Photoinduced Toxicity of Metals and PAHs to *Hyalella azteca*: UV-Mediated Toxicity and the Effects of Their Photoproducts

by

David Mark Isherwood

A thesis
presented to the University of Waterloo
in fulfillment of the
thesis requirement for the degree of
Master of Science
in
Biology

Waterloo, Ontario, Canada, 2009

I hereby declare that I am the sole author of this thesis. This is a true copy of the thesis, including any final revisions, as accepted by my examiners.

I understand that my thesis may be made electronically available to the public.

Abstract

Polycyclic aromatic hydrocarbons (PAH) are a class of common environmental contaminants known to be phototoxic. PAH Photoinduced toxicity is caused by two mechanisms: photomodification and photosensitization. The photomodification process results in modified PAHs, usually via oxygenation, forming new compounds (oxyPAHs), which are often more soluble than their parent PAHs. The process of photosensitization usually leads to the production of singlet oxygen, a reactive oxygen species (ROS), which in turn is extremely damaging to organic molecules. Both of these processes occur at environmentally relevant levels of actinic radiation.

Metals are ubiquitous environmental contaminants found extensively in many aquatic systems. Many metals are toxic at very low levels, and exhibit toxicity via ROS production or via direct binding to a ligand in an organism (Biotic Ligand Model). PAHs and metals often occur as co-contaminants in the environment, and there combined effects have only been examined in a few organisms.

The goal of this thesis was to examine the toxicity of PAHs, oxyPAHs, metals and their mixtures to *Hyalella azteca* in 96 h acute toxicity tests. All of the tests were performed under varying spectra of light; photosynthetically active radiation (PAR), PAR + UVA or simulated solar radiation (SSR) (PAR + UVA radiation + UVB radiation). In addition, chemical exposures in the Dark were performed to assess toxicity in the absence of light. The PAHs chosen represent 3 of the most common PAHs anthracene (ANT), phenanthrene (PHE), benzo(a)anthracene (BAA). The 12 oxyPAHs studied were quinolated analogues of the 3 parent compounds as well as anthraquinone derivatives that are hydroxylated at various positions. The toxicity of the parent PAHs increased in the

presence of increasing amounts of actinic radiation. The toxicity of the oxyPAHs also increased as PAR, UVA and UVB was added. Furthermore, most PAHs and oxyPAHs were found to be more toxic than the parent PAHs in the absence of actinic radiation.

The metals cadmium (Cd), copper (Cu), nickel (Ni) and zinc (Zn) were used in toxicity tests. These metals were selected based on their high prevalence in aquatic environments and the large amount of data in the published work. The order of metal toxicity in the Dark was Cd > Cu > Zn > Ni. The order of metal toxicity for the PAR and PAR/UV-A regime was Cd = Cu > Ni > Zn. The order of metal toxicity for the SSR treatment was Cu > Cd > Ni > Zn.

The toxicity of several metal/PAH mixtures was determined using one of the four metals and ANT, ATQ and 1-hATQ. The mixtures generally had additive toxicity under Dark and PAR lighting regimes. Under SSR lighting most mixtures showed a strictly additive toxicity, however synergistic toxicity was observed for the redox active metals (Cu, Ni) mixed with ANT. In the aquatic environment complex mixtures of PAHs and metals occur. The results of this study illustrate the effects that these mixtures may have on benthic invertebrates.

Acknowledgements

I am thankful to my supervisor, Dr. Bruce Greenberg for his support and knowledge in guiding me throughout this project. I appreciate the great deal of freedom that I have been given while completing my graduate studies.

I am grateful to my committee members, Brendan McConkey and Dr. Matthew Vijayan for their input and encouragement.

A special thank you goes to the members of the Greenberg lab especially Dr. Xiao-Dong Huang, Mark Lampi and Anabel Ueckermann for there help in creating a project that was both enjoyable and challenging, as well as their unique perspectives on life.

Finally, I want to thank my parents, Steven and Colleen Isherwood, for their unconditional love, encouragement, perspective, and for believing in me.

Table of Contents

List of Tables

List of Figures

List of Abbreviations

BLM - Biotic ligand model
DMSO - Dimethyl Sulfoxide
EC50 - Effective Concentration 50% mortality
ESS - Excited Singlet State
ETS - Excited Triplet State
LD50 - Lethal Concentration 50% mortality
OxyPAH - Oxygenated Polycyclic Aromatic Hydrocarbon
PAH - Polycyclic Aromatic Hydrocarbon
PAR - Photosynthetically active radiation
PCB - Polychloronated Biphenyl
QSAR - Quantitative Structure Activity Relationship
ROS - Reactive oxygen species
SSR - Simulated Solar Radiation

Metal Abbreviations

Cd - Cadmium
Cr - Chromium
Cu - Copper
Fe - Iron
Hg - Mercury
Ni - Nickel
Pb - Lead
Zn - Zinc

PAH Abbreviations

ANT – Anthracene
1,2,10-tANT – 1,2,10-trihydroxyanthracene
ATQ - Anthraquinone
1-hATQ – 1-hydroxyanthraquinone
2-hATQ – 2-hydroxyanthraquinone
1,2-dhATQ – 1,2-dihydroxyanthraquinone
1,3-dhATQ – 1,3-dihydroxyanthraquinone
1,4-hATQ – 1,4-dihydroxyanthraquinone
1,8-dhATQ – 1,8-dihydroxyanthraquinone
1,2,4-thATQ – 1,2,4-trihydroxyanthraquinone
1,2,5,8-thATQ- 1,2,5,8-tetrahydroxyanthraquinone
BAA – Benz(a)anthracene
BAQ – Benz(a)anthraquinone
PHE – Phenanthrene
PHQ – Phenanthrenequinone

Chapter 1
Introduction

1.0 Introduction

Over the past few decades, environmental contamination has risen from a minor concern in the 1950's and 1960's, to one of utmost importance in the present day. Xenobiotic chemicals produced by industrial processes often end up as environmental contaminants in terrestrial and aquatic ecosystems (Miller 1998, MacDonald et al. 2000). These contaminants are typically by-products of industrial processes, which are typically difficult to dispose of or remove. Environmental contaminants are often encountered as mixtures of two or more different chemicals. The field of environmental toxicology attempts to address the effects of these chemicals on the environment (Neff 1985, Landis et al. 1995, Klaassen 2001).

Environmental toxicology is a highly interdisciplinary science. It is comprised of several fields, including biology, microbiology, chemistry, engineering, ecology and many others (Oehme 1979). The question of assessing the effects of chemicals in the environment is complex; assessment depends upon the organism tested and involves not only toxicity testing of single chemicals, but also the interactive effects (synergism, antagonism) of chemical mixtures (Miller 1998). The issue of hazardous waste management is closely related to environmental toxicology, as most compounds studied in toxicology are deemed hazardous. There is a growing need for techniques and practices to minimize the environmental effects of chemicals, such as polycyclic aromatic hydrocarbons (PAHs), metals and their mixtures (Klaassen et al. 2001).

PAHs and metals are two abundant environmental contaminants. Both can be discharged into the environment via common industrial processes, including steel production and petroleum processing (Maliszewska-Kordybach et al. 2000, Gurst 2005, Gurst et al. 2005). Independently, PAHs and metals are highly toxic and when exposed to solar radiation these contaminants often exhibit an increase in toxicity (Huang et al. 1995;1997, Babu et al. 2001;2003;2005, Lampi et al. 2005, Xie et al. 2006;2007). To complicate matters further, these compounds are byproducts of the same industrial processes, and are almost always found together as mixtures in aquatic environments. In the current literature, the toxicities of many of these compounds have been tested individually and have been shown to cause toxicity at concentrations found in the environment (Huang et al. 1995a, Lampi et al. 2005, Gurst et al. 2005, Xie et al. 2007). However, these compounds are not found as single contaminants in the environment and are exposed to solar radiation. In particular the toxicity of PAHs has been shown to increase in the presence of solar radiation, via two processes, photomodification and photosensitization. Photosensitization produces reactive oxygen species (ROS) and photomodification leads to the formation of PAH photoproducts, such as oxygenated polycyclic aromatic hydrocarbons (oxyPAH). These processes complicate risk assessment, and have not been incorporated into current risk assessment protocols. As a result, it is likely that, the environmental impacts of these compounds are being underestimated. Currently, there is no legislation that addresses metals and PAHs as co-contaminants. Both the Canadian Council of Ministers of the Environment (CCME) and the U.S. Environmental Protection Agency (USEPA) still base their guidelines on single chemical toxicity data (CEPA 1999, USEPA 2004).

PAH and metal toxicities as single contaminants have been well documented (Babu et al. 2001, Borgmann et al. 2002, Lampi et al. 2005, Gurst 2005, Gurst et al. 2005). As well, several studies have looked at oxyPAHs as a single contaminant (McConkey et al. 1997, Lampi et al. 2005, Xie et al. 2007). It has also been found that when PAHs and metals are tested as a mixture, an increase in toxicity is often seen (Babu et al. 2005, Xie et al. 2006; 2007). Additionally, PAH toxicity has been shown to increase in the presence of actinic radiation (Diamond et al. 2003, Lampi et al. 2005). Due to their toxicity, mutagenicity, and carcinogenicity these compounds are of major environmental concern. The toxicity of PAHs under environmentally relevant lighting conditions to *Hyalella azteca,* a representative benthic organism, has not been investigated. This thesis addresses the effects of PAHs and metals have individually on *Hyalella azteca* under several different lighting regimes. It also attempts to further the understanding of the complex interactions that occur in mixtures of ANT, ATQ, 1-hATQ and metals in the presence of actinic radiation.

1.1 Polycyclic Aromatic Hydrocarbons

Polycyclic Aromatic Hydrocarbons (PAHs) are compounds made up of two or more fused benzene rings. The name also refers to PAH derivatives, which contain alkyl or other functional groups, such as hydroxyl or carbonyl groups (Health Canada Priority Substances List, 1999). PAHs are produced naturally, through the combustion of organic matter by forest fires and volcanoes. Additionally, very small amounts may be produced by diagenesis or biosynthesis (Neff 1985, Ankley et al. 1994, Burgess et al. 2003). Anthropogenically, PAHs are produced primarily by incomplete combustion of fossil

fuels, steel production, petroleum spills, as well as from power generation and home heating (Neff 1985, Ankley et al. 1994, Burgess et al. 2003). PAHs are only slightly soluble in water and thus readily associate with particulate matter in the water column (McKinney et al. 1999, Parkerton et al. 2000, MacDonald et al. 2000, Lampi et al. 2001, Kurihara et al. 2005), in airborne matter (Fox and Olive 1979, MacDonald et al. 2000) and in terrestrial soils (NRCC 1983, Parkerton et al. 2000, MacDonald et al. 2000). The hydrophobicity of PAHs often results in their accumulation in lipids of organisms ranging from bacteria (McConkey et al. 1996) and plants (Duxbury et al. 1997) to humans (Younglai et al. 2002). Additionally, these compounds have been found to have estrogenic activities in many organisms, causing endocrine disruption in rats (Nykamp et al. 2001), fish (Brasseur et al. 2007), and humans (Vondracek et al. 2002).

Due to their conjugated π-bonding orbitals, PAHs can absorb photons of light in the UV and blue regions of the electromagnetic spectrum (Foote 1968, Newsted and Giesy 1987, Huang et al. 1993, Diamond et al. 2000). Absorption of radiation at these wavelengths can alter the structure and toxicity of PAHs predominantly through two mechanisms: photosensitization and photomodification (Mallakin et al. 1999:2000). Photosensitization generally leads to the production of reactive oxygen species (ROS), which can damage biological molecules. Photomodification results in the modification of PAHs into new compounds through various processes including, photooxidation and photolysis. These compounds typically have increased water solubility and toxicity (Foote et al. 1987, Huang et al. 1997, Diamond et al. 2000, Lampi et al. 2005, Xie et al. 2007).

Risk assessment of PAHs and the photoinduced toxicity associated with their exposure to actinic radiation has proven to be difficult and complex. PAHs are often found in the environment as complex mixtures of highly substituted heterocyclic hydrocarbons. The composition and chemical profiles of PAHs can vary considerably from site to site (Sanders et al. 1995). Also each PAH in a mixture differs in its potential for photoactivation. Complicating matters further, a given PAHs photoactivation potential is strongly influenced by the milieu of co-contaminant PAHs and metals at a given site (Dabestani et al. 1999, Diamond et al. 2003, Xie et al. 2007). This poses a serious problem for the predictive modeling of PAHs. Furthermore many PAH photoproducts are more toxic than their parent compounds and their potential for toxicity is influenced by co-contaminants (McConkey et al. 1996, Duxbury et al. 1997, Diamond et al. 2000, Lampi et al. 2005, Xie et al. 2007). Due to these complicating factors there is little government regulation for PAHs and almost no regulation for PAH photoproducts.

1.2 Photosensitization

In almost any environmentally relevant scenario it is inevitable that an environmental contaminant will be exposed to sunlight, in particular to ultraviolet radiation (UV). When exposed to actinic radiation molecules capable of absorbing UV light will become excited, resulting in many different possible photochemical reactions (Burgess et al. 2003). These reactions are entirely dependent upon the chemical absorbing the light and the wavelength of light that the compound is exposed to. The absorbance spectrum of several representative PAHs are depicted in figure 1.1. If a

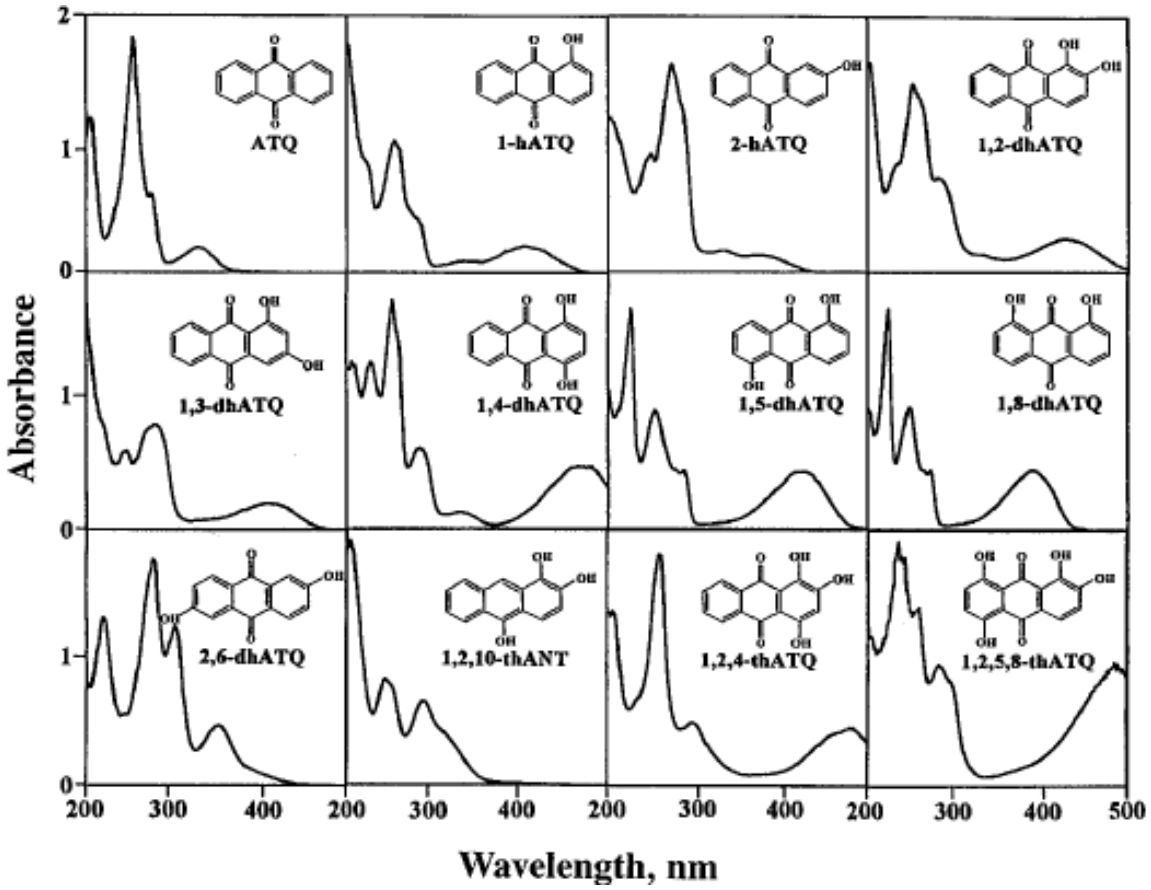

Figure 1.1 Absorbance spectrum of representative PAHs (Adapted from Mallakin et al. 1999)

molecule absorbs a wavelength of light that overlaps with its absorption spectrum, a photochemical reaction can take place. The wavelength range of solar radiation needed for most PAHs to become photoactivated is 290-480 nM (Burgess et al. 2003). Photoactivation often leads to photosensitization process, resulting in the production of ROS. Many natural organic compounds that have similar structures to PAHs are known photosensitizers including flavonoids, chlorophyll and phytoalexins (Figure 1.2) (Lazzaro et al. 2004). Researchers have found that a wide variety of PAHs, can cause a photosensitization effect long after the initial exposure due to the bioaccumulation of PAHs in organisms (Boese et al. 1999, Diamond et al. 2000, Nuutinen et al. 2003).

PAHs, like all organic compounds, exist in a ground state known as the singlet ground state (Figure 1.3). In this state PAHs have two electrons residing in their highest occupied molecular orbital (HOMO) (Foote 1968). When PAHs are exposed to actinic radiation they can absorb energy in the form of photons, in a process known as excitation. When a PAH absorbs a photon of energy and becomes photoactivated, one of the HOMO electrons undergoes a transition to a higher energy level known as the excited singlet state (ESS), designated as $^{1}PAH^{*}$ (Figure 1.3). From its ESS several things can occur. Firstly, the PAH can emit a photon via fluorescence, which in turn returns the molecule to its singlet ground state (Foote 1968). The PAH can also give off the energy through vibrational states as heat and return to its singlet ground state. However, while the molecule is in its ESS it can also undergo a process called intersystem crossing, during which there is a transition from the ESS to a spin state called the excited triplet state (ETS) designated $^{3}PAH^{*}$ (Figure 1.3). The ETS plays a key role in photochemistry. When a PAH is in its ETS it can return to its ground state by emitting a photon of light

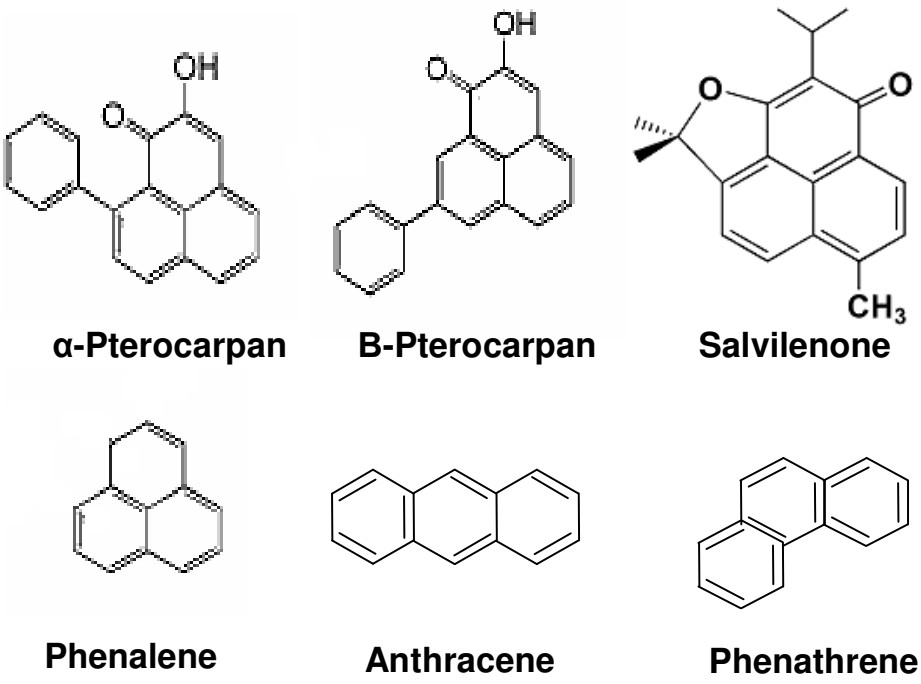

Figure 1.2 Structures of photosensitizers: Phytoalexins, Theraputics and PAHs.

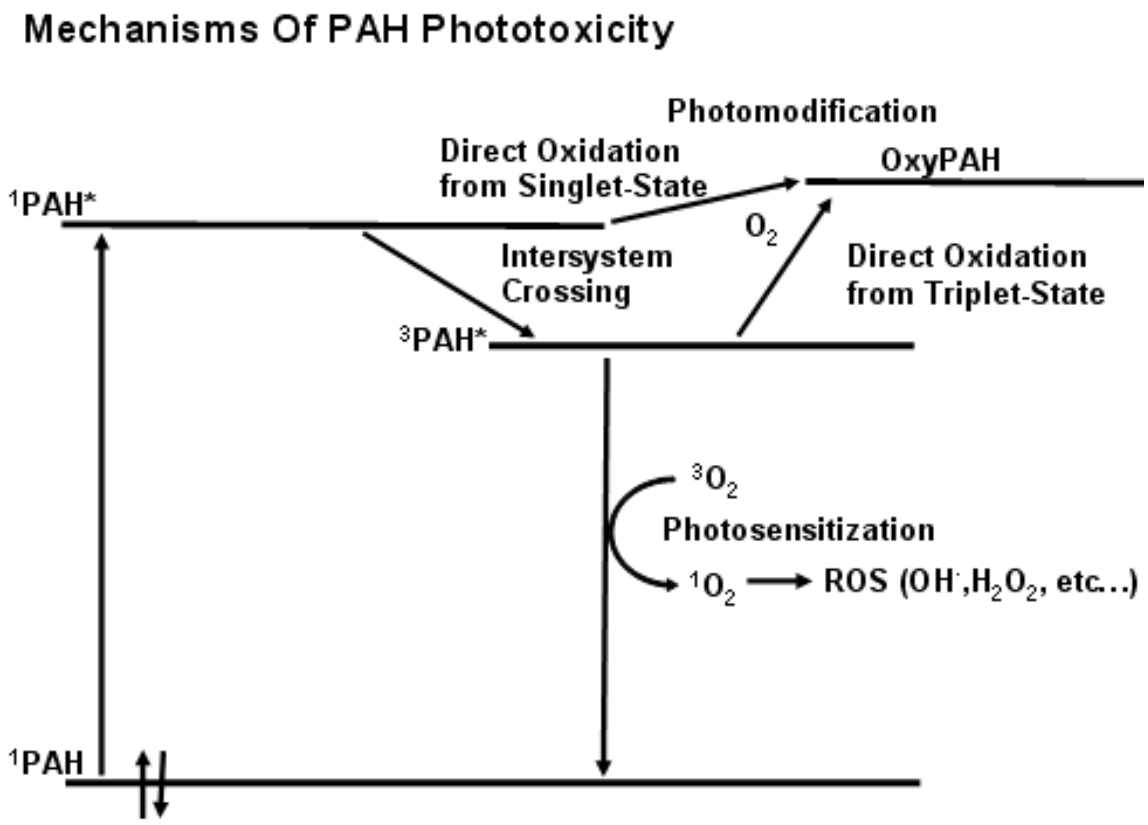

Figure 1.3 Jablonski Diagram Illustrating Photoinduced Toxicity of PAHs
Abbreviations ^{1}PAH, ground state PAH; ^{1}PAH*, excited singlet state PAH; ^{3}PAH*; excited triplet state PAH; $^{3}O_2$, triplet (ground) state oxygen; $^{1}O_2$, singlet (excited) state oxygen.

through phosphorescence. However, phosphorescence is a triplet-singlet state reaction and is quantum-mechanically forbidden by the Pauli Exclusion Principle. Therefore, the ETS is extremely long lived lasting 10^{-6} - 10^{-4} seconds, compared to that of the much shorter lived ESS, which lasts 10^{-9} seconds. This long lived state increases the probability of photochemical reactions occurring (Foote et al. 1976). While the PAH is in its excited triplet state it can react with molecular oxygen, transferring energy and elevating the triplet oxygen to its excited singlet state (a higher energy level for O_2).

Molecular oxygen in nature is primarily found in a ground triplet state ($^3O_2$). All biological molecules exist in a singlet ground state. The Pauli Exclusion Principle states that singlet-triplet state reactions are forbidden (Foote et al. 1968; 1976, Kohen et al. 1995). Singlet oxygen ($^1O_2$) is of a higher energy level than that of $^3O_2$ and as a result is extremely reactive, particularly with biological molecules, because the spin restrictions not longer exist. Singlet oxygen will typically react with the first molecule that it comes into contact with; this process is known as Type Two Photosensitization (Figure 1.4). Alternatively, if the PAH is in its ETS, it can interact with a molecule other than molecular oxygen. It then can transfer its energy causing the molecule to become excited, which results in a radical or triplet state molecule. This radical or triplet state molecule can then react with molecular oxygen or other biological molecules. This process is also referred to as Type One Photosensitization (Foote 1968; 1976; 1991).

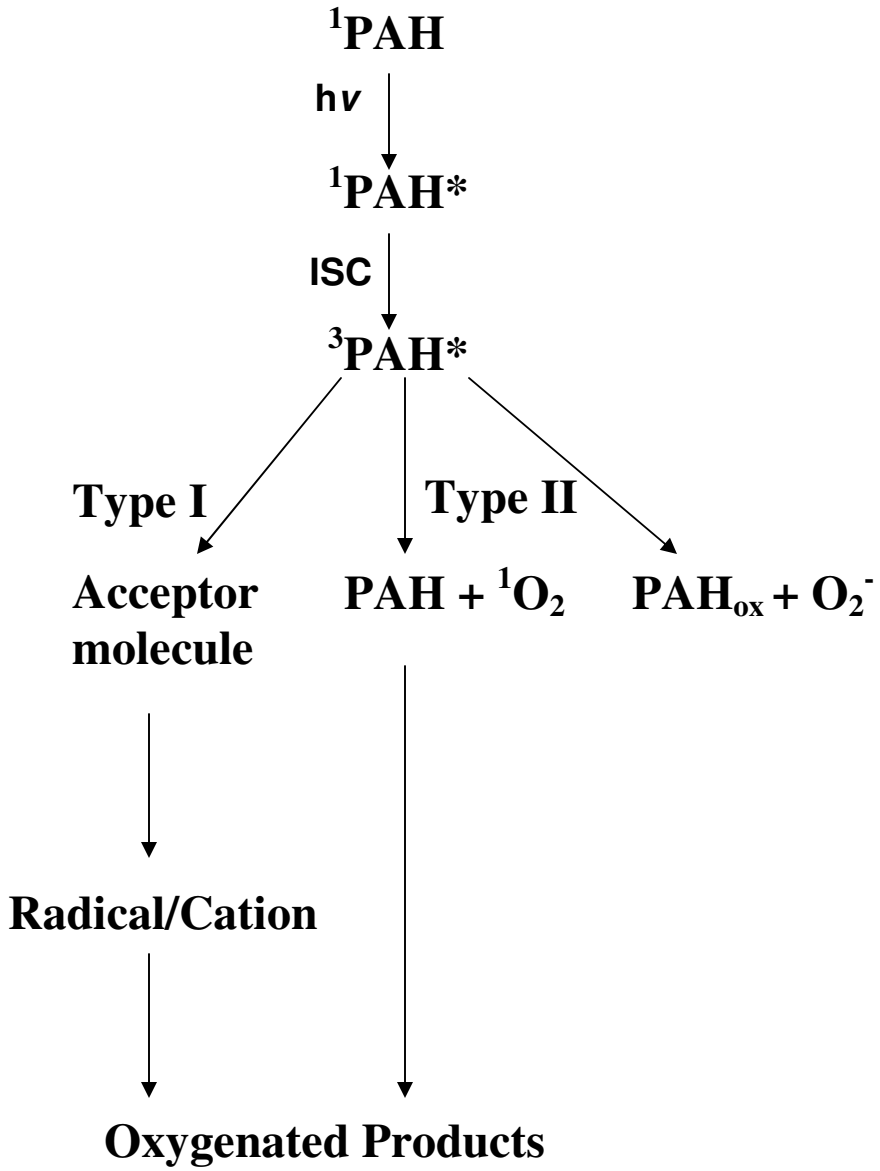

Figure 1.4. Mechanisms of Photosensitization; Type 1 and Type 2. Abbreviations: ^{1}PAH, singlet (ground) state PAH; ^{1}PAH*, singlet (excited) state PAH; ^{3}PAH*, triplet (excited) state PAH; hν, a photon of light; ISC, intersystem crossing.
Adapted from Foote 1991.

1.3 Photomodification

A second important process involved in PAH phototoxicity is photomodification, which occurs when a PAH is excited to its ESS or ETS. When a PAH in an excited state reacts with oxygen, it can result in the formation of oxygenated products (oxyPAHs). For instance, PHE oxidation occurs via 9,10 endoperoxidation of phenanthrene (PHE) resulting in the formation of its primary photoproduct phenanthrenequinone (PHQ) or via further reactions, a hydroxylated phenanthrenequinone (hPHQ) (Figure 1.5). This can also occur in other PAHs, such as anthracene (ANT), which also occurs by the formation of an endoperoxide, via 1,4 –cycloaddition of oxygen across its central ring. This results in the formation of anthraquinone (ATQ) (Mallakin et al 1999). Photomodification of PAHs is known to occur in the presence of natural sunlight in the biosphere and has been linked to increased toxicity (Huang et al. 1995, McConkey el al. 1997, Lampi et al. 2005). Often PAH photomodification leads to the formation of increasingly water soluble compounds (Mallakin et al. 1999:2000, Brack et al. 2003) (Figure 1.6). Photomodification can occur from the ETS where oxygen is added via oxidation. In studies performed by Huang et al (1995), Mallakin et al (1999) and Diamond et al (2000) anthracene, a common PAH, was found to oxidize into a variety of compounds, including 1,2-dihydroxyanthraquinone, which is known to disrupt mitochondrial and photosynthetic electron transport (McConkey et al. 1997, Huang et al. 1997, Mallakin et al. 2000, Xie et al. 2006). In addition, Huang et al. (1997) found evidence that several hydroxylated anthraquinones inhibit photosynthetic electron transport. Mallakin et al. (2000) demonstrated that in the presence of simulated solar radiation (SSR) anthracene becomes

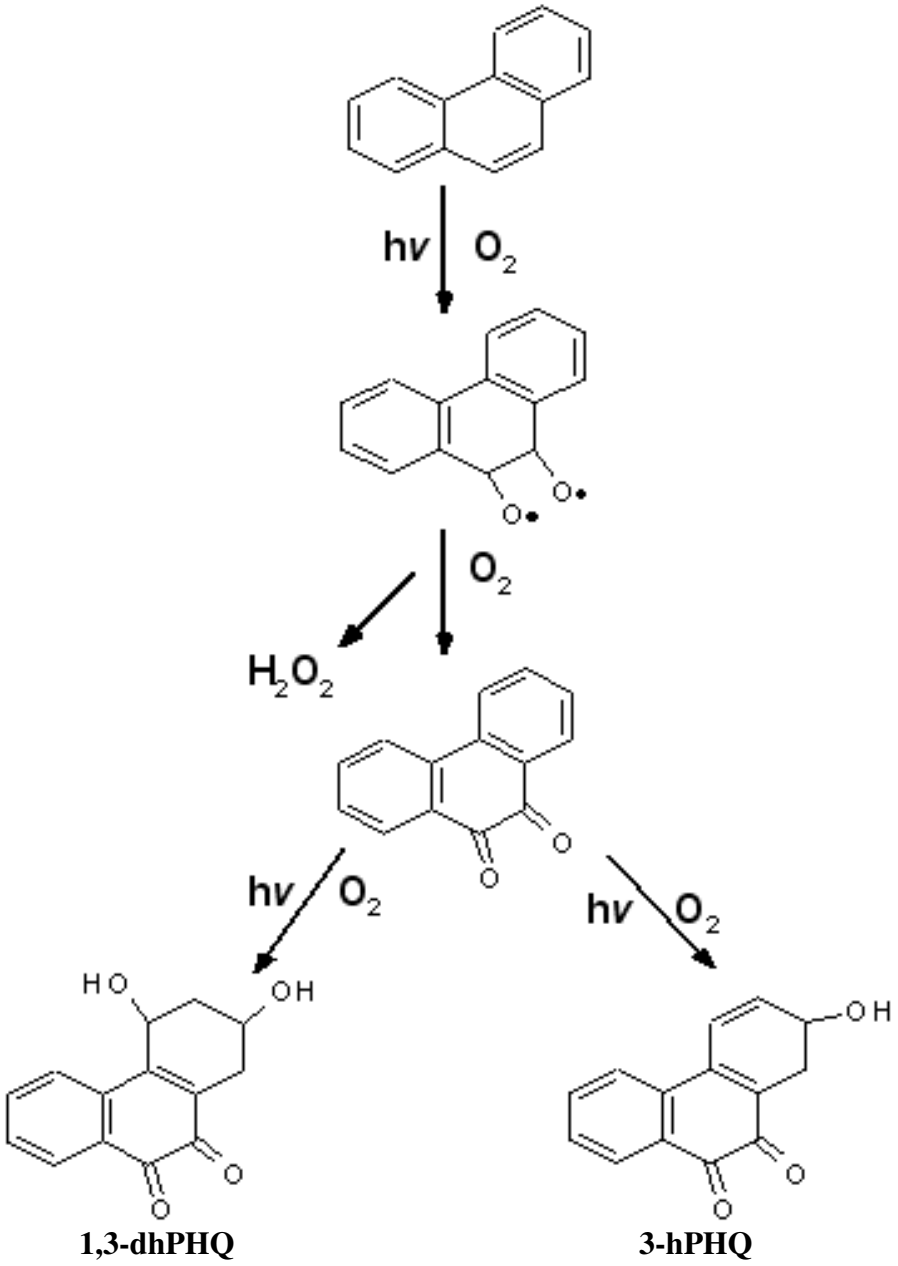

Figure 1.5 Photomodification of Phenanthrene. 1,3-dihydroxyphenanthraquinone (1,3-dhPHQ); 3-hydroxyphenanthraquinone (3-hPHQ)

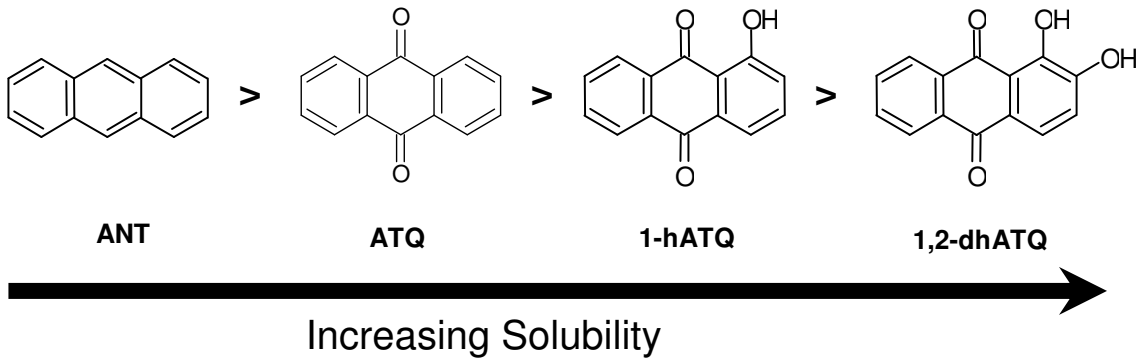

Figure 1.6 Solubility trends in PAHs. ANT, anthracene; ATQ, anthraquinone; 1-hATQ, 1-hydroxy-anthraquinone; 1,2-dhATQ, 1,2-dihydroxy-anthraquinone.

extensively modified and has a half-life of two hours, whereas anthraquinone, a primary anthracene photoproduct, is relatively stable. Mallakin et al. also found that anthracene when exposed to SSR becomes modified into more than 20 different photoproducts (Mallakin et al. 2000). Lampi et al. (2006) found that many intact PAHs exhibited UV mediated toxicity to *Daphnia magna* and found their photoproducts to be highly toxic even in the absence of actinic radiation. Phenanthrene, another unsubstituted PAH with 3 rings, has also been shown to undergo photomodification into a large number of photoproducts (Gurst et al, 2005).

1.4 Metals

Metals are environmental contaminants that are often released during steel production, through machinery exhaust, and via accidental spills/discharges. The most common metal contaminants found in freshwater are Cu, Cd, Cr, Ni and Pb (Abel 1989, Priority Substance List CEPA 1999, Toxic Substance List 2004).

Many metal ions are used in biological processes and, at low levels, are essential to life (Abel 1989, Edie 2003). They have roles as protein co-factors, in cellular signaling and as redox agents. However, even at low levels metals can be problematic, as metals do not biodegrade, are often water soluble, and have the potential to bioaccumulate in biological systems. At elevated levels metals can become toxic, as shown in work done by Borgmann et al. (2005), which determined the EC50s for 63 metals and metalloids in *Hyalella azteca*. Metals that are classified as heavy metals (atomic weight greater than 40) represent the most common and dangerous environmental contaminants. Metals including copper (Cu) and zinc (Zn) are essential

trace metals to most living organisms. Others, such as lead (Pb) and cadmium (Cd), have no known biological function. Most current research suggests that metals induce toxicity via different mechanisms, including enzyme inhibition based on the biotic ligand model (BLM) and by the formation of ROS (Kasprzak 1989, Pourahmad et al. 2000, Gurst et al. 2005, Xie et al. 2005). Metal-induced ROS production has recently been noted as an important mechanism of metal toxicity. Both redox-active metals (Cu, Fe, Ni) and non redox-active metals (Pb, Cd, Hg) can induce ROS formation, although they do this via different pathways (Li et al. 1993, Li et al. 1994, Pourahmad et al. 2000; 2003, Bolduc et al. 2004, Xie et al. 2006).

1.5 Copper

Copper (Cu) is a metal that has been utilized for its malleability and conductivity and is presently used in many aspects of industrialized life. It is found in casting, gas and water piping, roofing materials, cooking utensils, chemical and pharmaceutical equipment, and in currency (Tabershaw 1977). Cu compounds are used as dyes (cupric arsenate), insecticides (Cu flouroarsenate), fungicides (Cu sulfate), and various analytical reagents (Cupric Chloride). Cu contamination usually results from industrial discharges, mining, and smelting (Nriagu 1979, Fitzgerald 1998).

Cu is one of the most common metals of concern in aquatic ecosystems. It is found naturally in most freshwater systems with a concentration ranging from 3-12ng/L (Abel 1989, Environment Canada 2003). Cu is essential in many biological processes, including metalloprotien cofactors, cytochrome c oxidase, Cu-Zn superoxide dismutase, and azurin (a redox centre in microorganisms) (Fitzgerald 1998). Most terrestrial

vertebrates, including humans, are never exposed to lethal concentrations of Cu and are highly tolerant of Cu. For example, the rat oral LD50 for Cu is 114 mg/kg (Abel 1989). However, Cu is abundant in aquatic environments and is extremely toxic to aquatic invertebrates, plants, and fish, which are all sensitive to Cu in the low to high μM range (Babu et al. 2001, Hansen et al. 1996, Jeffrey et al. 2002, Borgmann et al. 2005, Xie et al. 2006).

Several mechanisms have been proposed to explain the toxicity of Cu, including DNA binding, disruption of divalent ion channels (Ca^{2+}), lipid peroxidation, lysosomal destabilization, and redox cycling (Pourahmad et al. 2000). Redox cycling plays an important role in many cellular pathways, such as cytochrome c oxidase and free radical defense (eg: superoxide dismutase). Redox cycling can also act as a mechanism of ROS production (Pourahmad et al. 2000). Several studies have been performed that demonstrate the Cu-based ROS mechanism through the use of the antioxidant enzyme assays; catalase, or superoxide dismutase assays (Pourahmad et al. 2000, Babu et al. 2001, Liang et al. 1999, Xie et al. 2006). ROS production can lead to DNA damage, peroxidation of lipids, and oxidation of protein thiol bonds (Abel 1989, Van Asscheet et al. 1990)

1.6 Cadmium

Cadmium (Cd) is an element that is relatively rare in the earth's crust with an average concentration of 0.15-0.2 mg/kg (Sadiq 1992). Cadmium contamination in the environment is almost always as a byproducts from various industrial processes. Some of its uses include battery production, in polymer stabilization and to make metal alloys

(Sadiq 1992). Cadmium concentrations in pristine aquatic environments are generally less than 2 ng/L. Levels above 50 ng/L have been reported in many industrialized environments and Japanese lakes have recorded standing levels of 3.5 μg/L and periodic levels of 8 μg/L (Yamagata 1979). Cadmium contamination is almost always the result of anthropogenic activities (Environment Canada 2003).

Cadmium is one of the most toxic elements and is regarded as a priority pollutant, especially in aquatic ecosystems (Environment Canada 2003, USEPA 2000). Cadmium toxicity in aquatic organisms has been extensively studied (McLusky et al., Borgmann et al. 2005, Gurst et al. 2005, Gurst 2005). The chemistry of cadmium is different in fresh water compared to marine environments and generally freshwater organisms are much more susceptible to cadmium toxicity than marine organisms. Surprisingly, unlike other metals, Cd has been found to only minimally bio-concentrate up the food chain (Sadiq 1992). A study by Amiard-Triquet et al. (1983) found higher levels of Cd in invertebrates than in their fish predators. Another study by Perceval et al. (2002) and Borgmann et al. (2004) demonstrated that the toxicity of Cd in water is a function of pH, ionic strength and temperature.

Cadmium, unlike Cu, is a non-redox active metal. Its primary mechanism of toxicity is thought to be based on the biotic ligand model (BLM). Cd is sulphophilic, preferentially binding to thiol groups over other molecules. As a result, Cd's primary mechanism of toxicity is thought to be through enzyme inhibition (Sadiq 1992, Takameure et al. 2005). As a divalent cation Cd can also compete with Ca^{2+} uptake in many intracellular processes (Kelly 1988). However, despite being a non-redox active metal studies have shown that Cd does elicit a ROS mediated toxicity, the mechanisms of

which are theorized to be based on Cd/Protein interactions (Stacy et al. 1980, Snyder 1988, Xie et al, 2006).

1.7 Nickel

Nickel (Ni) is an element found abundantly in the Earth's crust at a concentration of 5-10 mg/kg. It is used in industrial processes including the manufacture of stainless steel, magnets, coinage, batteries and other metal alloys. Though a common element, Ni is not often found in large deposits, with the exception being the southern Canadian Shield in particular Sudbury Ontario, which is responsible for 30% of the worlds nickel supplies. Nickel while not essential for animals, is an essential element for plants and many microorganisms. In particular, many plants contain a Ni based superoxide dismutase and Ni-Fe hydrogenases (Szilagyi et al. 2004, Jaoun 2006).

Environmental contamination by Ni is a common occurrence with contamination often arising from anthropogenic sources. In pristine lakes nickel is found at a concentration of 0.1-1.0 μg/L, whereas contaminated lakes can have concentrations as high as 100-1000 μg/L (Eisler 1998). Nickel, is not acutely toxic to animals, but is highly carcinogenic, genotoxic and mutagenic (Kasprzak 1989, Kasprzak et al. 2003, Pourahmad et al. 2000, Szilagyi et al. 2004). Though Ni is only mildly toxic to aquatic organisms, the mutagenic and carcinogenic effects can be staggering. Ni contamination in aquatic systems has been shown to increase levels of carcinomas in populations of fish (Anderson 1992, Doig and Liber 2006; 2007).

Ni toxicity is thought to occur through direct binding to ligands (BLM). However, recent experimental evidence has suggested that ROS plays an important role in Ni

toxicity (Kasprzak 1991, Kang et al. 2003, Doig and Liber 2006). Kang et al. (2003) found that Ni in human hepatocytes induced the production of hydrogen peroxide, lipid peroxidation and up-regulation of ROS scavenger compounds. Despite this evidence, the primary toxicity mechanism is thought to be that of direct binding to proteins.

1.8 Zinc

Zinc (Zn) is an essential biological element and is abundant in nature (Kelly 1988). Many proteins and enzymes in animals and plants contain zinc prosthetic groups. These include zinc fingers, carboxypeptidase A, and retinol-binding protein (Christian et al. 1998, King et al. 2006). In addition, there are over a dozen types of cells in the human body that secrete zinc ions, which are thought to have roles in cellular signaling. For instance, Hershfinkel et al. (2007) found that zinc ions act as neurotransmitters between human neurons.

Zinc contamination is primarily from anthropogenic sources. Often zinc contamination results from the corrosion of stainless steel piping, mining, industrial processes and pharmaceutical waste (Environment Canada 2003). Zinc is relatively non-toxic to most aquatic organisms, but at elevated levels can have acute toxic effects (Timmermans 1993). The toxicity of Zinc has is primarily attributed to direct ligand binding based on the BLM. Zinc interferes with other divalent ion uptake, as well as competing with other ions as enzymatic cofactors. One example of Zn toxicity Hemolytic Anemia results from human ingestion of as little as 100-300 mg of zinc (Stowe et al. 1978).

1.9 Metals and PAHs

Metals and PAHs often exist in the environment together as complex mixtures. Sediments, sewage, and aquatic systems are often co-contaminated with mixtures of Cu, Ni, Cd, Zn and PAHs. Almost all of this contamination is from anthropogenic sources, primarily industrial processes. It has been demonstrated that potential interactions between the metals and PAHs can increase the overall toxicity of the contaminant mixtures (CEPA 1999, Tabak et al. 2003, Xie et al. 2005, Doig and Liber 2006, Xie et al. 2007). Experiments performed by Tabak et al. (2003) showed that contaminated sediments from the East River (NY, USA) were acutely toxic to 12 freshwater and marine organisms including *Hyalella azteca*. Despite the pressing issue of PAH and metal mixture contamination, very few studies have looked at the toxic interactions between PAHs and metals, and the underlying mechanisms of toxicity.

As stated above, PAHs undergo photosensitization and photomodification in the presence of actinic radiation, resulting in the production of oxyPAHs and reactive oxygen species. As a result co-contamination with other chemicals is further complicated by the potential presence of these oxyPAHs. Co-contamination of PAHs/oxyPAHs and metals have the potential to have an increased toxic effect. This toxicity can be further amplified in the presence of actinic radiation. When a PAH exposed to sunlight is coupled with a redox active metal (Cu, Fe, or Ni), there can be a marked increase in the formation of oxyPAHs and ROS production (Goldstein et al. 1993, Xie et al. 2007). In particular, if a metal is redox active the potential for toxicity in a PAH/metal mixture is greatly increased (Li et al. 1993, Xie et al. 2005; 2007). Xie et al. (2005) examined the effects that mixtures of Phenanthrenequinone (PHQ), Cu, and a number of antioxidants on

Daphnia magna. It was found that PHQ and Cu mixtures caused a marked increase in toxicity that was diminished when the antioxidants were present. This study showed that ROS production is an important mechanism for Cu and PHQ co-toxicity (Xie et al. 2005). In a follow-up study Xie et al. (2007) found that the relative toxicity of PHQ/Cd mixtures, (in *Daphnia magna*) was not necessarily related to the amount of ROS generated by the compounds. The study also implied that ROS played only a part in the toxicity of the PHQ/Cd mixture.

1.10 Reactive Oxygen and ROS Cycling

PAHs and metals can independently interfere with biological processes. In particular the presence of PAHs and redox-active metals, such as copper and nickel, can perturb biological electron transport in mitochondria and chloroplasts (Huang et al. 1997a, 1997b, Xie et al. 2005:2007). The primary cause of biological damage in this case is reactive oxygen species (ROS). ROS are derivatives of molecular oxygen, including free radicals such as the hydroxyl ion (OH^-), superoxide anion ($O_2^{\bullet-}$), hydroxide radical ($^{\bullet}OH$), and hydrogen peroxide (H_2O_2) (Foote 1968) (Figure 1.7). These free radicals are found in most organisms and play a role in cellular signaling, immune responses, and apoptosis. However, these compounds are also extremely detrimental to cells in uncontrolled settings, such as metal toxicity or PAH photosensitization. They can cause lipid peroxidation and are known to disrupt proteins (Foote 1978)

Reactive oxygen species are almost always formed during the reduction of molecular oxygen (O_2) into water (H_2O) in the mitochondrial electron transport chain. This reduction results in the acceptance of four electrons. This occurs as a stepwise

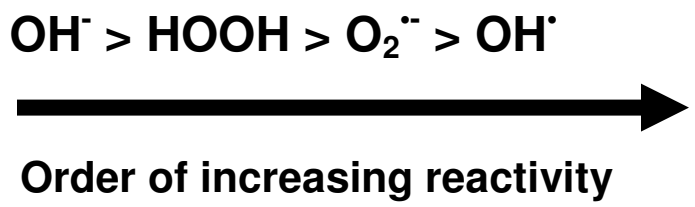

Figure 1.7 Reactivity of Oxygen species. O_2, molecular Oxygen; OH-, hydroxyl ion; HOOH, hydrogen peroxide; $O_2^{\bullet-}$, superoxide radical; $OH^{\bullet}$, Hydroxyl radical.

reduction. Due to electron spin restrictions, molecular oxygen must accept each of the four electrons individually (King et al. 1975). Reactive oxygen species can also be formed when PAHs and metals are present by a process known as redox cycling.

Redox cycling with metals is based on Fenton-chemistry and occurs because the PAH/oxyPAH and the redox active metal can cycle between two redox states. Redox cycling can facilitate the transfer of electrons from donor molecules to other electron acceptors, such as molecular oxygen, leading to the generation of ROS (Figure 1.8) (Foote 1991, Huang et al. 1995;1997, Xia et al. 2004, Xie et al. 2006;2007). These ROS can cause lipid peroxidation and disrupt nucleic acids and are considered to be key contributors to metal/PAH toxicity. This toxicity is further increased in the presence of actinic radiation. When PAHs are exposed to actinic radiation they photosensitize, leading to the production of ROS, which in turn redox cycles in the presence of redox active metals (Cu, Ni, Fe) greatly increasing the toxicity of the mixture (Weckx and Clijsters 1996, Xia et al. 2004, Xie et al. 2005, Xie et al. 2007).

1.11 *Hyalella azteca* as a Model Organism

In this study *Hyalella azteca* (Crustacea, Amphopida) was chosen as a model organism for toxicity testing. *Hyalella azteca* is a representative freshwater invertebrate commonly found in the littoral zone of lakes, rivers, streams, and ponds throughout North America (Kruschwitz 1978, USEPA 2000). *Hyalella azteca* feed primarily on decaying organic matter and are omnivorous. They reproduce sexually and reach reproductive age after two weeks. *Hyalella* have a lifespan of approximately four months and are sexually active until death (Kruschwitz 1978). *Hyalella azteca* were chosen as a test organism

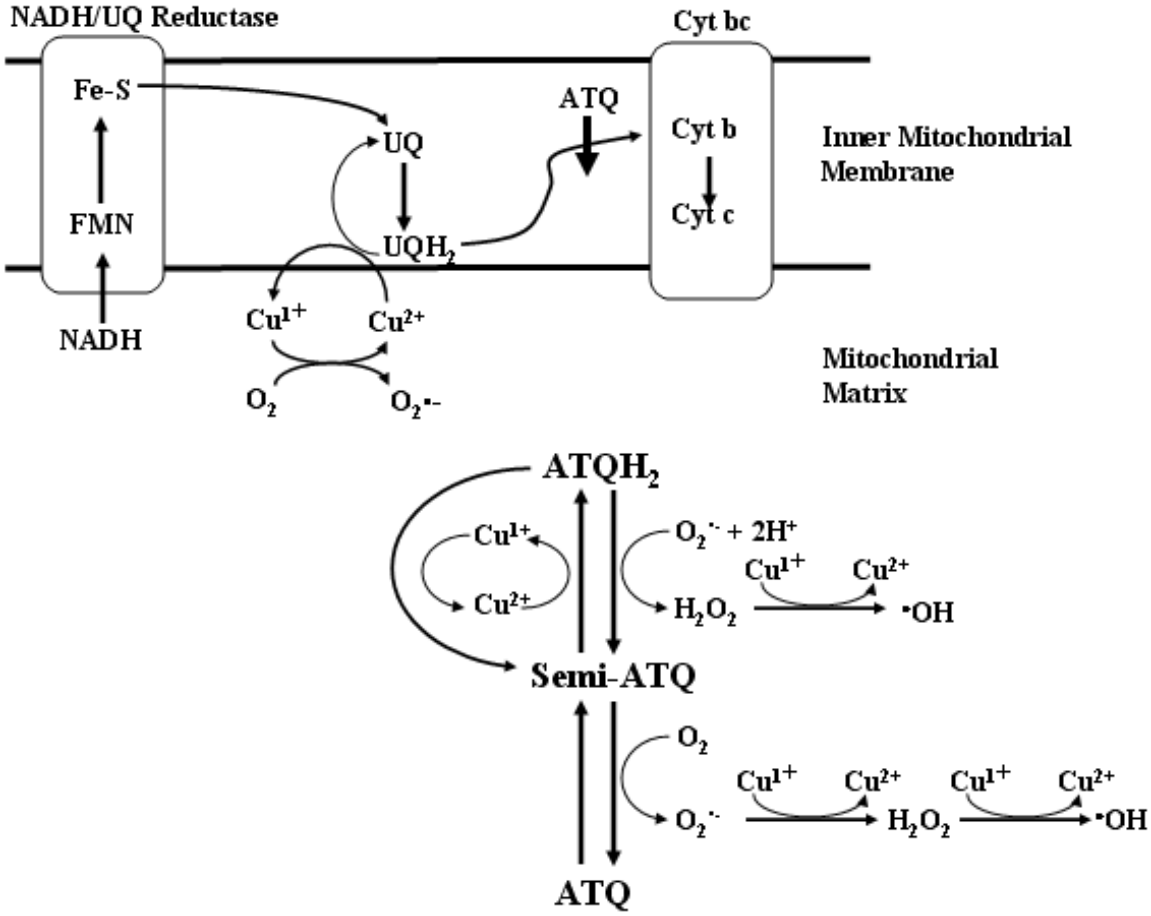

Figure 1.8. Redox cycling of ATQ and Cu (adapted from Xie et al. 2005)

because they represent a keystone species in aquatic food webs across the Americas as both a food source and scavenger. *Hyalella azteca* are relatively easy to culture and have an average sensitivity to common contaminants. This, along with the large amount of toxicity data about them, makes *Hyalella azteca* an ideal test organism (USEPA 2000).

1.12 Goals of this Study

PAHs and metals are two classes of environmentally important contaminants. They can often be found in the environment as co-contaminants primarily as a result of industrial processes like smelting and petroleum refining (Tabak et al. 2003). The toxicities of metals and PAHs alone in aquatic systems have been well documented; however, the effects that actinic radiation has on their toxicities has not been studied in *Hyalella azteca*. Furthermore, there is very little data on the combined effects of PAHs and metal mixtures under actinic radiation in aquatic systems.

This thesis attempts to fill in some of the gaps in our knowledge of PAH and Metal toxicities under actinic radiation. Using the *Hyalella azteca* whole organism system, the combined toxicity of PAH and metals were assessed by varying the levels of actinic radiation the organisms are exposed to. The PAHs chosen are representative chemicals based on abundance and varying oxygenated positions (ANT, ATQ, 1-hATQ, 2-hATQ, 1,2-dhATQ, 1,3-dhATQ, 1,4-dhATQ, 1,8-dhATQ, 1,2,4-thATQ, 1,2,5,8-thATQ, 1,210-thANT, BAA, BAQ, PHE, PHQ). The metals Cu, Cd, Ni, Zn are all common aquatic contaminants and are likely to have different mechanisms of toxicity. Additionally, there is a large amount of data to compare with on each of the single chemical toxicities. The data produced in this thesis will be used to deduce the role of

photoinduced toxicity on single toxicants and mixtures. The phototoxicity assays will be based on varying the irradiance spectra, to examine the effects that different environmentally relevant wavelengths have on toxicity. The first goal was to determine the effects of actinic radiation on 15 PAHs to *Hyalella azteca*, and is addressed in Chapter 2. The second goal was to determine the affect of actinic radiation on four metals to *Hyalella azteca*, and is addressed in Chapter 3. The third goal was to determine the affects that actinic radiation has on the toxicity of mixtures of PAHs and metals to *Hyalella azteca*, and is addressed in Chapter 4. Using these data sets this thesis aims to fill in the gaps in current data and help to develop further policy for the regulation of these contaminants.

Chapter 2

Photoinduced Toxicity of PAHs to *Hyalella azteca*. Effects of PAR and UV mediated mechanisms and the formation of Photoproducts.

2.0 Introduction

Polycyclic aromatic hydrocarbons (PAHs) are contaminants commonly found in many aquatic environments. The majority of PAH contamination arises from anthropogenic sources including electrical power generation, industrial processes, and the incomplete combustion of fossil fuels (Neff 1985, Ankley et al. 1994). They are highly lipophillic and are considered priority contaminants by Environment Canada (CEPA 1999, Environment Canada 2003).

The toxicity of PAHs to aquatic organisms is often enhanced by the exposure to sunlight (simulated or natural) (Newsted et al. 1987, Huang et al. 1995, McConkey et al. 1997, Diamond et al. 2000, Xie et al. 2005, Lampi et al. 2005, Xie et al. 2007). PAH photoinduced toxicity is based on two different mechanisms: photosensitization and photomodification (Oris et al. 1985, Landrum et al. 1986, Lehto et al. 2003). Photosensitization leads to the production of reactive oxygen species, which can result in significant damage to biological molecules (Foote 1976, Foote 1991, Landrum et al. 1986,). The other mechanism, photomodification, involves the structural modification of PAHs into a variety of oxygenated products (oxyPAHs) (Mallakin et al. 1999). This often results in increased water solubility and toxicity compared to that of their parent PAH (Huang et al. 1995, McConkey et al. 1997, Diamond et al. 2000, Lampi et al. 2005).

The presence and toxicity of oxyPAHs in the environment has recently come to be recognized as a cause for concern (Health Canada 1999). Many studies have found that the prevalence of these compounds is increasing, possibly due to photomodification of the parent PAHs. A study by Mallakin et al. (1999) demonstrated that anthracene when exposed to sunlight degrades rapidly into its photoproducts in the presence of actinic radiation. These photoproducts include ATQ, 1-hATQ, 1,2-hATQ and many more. Recently it has been clear that oxyPAHs are present in environment where PAHs are found (CEPA 1999, McKinney et al. 1999, Barbosa et al. 2004, Kurihara et al. 2005). The apparent increase in oxyPAH concentrations is likely in part due to the fact that scientists are now aware of them and have developed new methods for detecting them. This is a cause for concern as many of these compounds are unregulated (Kurihara et al. 2005).

Despite the known sensitivity of *Hyalella azteca* to PAHs and the prevalence of PAHs in the environment, very little toxicity data is available on PAHs or oxyPAHs. In particular, no data is available on the toxicity of the oxygenated PAHs to *Hyalella azteca*, exposed to actinic radiation. In the present study the toxicities of 15 PAHs and oxyPAHs were assayed under 4 different irradiation sources; Dark (no light), Photosynthetically Active Radiation (PAR) light (400-700nm), PAR/UV-A light (320-700nm) and Simulated Solar Radiation (SSR) light (290-700nm). In addition, the oxyPAHs chosen have all been shown to be photomodification products of the parent PAHs used in the study (ANT, PHE, BAA) (Huang et al 1995, Mallakin et al 1999). This chapter aims to address the gaps in the current data sets to further our understanding of PAH phototoxicity.

2.1 Materials and Methods

2.1.1 Test Organism

A stock culture of *Hyalella azteca* was obtained from Warren Norwood and Uwe Borgmann at the Canada Centre for Inland Waters (CCIW). This culture was maintained in mixed age cultures following the guidelines published by the USEPA for static cultures (USEPA 2000). Cultures used for experimentation were optimized for breeding. To create these cultures, paired (mating) adults were separated from the stock cultures and placed into breeding tanks, 1L in volume consisting of 30 pairs. The breeding cultures were harvested after 7 days and the juveniles separated manually by visual identification based on size, and placed into a holding tank. After 7 days these immature *Hyalella azteca* were used in the treatments. The culture water used consisted of Waterloo, Ontario, Canada well water, diluted 1:1 with reverse-osmosis-purified water, and the water was changed once every 7 days. The cultures were fed twice per week with 5 mg TetraMin® Flakes (TetraMelle, Germany). The stock tanks were maintained at 22°C ± 1ºC, and the breeding tanks were maintained at 27°C ± 1ºC the optimal breeding temperature, for *Hyalella azteca* (Kruschwitz et al. 1978). The animals were cultured using a 16:8 light:dark photoperiod under cool white fluorescent light. The water hardness was maintained at 240 mg/L $CaCO_3$ and the pH was kept constant at 7.4. This culture was found to have average sensitivity to several common contaminants similar to those found in other published studies (Verrhiest et al. 2001, Schuler et al. 2003, Borgmann et al. 2005).

2.1.2 96h PAH Phototoxicity Assay

The assays were performed to determine the EC50 values for juvenile (7-14 day old) *Hyalella* according to the USEPA standard method (USEPA 2000). Fifteen PAHs were assayed to determine their toxicity to *Hyalella azteca* under varying lighting sources (Figure 2.1). These PAHs were purchased from a Fisher Scientific (Ottawa, Canada) and Sigma-Aldrich (Oakville, Canada) and were of the highest purity available (Table 2.1). Since most PAHs have limited water solubility; dimyethylsulfoxide (DMSO; Fisher Scientific, Nepean, ON, Canada) was used as a carrier solution to add stock solutions of the PAH to the test containers. The stock solutions were prepared in molecular biology grade DMSO to a concentration of 1 mg/L. These stock solutions were serially diluted to the relevant testing concentrations. Each assay was performed using one of seven different concentrations of a given PAH and a positive control consisting of DMSO in water at a concentration of 0.1 % (v/v). Thus the level of DMSO used had no impact on the test organisms and was used in the controls. In all cases the concentration of DMSO never exceeded 0.1% of the final volume of the experiment compartments. To ensure constant concentrations of PAH, the test solution was statically renewed after 48 hours. During the toxicity assay, the photoperiod was maintained on a 16:8 hour light:dark cycle for each of the lighting regimes described below. After 96 hours, mobility was assessed by gentle prodding, and immobility was considered to be mortality. Each test was performed with 10 *Hyalella azteca* in 200 mL of PAH test solution. Each treatment was completed in triplicate on 3 separate days. During the assay the animals were not fed, which had minimal impact on the organisms (Strong 1972). Water loss due to evaporation was approximately 10 mL/week, but the loss was considered negligible due

Table 2.1 Purities of PAHs in *Hyalella azteca* Assay

PAH			
Compound	**Purity (%)**	**Compound**	**Purity (%)**
ANT	99	**1,2,4-thATQ**	90
ATQ	99	**1,2,5,8-thATQ**	93
1-hATQ	97	**1,2,10-thANT**	91
2-hATQ	96	**BAA**	99
1,2-dhATQ	98	**BaQ**	96
1,3-dhATQ	98	**PHE**	96
1,4-dhATQ	96	**PHQ**	96
1,8-dhATQ	98		

Acronyms for PAHs: ANT = Anthracene; ATQ = Anthraquinone; 1-hATQ = 1-hydroxyanthraquinone; 2-hATQ = 2-hydroxyanthraquinone; 1,2-dhATQ = 1,2-dihydroxyanthraquinone; 1,3-dhATQ = 1,3-dihydroxyanthraquinone; 1,4-dhATQ = 1,4-dihydroxyanthraquinone; 1,8-dhATQ = 1,8-dihydroxyanthraquinone; 1,2,4-thATQ = 1,2,4-trihydroxyanthraquinone; 1,2,10-thANT = 1,2,10-trihydroxyanthracene; 1,2,5,8-thATQ = 1,2,5,8-tetrahydroxyanthraquinone; BAA = Benz[a]anthracene; BaQ = Benz[a]anthraquinone; PHE = Phenanthrene; PHQ = Phenanthraquinone.

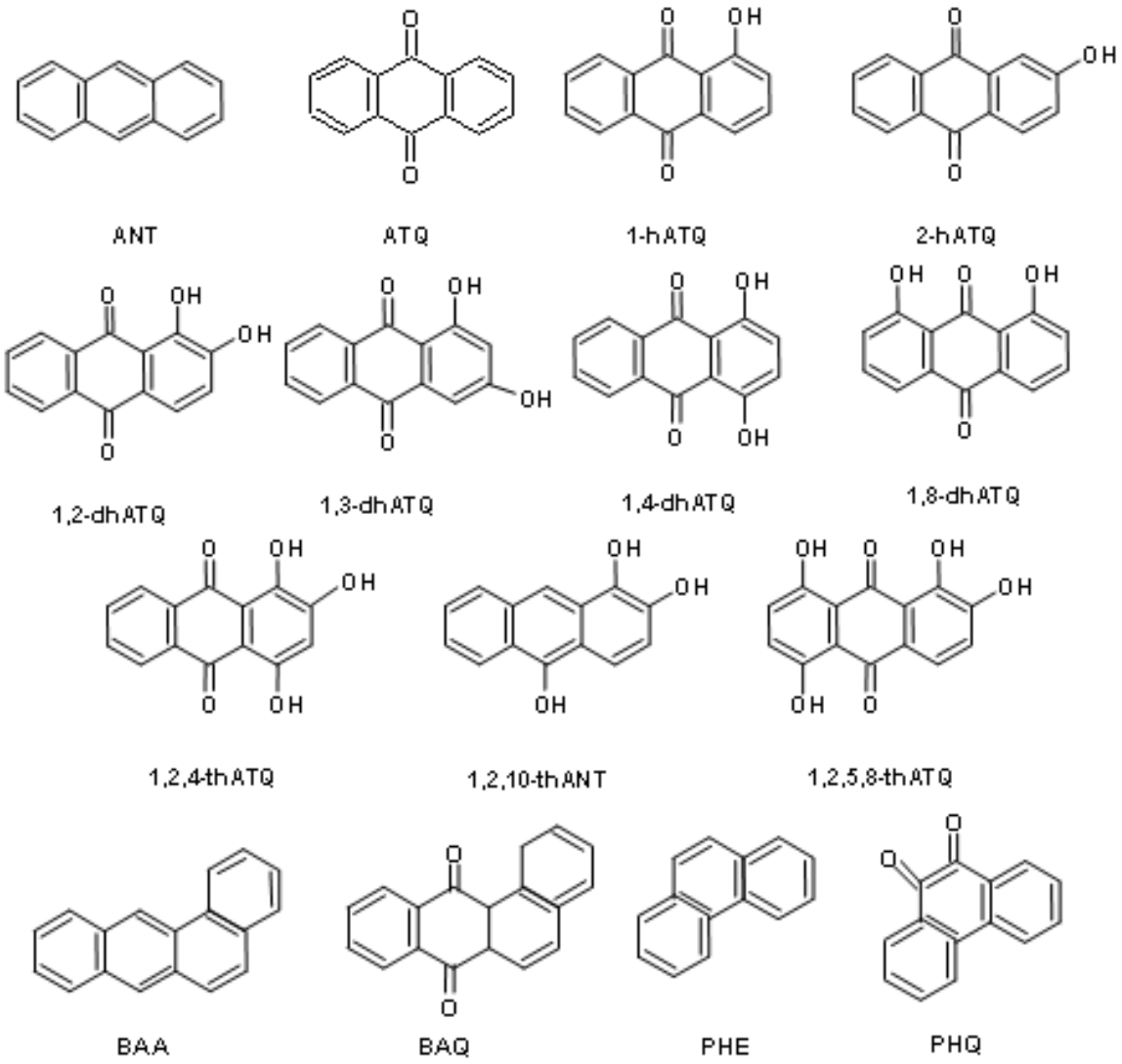

Figure 2.1 Structures of PAHs and photomodified PAHs used in this study.
ANT, anthracene; ATQ, anthraquinone; 1-hATQ, 1-hydroxy-anthraquinone; 2-hATQ, 2-hydroxy-anthraquinone; 1,2-dhATQ, 1,2-dihydroxy-anthraquinone; 1,3-dhATQ, 1,3-dihydroxy-anthraquinone; 1,4-dhATQ, 1,4-dihydroxy-anthraquinone; 1,8-dhATQ, 1,8-dihydroxy-anthraquinone; 1,2,4-thATQ, 1,2,4-trihydroxy-anthraquinone; 1,2,10-thANT, 1,2,10-trihydroxy-anthracene; 1,2,5,8-tetra-hydroxy-anthraquinone; BAA, benzo(a)anthracene; BaQ, benzanthraquinone; PHE, phenanthrene; PHQ, phenanthrenequinone.

to the static renewal of the water every 48 hours and the limited duration of the experiment (96 hours).

2.1.3 Radiation Sources

The irradiation sources for the toxicity assays consisted of three distinct lighting regimes and a dark treatment. The first experimental condition consisted of only photosynthetically active radiation (PAR) (400-700nm) (PAR, 56 $\mu mol \bullet m^{-2} \bullet s^{-1}$), provided by cool white fluorescent lamps (CWF)(Southern New England Ultraviolet Co., Branford, USA). The second lighting regime consisted of PAR light + UV-A light (320-700nm) (PAR:UVA, 56:4.6 $\mu mol \bullet m^{-2} \bullet s^{-1}$). The PAR light was provided by CWF lamps, while an RPR-3500 (UV-A lamps) was used to provide the UV-A light (Southern New England Ultraviolet Co., Branford, USA). The third lighting system was a full spectrum of simulated solar radiation (SSR) (290-700nm) (PAR:UVA:UVB, 60:4.6:0.46 $\mu mol \bullet m^{-2} \bullet s^{-1}$), which consists of PAR, UV-A, and UV-B. To produce the SSR, cool white fluorescent lamps, an RPR-3500 (UV-A lamps) and RPR-3000 (UV-B lamps) (Southern New England Ultraviolet Co., Branford, USA) were used to produce the full spectrum of visible/UV-A/UV-B. Due to the fact that RPR-3000 lamps produce some UV-C light which will on its own kill most amphipods, three layers of cellulose diacetate (0.08mm) were used to screen out wavelengths of light <290 nM (UV-C light) (Lampi et al. 2006).

2.1.4 Data Analysis

Survival data as a function of chemical concentration, from each assay were used to determine the EC50s of each compound. The data were first transformed using equation 1. This enables us to include zero values when calculating the EC50s.

Equation 1

$$\text{Survival} = \frac{m + 0.5}{n + 1}$$

Where *m* is the number of surviving juveniles in a given replicate and n is the total number of juveniles present at the start of the assay. The survival data were then fit into a logistic regression model, (Equation 2) adapted from Stephenson et al. (2000).

Equation 2

$$\text{Survival} = \frac{1}{1 + \left[\left(\frac{0.5}{0.5}\right) \cdot \left(\frac{x}{\mu}\right)^{b}\right]}$$

Where x is the log of the PAH concentration, μ is the log of the EC50, and b is a measure of the concentration response curves slope. To solve for the EC50 and the slope, a regression with the nonlinear function of Systat 10 (Systat Software, Point Richmond, CA, USA) was used. The concentration response curves themselves were generated by inserting these values into equation 2. The average of the generated EC50s and standard deviations were then obtained.

2.2 Results

A 96 h acute assay was performed to determine the toxicities of 15 PAHs and oxyPAHs under 4 different lighting regimes. These EC50s were determined from concentration response curves based on mortality data from each of the chemicals shown in table 2.2. Most of the PAHs increased in toxicity as the lighting conditions were

Table 2.2 Toxicity of 15 PAHs to *Hyalella azteca* under Dark, PAR, PAR/UV-A and Simulated Solar Radiation (SSR).

	EC50			
PAH	**Dark (*nM*) ± SD**	**PAR (*nM*) ± SD**	**PAR + UV-A (*nM*) ± SD**	**SSR (*nM*) ± SD**
ANT	4902 ± 169	108 ± 19.7	164 ± 32.7	4.87 ± 0.36
ATQ	1624 ± 192	188 ± 48.4	156 ± 45.9	142 ± 38.9
1-hATQ	NT	332 ± 68.4	378 ± 117	24.4 ± 1.43
2-hATQ	NT	641 ± 77.9	501 ± 90.6	21.7 ± 3.93
1,2-dhATQ	6645 ± 1629	860 ± 170	479 ± 147	54.1 ± 21.1
1,3-dhATQ	6824 ± 1171	1008 ± 156	680 ± 99.7	49.5 ± 10.2
1,4-dhATQ	1089 ± 342	989 ± 205	457 ± 63.7	6.19 ± 1.39
1,8-dhATQ	910 ± 150	923 ± 182	397 ± 71.6	28.1 ± 7.48
1,2,4-thATQ	5034 ± 645	1295 ± 204	540 ± 42.1	73.1 ± 18.8
1,2,5,8-thATQ	NT	422 ± 48.9	364 ± 90.1	31.5 ± 6.14
1,2,10-thANT	NT	4890 ± 398	894 ± 59.6	40.1 ± 3.83
BAA	2404 ± 277	567 ± 89.3	129 ± 34.7	10.9 ± 3.64
BaQ	1387 ± 283	534 ± 98.4	103 ± 41.2	5.82 ± 2.54
PHE	3167 ± 232	444 ± 111	106 ± 38.9	12.2 ± 0.77
PHQ	2078 ± 388	524 ± 94.8	322 ± 1009	5.89 ± 1.06

Each experiment was repeated independently at least 3 times.
*** NT = Non Toxic at levels below maximum solubility of 8000 nM**

changed from dark to SSR. The greatest change in toxicity was more often than not in the PAR/UV-A to the SSR. The exception to this trend was ATQ which showed no statistical change in toxicity across PAR, PAR/UV-A and SSR treatments.

The concentration response curves for the dark treatments, showed a four fold difference in toxicity of each of the PAHs to *Hyalella azteca* (Fig 2.2-2.15). The most toxic PAH in the dark treatment was 1,8-dhATQ with an EC50 910 nM. Several of the PAHs (1-hATQ, 2-hATQ, 1,2,5,8-thATQ, 1,2,10-thANT) showed no acute toxicity under the dark treatment and were non-toxic at levels below maximum solubility of 8000 nM. The slopes of the concentration response curves, in the dark treatments generally differed from PAH to PAH. The parent quinones (ATQ, BAQ, PHQ) all had similar slopes and EC50 values that were similar in magnitude. The dihydroxyanthraquinones (1,2-dhATQ, 1,3-dhATQ, 1,4-dhATQ, 1,8-dhATQ) had slopes that were very similar to each other, however their EC50s varied over 3 orders of magnitude. The slopes of the dihydroxyanthraquinones differed from those of the parent compounds; with the slopes of the parent PAHs being much shallower than those of the dihydroxylated quinones. The concentration response curve for ANT in the dark treatment differed from the other PAHs being much shallower (Fig. 2.2). The slope of 1,2,4-thATQ was found to be the steepest of the dark concentration response curves (Fig. 2.10).

The results of the PAR treatment showed varying EC50s across 3 orders of magnitude (Table 2.2). The PAHs under the PAR treatment were all found to be much more toxic than in the dark treatment, increasing in toxicity by 4-50 fold. The most toxic of the PAH to *Hyalella azteca* under PAR lighting was ANT, with an EC50 of 108.3 nM. The least toxic PAH was found to be 1,2,10-thANT with an EC50 of 4890 nM. All of the

parent PAHs (ANT, BAA, PHE) had very similar EC50s to their primary photoproducts (ATQ, BAQ, PHQ). One of the primary photoproducts of ATQ (1,2-dhATQ) was found to be 4 fold less toxic than that of ATQ under PAR lighting.

The concentration response curves for the PAR treatments showed differing slopes between many of the PAHs. ANT, had a shallowest slope that mirrored that of ATQ, except ATQ was much less toxic than ANT. 1-hATQ (Fig. 2.4), 2-hATQ (Fig. 2.5) and 1,2,5,8-thATQ (Fig. 2.11) showed similar slopes. The dihydroxy-anthraquinones (1,2-dhATQ, 1,3-dhATQ, 1,4-dhATQ,1,8-dhATQ) all shared similar slopes. 1,2,10-thANT was found to have the steepest slope of the PAR treatments, and was not similar to any of the other PAHs.

The PAR/UV-A treatment showed a wide range of EC50s, which varied over 2 orders of magnitude. Almost all of the PAHs increased in toxicity over the PAR treatments and were generally 2-5 fold more toxic. The PAH with the lowest EC50 in the PAR/UVA treatment was BAQ with an EC50 of 103 nM, followed closely by PHE with an EC50 of 106 nM. The least toxic PAH of the PAR/UV-A treatments was 1,2,10-thANT, with an EC50 of 894 nM. 1,2,10-thANT increased in toxicity from the PAR treatment by 10 fold but was still the least toxic of the PAR/UV-A treatments. All of the hydroxylated anthraquinones (1-hATQ, 2-hATQ, 1,2-dhATQ, 1,4-dhATQ,1,8-dhATQ, 1,2,4-thATQ, and 1,2,5,8-thATQ) with the exception of 1,3-dhATQ had EC50s that were very close in magnitude between 364 nM and 540 nM. The EC50 of 1,3-dhATQ was 680 nM which was not statistically similar enough to group it with the other hydroxyanthraquinones (Fig. 2.7).

The PAR/UV-A treatments showed a wide range of slopes for the different PAHs. The shallowest slope in the PAR/UV-A treatment was ATQ. The mono hydroxylated anthraquinones (1-hATQ, 2-hATQ) had slopes that were very similar, but slightly steeper than that of ATQ. 1,2-dhATQ showed a unique slope that did not closely resemble any of the other PAHs. The PAH in the PAR/UV-A treatment with the steepest slope was PHQ, however the slopes of BAA, PHE, and BAQ were very similar albeit slightly shallower to that of PHQ.

Under the SSR treatment the EC50s increased over that of the PAR/UV-A treatments. They generally increased by a factor of 5-50, the exception being ATQ which showed no statistical change in toxicity from the PAR/UV-A treatment, with an EC50 of 156 nM (PAR/UV-A) and an EC50 of 142 nM (SSR). The most toxic compound under SSR was found to be ANT with an EC50 of 4.87 nM. The other parent PAHs (BAA, PHE) were also found to be very toxic with EC50s of 10.9 nM and 12.2 nM respectively. ATQ was found to be the least toxic of the PAHs under SSR with an EC50 of 142 nM. 1,2-dhATQ an extensively studied PAH was found to be only moderately toxic under SSR, with an EC50 of 54.

The slopes of the SSR treatment concentration response curves were generally much steeper than those of the other radiation treatments. ANT was found to have the steepest slope in the SSR treatment. PHE and PHQ were found to have slopes that were slightly shallower than that of ANT but were similar enough that they might be sharing the same mechanism of toxicity. ATQ was found to have the shallowest slope in the SSR treatment. ATQ was also found to have a very similar slope in the SSR treatment to that of the PAR/UV-A treatment. The monohydroxylated ATQs (1-hATQ, 2-hATQ) had

very similar slopes to each other. These slopes closely matched those of 1-hATQ and 2-hATQ in the PAR/UV-A treatments.

The concentration response curves for ANT across all lighting regimes showed a 1000 fold change in concentration from dark regimes to the SSR regimes (Fig 2.2). The ANT concentration response curves also showed very different slopes across the four lighting conditions. The EC50s varied from the 4902 nM in the dark to an EC50 of 4.87 under SSR.

The EC50s for ATQ showed a tenfold change in toxicity from the dark to the PAR treatment. However, the ATQ EC50s for the PAR, PAR/UV-A and SSR treatment were not statistically different, at 188, 156 and 142 nM respectively. The dark treatment produced an EC50 of 1625 nM. Interestingly the slopes of all of the ATQ concentration response curves were very similar across all four of the lighting regimes.

The concentration response curves for both 2-hATQ and 1-hATQ were very similar across all of the lighting regimes. The EC50s for 1-hATQ ranged from greater than maximum solubility (8000 nM) under dark conditions to 24.4 nM under SSR conditions. When exposed to PAR lighting, 1-hATQ increased in toxicity by 10 fold over that of the dark treatment to 332 nM. The addition of UV-A light did not have an impact on the toxicity of 1-hATQ. The EC50 for the 1-hATQ PAR/UV-A treatment was 378 nM, which was not found to be statistically different from that of the PAR only treatment. 2-hATQ was found to be remarkably similar to 1-hATQ with the PAR and PAR/UV-A treatments having EC50s that were not statistically different.

1,2-dhATQ, 1,3-dhATQ, and 1,2,4-thATQ, were all found to have similar EC50s across all 4 of the lighting regimes. The EC50s of the dark treatment were similar for the

3 PAHs and were not statistically different at 6646 nM (1,2-dhATQ), 6825 nM (1,3-dhATQ) and 5034 nM (1,2,4-thATQ). The EC50s for the PAR and PAR/UV-A treatments were similar but statistically different. However the SSR treatments EC50s were not statistically different from each other for 1,2-dhATQ, 1,3-dhATQ and 1,2,4-thATQ. The slopes of 1,2-dhATQ, 1,3-dhATQ and 1,2,4-thATQ were also very similar to each other across all four of the lighting regimes, with the exception of 1,2,4-thATQ under the dark treatment which the steepest slope of any of the 15 PAHs tested.

The EC50s for 1,4-dhATQ and 1,8-dhATQ showed similar trends across all 4 of the lighting regimes. The EC50s for 1,4-dhATQ and 1,8-dhATQ in the dark, PAR and PAR/UV-A treatments were not statistically different from each other across each of the 3 treatments. However, the EC50s for each of the treatment showed an increase in toxicity from dark (Low toxicity) to PAR/UV-A (High toxicity). The EC50s for the SSR treatment were statistically different from each other, with 1,4-dhATQ having a EC50 of 6.19 nM and 1,8-dhATQ having a EC50 of 28.1 nM. The slopes of the concentration response curves for the dark, PAR, PAR/ UV-A and SSR treatments were very similar for 1,4-dhATQ and 1,8-dhATQ. The slopes of the dark and the PAR treatments of both compounds were both unique, and did not match the slopes of the other treatments. The PAR/UV-A and the SSR treatments for both compounds, had slopes that were very similar.

BAA was found to be less toxic than its primary photoproduct BAQ in the dark treatment, with EC50s of 2404 nM and 1388 nM respectively. The EC50s for the two compounds decreased as the amount of actinic radiation increased. Both compounds had comparable EC50s across the PAR, PAR/UV-A and SSR treatments and were found not

to be statistically different. The slopes of BAA varied across all four of the lighting regimes. BAQ had slopes in each of the 4 lighting regimes that mirrored BAA almost perfectly, with the exception being BAQ under SSR which had a much steeper slope than BAA.

The EC50 for PHE was found to be 50% less toxic in the dark than its primary photoproduct PHQ, with EC50s of 3167 nM and 2078 nM respectively. The EC50s of the PAR treatments for PHE (444 nM) and PHQ (524 nM) were found to be statistically the same. The PAR/UV-A and SSR treatments for both compounds were found to be different from each other (PHE > PHQ in PAR+ UV-A, PHE < PHQ SSR). The concentration response curves for both PHE and PHQ were found to be very similar in the dark and PAR treatments. Under the PAR/UV-A and SSR treatments however, PHE was found to have a much steeper slope compared to that of PHQ.

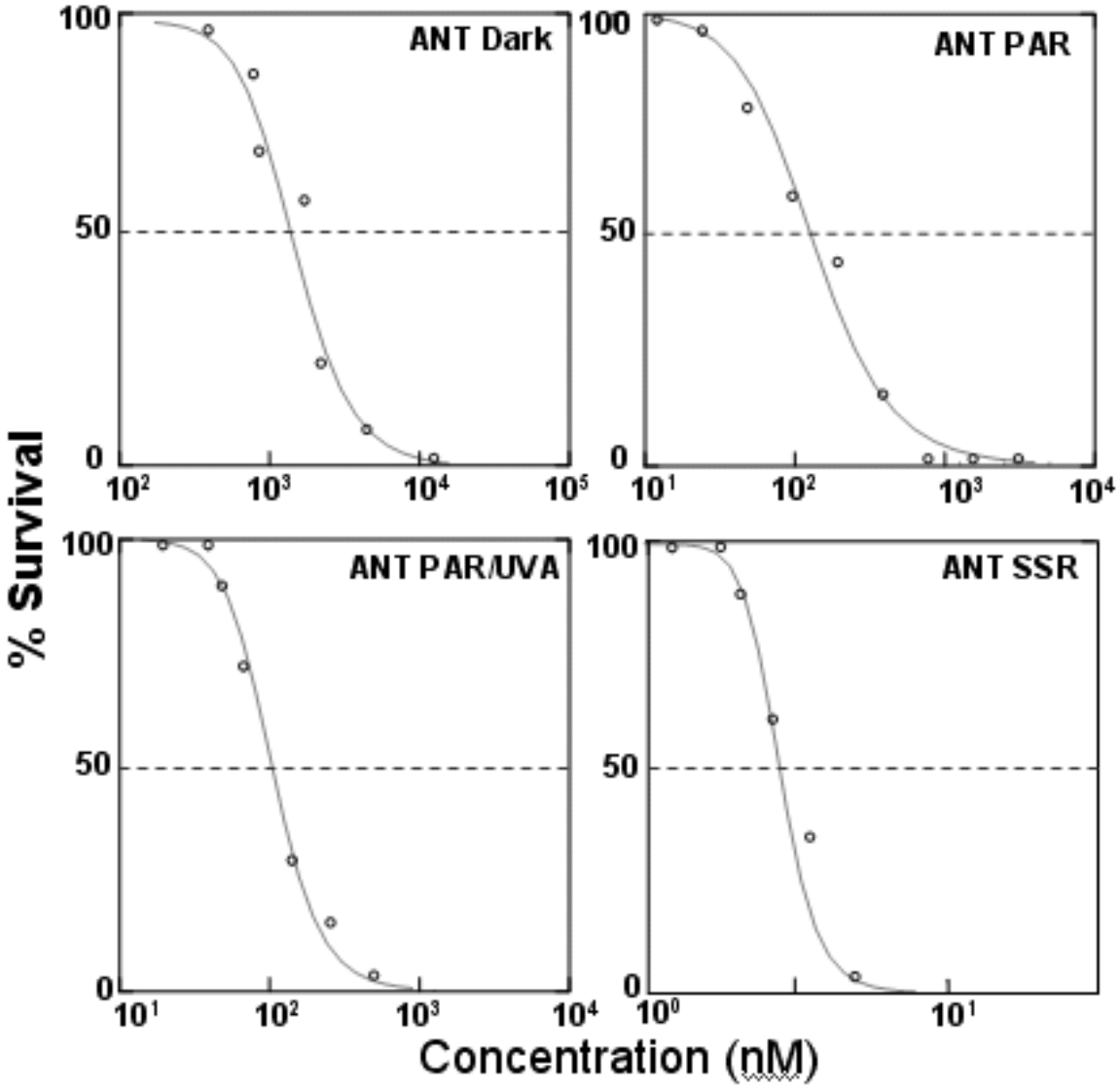

Figure 2.2 Concentration response curves for anthracene (ANT) to *Hyalella azteca* under four lighting conditions. Photosynthetically Active Radiation (PAR, 400-700 nm), Ultraviolet Radiation A (UV-A, 320-400 nm), Ultraviolet Radiation B (UV-B, 290-320 nm).

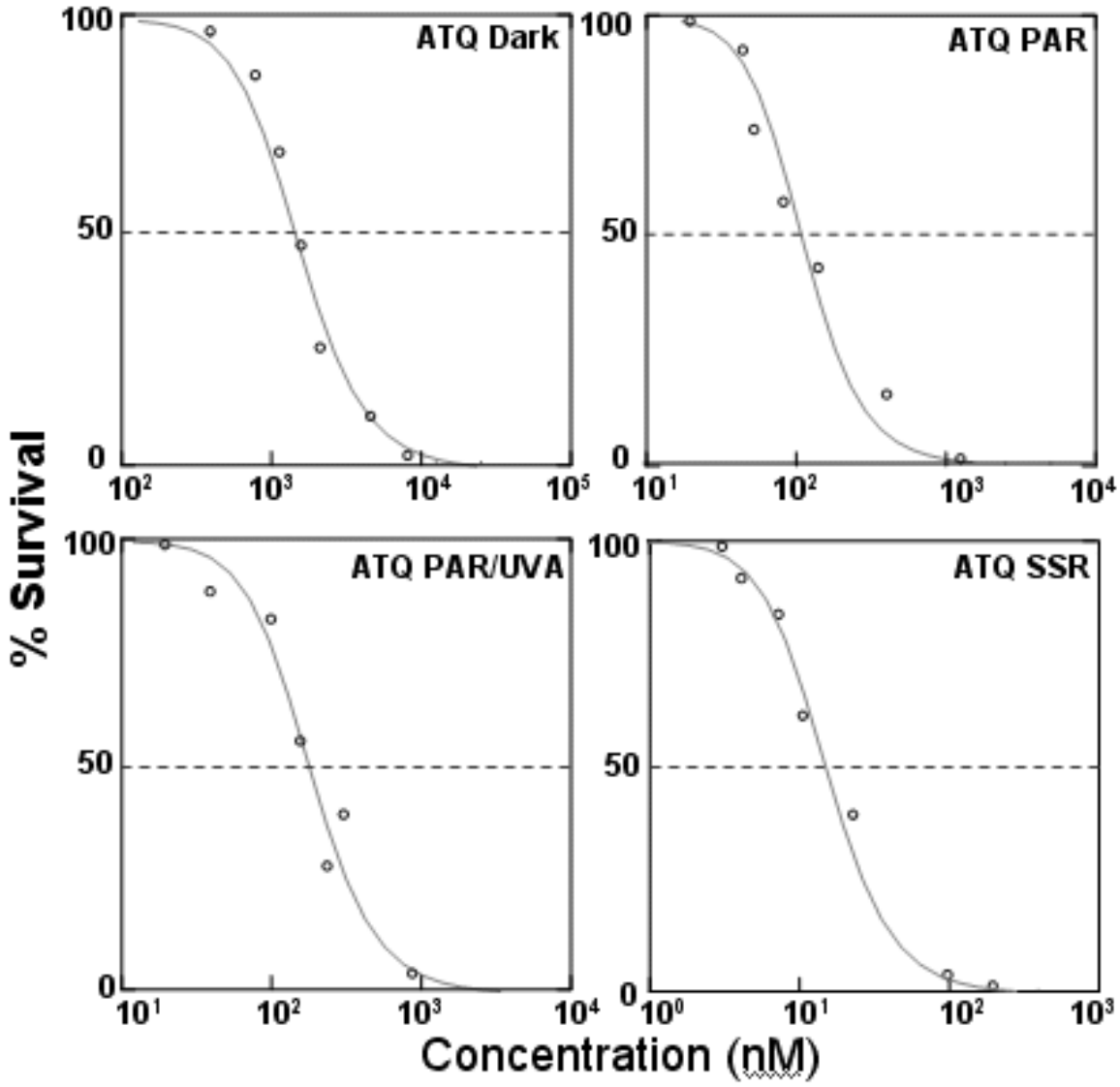

Figure 2. Concentration response curves for anthraquinone (ATQ) to *Hyalella azteca* four three lighting conditions. Photosynthetically Active Radiation (PAR, 400-700 nm), Ultraviolet Radiation A (UV-A, 320-400 nm), Ultraviolet Radiation B (UV-B, 290-320 nm).

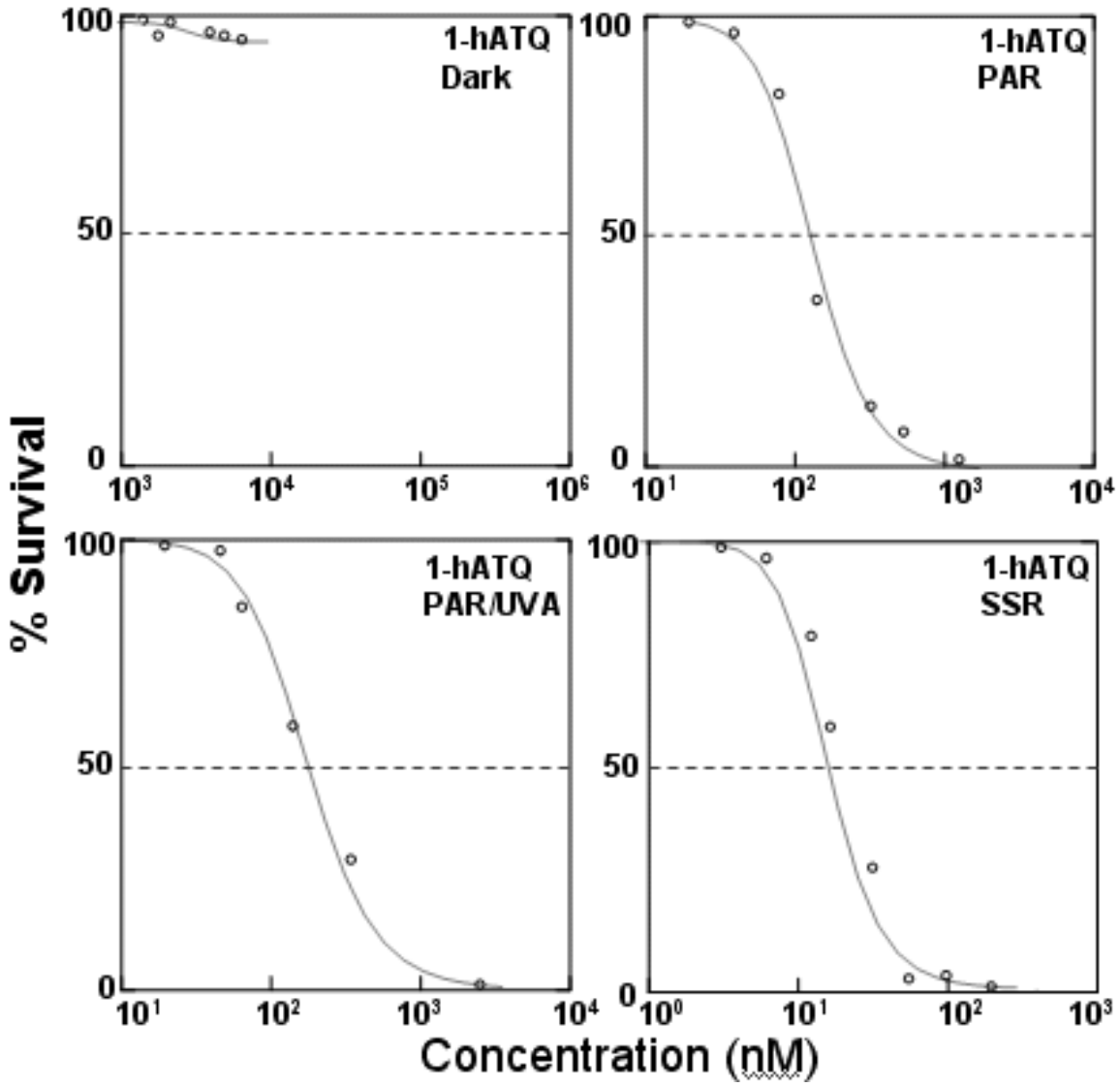

Figure 2.4 Concentration response curves for 1-hydroxyanthraquinone (1-hATQ) to *Hyalella azteca* under four lighting conditions. Photosynthetically Active Radiation (PAR, 400-700 nm), Ultraviolet Radiation A (UV-A, 320-400 nm), Ultraviolet Radiation B (UV-B, 290-320 nm).

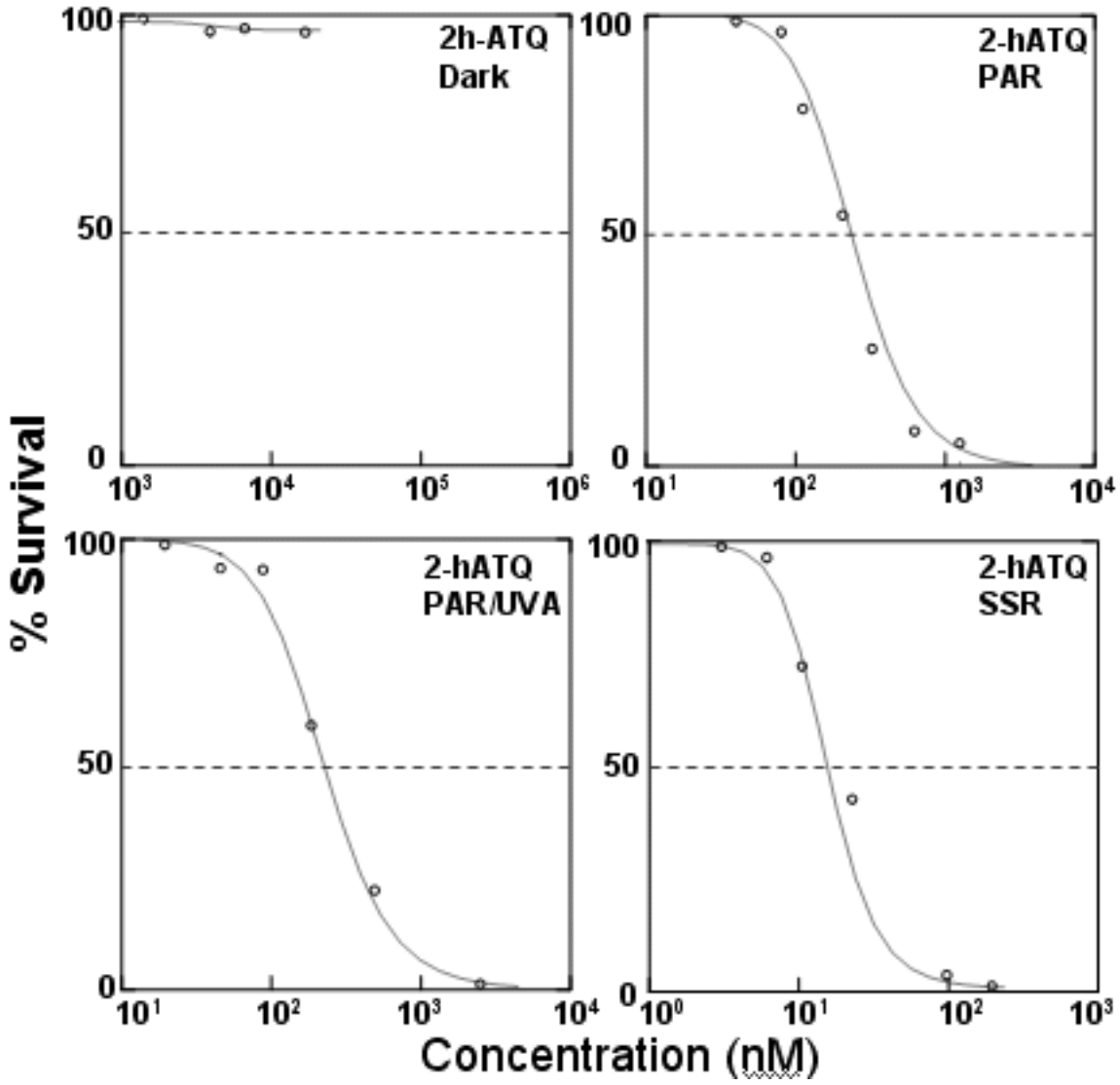

Figure 2.5 Concentration response curves for 2-hydroxyanthraquinone (2-hATQ) to *Hyalella azteca* under four lighting conditions. Photosynthetically Active Radiation (PAR, 400-700 nm), Ultraviolet Radiation A (UV-A, 320-400 nm), Ultraviolet Radiation B (UV-B, 290-320 nm).

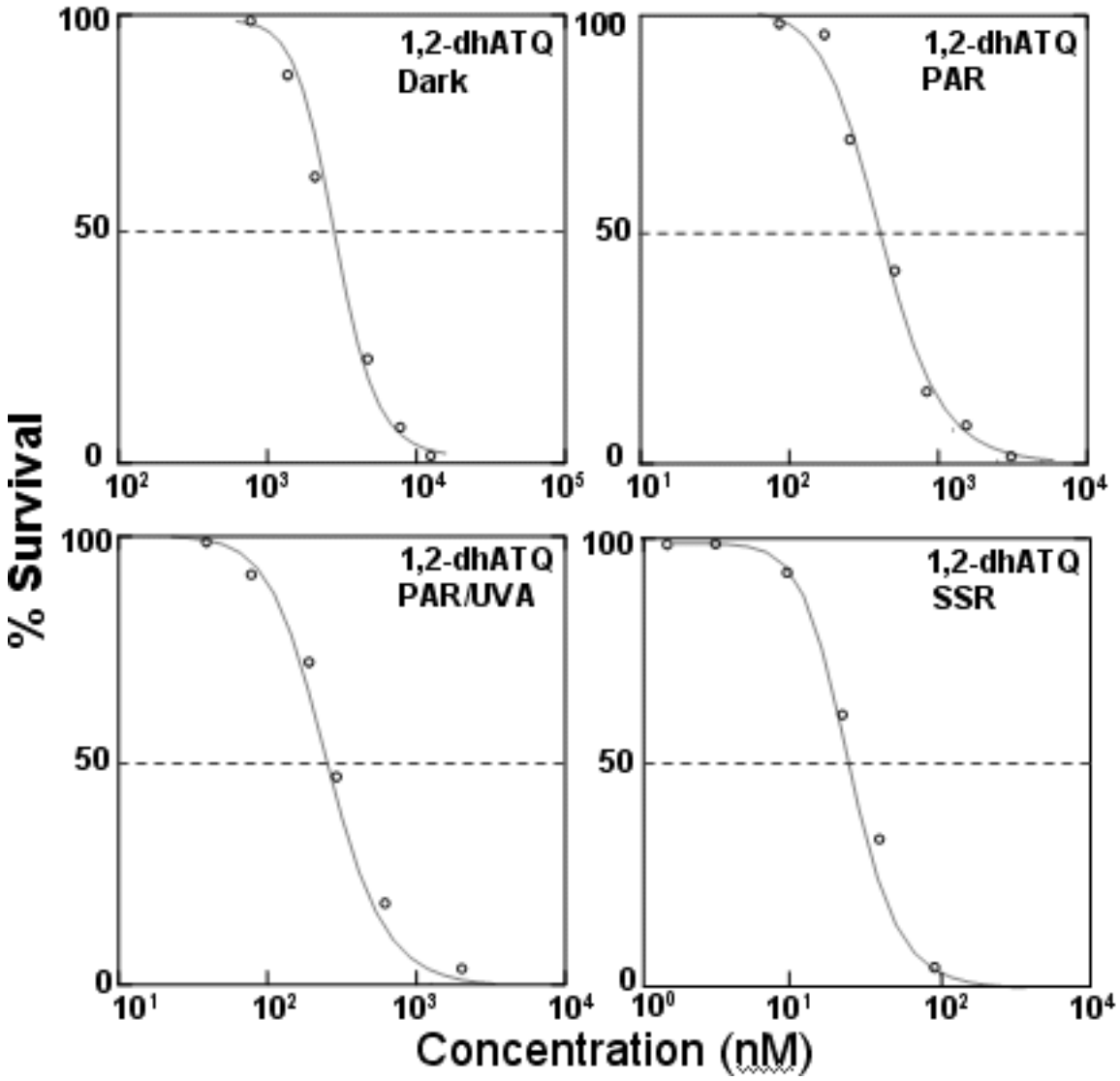

Figure 2.6 Concentration response curves for 1,2-dihydroxyanthraquinone (1,2-dhATQ) to *Hyalella azteca* under four lighting conditions. Photosynthetically Active Radiation (PAR, 400-700 nm), Ultraviolet Radiation A (UV-A, 320-400 nm), Ultraviolet Radiation B (UV-B, 290-320 nm).

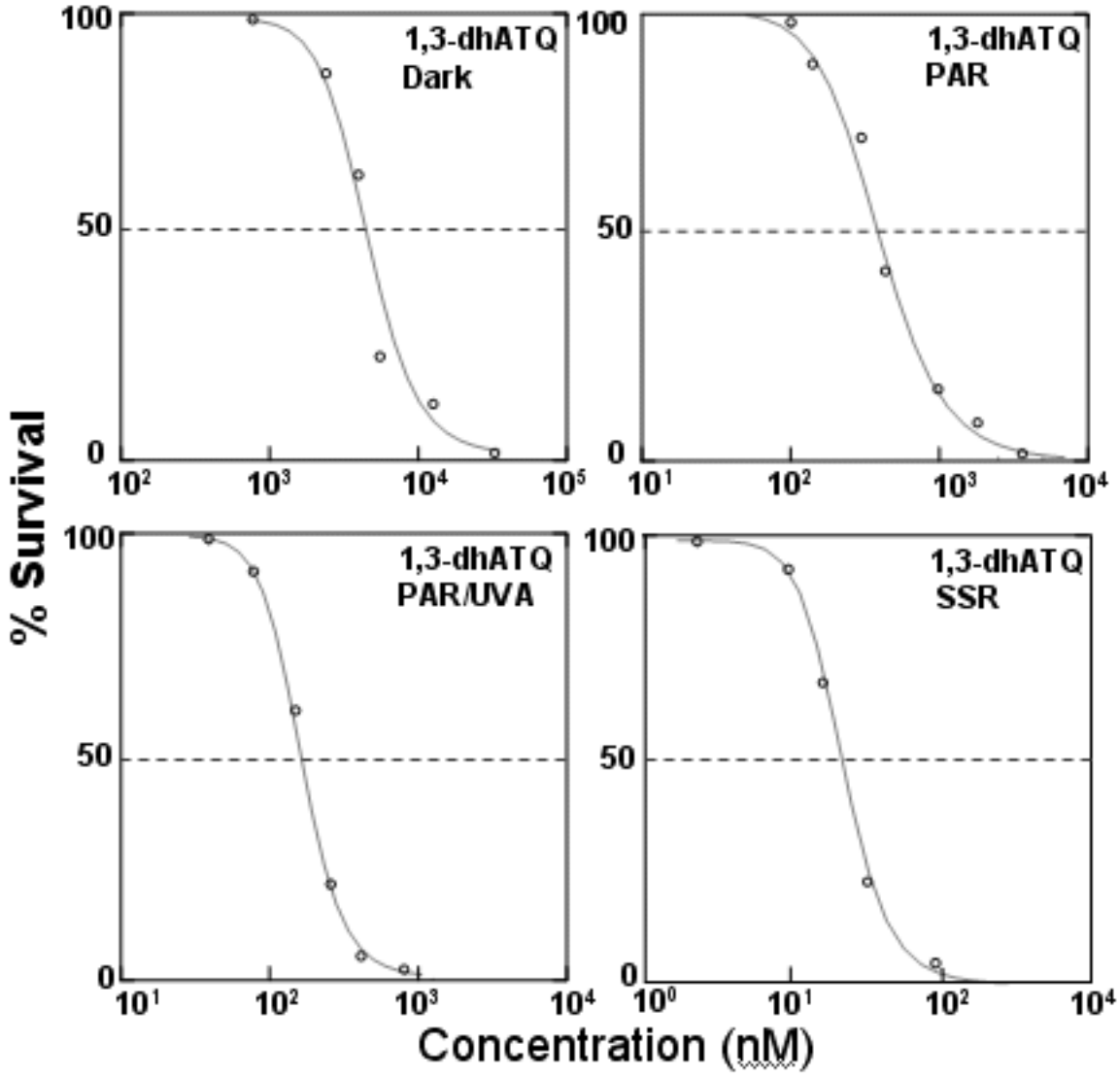

Figure 2.7 Concentration response curves for 1,3-dihydroxyanthraquinone (1,3-dhATQ) to *Hyalella azteca* under four lighting conditions. Photosynthetically Active Radiation (PAR, 400-700 nm), Ultraviolet Radiation A (UV-A, 320-400 nm), Ultraviolet Radiation B (UV-B, 290-320 nm).

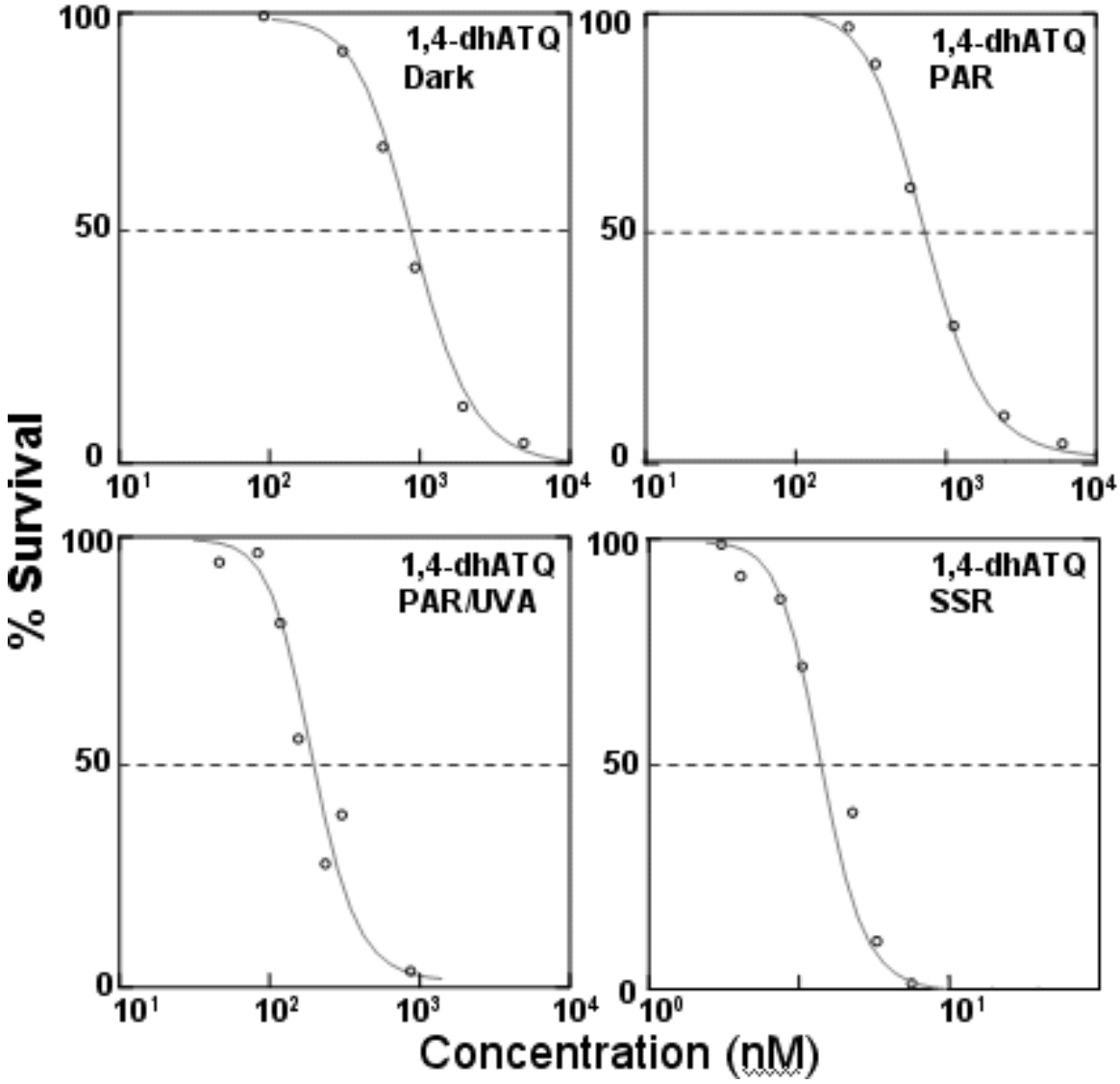

Figure 2.8 Concentration response curves for 1,4-dihydroxyanthraquinone (1,4-dhATQ) to *Hyalella azteca* under four lighting conditions. Photosynthetically Active Radiation (PAR, 400-700 nm), Ultraviolet Radiation A (UV-A, 320-400 nm), Ultraviolet Radiation B (UV-B, 290-320 nm).

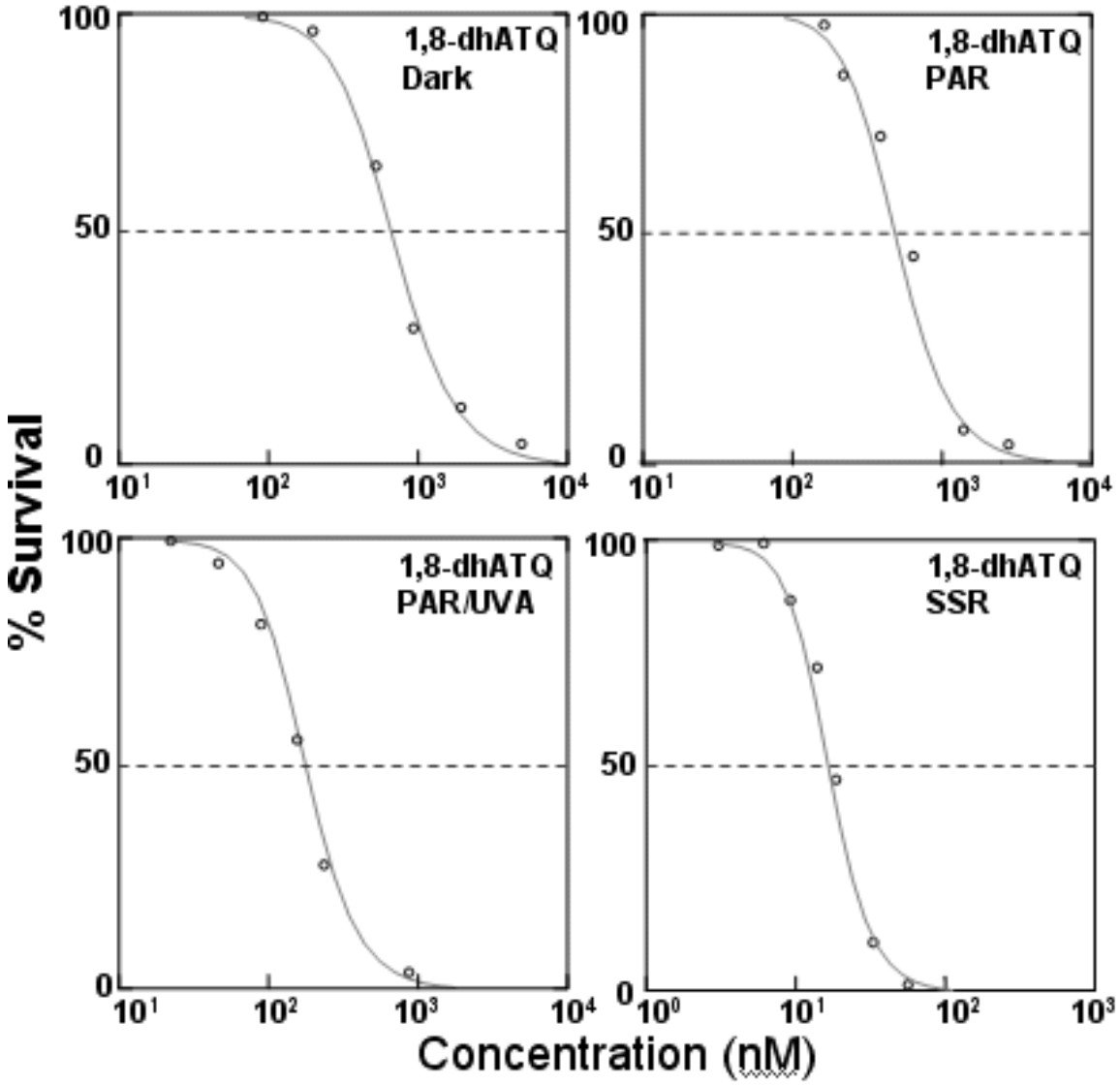

Figure 2.9 Concentration response curves for 1,8-dihydroxyanthraquinone (1,8-dhATQ) to *Hyalella azteca* under four lighting conditions. Photosynthetically Active Radiation (PAR, 400-700 nm), Ultraviolet Radiation A (UV-A, 320-400 nm), Ultraviolet Radiation B (UV-B, 290-320 nm).

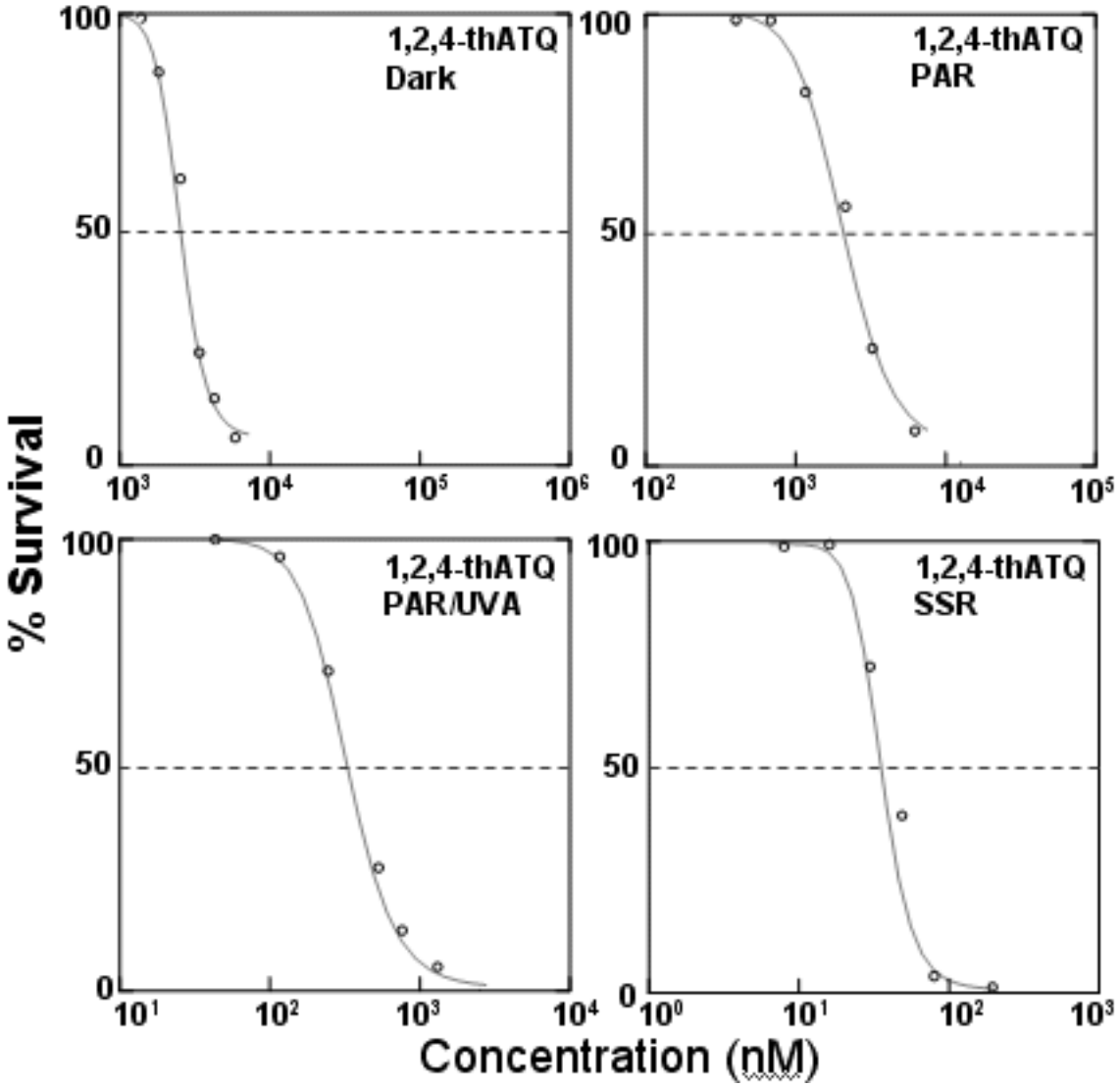

Figure 2.10 Concentration response curves for 1,2,4-trihydroxyanthraquinone (1,2,4-thATQ) to *Hyalella azteca* under four lighting conditions. Photosynthetically Active Radiation (PAR, 400-700 nm), Ultraviolet Radiation A (UV-A, 320-400 nm), Ultraviolet Radiation B (UV-B, 290-320 nm).

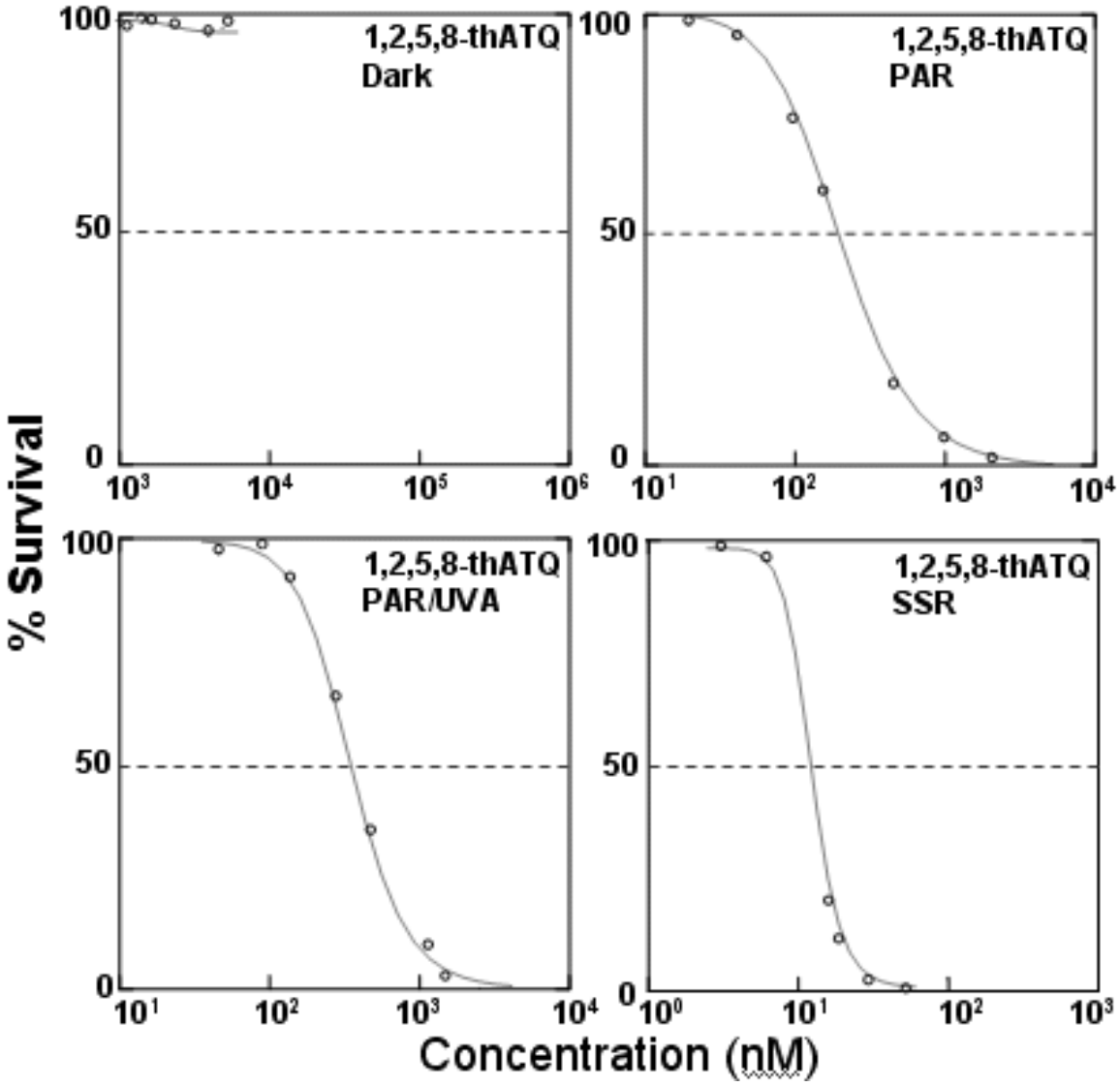

Figure 2.11 Concentration response curves for 1,2,5,8-tetrahydroxyanthraquinone (1,2,5,8-thATQ) to *Hyalella azteca* under four lighting conditions. Photosynthetically Active Radiation (PAR, 400-700 nm), Ultraviolet Radiation A (UV-A, 320-400 nm), Ultraviolet Radiation B (UV-B, 290-320 nm).

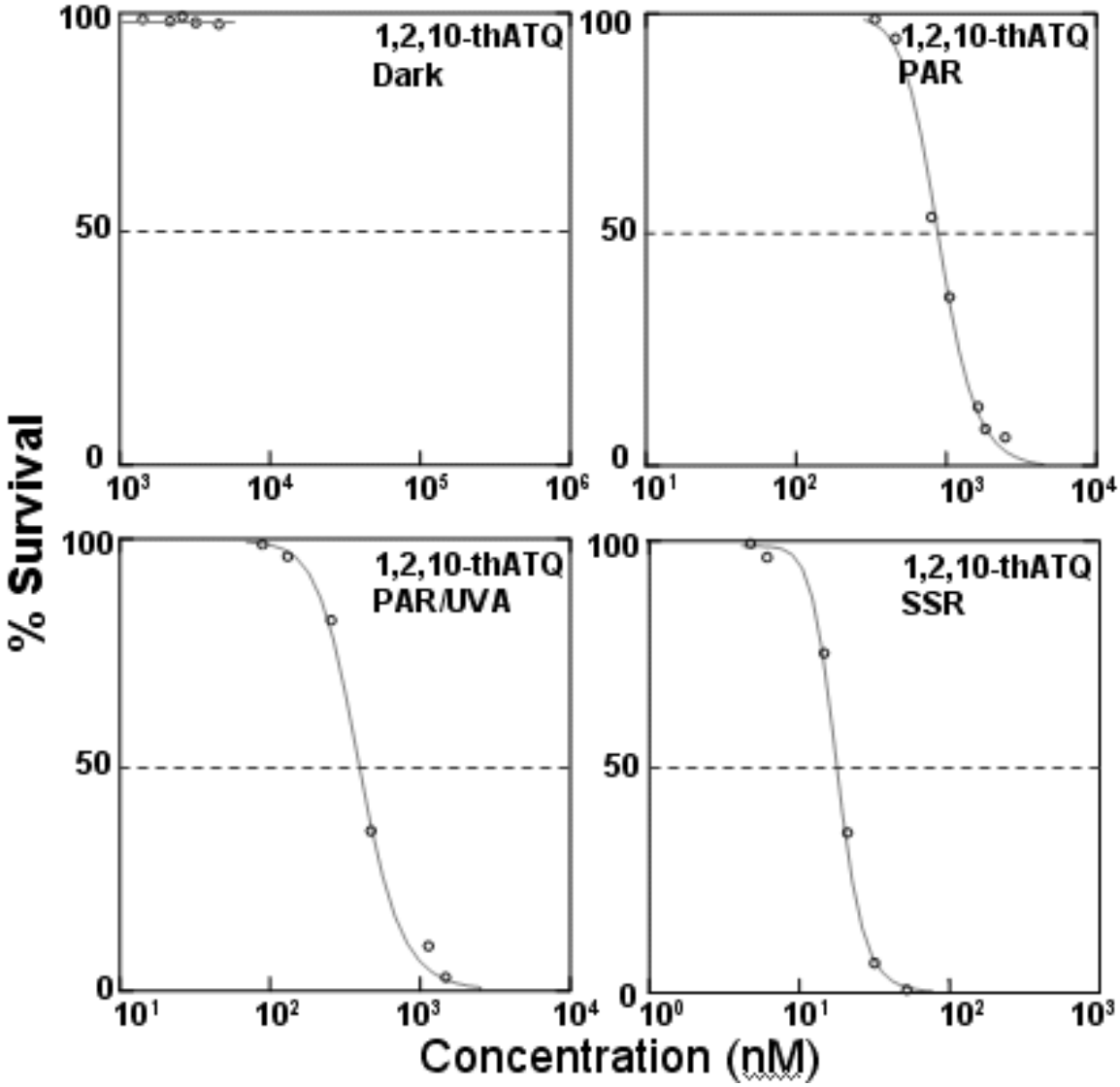

Figure 2.12 Concentration response curves for 1,2,10-trihydroxyanthracene (1,2,10-thANT) to *Hyalella azteca* under four lighting conditions. Photosynthetically Active Radiation (PAR, 400-700 nm), Ultraviolet Radiation A (UV-A, 320-400 nm), Ultraviolet Radiation B (UV-B, 290-320 nm).

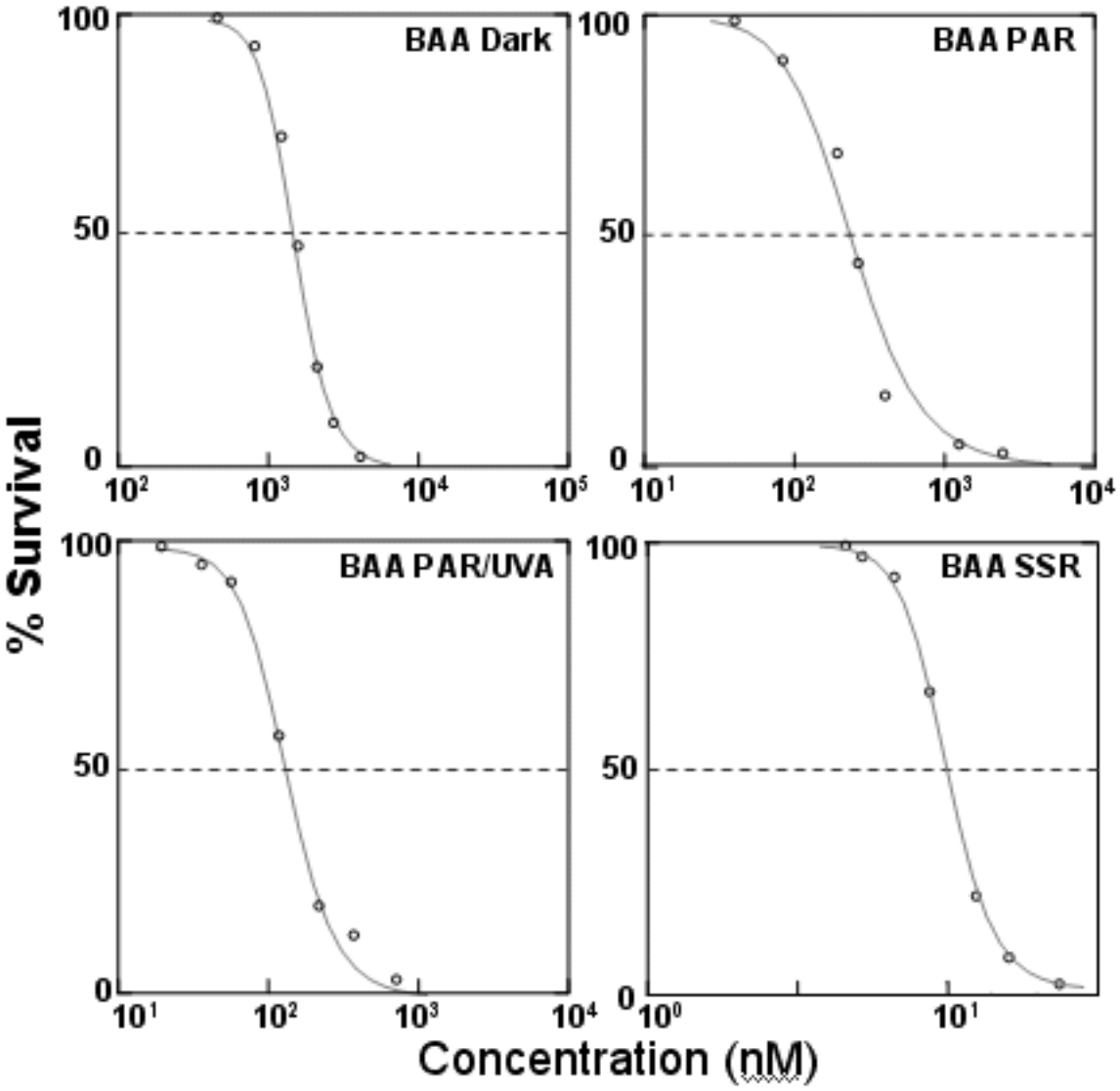

Figure 2.13 Concentration response curves for benzo(a)anthracene (BAA) to *Hyalella azteca* under four lighting conditions. Photosynthetically Active Radiation (PAR, 400-700 nm), Ultraviolet Radiation A (UV-A, 320-400 nm), Ultraviolet Radiation B (UV-B, 290-320 nm).

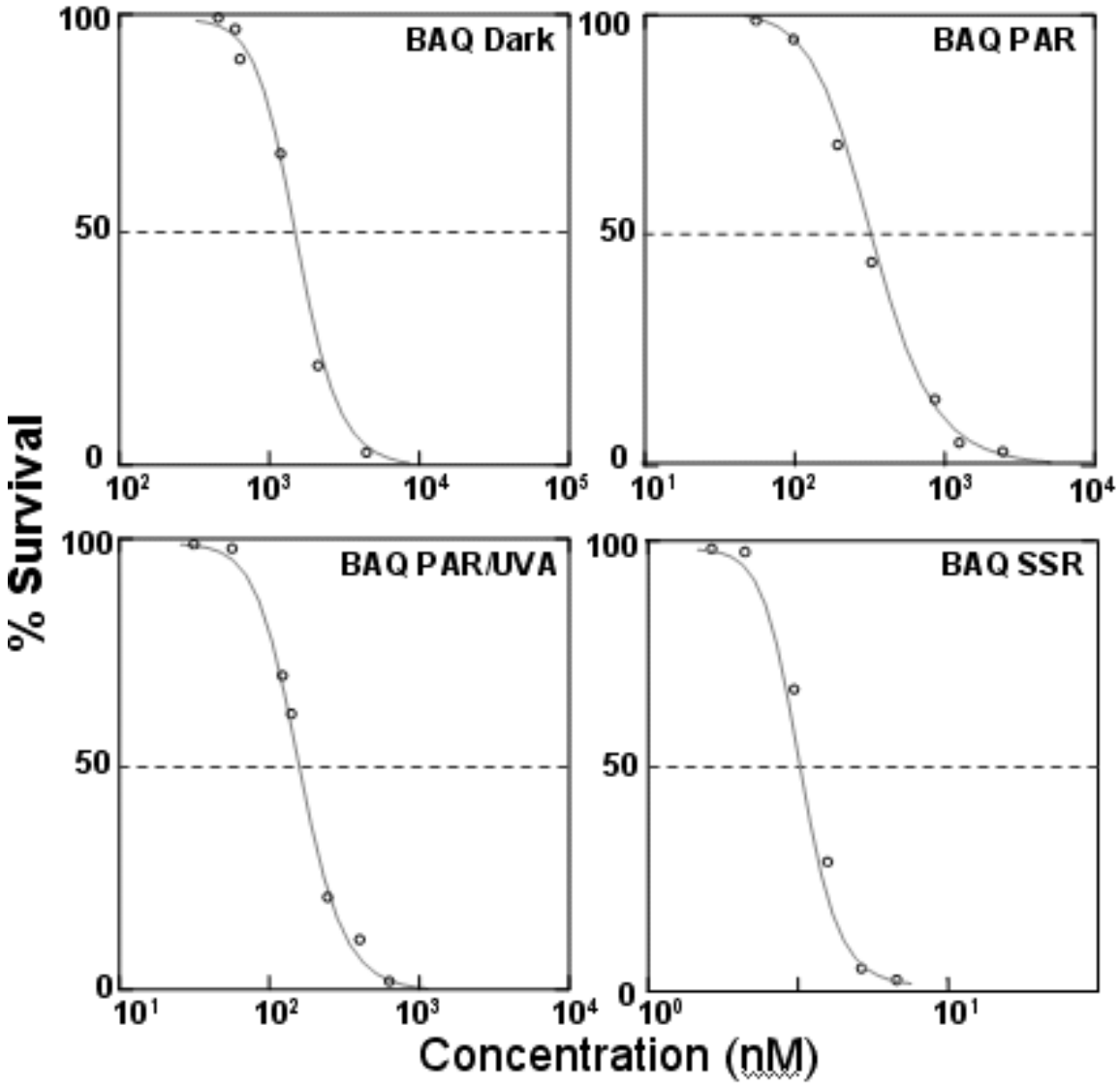

Figure 2.14 Concentration response curves for benzo(a)anthraquinone (BAQ) to *Hyalella azteca* under four lighting conditions. Photosynthetically Active Radiation (PAR, 400-700 nm), Ultraviolet Radiation A (UV-A, 320-400 nm), Ultraviolet Radiation B (UV-B, 290-320 nm).

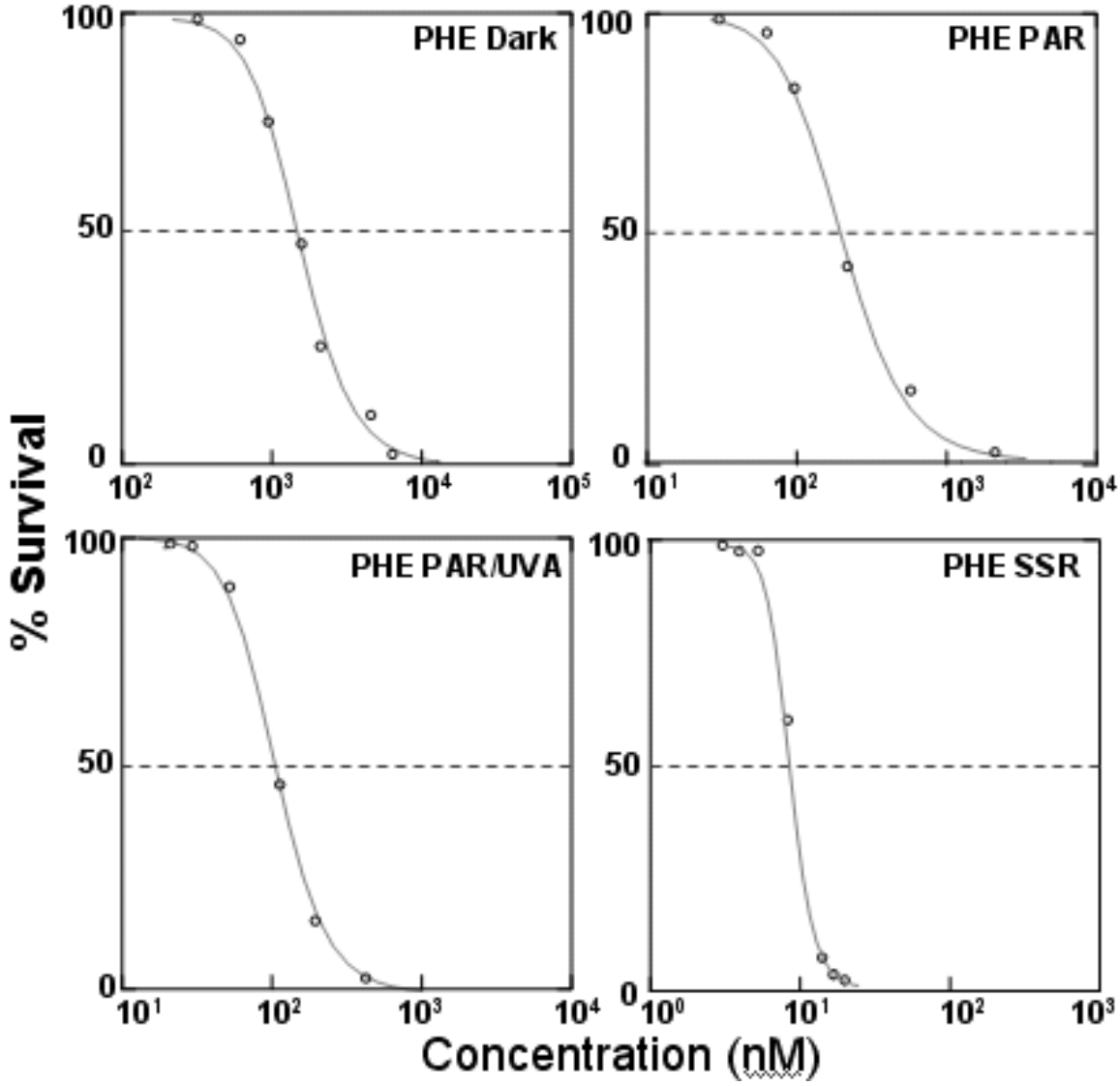

Figure 2.15 Concentration response curves for phenanthrene (PHE) to *Hyalella azteca* under four lighting conditions. Photosynthetically Active Radiation (PAR, 400-700 nm), Ultraviolet Radiation A (UV-A, 320-400 nm), Ultraviolet Radiation B (UV-B, 290-320 nm).

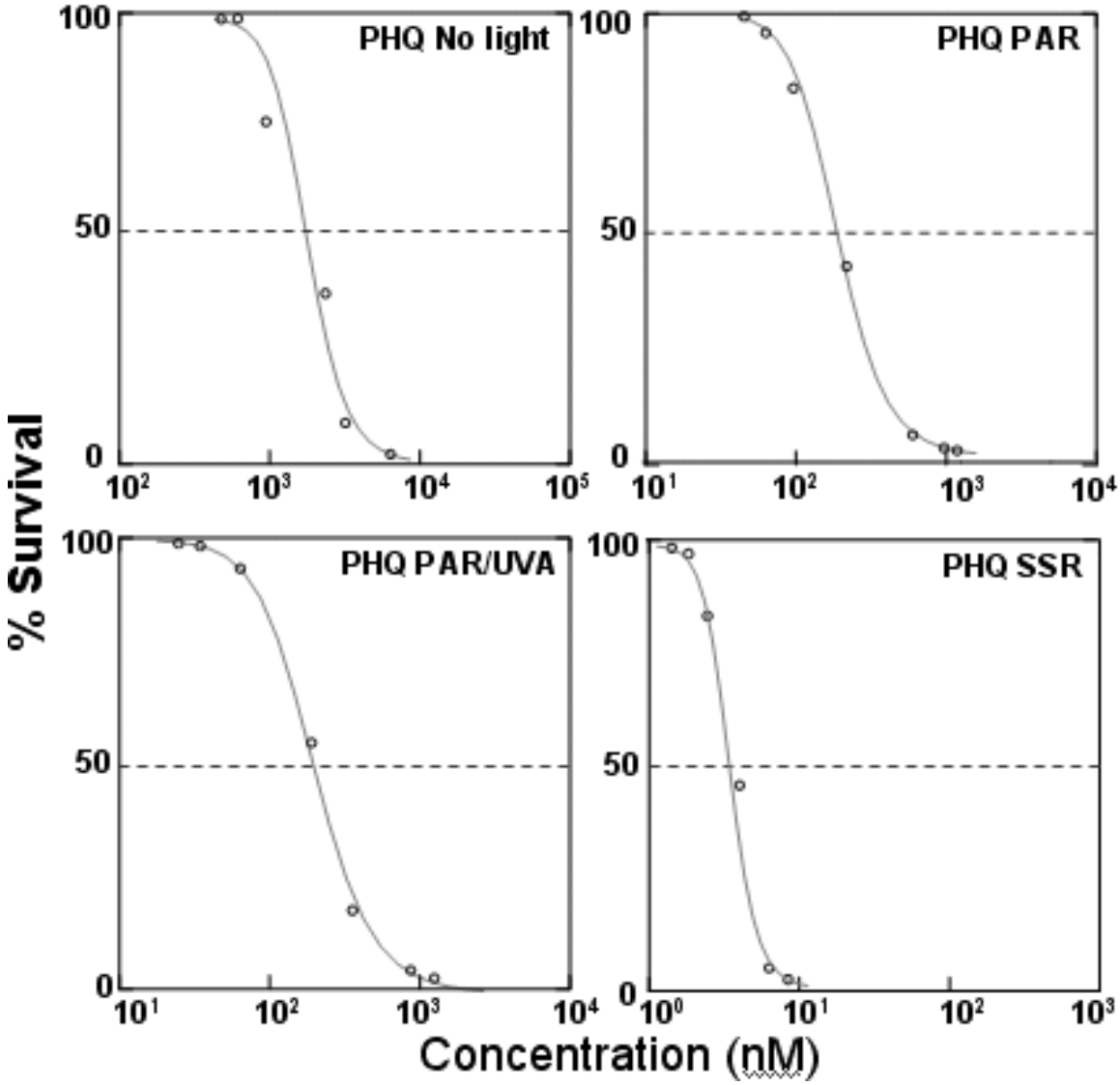

Figure 2.16 Concentration response curves for phenanthraquinone (PHQ) to *Hyalella azteca* under four lighting conditions. Photosynthetically Active Radiation (PAR, 400-700 nm), Ultraviolet Radiation A (UV-A, 320-400 nm), Ultraviolet Radiation B (UV-B, 290-320 nm).

2.3 Discussion

The toxicities for 15 PAHS and oxyPAHs were determined under 4 different irradiation regimes: Dark, PAR, PAR/UV-A and SSR (Table 2.2). The PAHs and oxyPAHs were generally found to be toxic to *Hyalella azteca*, under all of the lighting regimes. They generally became more toxic as increasing amounts UV radiation was added. Much of the dark and several of the SSR EC50s are in agreement with published data for *Hyalella azteca* (Wilcoxen et al. 2003, Hatch 1999). Much of the data showed similar trends in toxicity to those found by Lampi et al. (2005) and Xie et al. (2006) for *Daphnia magna*. The major exceptions were ANT, PHE and 1,2dh-ATQ which were found to be more toxic in *Hyalella azteca* than in *Daphnia magna.*

PAHs under all lighting regimes were considered acutely toxic if the 96h EC50 value was less than 3000 nM. Under these conditions 6 of the 12 oxyPAHs (ATQ, 1,4-dhATQ, 1,8-dhATQ, BaQ and PHQ) and one of the parent PAHs (BAA) exhibited acute toxicity in the dark treatments. Of the 6 oxyPAHs that exhibited toxicity without a lighting source, 1,8-dhATQ was the most toxic with an EC50 of 910 nM. Four of the oxyPAHs had EC50s that were greater than the maximum solubility of the oxyPAH, including, 1-hATQ, 2-hATQ, 1,2,5,8-thATQ and 1,2,10-thANT. This finding is similar to that of Lampi et al. 2005 who found that 1-hATQ and 2-hATQ did not display adequate toxicity below their solubility limits to calculate an EC50 value for *Daphnia magna* (Lampi et al. 2005). This finding also suggests that several oxyPAHs may not be acutely toxic in the absence of actinic radiation. Surprisingly only 2 of the 4 regulated compounds (BAA, ATQ) were found to be acutely toxic to *Hyalella azteca* in the dark. The other 2 regulated compounds (ANT and PHE) were found not to be acutely toxic in

the dark treatments with EC50s around 5000 nM. Also BAA was one of the least toxic compounds in the Dark treatment, which suggests that regulation of some of the more toxic compounds (1,8-dhATQ, 1,4-dhATQ) is needed.

When looking at concentration response curves, in the dark treatment, the three unhydroxylated quinones (ATQ, BAQ, PHQ) were all found to have similar slopes. They also all had EC50s that were similar in magnitude. This suggests that these "parent" quinones possibly share a similar mechanism of toxicity under dark conditions. Many researchers have found that PAHs with similar structures have similar modes of toxicity, and structure activity models have been developed based on these data sets (Huang et al. 1997, El-alawi et al. 2002, Lampi et al. 2007). One mechanism that has been suggested for quinones is mitochondrial disruption and ROS production via redox cycling (Xia et al. 2004, Xie et al. 2007). In two separate studies, it was found with PHQ (Xie et al. 2007), ATQ, and BAQ (Xia et al. 2004) that these 3 PAHs can disrupt mitochondrial electron transport, and produce ROS, which in turn can cause irreversible oxidative damage to the organism.

The concentration response curves for the dihydroxyanthraquinones (1,2-dhATQ, 1,3-dhATQ, 1,4-dhATQ, 1,8-dhATQ) in the dark treatment also exhibited very similar slopes. However the EC50s for these compounds varied over four orders of magnitude, with 1,4-dhATQ (EC50: 1089 nM) and 1,8-dhATQ (EC50: 910 nM) being much more toxic than 1,2-dhATQ (EC50: 6645 nM) and 1,3-dhATQ (EC50: 6824 nM) This suggests that these compounds all share a similar mechanism of toxicity. Two mechanisms have been proposed for the acute toxicity of these compounds. Babu et al (2001) found that 1,2-dhATQ disrupts the chloroplast electron transport chain, via redox

cycling in *Lemna gibba*. A study performed by Bondy et al. (1994) found that 1,4-dhATQ and 1,8-dhATQ due to their planar structure, are able to intercalate into DNA strands in mammals, disrupting hydrogen bonding.

The data from the PAR lighting regime produced EC50 values that were on average 2-20 fold lower (more toxic) than the EC50s for the dark treatments. These EC50s ranged from 108 nM for ANT, to 1295 nM for 1,2,5,8-thATQ. 1-hATQ, 2-hATQ and 1,2,5,8-thATQ showed a the largest increase in toxicity under the PAR treatment increasing by 15-20 fold, compared to that of the dark treatment. This large jump in EC50 is most likely due to the ability of each of these three quinines (1-hATQ, 2-hATQ and 1,2,5,8-thATQ) to absorb PAR (Mallakin et al. 1999). The least toxic of the PAHs in the PAR treatment was 1,2,10-thANT, with an EC50 of 4890 nM. This compound does not absorb PAR light, which is likely the reason for the change in toxicity. ANT which was found not to be acutely toxic in the dark treatment, when exposed to PAR became the most toxic compounds with an EC50 of 108 nM. This result is surprising as ANT is not known to absorb PAR light. One possible reason for this is ANT once ingested/inhaled can intercalate into DNA and bind to guanine bases causing base mis-pairing. This DNA disruption has been known to be influenced by the amount of CytP450 and other mono-oxygenases, which modify ANT into epoxides with greater bioavailability and a different absorption spectrum (Shou et al. 1996). This mechanism usually results in chronic toxicity, however several studies have linked acute PAH toxicity to this mechanism (Shou et al. 1996, Kurihara et al 2005).

It is interesting to note that the parent PAHs (ANT, BAA, PHE) under the PAR lighting showed remarkable similarities in EC50s to their primary photoproducts (ATQ,

BAQ, PHQ). In particular the EC50s of BAA and BAQ were compared, and PHE and PHQ were compared, they were found not to be statistically different. Also the concentration-response-curve for the parent PAH (BAA, PHE) when compared to its primary photoproduct (BAQ, PHQ) had very similar slopes. This suggests that these compounds likely share a similar mechanism of toxicity. It is also very likely that ANT, BAA and PHE are being partially or completely photomodified into their primary photoproducts (ATQ, BAQ, PHE) (Huang et al 1997, Mallakin et al. 1999, Lampi et al. 2005).

In the PAR/UV-A treatments the EC50 values ranged from 103 nM in BAQ to 894 nM in 1,2,10-thANT. Under this regime, the EC50s showed a 2-5 fold increase in toxicity over that of the PAR treatments. This increase in toxicity is likely due to the increase in radiation being absorbed as most PAHs absorb more strongly in the UV-A region of the spectrum than in the PAR region of the spectrum. The exception to this was ANT and ATQ which showed no statistical change in toxicity from PAR to PAR/UV-A. This is surprising as ANT only absorbs UV-B light and should not increase in toxicity in the presence of PAR or UV-A. One possible explanation for this might be that the addition of UV-A radiation and PAR influence the toxicity of ANT in a similar fashion, minimizing any change in toxicity in the presence of both types of radiation. For ATQ this result was not expected as ATQ does not absorb PAR light and should increase in toxicity only when absorbing UVA. It is likely that the toxicity of the ATQ treatments is predominantly due to interference with a biological process, likely the mitochondrial electron transport chain in *Hyalella azteca*. This type of interference has been

documented in other PAHs the presence of PAR light in similar compounds (1,2-dhATQ) and is a result of ROS damage via redox cycling (Babu et al. 2001).

Under the PAR/UV-A treatment the greatest change in EC50 was observed in 1,2,10-thANT. 1,2,10-thANT increased in toxicity 5 fold, from 4890 nM for the PAR treatment to 894 nM in the PAR/UV-A treatment. This large change in EC50 can be attributed to 1,2,10-thANTs strong absorption of UV-A. Interestingly, even with this large change in EC50, 1,2,10-thANT remains the least toxic of all of the PAR/UV-A trials.

An interesting observation was that all of the hydroxylated anthraquinones (1-hATQ, 2-hATQ, 1,2-dhATQ, 1,4-dhATQ, 1,8-dhATQ, 1,2,4-thATQ and 1,2,5,8-thATQ) with the exception of 1,3-dhATQ had EC50s that were similar in magnitude. However the slopes of the hydroxylated anthraquinones concentration response curve varied for each of the different chemicals. This suggests that even though they share similar EC50s the mechanisms of toxicity might be different for each of the hydroxylated anthraquinones.

ANT and BAA were found to have similar slopes and EC50s to their primary photoproducts ATQ and BAQ. This suggests that these compounds share a common mechanism of toxicity with their primary photoproducts. PHQ was found to have the steepest slope in the PAR/UV-A treatment. PHE shared a similar albeit slightly shallower slope to that of PHQ. Their EC50s however were not close, which suggests that PHQ and PHE unlike the other parent/primary photoproduct pairs do not share a similar mechanism of toxicity under PAR/UV-A lighting. Also PHE under UV-A rapidly

becomes photomodified into PHQ, whereas PHQ is realatively stable under UV-A light (McConkey et al. 1997)

In general most PAHs in the SSR treatment were found to increase in toxicity by 5-20 fold over that of the PAR/UV-A treatments. The most toxic compounds in the SSR treatment were ANT and BAQ with EC50s of 4.87 nM and 5.82 nM respectively. These two compounds were predicted to be the most toxic due to their ability to form copious numbers of photoproducts. ANT in particular has been shown to form more than 20 photoproducts when irradiated with SSR, and becomes almost completely photomodified (undetectable in samples) after four hours (Mallakin et al. 1999, 2000). Due to ANTs degradation to other products under SSR, the complex interactions and the multiple photoproducts produced, it is not surprising that the EC50 of ANT is the lowest of any of the chemicals tested. The other parent PAHs (PHE, BAA) were also very toxic in the SSR treatment with EC50s of 10.9 nM and 12.2 nM respectively. These compounds were found to be slightly less toxic than their primary photoproducts (BAQ, PHQ). BAA however had a concentration response curve slope that was almost identical to that of BAQ. This is indicative that these chemicals likely share a similar toxicity mechanism. It could also indicate that BAA is being photomodified into BAQ, based on the similarities in their slopes and EC50s. This also suggests that UV-B plays a key role in PAH phototoxicity. Lampi et al. (2005) and Huang et al. (1995; 1997) found similar results in *Daphnia magna* and *Lemna gibba* respectively.

The EC50s for ANT for the four different treatments showed a 1000 fold change in toxicity from the Dark treatment (EC50: 4902 nM) to the SSR treatment (4.87 nM). The SSR values matched results found by Mallakin et al. (1999) under the same

conditions (10.6 nM). The slopes of the concentration response curves across the four treatments showed four unique slopes. This suggests that ANT under each of the treatments might have different toxicity mechanisms. Interestingly the PAR/UV-A treatment was slightly less toxic than that of the PAR treatment. One possible reason for this is that under PAR lighting some oxidative stress defenses (Mono-oxygenases, Catalase, Superoxide dismutase) may not be up-regulated as much as when UV-A is present. A study by Fernadez and L'Haridon (1992) showed that ANT in the presence of UV-A light causes CytP450, and Catalase to be up-regulated in *Triturus vulgaris* (Newts). They also showed that ANT under PAR lighting does up-regulate these genes but at about 40% of that of the UV-A trials (Fernandez and L'Haridon. 1992). Also it has been shown that in the presence of UV-A ANT can undergo some photomodification which leads to a wide range of photoproducts, including ATQ (Mallakin et al. 1999, Lehto et al. 2003). Under PAR and PAR/UV-A light the EC50s for ANT and ATQ correlated very well. This is indicative that ANT might be photomodified into ATQ, which in turn might be eliciting the responses observed (Lehto et al. 2003).

One set of data that did not seem to fit with the other PAHs was the EC50 values of ATQ, which did not decrease across PAR, PAR/UV-A and SSR treatments. ATQ was found to be relatively non-toxic in the absence of light, but in the presence of PAR lighting, it became one of the most toxic of the PAHs. However in the presence of PAR/UV-A the compound only slightly increased in toxicity. Furthermore the difference between the PAR/UV-A EC50 (156 nM) and the SSR EC50 (142 nM) were found not to be statistically different. This finding is surprising due to the fact that ATQ absorbs strongly in the UV-A/UV-B portion of the electromagnetic spectrum and minimally in

the PAR region (Mallakin et al. 1999). One reason for this might be that ATQ is more water soluble than other PAHs, and therefore may be easily excreted or metabolized by the organism, leaving only photosensitization as the primary mechanism of action. The data also suggests that the stability of ATQ might contribute to the lack of further toxicity under UV-A/UV-B lighting, due to lack of further photoproducts being produced.

The EC50 for 1-hATQ under each of the four treatments became increasingly more toxic as more UV radiation was added. The EC50s increased in toxicity from being acutely non-toxic in the dark treatment to being very toxic in the SSR treatment with an EC50 of 24.4 nM. The greatest change in 1-hATQ toxicity was observed under the PAR treatment increasing 100 fold over that of the dark treatment. The strong PAR absorbance of 1-hATQ is likely responsible for this large increase in toxicity (Mallakin et al. 1999). The slopes of 1-hATQs concentration response curves are all very similar, in the PAR, PAR/UV-A and SSR treatments. This suggests that 1-hATQ under PAR, PAR/UV-A and SSR all share a similar toxicity mechanism. One proposed mechanism is that 1-hATQ forms Michael-adducts with biological molecules, resulting in disruption of biological processes (Tanaka et al. 1995, Briggs et al. 2003).

Interestingly one of the most studied PAHs 1,2-dhATQ was found to be one of the least toxic. 1,2-dhATQ was found to have an EC50 in the dark treatment of 6645 nM. This value is comparable to EC50s determined in *Daphnia magna* (Lampi et al. 2006) and *Lemna gibba* (Mallakin et al. 1999). 1,2-dhATQ was found to increase in toxicity as the wavelengths of radiation added was increased from PAR to SSR. The EC50 increased by 100 fold over the four treatments. The slopes of the concentration response curves for 1,2-dhATQ were almost identical across all four treatments. This suggests

that 1,2-dhATQ has a similar mechanism of toxicity across all of the different conditions. One proposed mechanism has been intensively studied in dark reactions suggests that 1,2-dhATQ blocks mitochondrial electron transport (Tripuranthakam et al. 1999). A similar mechanism has shown that 1,2-dhATQ in the presence of Cu can redox cycle, resulting in the depletion of the ubiquinone pool and the production of large amounts of ROS (Babu et al. 2001). Babu et al (2003) found that SSR radiation can elicit a similar response in the place of Cu in the mitochondrial electron transport chain when 1,2-dhATQ is present.

1,3-dhATQ was found not to have statistically different EC50s from 1,2-dhATQ across all four of the radiation treatments. 1,3-dhATQ also had slopes that were almost identical to those of 1,2-dhATQ. This indicates that 1,3-dhATQ may share a similar mechanism of toxicity to that of 1,2-dhATQ, which is likely that of mitochondrial disruption and ROS production indicated in the previous paragraph.

1,4-dhATQ and 1,8-dhATQ showed similar trends in their EC50s across all four of the lighting regimes. The EC50s for 1,4-dhATQ and 1,8-dhATQ in the dark, PAR and PAR/UV-A treatments were not statistically different from each other. The EC50s however did decrease as UV radiation was added. The EC50s for the SSR treatment were statistically different, with 1,4-dhATQ having a EC50 of 6.19 nM and 1,8-dhATQ having a EC50 of 28.1 nM. The slopes of the concentration response curves for the dark, PAR, PAR/ UV-A and SSR treatments were very similar for 1,4-dhATQ and 1,8-dhATQ. The slopes of the dark and the PAR treatments of both compounds were both unique, and did not match the slopes of the PAR/UV-A and the SSR treatments which had slopes that were almost identical. This suggests that both 1,4-dhATQ and 1,8-dhATQ share similar

toxicity mechanisms under each of the three different lighting treatments. It also suggests that the there are 3 different toxicity mechanism present for these chemicals. The first being a toxicity mechanism in the absence of light, the second being mechanism under PAR lighting and the third mechanism in the presence of PAR/UV-A or SSR. The dark treatment toxicity of 1,4-dhATQ and 1,8-dhATQ has been shown to be caused by inhibition of topoisomerase II, and via DNA adducts (Bondy et al. 1994, Flowers-Geary et al. 1996). Two other mechanisms have been speculated for toxicity of these chemicals under SSR lighting. These mechanisms are ROS production via mitochondrial inhibition and adduct formation with biological molecules (Ankley et al. 1994, Lampi et al 2006).

Benzo(a)anthracene and its derivatives are known to be acutely toxic (Dong et al. 2002, Feldmannová et al. 2006). BAA was found to be about 2 fold less toxic than its primary photoproduct BAQ, with EC50s of 2404 nM and 1387 nM. The Dark EC50 for BAA (2404 nM) corresponds well to that in the literature of 3583 nM for *Daphnia magna*. The EC50s of BAA and BAQ however were not statistically different for the PAR, PAR/UV-A and SSR treatments. The slopes of the concentration response curves were also very similar in shape, with the exception of BAQ in the SSR treatment which was much steeper than that of BAA. This data suggests that BAA and BAQ share similar toxicity mechanisms in the dark, PAR and PAR/UV-A treatments. It also suggests that the mechanism varies for each of the lighting conditions as the slopes of the concentration response curves are different for each of the lighting regimes. It is also very likely that BAA and BAQ under SSR do not share the same toxicity mechanism. One explanation for this similarity in EC50s and slope in the PAR and PAR/UV-A treatments is that BAA is becoming photomodified into BAQ. However if this is the case

then we should expect that BAA and under SSR would have the same slope, which is not the case. A known mechanism for BAQ toxicity is via DNA cleavage in the dark treatments. In the presence of UV-B the suggested toxicity mechanism is ROS (Dong et al. 2002, Lehto et al. 2003).

PHE has been shown in many studies to be very toxic to organisms (McConkey et al 1997, Xie et al. 2005). The EC50 for PHE in the dark treatment was 3167 nM. This EC50 corresponds well to EC50s published for other organisms, Daphnia magna (3923 nM) (Lampi et al. 2005), *Vibrio fischeri* (2973 nM) (McConkey et al 1997) and Lemna gibba (5890 nM). PHQ, the primary photoproduct of PHE, was found to be more toxic than PHE under the dark treatment, with an EC50 of 2078 nM. This value is very similar to that found in *Daphnia magna* (1720 nM) (Xie et al. 2005). Xie et al. (2005) suggested that this increase in toxicity might be due in part to the higher water solubility of PHQ compared to that of PHE. The EC50s for the PAR and PAR/UV-A treatments showed that PHE was more toxic than PHQ. The slopes of the PAR and PAR/UV-A treatment curves for both compounds are very similar. This result is surprising as PHE in the presence of PAR or UV light becomes photomodified into PHQ and other photoproducts (McConkey et al. 1997, Lehto et al. 2003). One possible explanation is that PHE is becoming photomodified into another more toxic product than PHQ, possibly 1,2-dhPHQ (Lehto et al. 2003). The toxicity mechanism that has been proposed for PHQ toxicity is via an ortho-quinone redox cycling mechanism (Flowers-Geary et al. 1996, Xie et al. 2006). The EC50s for the SSR treatment for PHE and PHQ differed from each other, with PHQ (5.89 nM) being more toxic than PHE (12.2 nM). This is reversal in trends from the PAR and PAR/UV-A data was not expected. The increase in PHQ toxicity over

that of PHE is likely due to the slight dip in absorbance that PHE has around the UV-B wavelength (315 nM), whereas PHQ has a strong absorption throughout the UV-B range (290 nM-320 nM).

Among the EC50s no clear trend emerged, when analyzing the EC50 compared to the positions of the hydroxyl groups. Also the slopes of the concentration response curves showed no clear trend, suggesting that their might be several mechanisms of toxicity across for each of the PAHs. This is indicative that PAHs and oxyPAHs most likely have distinct mechanisms of toxicity. This might also be explained by the differences of PAHs absorbance and the resulting production of reactive oxygen species (ROS) from photon absorbance.

Throughout all of the varying spectra, the toxicities of the parent PAHs ANT, PHE, and BAA showed a clear increase in toxicity in the presence of UV light. The toxicities of the parent PAHs was as follows: ANT > PHE > BAA. This ordering of toxicity, matched the rates of photo-oxidation found by Huang et al. (1995) for these three PAHs (ANT >> PHE > BAA). This finding suggests that the toxicity of these compounds is linked to its rate of photomodification. It also suggests that the primary mechanism for toxicity of these compounds is likely due to their photomodification into photoproducts.

Chapter 3

Toxicity of Cu, Cd, Ni and Zn to *Hyalella azteca*: The effects of PAR and UV radiation.

3.0 Introduction

Metals, a class of environmental contaminants that primarily come from anthropogenic sources, are common contaminants in both aquatic and terrestrial environments. Many metals are beneficial to organisms in low amounts and are essential to life (Abel, 1989). However, when present at environmentally relevant concentrations, metals also induce a large assortment of toxic effects on organisms, and can be cytotoxic and carcinogenic. Many metals, including Cd, Cu, Ni, and Fe are capable of inducing ROS formation, which is thought to be one of the primary causes of metal cytotoxicity and carcinogenicity (Kasprzak 1989, Pourahmad et al. 2000, Xie et al. 2006;2007).

A study by Borgmann et al. (2005) showed that the toxicity of 63 metals to *Hyalella azteca* was directly linked to water hardness. This study also showed that the charge on the metal ion did not correlate directly with the relative toxicity. In separate studies, Goldstein et al. (1993) and Pourahmad et al. (2003) both demonstrated that Cu in the presence of a biological reducing agent can produce hydroxyl radicals from hydrogen peroxide via Fenton-Type reactions (Goldstein et al. 1993, Pourahmad et al. 2003). Studies have also demonstrated that in the presence of SSR, Cu toxicity is greatly increased in the aquatic plant *Lemna gibba* (Babu et al. 2003, Akhtar 2004). Babu et al (2003) also found that both Cu and UV-B light elicited similar ROS production, indicating that they likely share a similar toxic mechanism. A separate study

demonstrated that the toxicity of Cd is likely due to mitochondrial disruption via an oxidative stress mechanism (Bolduc et al. 2004).

Metal toxicity to *Hyalella azteca* has been widely documented in the literature, but very little work has been done that examines the effects of metals combined with actinic radiation in *Hyalella azteca*. This chapter addresses the gaps in the current literatures, attempting to determine the effects of different wavelengths of light on metal toxicity in *Hyalella azteca.*

3.1 Materials and Methods

The metals cadmium (Cd), copper (Cu), nickel (Ni) and zinc (Zn) were tested at seven different concentrations to determine the EC50 values for each metal. Assay conditions were performed the same as in the 96h PAH assay (section 2.2), except that metal salts were added instead of PAHs. Stock solutions of metals were of the highest purity available (Table 3.1) and purchased from Sigma Chemical Company (St Louis, MO, USA). These metals were tested under 3 different lighting regimes using a 16:8 light:dark cycle and a Dark treatment. The test solution was statically renewed after 48 hours to ensure a constant concentration of metals. After 96 hours, mobility was assessed by gentle prodding. Immobility was considered mortality. Each treatment was performed in triplicate. Water loss due to evaporation was 10mL/week, which was considered negligible. Test conditions were kept the same as in the previous experiment described in Chapter 2. The animals were grown and maintained under the same conditions described in Chapter 2.1.1 – Test Organisms. The lighting conditions were as described in Chapter

Table 3.1 Purities of Metals used in the 96h Metal Assays.

Metal Compound	Purity (%)
$CuSO_4$	98
$CdCl_2$	99
$NiCl_2$	99
$ZnCl_2$	99

Abbreviations for Metals: Copper (Cu), Cadmium (Cd), Nickel (Ni), Zinc (Zn)

2.1.3 – Lighting Sources. The data were analyzed as described in Chapter 2.1.4 – Data Analysis.

3.2 Results

The toxicity of Cu, Cd, Ni, and Zn were determined by using the regression model described in section 2.1.4. From this data, concentration response curves were plotted and EC50s determined. The toxicities for each of the treatments are shown in Table 3.2. The responses to the metals varied greatly with lighting conditions ranging from Cd with no response to light, to that of Cu which became increasingly toxic as the amount of UV radiation increased from Dark to SSR. The metal concentration response curves varied from metal to metal, and the slopes varied across the lighting conditions. The differences in slopes are illustrated for each of the metals in Figures 3.1-3.4.

In the dark treatment, Ni was found to be the least toxic metal with an EC50 of 3032 nM, and Cd was found to be the most toxic metal with an EC50 of 97.8 nM. Zn was found to have low toxicity under the dark conditions with an EC50 of 2110 nM. Cu was found to be moderately toxic in the dark treatment with an EC50 of 1400 nM. The slopes of the metals under the dark treatment varied from metal to metal. Cd was found to have the steepest slope. Zn and Ni had slopes that were very similar in shape, and were both the shallowest slopes in the dark treatment. Cu had a slope that was not similar to the other 3 metals and was steeper than that of Zn and Ni.

Under the PAR lighting regimes the toxicities of Cu and Ni showed a slight decrease in EC50s. Cu increased in toxicity from 1400 nM in the dark treatment to 975 nM in the PAR treatment. Ni increased in toxicity slightly from 3032 nM to 2691 nM. The

toxicities of Zn and Cd showed no statically significant change in toxicity from the dark treatment to the PAR treatment. The concentration response curves for the PAR treatment showed a wide range of slopes. The slopes of all four metals in the PAR treatments were almost identical to those of each of the metals in the dark treatments.

The PAR/UV-A treatments showed an increase in toxicity for Cu and Ni. Cu in the presence of PAR/UV-A light showed a 5 fold increase in toxicity from 975 nM under PAR to 180 nM under PAR/UV-A treatment. With the addition of UV-A light Ni also showed an increase in toxicity from 2691 nM to 1761 nM. Cd and Zn did not show a statistically significant change in toxicity as UV-A was added. The slopes of the concentration response curves for Zn and Cd stayed the same as in the dark and PAR treatments, with Cd being the steepest and Zn being the shallowest. The slope of the Cu treatment however was slightly steeper in the PAR/UV-A treatments than in the Cu dark and PAR treatments. The Ni concentration response curve was much shallower in the PAR/UV-A treatment compared to Ni in the dark and PAR treatments.

The SSR treatment resulted in an increase in toxicity for Cu and Ni relative to the PAR/UV-A treatment. Cd and Zn however did not increase in toxicity under the SSR treatment. When exposed to SSR, Cu showed a greater than 10 fold increase in toxicity, compared to the PAR/UV-A treatment, increasing from 180 nM to 10.5 nM. Ni increased in toxicity by 10% from 1761 nM to 1550 nM. Cd and Zn showed no statistical change in toxicity under the SSR treatment compared to that of the PAR/UV-A. The concentration response curves for the SSR treatment showed no change in slopes for Cd and Zn. Cu however had the steepest slope, which did not look similar to any of the other treatments.

Table 3.2 Toxicity of four Metals to Hyalella azteca under Dark, PAR, PAR/UV-A and Simulated Solar Radiation (SSR).

Metal	Dark (*nM*) ± SD	PAR (*nM*) ± SD	PAR + UV-A (*nM*) ± SD	SSR (*nM*) ± SD
Cu	1400 ± 303	975 ± 45.8	180 ± 58.4	10.5 ± 0.35
Cd	97.8 ± 8.41	92.6 ± 11.4	110 ± 7.65	106 ± 12.5
Ni	3033 ± 156	2691 ± 308	1761 ± 261	1550 ± 218
Zn	2110 ± 400	2346 ± 217	2089 ± 189	1957 ± 298

Animals were incubated with metals under dark, PAR, PAR/UV-A and (SSR) lighting regimes. Each experiment was repeated independently at least 3 times.

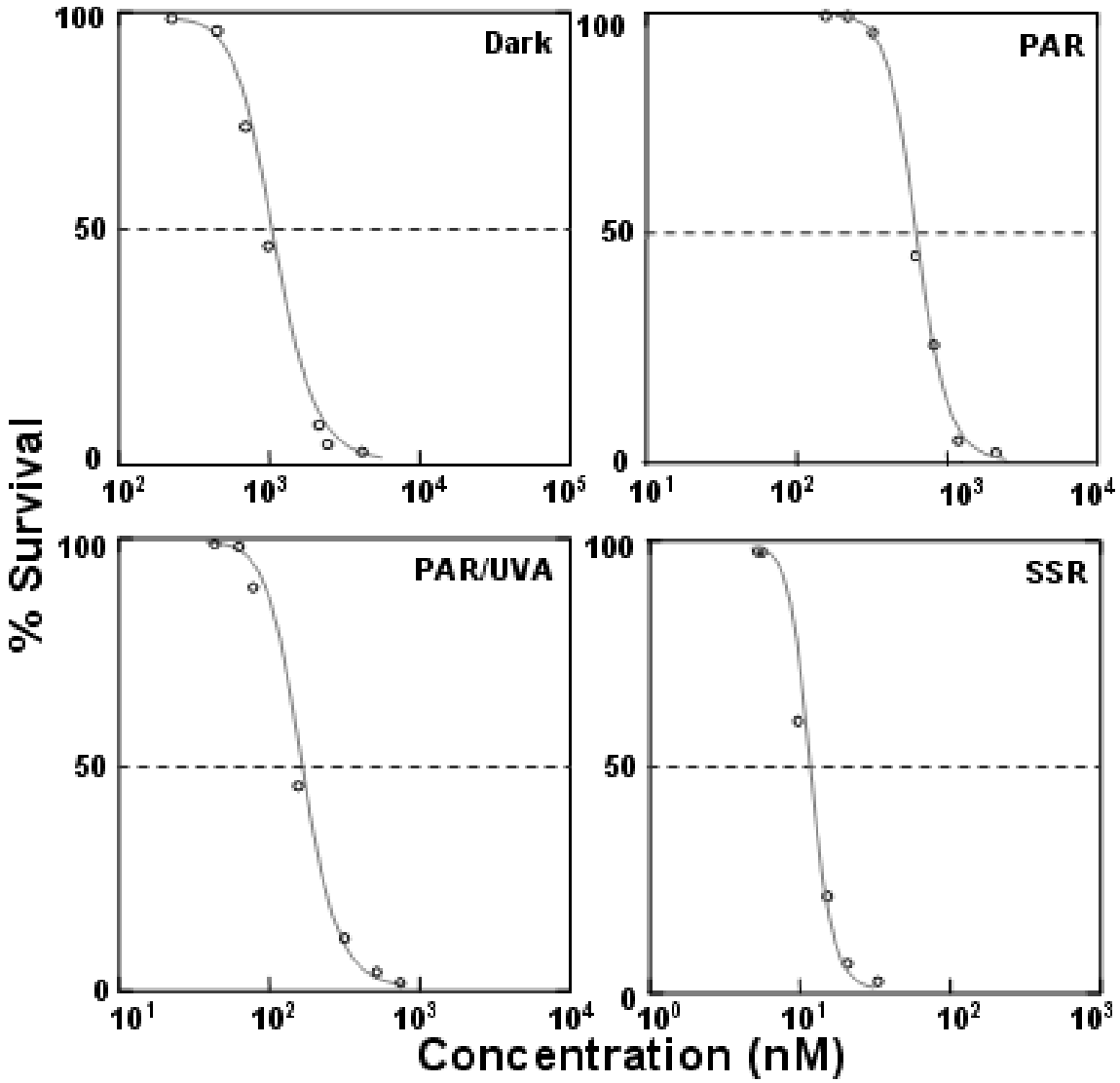

Figure 3.1 Concentration response curves for Copper (Cu) to *Hyalella azteca* under four lighting conditions. Dashed red line represents 50% survival.

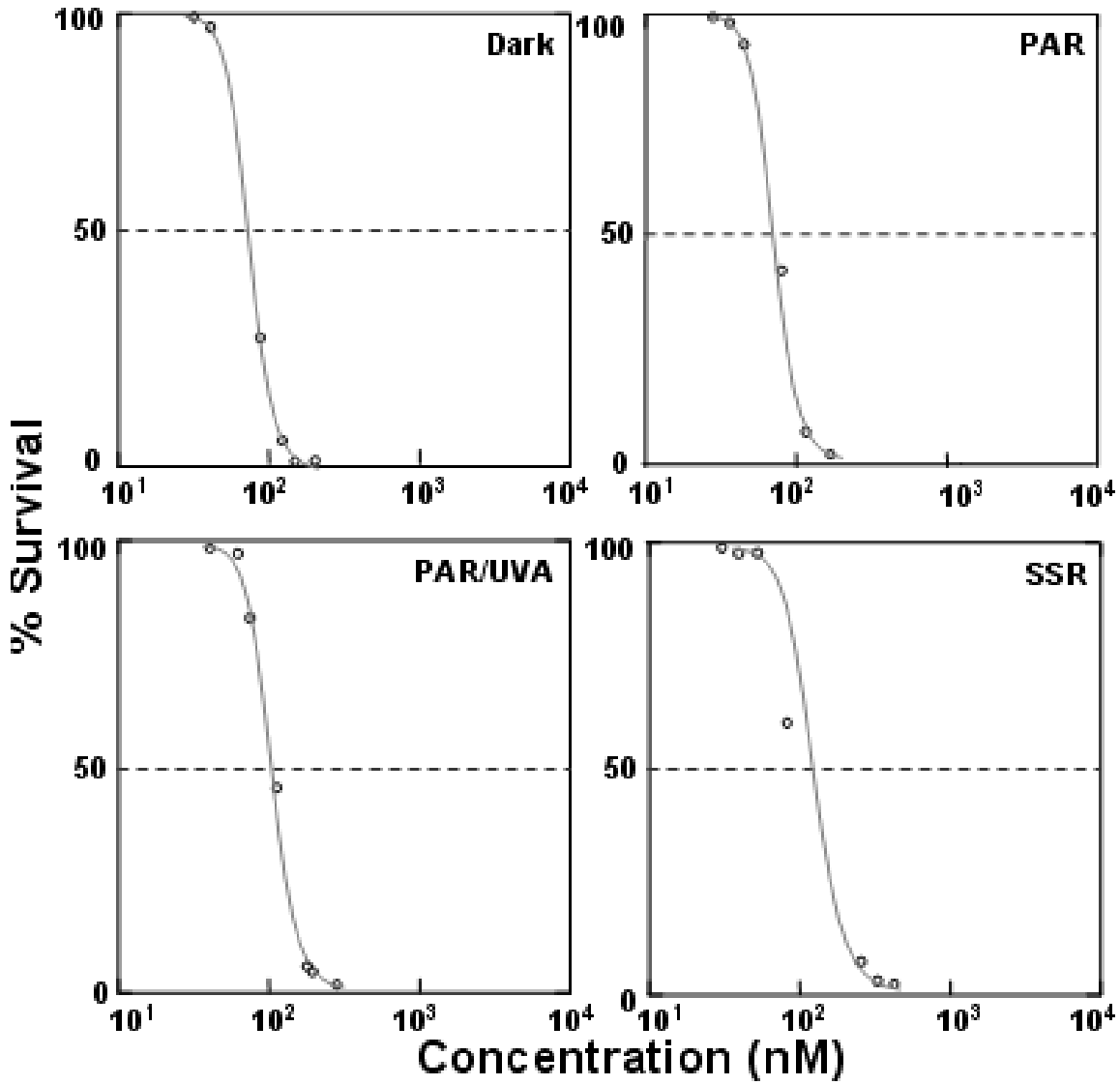

Figure 3.2 Concentration response curves for Cadmium (Cd) to *Hyalella azteca* under four lighting conditions. Dashed red line represents 50% survival.

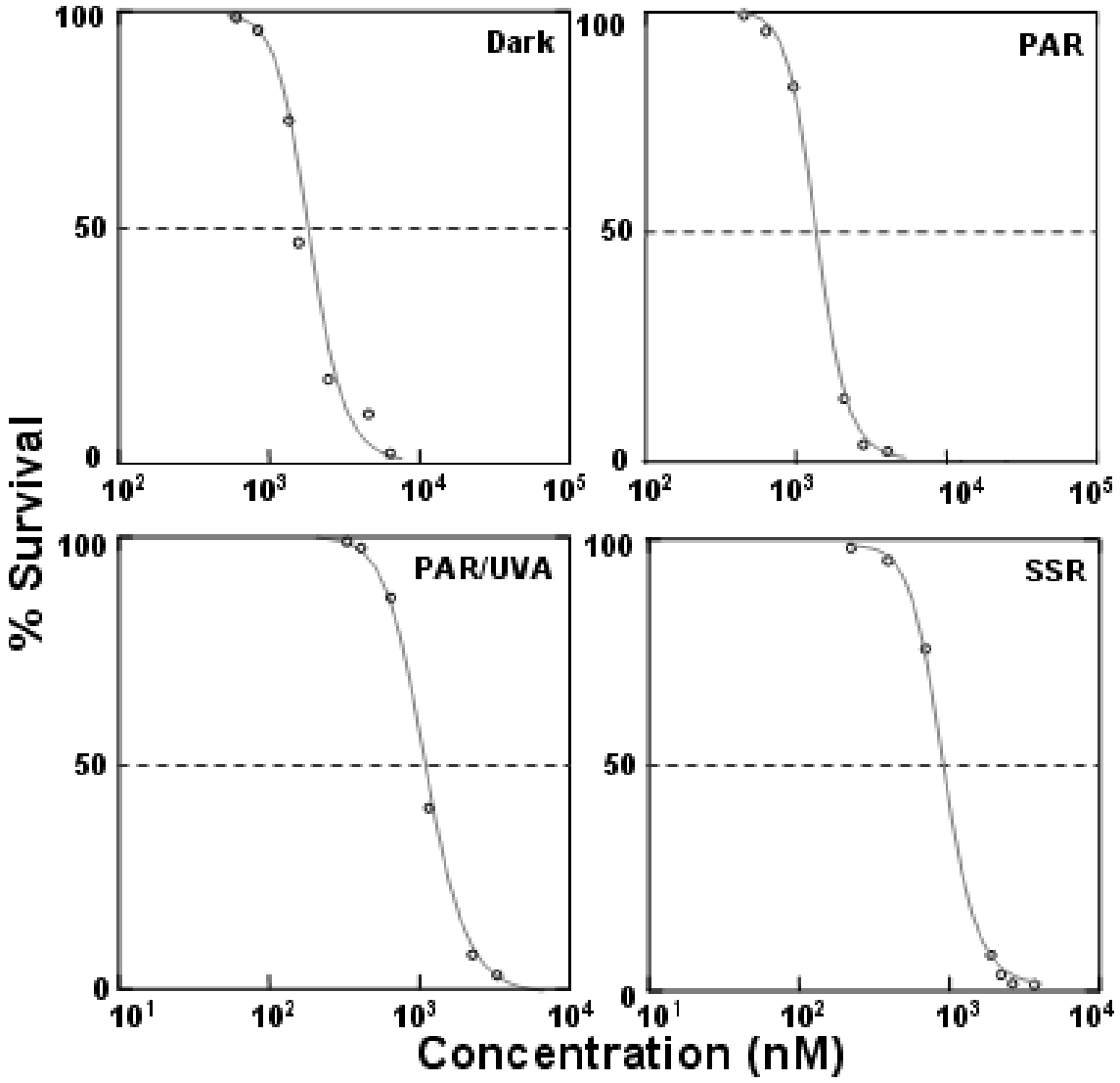

Figure 3.3 Concentration response curves for Nickel (Ni) to *Hyalella azteca* under four lighting conditions. Dashed red line represents 50% survival.

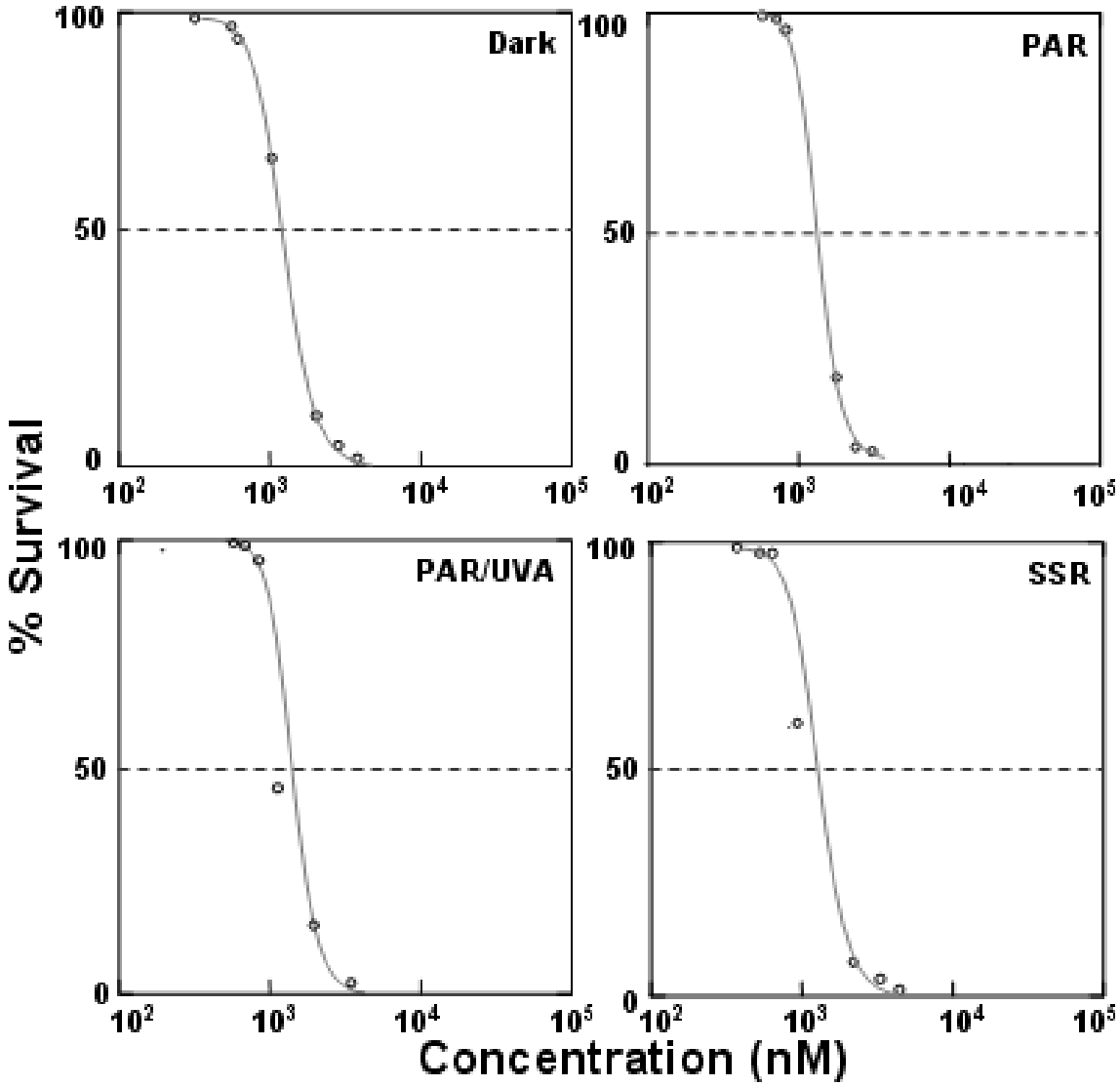

Figure 3.4 Concentration response curves for Zinc (Zn) to *Hyalella azteca* under four lighting conditions. Dashed red line represents 50% survival.

3.3 Discussion

The toxicity of Cd, Cu, Ni, Zn were assessed under 4 different lighting conditions, dark, PAR, PAR/UV-A and SSR (Table 3.2). The metals were generally found to be non-toxic at environmentally relevant levels (Borgmann et al. 2005). However, when exposed to increasing levels of actinic radiation each of the metals acted differently, some becoming exceedingly toxic at environmentally relevant levels (Cu) and some showed no change in toxicity with varying lighting conditions (Cd). The differences in metal toxicity are likely due to differences reactivity and ROS generation, although there are several other proposed mechanisms..

Under the Dark conditions, Ni and Zn were found to be relatively non-toxic at environmentally relevant conditions with EC50s of 3033 nM and 2110 nM respectively. As expected Cu was found to be mildly toxic in the dark with an EC50 of 1400 nM which are similar to published results (Borgmann et al. 2005). Cd was found to be exceedingly toxic in the absence of light with an EC50 of 97.8 nM. These values correlate well with published data from Gurst et al. (2005), who found Cd has an EC50 134 nM in the absence of light. These results is not surprising as most studies show that cadmium is acutely toxic to benthic invertebrates (Collyard et al. 1994, Gurst 2005). Several studies have shown that Cd induced ROS production in Chinese Hamster Ovary cells (CHO) (Yang et al. 1996) and in protists (Wantanabe and Suzuki 2001). Bolduc et al. (2004) suggested that in *in-vitro* studies Cd-induced mitochondrial disruption is the primary cause of acute toxicity in animal cells through oxidative stress. These results suggest that if Cd is already producing ROS and inducing toxicity via this mechanism any further ROS production via phototoxicity will have little or no effect. The presented Data shows

that the toxicity of Cd did not change across the lighting regimes. The order of metal toxicity in the dark treatment was Cd>Cu>Zn>Ni. All of the EC50s obtained from the dark treatments were similar to those in previously published studies (Collyard et al. 1994, Keithly et al. 2004, Borgmann et al. 2005, Gurst et al. 2005).

The results for the PAR treatment generally showed no statistically significant change in toxicity over that of the dark treatments, with Cu being the exception. The EC50 for Cu showed a 30% decrease in the EC50 value going from 1400 nM in the dark to 975 nM in the PAR treatment. This result is surprising as Cu has only a very weak absorbance in PAR (minimal absorbance at 610-700 nm, peaking at 810 nm), and therefore should not exhibit a large increase in toxicity under PAR. Also the level at which the Cu is present is two fold lower than acute toxicity seen based on the biotic ligand model (BLM) (2561 nM) (Borgmann et al. 2004). This suggests that there is another mechanism at work other than the BLM. Several studies have shown that the effects of Cu has almost no impact under cool white fluorescent light unless present at high (BLM) concentrations (Babu et al. 2001:2003, Akhtar et al. 2004). However, it should be noted that most of these studies were performed on plants (Peterson et al. 2000, Babu et al. 2001:2003), and the animal tests performed on a much shorter timescale (48h), on a different organism (*Daphnia magna*)(Kramer et al. 2004). Previous work by Babu et al. (2001) and Xie et al. (2006) have shown that Cu is a redox active metal. They showed that redox active metals interfere with mitochondrial electron transport chains (ETC) in both plants and animals at levels when exposed to UV radiation (Babu et al. 2001;2003, Xie et al. 2006). Babu et al. (2001) suggested that when exposed to UV light there is an increase in ROS production which in turn leads to an increase in toxicity. This

data suggests that PAR light might also increase the production of ROS possibly through a PAR light chromophore. The most likely mitochondrial chromophore is Cytochrome C oxidase which has an absorption peak at 684 nM (Hamblin et al. 2007). The PAR light controls showed no noticeable toxicity in *Hyalella azteca* and were run alongside the PAR treatments. The toxicity that Cu and PAR light elicited was a marked increase from that of the Cu on its own (1400 nM to 975 nM) suggesting that PAR has an influence on Cu's toxicity. One reason for this increase is redox cycling based on the interference in the mitochondrial ETC and a direct increase in ROS production. Another theory is that in the presence of a single stressor (Radiation or Metal) organisms are often able to adapt to the stressor; however, in the presence of a second stressor the load on the ROS scavengers and other defense mechanisms might be too great, leading to an increase of ROS and mortality. This increase in ROS would likely lead to protein oxidation, lipid cross-linking and other cellular damage (Borgmann and Norwood 1997, Brennan et al. 2008).

When exposed to UV-A treatments no statistical difference was seen in the toxicities of Zn and Cd when compared to either the Dark treatment or the PAR treatment. The Cu treatment with PAR/UV-A light showed a 6 fold increase in toxicity from PAR to PAR/UV-A. Most studies done using Cu and actinic radiation focused on UV-B light, however UV-B light does not penetrate as deep into the water column as UV-A and PAR (A-H-Mackerness et al. 1999, Babu et al. 1999:2003). These studies also show that full spectrum SSR (PAR/UV-A/UV-B) causes a large increase in toxicity when compared to that of PAR lighting on average a 10 fold increase in toxicity. These studies also suggest that UV-B is responsible for the large increase in toxicity and that UV-A

contributes relatively little to the toxic effects. PAR/UV-A data presented in this thesis suggests that some of the toxicity of Cu under full SSR radiation is likely due to UV-A mechanism and that it cannot be discounted. The slopes of the Cu concentration response curves all show different slopes. This indicates that they each have a distinct mechanism of toxicity.

Ni was also found to become more toxic with the addition of UV-A resulting in a 60% increase in toxicity over the PAR treatment, from an EC50 of 2691 nM to1761 nM. This increase is also surprising as most studies done on Ni/UV focus on the toxicity of UV-B via a redox cycling mechanism. These studies suggest that UV-A has a negligible effect on metal toxicity (Lynn et al. 1997, Huang et al. 2001). However with Ni the concentration response curves show very similar slopes in the PAR/UVA and SSR regimes. This likely indicates that the PAR/UVA and SSR treatments are both caused by a similar toxicity mechanism. These findings with Ni toxicity indicate that UV-A has a substantial impact and is likely acting in a similar fashion to that of UV-B.

The exposure to full spectrum simulated solar radiation (SSR) caused no statistical change in EC50s for Cd and Zn. This result is not surprising as Cd is intrinsically toxic at low concentrations (Watanabe and Suzuki 2001, Bolduc et al. 2004) and the toxicity of Zn has not been shown to be influenced any kind of actinic radiation (Gouvea et al. 2008). Both of the redox active metals showed a marked increase in toxicity from that of the PAR/UV-A treatments. Cu, when exposed to full SSR, increased in toxicity by a factor of 10. This result is similar to that in the literature, which shows that Cu toxicity increases when exposed to UV-B light in other organisms (A-H-Mackerness et al. 1999, Babu et al. 2003, Gouvea et al. 2008). However, based on the results from the PAR/UV-

A treatment, the potential impact of UV-A toxicity cannot be discounted. Previous studies do not consider UV-A as a contributor to Cu toxicity as UV-A does not penetrate deep into the water column. *Hyalella azteca* and many other aquatic organisms live in the littoral zone around lakes, where the water is shallow enough for UV-A light to penetrate. As such, when future ecological risk assessment models are created to predict metal toxicity, the effects of UV-A on these systems should not be discounted.

All of the metals were found to exhibit some degree of toxicity to *Hyalella azteca*. Zn was found to be the least toxic of the chemicals, and the toxicity of Zn did not seem to be influenced at all by any amount of actinic radiation. The most toxic chemical across the dark and PAR/UVA treatments was found to be Cd. The toxicity of Cd was not affected at all by any change in levels of actinic radiation. This leads us to conclude that Cd is not photoactive under wavelengths of UVB to PAR (290 nm - 700 nm).

Cu was found to be toxic under all of the lighting treatments. The greatest toxicity for Cu was observed under the SSR treatment, which showed Cu to be the most toxic of the four metals tested under SSR. Cu was found to be photoactive, with the response to Cu increasing in toxicity as the amount of actinic radiation increased, from dark through PAR, PAR/UVA to SSR. Ni was found to have moderate toxicity across all four treatments. The toxicity of Ni increased at the amount of actinic radiation increased, however the addition of UVB in the SSR treatment showed no statistically significant increase in toxicity over that of the PAR/UVA treatment. Therefore it can be said that Cu and Ni are photoactive. It can also be said that Cu phototoxicity is affected by PAR, UVA and UVB radiation. Ni phototoxicity however is likely only affected by PAR and UVA.

When developing environmental contaminant guidelines, it is important to ensure that the contaminant impact is properly assessed. The data presented here supports the need to regulate contaminants not only by their nominal toxicity data but also by their potential toxicities in combination with other environmental stressors.

Chapter 4

Effects of PAH and Metal Mixtures on *Hyalella azteca*

4.0 Introduction

Polycyclic aromatic hydrocarbons (PAHs) and metals are common environmental contaminants, often found together as mixtures (CEPA 1999, Gurst et al. 2005, Tabak et al. 2005). Contamination in most aquatic environments is primarily due to anthropogenic sources, such as steel production and petroleum refining. These processes often discharge large amounts of contaminants including PAHs, metals, and PCBs into lakes and rivers. In the water column PAHs are usually associated with particulate matter; however, when exposed to sunlight, some PAHs can undergo photomodification, becoming more water soluble and more bioavailable (McConkey et al. 1997, Huang et al. 1997, Mallakin et al. 1999, Lehto et al.2003, Lampi et al. 2005). Furthermore, when exposed to sunlight, PAHs are active photosensitizers, and can produce ROS, which are can disrupt biological membranes (Foote 1968, Foote 1991, Xia et al. 2004). Metals are also associated with particulate matter and have been shown to be toxic at environmentally relevant levels (Babu et al. 2003, Borgmann et al. 2005, Gurst et al. 2005, Xie et al. 2006:2007). Metals vary in their toxicity mechanisms, many of which (Cd, Cu, Ni, Fe) have been linked to ROS production (Babu et al. 2003, Bolduc et al. 2004, Doig and Liber 2006, Xie et al. 2007).

Co-contamination of aquatic environments with PAHs and metals makes studying their potential interactions of high priority. In particular, studies on these interactions need to be conducted on a keystone species. A Benthic invertebrate like *Hyalella azteca* is an ideal model organism, as they are primary heterotrophs and play an important role

in the recycling of organic matter in many ecosystems. *Hyalella azteca* is also relatively stationary in their habitat and do not typically travel more than 20 m from where they were hatched, and thus will have constant exposure to a given contaminant mixture over their lifetime (Kruschwitz 1978).

PAHs and metal mixtures have been shown to have increased toxicity over that of either contaminant alone. Xie et al. (2005) found that mixtures of Cu and PHQ resulted in the production of ROS and a greater than additive toxicity to *Daphnia magna*. A study performed by Babu et al (2001) found that mixture of Cu and 1,2-dihydroxyanthraquinone lead to the formation of ROS and redox cycling in *Lemna gibba*. They also showed that the redox cycling in these mixtures showed synergistic toxicity compared to the toxicity of either contaminant alone (Babu et al. 2001;2003). Xie et al. (2007) found that mixtures of Cd/PHQ did not lead to ROS formation and that mixtures of Ni/PHQ did. Wilcoxen et al. (2003) found that adding UV-B light to *Hyalella azteca* in the presence of flouranthene increased the toxicity of the PAH. Despite the data available on other organisms, there have been no studies performed on the interactions of metals and PAHs under actinic radiation with *Hyalella azteca*. The potential for interactions in the presence of sunlight are immense, as sunlight usually increases the toxicity of these compounds. Without these studies the toxicity of these mixtures might be overlooked, leading to an underestimation of risk. The PAHs chosen in for this study were ANT, ATQ, and 1-hATQ. These PAHs were chosen based on their similar structures and the large amount of data already known about their response to actinic radiation. Cu, Cd, Ni, and Zn were chosen based on their differing redox states and the large amount of toxicity data in the literature. In this chapter, the effects of mixtures of

metals and PAHs to *Hyalella azteca*, in the presence of varying spectra of light were examined, in an attempt to asses the potential impact of these chemicals as a mixture.

4.1 Materials and Methods

Four metals (Cu, Cd, Ni, Zn) and three PAHs (ANT, ATQ, 1-hATQ) were tested using metal concentrations based on the data obtained in Chapter 2 and Chapter 3. Assay conditions were kept the same as in the 96h PAH assay and the 96h Metal Assay (Chapter 2 and Chapter 3). These mixtures were tested under 2 PAR (400-700 nm) and SSR (290-320 nm) lighting using a 16:8h light:dark cycle and a darkness treatment. The PAR/UV-A lighting regime was excluded form this assay, because most metals did not show an increase in toxicity under PAR/UV-A lighting compared to that of the PAR treatment, and therefore the results of PAH/Metals assay under PAR/UV-A light would likely resemble that of the PAH PAR treatments. For these assays, the metal concentrations were kept constant at one of four levels (1, 10, 100 or 1000 nM) while the PAH concentration was varied over 7 different concentrations. These concentrations were based on EC50s found during previous studies. Each treatment was performed in quadruplicate and repeated when necessary. The metal concentrations used were based on the toxicity data from previous experiments (Section 3.1 – Metal 96h Toxicity Test). The three PAH concentrations used were chosen based on previous experimental data (Section 2.1.2 – PAH 96h Phototoxicity Assay). The *Hyalella azteca* were grown and maintained under the same conditions described in section 2.1.1 – Test Organisms. The lighting conditions were the same as described in section 2.1.3 – Lighting Sources, with the exception that PAR/UV-A lighting was excluded from the treatments.

4.1.1 Data Analysis

Analysis of the data was performed as described in section 2.1.4. Additionally the effects of the mixtures based on the previous two experiments were analyzed by response addition as described by Norwood et al. (2003) and concentration addition as described in Sorensen et al. (2007). In response addition, the effects of each of the individual components are analyzed and the predicted effect of the mixture is generated. The two chemicals are assumed to act additively such that the actual effect of the mixture will equal the sum of the effects of each of the individual components added together. The metals based on the previous data in chapter 3 were assumed to have no measurable toxic effect below 10 nM and as a result the predicted values for metal concentrations of 1 nM and 10 nM reflect this. If the effect of the mixture was statistically greater than that of the predicted effect, the mixture is said to be synergistic. If the effect of the mixture was statistically smaller than that predicted it is said to be antagonistic. If the effects were not statistically different from that of the predicted value it is said to be additive in toxicity. To determine predicted mortality, data from the two previous experiments was plotted into equation 4.1 with the PAH mortality being A and the metal mortality B. If the effect of chemical A results in X% mortality and the effect of chemical B results in Y% mortality, then the predicted mortality of a given mixture (P_m) of chemicals A and B, can be calculated using equation 4.1 (Norwood et al. 2003).

Equation 4.1 $P_m = 1-(1-X/100)(1-Y/100)$

To analyze the mixture toxicity data further, a concentration addition model was also applied to the data; the model chosen for this was a two sided effect isobole model. This model allows us to graphically represent our data in an easily presentable manner. It

was used in this study because it allows use to clearly show when mixture toxicity is additive, synergistic and antagonistic. Based on this idea the basic model has chemical A plotted on the X axis and chemical B plotted on the Y axis. The EC50s of chemical A and chemical B are plotted on the graph and a strait line joining the EC50s is drawn. The 95% confidence intervals (C.I.) of each of the EC50s are then plotted and joined by dashed lines in a similar fashion. The EC50s of mixtures of PAH + metals are then plotted on the graph as a series and the resulting effects are easily read off the graph. If the data point is below the 95% C.I. of the additive line it is said to be synergistic in toxicity. If the point is above the 95% C.I. of the additive line it is said to be antagonistic in toxicity.

4.2 Results

The toxicity of metal/PAH mixtures under the different irradiation conditions were determined for *Hyalella azteca*. The mixtures consisted of one of four concentrations of metals (1, 10, 100, 1000 nM) with varying concentrations of PAH. The EC50s were determined using a logistic regression model as described in section 4.1.1 and are summarized in Tables 4.1-4.9. These results are displayed graphically in figures 4.1-4.8. The Isobolic mixture toxicity models are presented in figures 4.9-4.32. Most of the PAH/metal mixtures at low metal concentration (1 nM, 10 nM) showed EC50s that were very close to their PAH counterpart alone. Some mixtures were found to be synergistic, some and some additive and a few were antagonistic. The predicted values were then plotted and compared to those of the observed values, along with concentration response curves for the metal on its own and for the PAH on its own. The concentration response curves are shown for ANT + metals in figures 4.33 - 4.56. The concentration

Table 4.1: Predicted and observed mixture toxicity of ANT + Metals to *Hyalella azteca* under dark conditions.

Treatment	Dark Observed (*nM*) ± SD	Dark Predicted (*nM*)
ANT	4902 ± 169	N/A
ANT + 1 nM Cu	4302 ± 295	4902
ANT + 10 *nM* Cu	4518 ± 278	4902
ANT + 100 *nM* Cu	2056 ± 254	2890
ANT + 1000 nM Cu	537 ± 35.9	673
ANT + 1 nM Cd	3964 ± 692	4902
ANT + 10 nM Cd	491 ± 71.1	4902
ANT + 100 nM Cd	5.78 ± 1.19	AT
ANT + 1000 nM Cd	AT	AT
ANT + 1 nM Ni	4893 ± 407	4902
ANT + 10 *nM* Ni	4389 ± 98.8	4902
ANT + 100 *nM* Ni	3894 ± 187	3874
ANT + 1000 nM Ni	1259 ± 45.9	723
ANT + 1 nM Zn	4579 ± 509	4902
ANT + 10 nM Zn	4374 ± 308	4902
ANT + 100 nM Zn	3925 ± 206	4139
ANT + 1000 nM Zn	1432 ± 96.5	1557

Each Experiment was repeated independently at least three times.

*AT = Acutely toxic at all concentrations of anthracene under given lighting conditions.

Table 4.2: Predicted and observed mixture toxicity of ANT + Metals to *Hyalella azteca* under PAR conditions.

Treatment	PAR Observed (*nM*) ± SD	PAR Predicted (*nM*)
ANT	108 ± 19.7	N/A
ANT + 1 nM Cu	122 ± 25.8	108
ANT + 10 *nM* Cu	103 ± 52.7	108
ANT + 100 *nM* Cu	23.6 ± 12.4	77.9
ANT + 1000 nM Cu	2.58 ± 0.56	8.68
ANT + 1 nM Cd	142 ± 51.6	108
ANT + 10 nM Cd	100 ± 41.6	108
ANT + 100 nM Cd	AT	AT
ANT + 1000 nM Cd	AT	AT
ANT + 1 nM Ni	102 ± 67.4	108
ANT + 10 *nM* Ni	84.2 ± 47.4	108
ANT + 100 *nM* Ni	76.9 ± 30.2	94.7
ANT + 1000 nM Ni	48.4 ± 12.6	34.1
ANT + 1 nM Zn	95.4 ± 34.7	108
ANT + 10 nM Zn	98.3 ± 20.4	108
ANT + 100 nM Zn	67.5 ± 18.8	102
ANT + 1000 nM Zn	30.6 ± 12.4	89.5

Each Experiment was repeated independently at least three times.

*AT = Acutely toxic at all concentrations of anthracene under given lighting conditions.

Table 4.3: Predicted and observed mixture toxicity of ANT + Metals to *Hyalella azteca* under SSR conditions.

Treatment	SSR Observed (*nM*) ± SD	SSR Predicted (*nM*)
ANT	4.87 ± 0.36	N/A
ANT + 1 nM Cu	4.56 ± 0.71	4.87
ANT + 10 *nM* Cu	0.89 ± 0.30	4.87
ANT + 100 *nM* Cu	AT	AT
ANT + 1000 nM Cu	AT	AT
ANT + 1 nM Cd	2.21 ± 0.31	4.87
ANT + 10 nM Cd	AT	4.87
ANT + 100 nM Cd	AT	AT
ANT + 1000 nM Cd	AT	AT
ANT + 1 nM Ni	5.12 ± 0.14	4.87
ANT + 10 *nM* Ni	2.08 ± 0.32	4.87
ANT + 100 *nM* Ni	1.64 ± 0.89	3.57
ANT + 1000 nM Ni	AT	AT
ANT + 1 nM Zn	8.72 ± 0.23	4.87
ANT + 10 nM Zn	4.37 ± 0.41	4.87
ANT + 100 nM Zn	3.25 ± 0.21	4.56
ANT + 1000 nM Zn	1.09 ± 0.53	4.37

Each Experiment was repeated independently at least three times.

*AT = Acutely toxic at all concentrations of anthracene under given lighting conditions.

Table 4.4: Predicted and observed mixture toxicity of ATQ + Metals to *Hyalella azteca* under dark conditions.

Treatment	Dark Observed (*nM*) ± SD	Dark Predicted (*nM*)
ATQ	1624 ± 192	N/A
ATQ + 1 *ηM* Cu	1284 ± 152	1624
ATQ + 10*ηM* Cu	1251 ± 62.6	1624
ATQ + 100 *ηM* Cu	203 ± 27.6	640
ATQ + 1000 *ηM* Cu	37.7 ± 8.69	112
ATQ + 1 *ηM* Cd	1671 ± 35.8	1624
ATQ + 10 *ηM* Cd	577 ± 79.4	1624
ATQ + 100 *ηM* Cd	AT	AT
ATQ + 1000 *ηM* Cd	AT	AT
ATQ + 1 *ηM* Ni	1428 ± 191	1624
ATQ + 10 *ηM* Ni	1145 ± 215	1624
ATQ + 100 *ηM* Ni	859 ± 61.7	1167
ATQ + 1000 *ηM* Ni	109 ± 16.8	434
ATQ + 1 *ηM* Zn	1797 ± 429	1624
ATQ + 10 *ηM* Zn	1587 ± 273	1624
ATQ + 100 *ηM* Zn	1467 ± 230	1359
ATQ + 1000 *ηM* Zn	899 ± 22.9	903

Each Experiment was repeated independently at least three times.

* AT = Acutely toxic at all concentrations of anthracene under given lighting conditions.

Table 4.5: Predicted and observed mixture toxicity of ATQ + Metals to *Hyalella azteca* under PAR conditions.

Treatment	PAR Observed (*nM*) ± SD	PAR Predicted (*nM*)
ATQ	188 ± 48.4	N/A
ATQ + 1 *ηM* Cu	179 ± 25.7	188
ATQ + 10*ηM* Cu	181 ± 62.2	188
ATQ + 100 *ηM* Cu	43.6 ± 81.9	129
ATQ + 1000 *ηM* Cu	AT	AT
ATQ + 1 *ηM* Cd	169 ± 77.8	188
ATQ + 10 *ηM* Cd	82.8 ± 54.3	188
ATQ + 100 *ηM* Cd	AT	AT
ATQ + 1000 *ηM* Cd	AT	AT
ATQ + 1 *ηM* Ni	154 ± 44.1	188
ATQ + 10 *ηM* Ni	146 ± 63.7	188
ATQ + 100 *ηM* Ni	62.7 ± 36.1	135
ATQ + 1000 *ηM* Ni	46.8 ± 8.92	89.4
ATQ + 1 *ηM* Zn	176 ± 78.8	188
ATQ + 10 *ηM* Zn	147 ± 62.8	188
ATQ + 100 *ηM* Zn	146 ± 42.9	145
ATQ + 1000 *ηM* Zn	30.7 ± 17.8	102

Each Experiment was repeated independently at least three times.

* AT = Acutely toxic at all concentrations of anthracene under given lighting conditions.

Table 4.6: Predicted and observed mixture toxicity of ATQ + Metals to *Hyalella azteca* under SSR conditions.

Treatment	SSR Observed (*nM*) ± SD	SSR Predicted (*nM*)
ATQ	142 ± 38.9	N/A
ATQ + 1 *ηM* Cu	164 ± 15.8	142
ATQ + 10*ηM* Cu	13.7 ± 6.17	23.5
ATQ + 100 *ηM* Cu	1.51 ± 0.71	AT
ATQ + 1000 *ηM* Cu	AT	AT
ATQ + 1 *ηM* Cd	89.8 ± 17.6	142
ATQ + 10 *ηM* Cd	7.62 ± 1.39	142
ATQ + 100 *ηM* Cd	AT	AT
ATQ + 1000 *ηM* Cd	AT	AT
ATQ + 1 *ηM* Ni	166 ± 45.6	142
ATQ + 10 *ηM* Ni	27.7 ± 3.56	118
ATQ + 100 *ηM* Ni	19.6 ± 2.63	34.5
ATQ + 1000 *ηM* Ni	4.81 ± 0.86	1.46
ATQ + 1 *ηM* Zn	169 ± 18.2	142
ATQ + 10 *ηM* Zn	146 ± 32.8	142
ATQ + 100 *ηM* Zn	139 ± 45.0	125
ATQ + 1000 *ηM* Zn	50.8 ± 12.5	59.2

Each Experiment was repeated independently at least three times.

* AT = Acutely toxic at all concentrations of anthracene under given lighting conditions.

Table 4.7: Predicted and observed mixture toxicity of 1-hATQ + Metals to *Hyalella azteca* under dark conditions.

Treatment	Dark Observed (*nM*) ± SD	Dark Predicted (*nM*)
1-hATQ	NT	N/A
1-hATQ + 1 *ηM* Cu	NT	NT
1-hATQ + 10*ηM* Cu	5473 ± 468	NT
1-hATQ + 100 *ηM* Cu	4667 ± 385	NT
1-hATQ + 1000 *ηM* Cu	1005 ± 98.2	2005
1-hATQ + 1 *ηM* Cd	5933 ± 607	NT
1-hATQ + 10 *ηM* Cd	1046 ± 47.8	NT
1-hATQ + 100 *ηM* Cd	AT	AT
1-hATQ + 1000 *ηM* Cd	AT	AT
1-hATQ + 1 *ηM* Ni	NT	NT
1-hATQ + 10 *ηM* Ni	NT	NT
1-hATQ + 100 *ηM* Ni	3954 ± 254	NT
1-hATQ + 1000 *ηM* Ni	1142 ± 189	4105
1-hATQ + 1 *ηM* Zn	NT	NT
1-hATQ + 10 *ηM* Zn	5830 ± 257	NT
1-hATQ + 100 *ηM* Zn	2854 ± 563	3982
1-hATQ + 1000 *ηM* Zn	756 ± 54.5	1547

Each Experiment was repeated independently at least three times.

* NT = Non Toxic at levels below maximum solubility of 8000 *η*M

* AT = Acutely toxic at all concentrations of anthracene under given lighting conditions.

Table 4.8: Predicted and observed mixture toxicity of 1-hATQ + Metals to *Hyalella azteca* under PAR conditions.

Treatment	PAR Observed (*nM*) ± SD	PAR Predicted (*nM*)
1-hATQ	332 ± 68.4	N/A
1-hATQ + 1 *ηM* Cu	310 ± 26.2	332
1-hATQ + 10*ηM* Cu	134 ± 31.4	332
1-hATQ + 100 *ηM* Cu	31.5 ± 11.8	50.4
1-hATQ + 1000 *ηM* Cu	AT	3.78
1-hATQ + 1 *ηM* Cd	348 ± 42.1	332
1-hATQ + 10 *ηM* Cd	138 ± 13.2	332
1-hATQ + 100 *ηM* Cd	AT	AT
1-hATQ + 1000 *ηM* Cd	AT	AT
1-hATQ + 1 *ηM* Ni	182 ± 35.6	332
1-hATQ + 10 *ηM* Ni	167 ± 27.6	332
1-hATQ + 100 *ηM* Ni	123 ± 16.9	150
1-hATQ + 1000 *ηM* Ni	67.2 ± 19.0	78.7
1-hATQ + 1 *ηM* Zn	341 ± 36.2	332
1-hATQ + 10 *ηM* Zn	289 ± 28.4	332
1-hATQ + 100 *ηM* Zn	183 ± 41.2	289
1-hATQ + 1000 *ηM* Zn	40.1 ± 12.7	189

Each Experiment was repeated independently at least three times.

* AT = Acutely toxic at all concentrations of anthracene under given lighting conditions.

Table 4.9: Predicted and observed mixture toxicity of 1-hATQ + Metals to *Hyalella azteca* under SSR conditions.

Treatment	SSR Observed (*nM*) ± SD	SSR Predicted (*nM*)
1-hATQ	24.4 ± 1.43	N/A
1-hATQ + 1 *ηM* Cu	38.5 ± 12.9	24.4
1-hATQ + 10*ηM* Cu	15.3 ± 3.64	24.4
1-hATQ + 100 *ηM* Cu	AT	3.67
1-hATQ + 1000 *ηM* Cu	AT	AT
1-hATQ + 1 *ηM* Cd	36.6 ± 8.92	24.4
1-hATQ + 10 *ηM* Cd	9.16 ± 2.62	24.4
1-hATQ + 100 *ηM* Cd	AT	AT
1-hATQ + 1000 *ηM* Cd	AT	AT
1-hATQ + 1 *ηM* Ni	30.6 ± 10.4	24.4
1-hATQ + 10 *ηM* Ni	27.1 ± 8.90	24.4
1-hATQ + 100 *ηM* Ni	16.1 ± 4.87	15.7
1-hATQ + 1000 *ηM* Ni	9.13 ± 2.01	5.38
1-hATQ + 1 *ηM* Zn	35.5 ± 3.29	24.4
1-hATQ + 10 *ηM* Zn	32.4 ± 6.34	24.4
1-hATQ + 100 *ηM* Zn	15.2 ± 2.73	23.8
1-hATQ + 1000 *ηM* Zn	9.76 ± 15.6	6.76

Each Experiment was repeated independently at least three times.

* AT = Acutely toxic at all concentrations of anthracene under given lighting conditions.

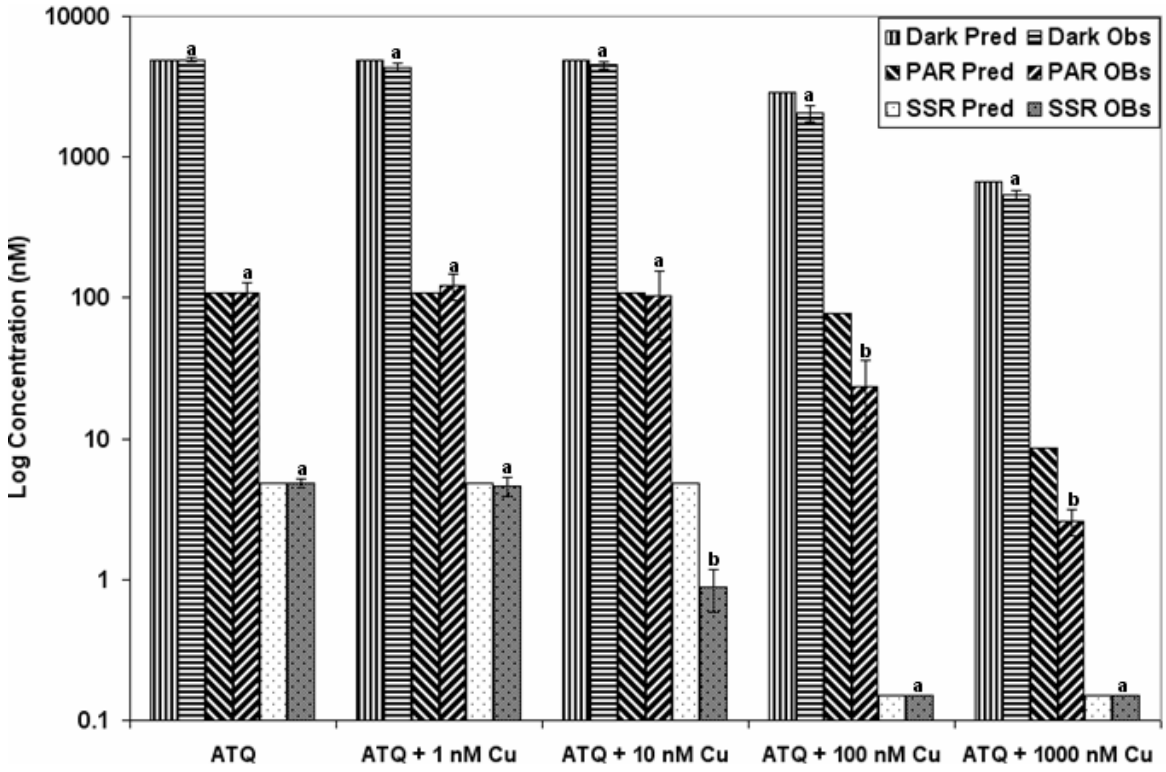

Figure 4.1 ANT + Cu mixture toxicity using response addition: predicted vs. observed. The data are EC50s mixtures of ANT with four concentrations of Cu. [a] Statistically identical to predicted value indicating additive toxicity. [b] Statistically different from the predicted value, indicating synergistic toxicity. [c] Statistically different from the predicted value, indicating antagonistic toxicity.

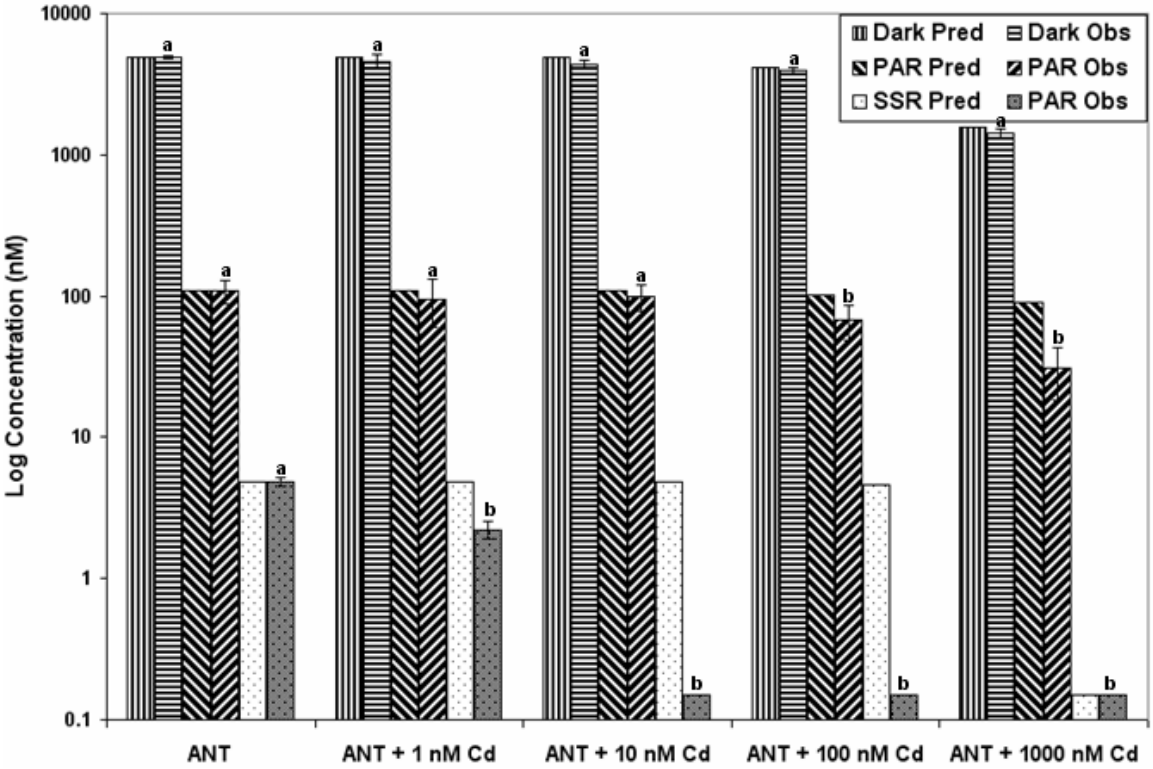

Figure 4.2 ANT + Cd mixture toxicity using response addition: predicted vs. observed. The data are EC50s mixtures of ANT with four concentrations of Ni. [a] Statistically identical to predicted value indicating additive toxicity. [b] Statistically different from the predicted value, indicating synergistic toxicity. [c] Statistically different from the predicted value, indicating antagonistic toxicity.

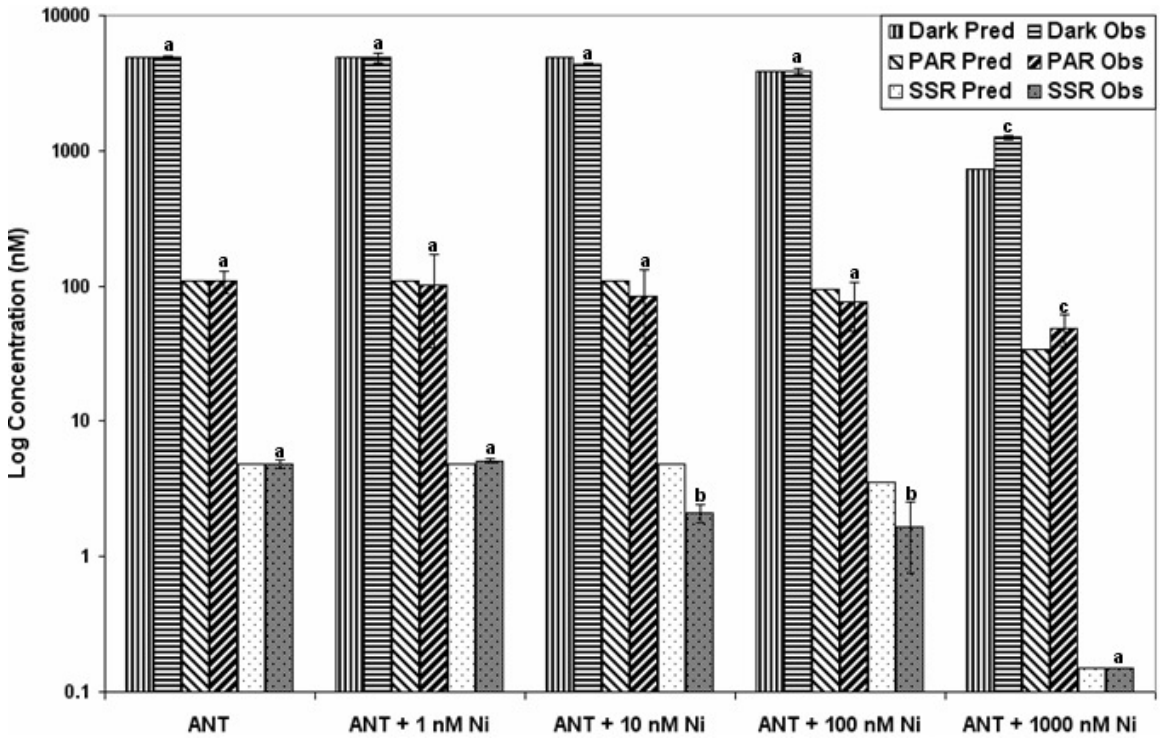

Figure 4.3 ANT + Ni mixture toxicity using response addition: predicted vs. observed. The data are EC50s mixtures of ANT with four concentrations of Ni. [a] Statistically identical to predicted value indicating additive toxicity. [b] Statistically different from the predicted value, indicating synergistic toxicity. [c] Statistically different from the predicted value, indicating antagonistic toxicity.

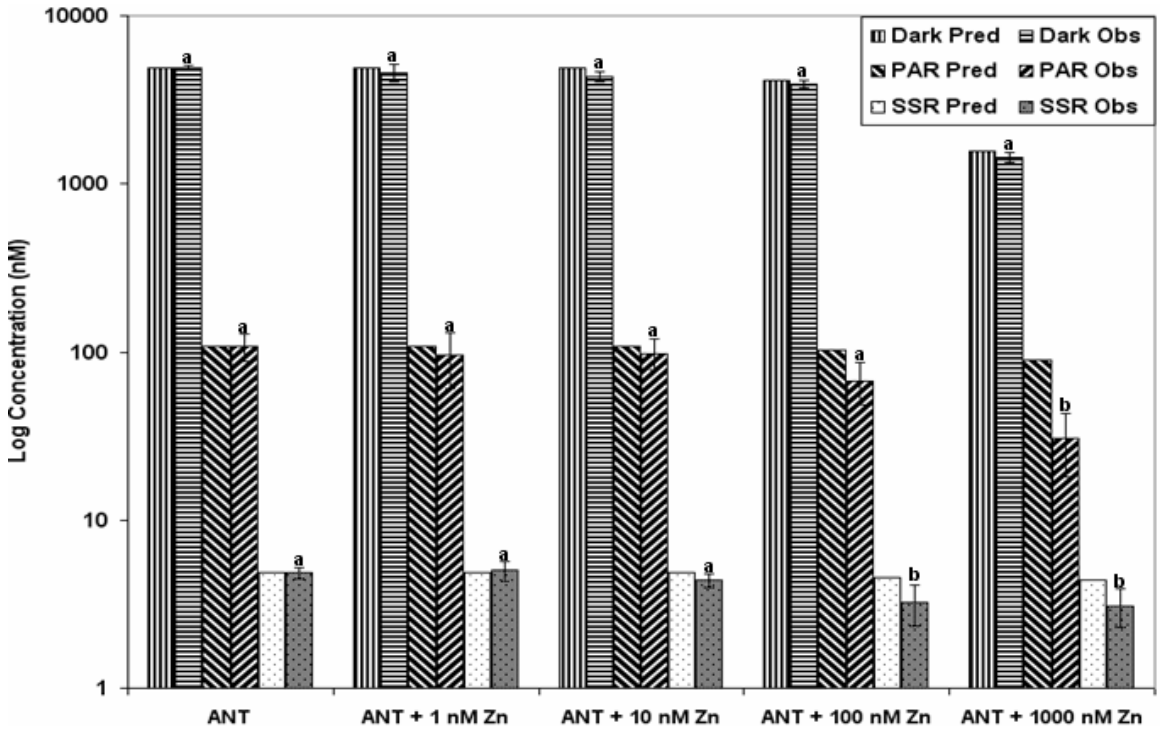

Figure 4.4 ANT + Zn mixture toxicity using response addition: predicted vs. observed. The data are EC50s mixtures of ANT with four concentrations of Zn. [a] Statistically identical to predicted value indicating additive toxicity. [b] Statistically different from the predicted value, indicating synergistic toxicity. [c] Statistically different from the predicted value, indicating antagonistic toxicity.

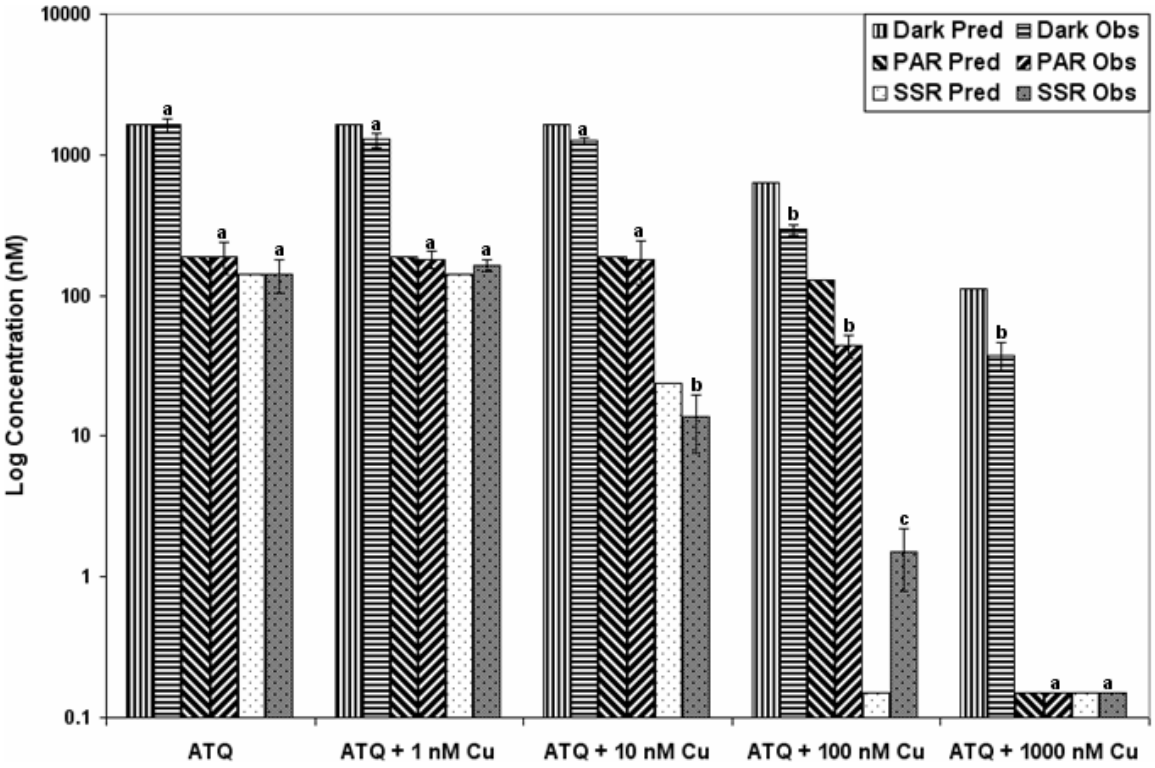

Figure 4.5 ATQ + Cu mixture toxicity using response addition: predicted vs. observed. The data are EC50s mixtures of ATQ with four concentrations of Cu. [a] Statistically identical to predicted value indicating additive toxicity. [b] Statistically different from the predicted value, indicating synergistic toxicity. [c] Statistically different from the predicted value, indicating antagonistic toxicity.

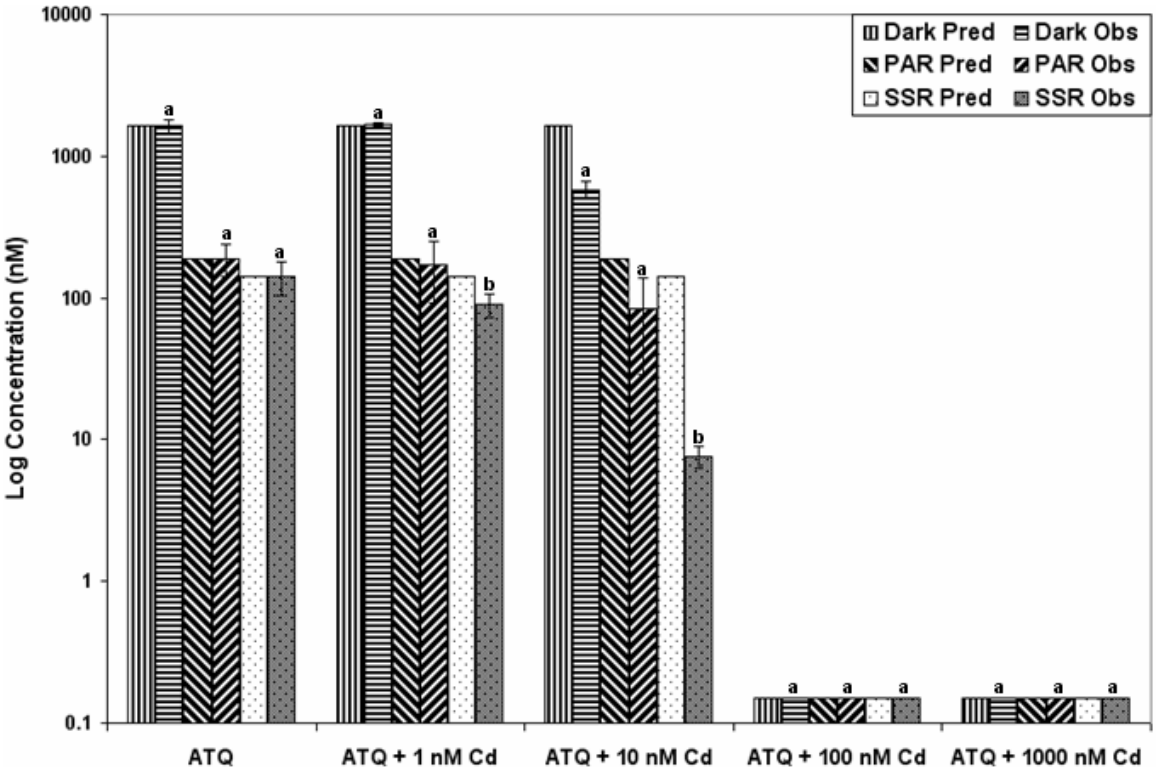

Figure 4.6 ATQ + Cd mixture toxicity using response addition: predicted vs. observed. The data are EC50s mixtures of ATQ with four concentrations of Cd. [a] Statistically identical to predicted value indicating additive toxicity. [b] Statistically different from the predicted value, indicating synergistic toxicity. [c] Statistically different from the predicted value, indicating antagonistic toxicity.

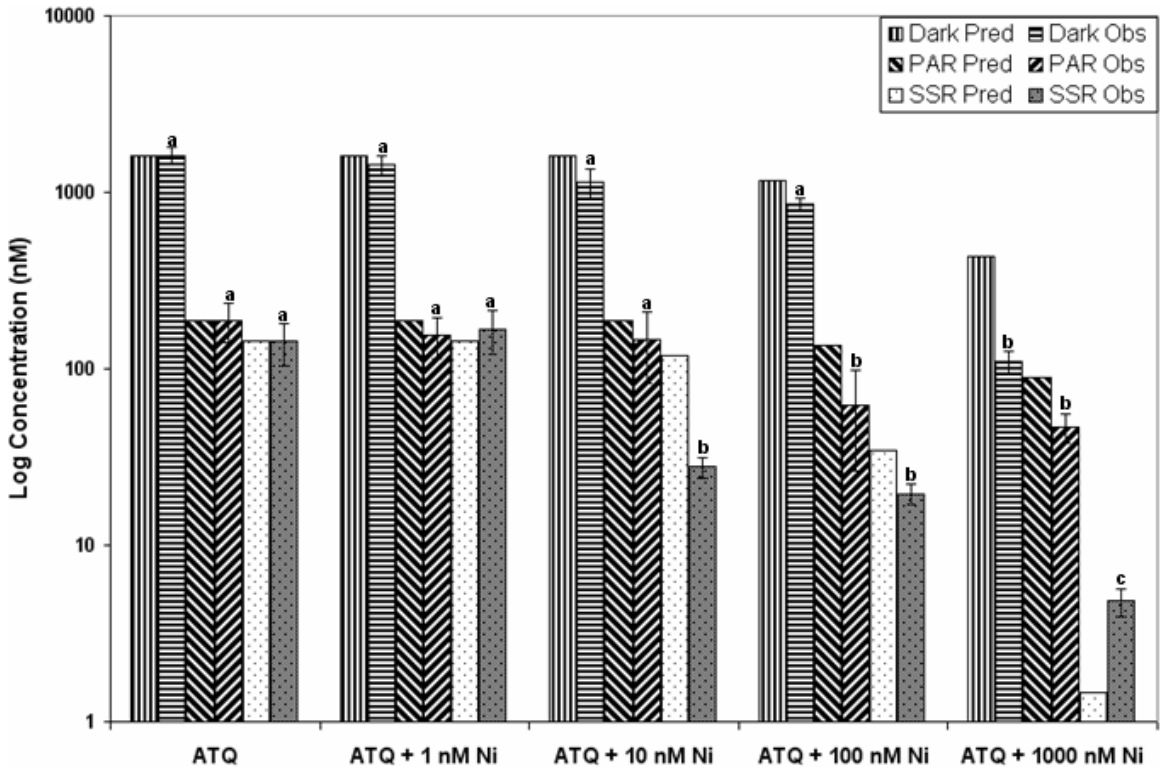

Figure 4.7 ATQ + Ni mixture toxicity using response addition: predicted vs. observed. The data are EC50s mixtures of ATQ with four concentrations of Ni. [a] Statistically identical to predicted value indicating additive toxicity. [b] Statistically different from the predicted value, indicating synergistic toxicity. [c] Statistically different from the predicted value, indicating antagonistic toxicity.

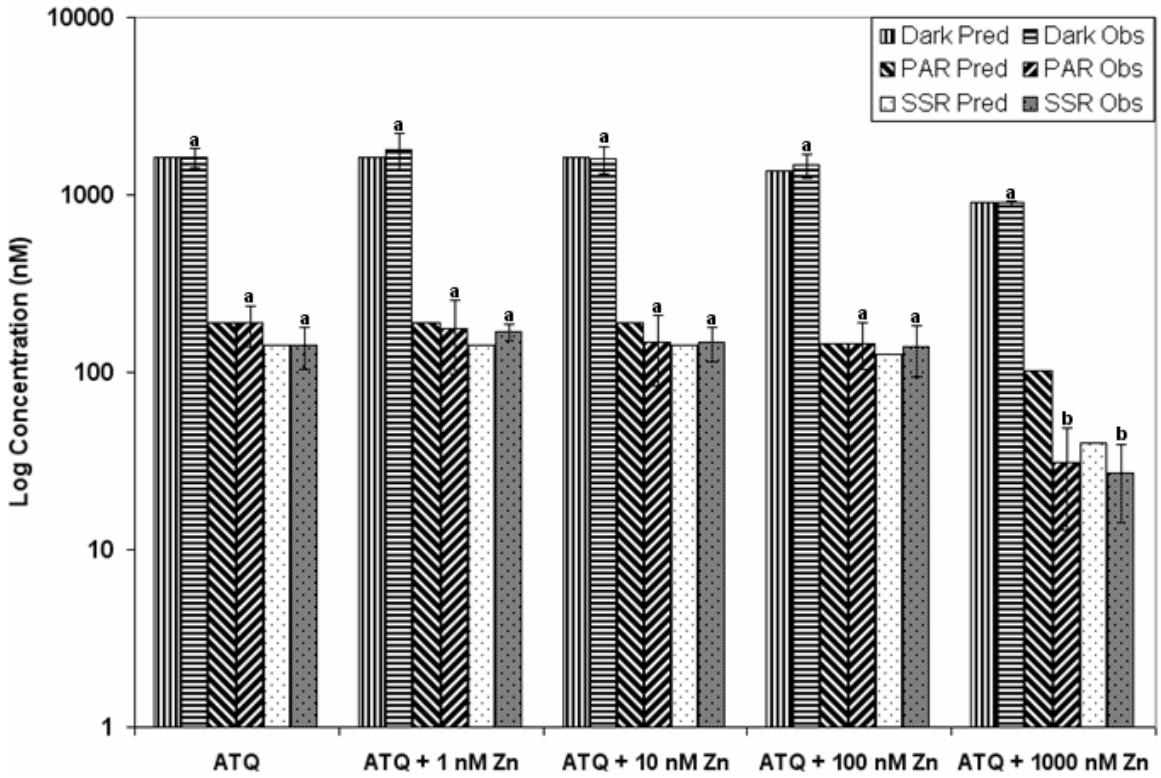

Figure 4.8 ATQ + Zn mixture toxicity using response addition: predicted vs. observed. The data are EC50s mixtures of ATQ with four concentrations of Zn. [a] Statistically identical to predicted value indicating additive toxicity. [b] Statistically different from the predicted value, indicating synergistic toxicity. [c] Statistically different from the predicted value, indicating antagonistic toxicity.

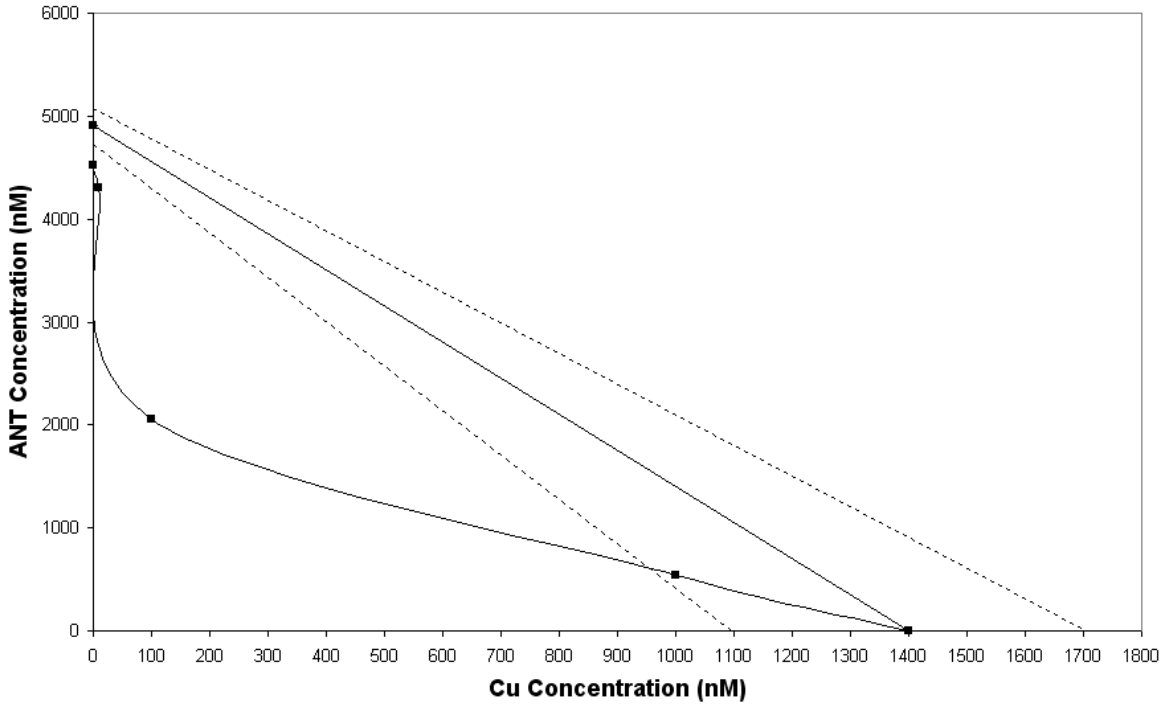

Figure 4.9 Isobologram for EC50s of binary mixtures of ANT + Cu under dark. Dotted lines represent 95% confidence intervals. EC50s of the varying mixtures of ANT + Cu were plotted on the isobologram with their 95% confidence limits. Within the 95% confidence intervals simple additive toxicity is observed. Points residing above, on, and under the lines indicate antagonistic, additive and synergistic toxicity respectively.

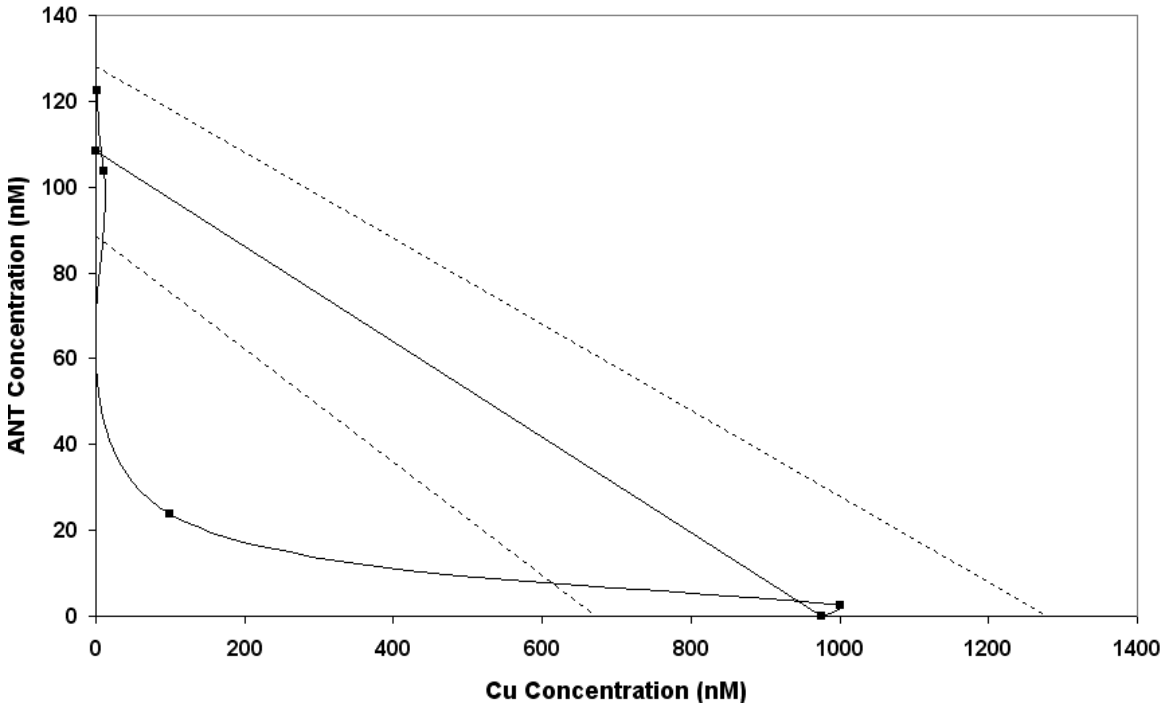

Figure 4.10 Isobologram for EC50s of binary mixtures of ANT + Cu under PAR. Dotted lines represent 95% confidence intervals. EC50s of the varying mixtures of ANT + Cu were plotted on the isobologram with their 95% confidence limits. Within the 95% confidence intervals simple additive toxicity is observed. Points residing above, on, and under the lines indicate antagonistic, additive and synergistic toxicity respectively.

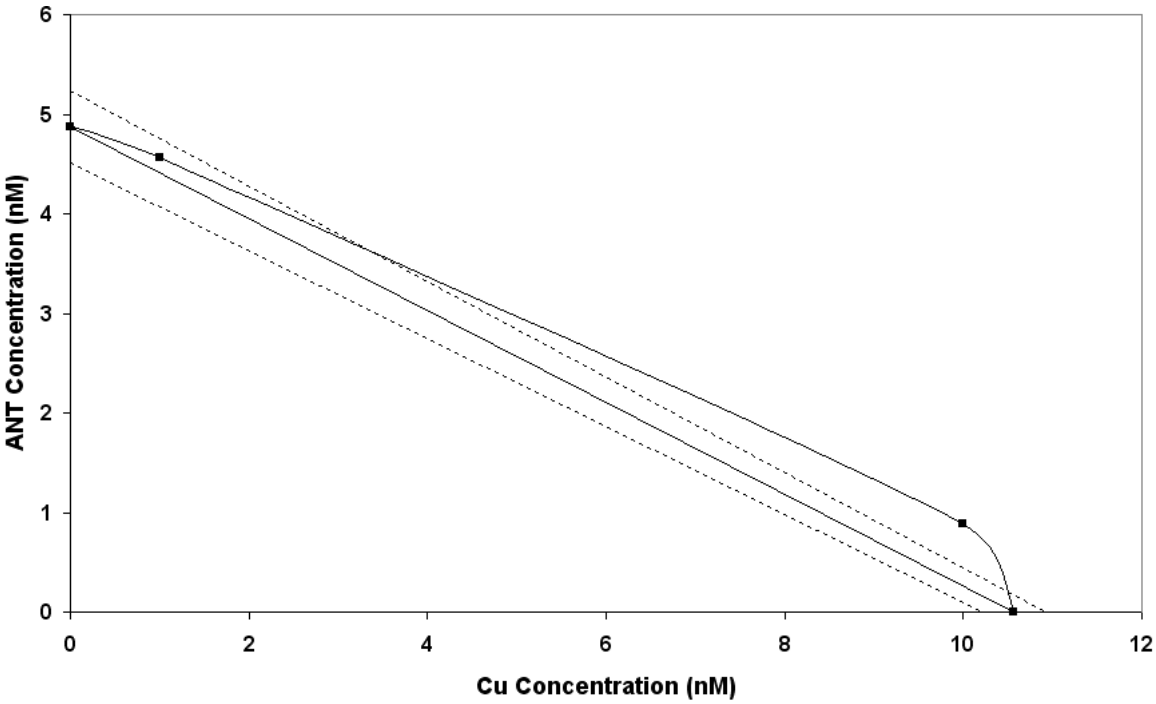

Figure 4.11 Isobologram for EC50s of binary mixtures of ANT + Cu under SSR. Dotted lines represent 95% confidence intervals. EC50s of the varying mixtures of ANT + Cu were plotted on the isobologram with their 95% confidence limits. Within the 95% confidence intervals simple additive toxicity is observed. Points residing above, on, and under the lines indicate antagonistic, additive and synergistic toxicity respectively.

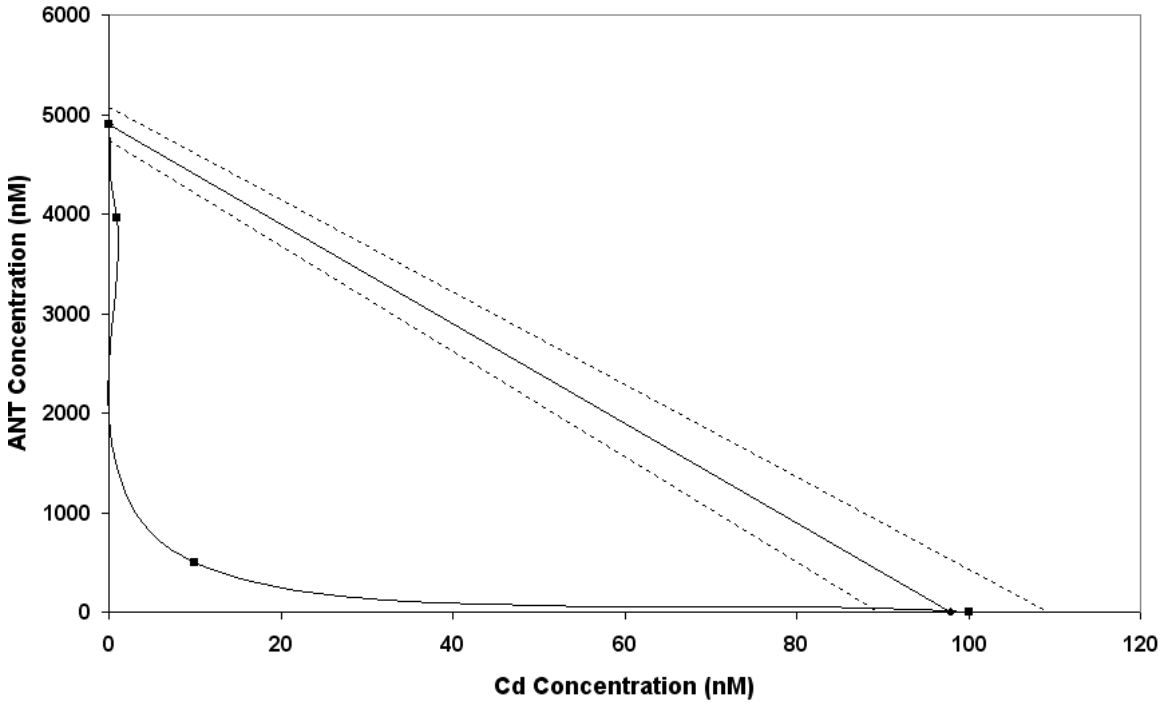

Figure 4.12 Isobologram for EC50s of binary mixtures of ANT + Cd under dark. Dotted lines represent 95% confidence intervals. EC50s of the varying mixtures of ANT + Cd were plotted on the isobologram with their 95% confidence limits. Within the 95% confidence intervals simple additive toxicity is observed. Points residing above, on, and under the lines indicate antagonistic, additive and synergistic toxicity respectively.

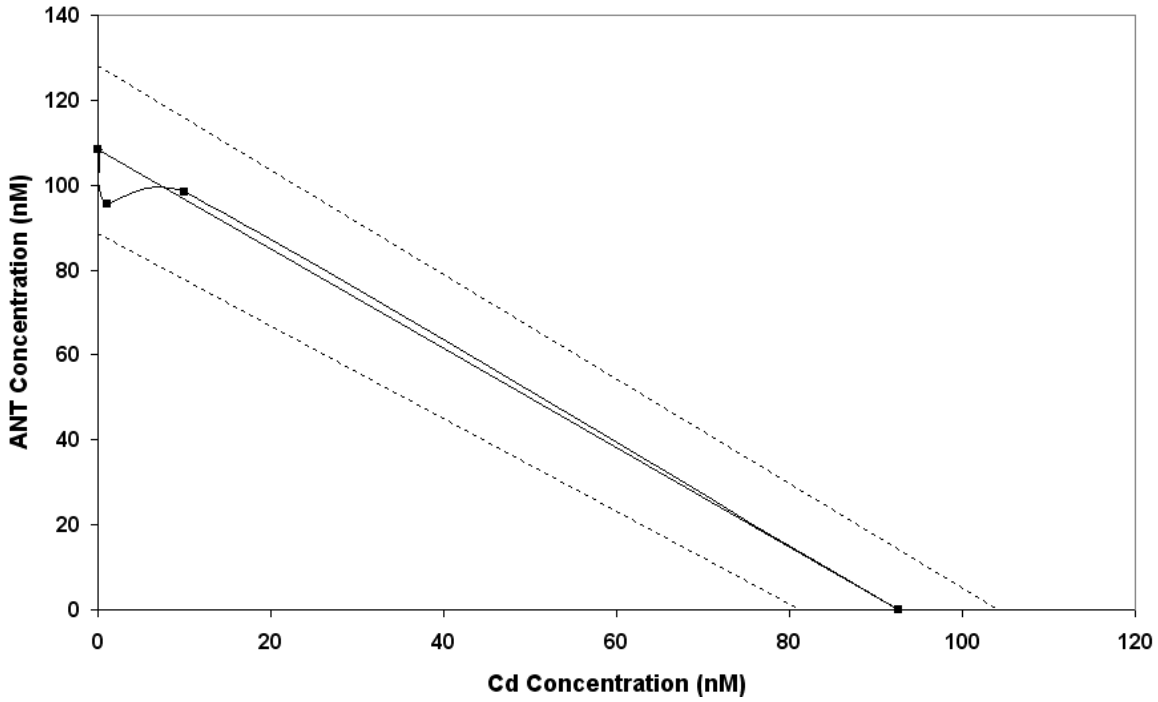

Figure 4.13 Isobologram for EC50s of binary mixtures of ANT + Cd under PAR. Dotted lines represent 95% confidence intervals. EC50s of the varying mixtures of ANT + Cd were plotted on the isobologram with their 95% confidence limits. Within the 95% confidence intervals simple additive toxicity is observed. Points residing above, on, and under the lines indicate antagonistic, additive and synergistic toxicity respectively.

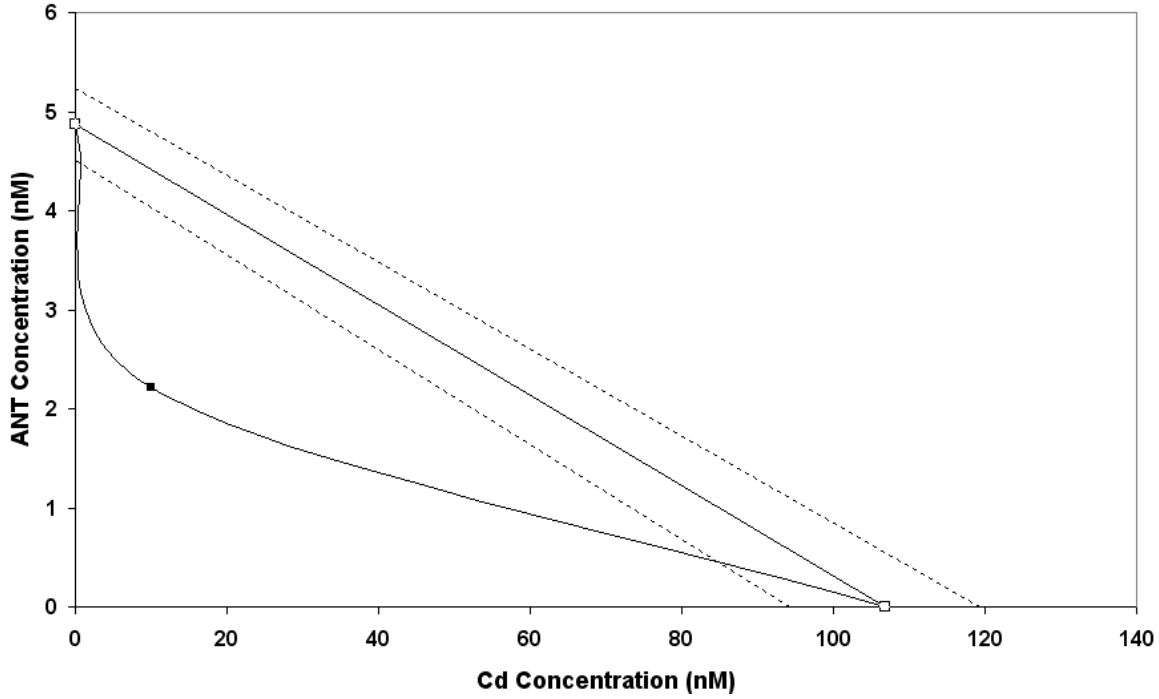

Figure 4.14 Isobologram for EC50s of binary mixtures of ANT + Cd under SSR. Dotted lines represent 95% confidence intervals. EC50s of the varying mixtures of ANT + Cd were plotted on the isobologram with their 95% confidence limits. Within the 95% confidence intervals simple additive toxicity is observed. Points residing above, on, and under the lines indicate antagonistic, additive and synergistic toxicity respectively.

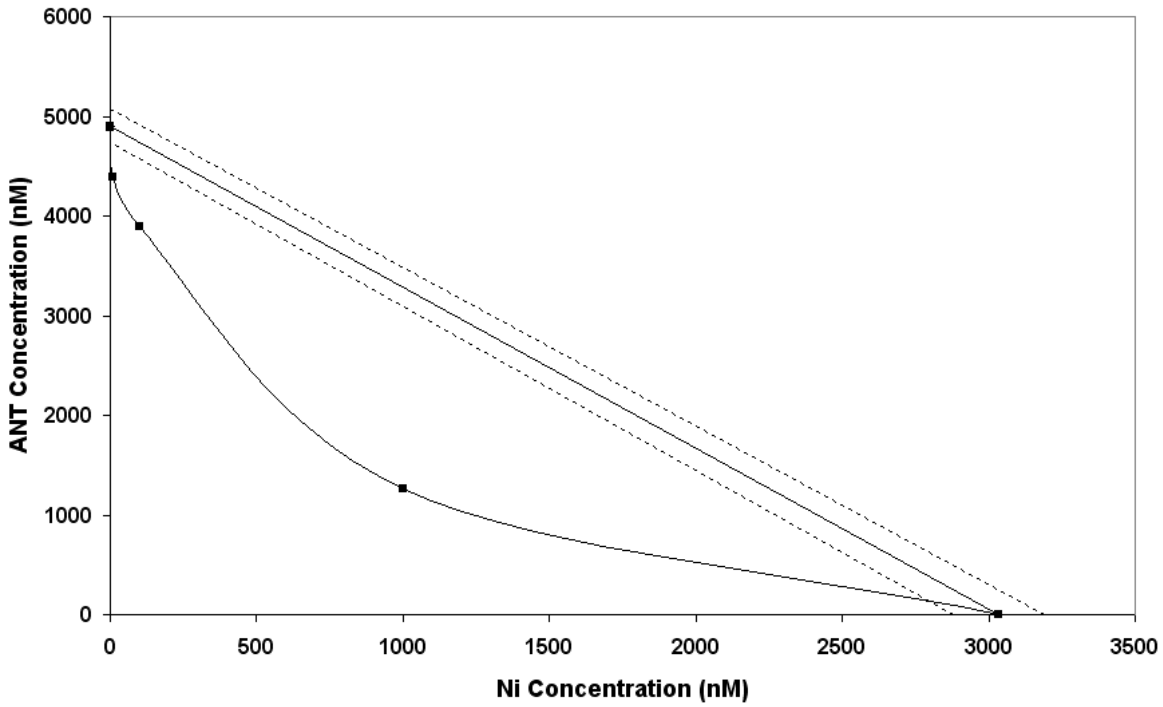

Figure 4.15 Isobologram for EC50s of binary mixtures of ANT + Ni under dark. Dotted lines represent 95% confidence intervals. EC50s of the varying mixtures of ANT + Ni were plotted on the isobologram with their 95% confidence limits. Within the 95% confidence intervals simple additive toxicity is observed. Points residing above, on, and under the lines indicate antagonistic, additive and synergistic toxicity respectively.

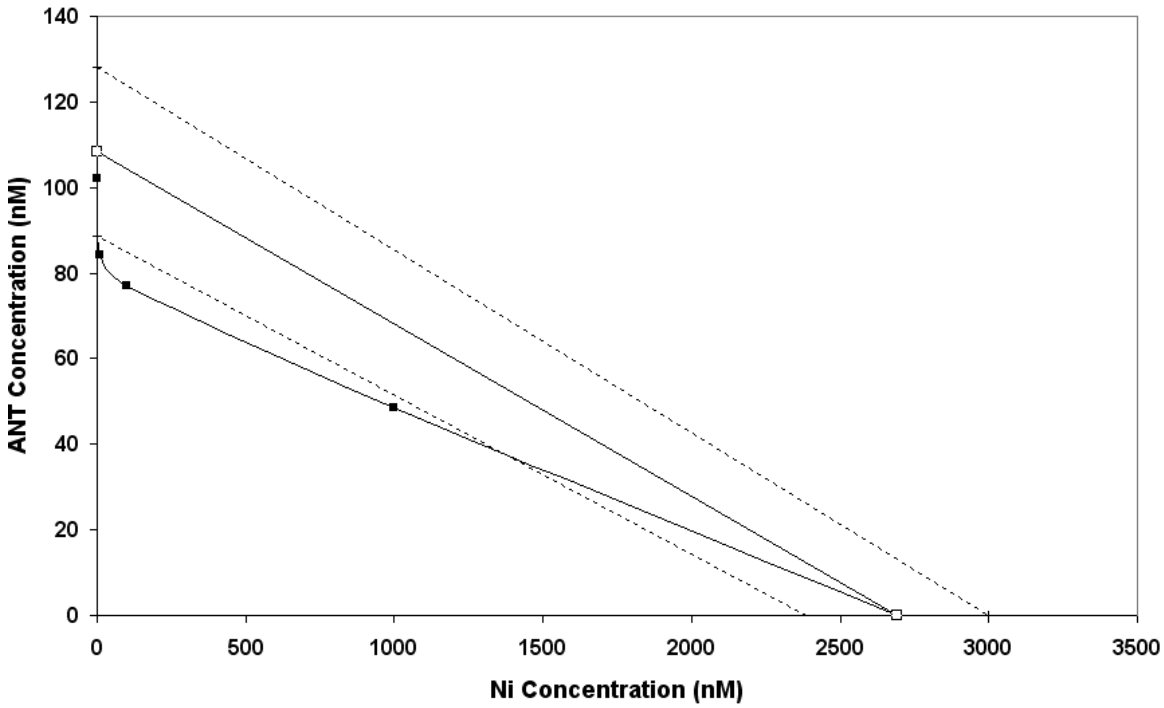

Figure 4.16 Isobologram for EC50s of binary mixtures of ANT + Ni under PAR. Dotted lines represent 95% confidence intervals. EC50s of the varying mixtures of ANT + Ni were plotted on the isobologram with their 95% confidence limits. Within the 95% confidence intervals simple additive toxicity is observed. Points residing above, on, and under the lines indicate antagonistic, additive and synergistic toxicity respectively.

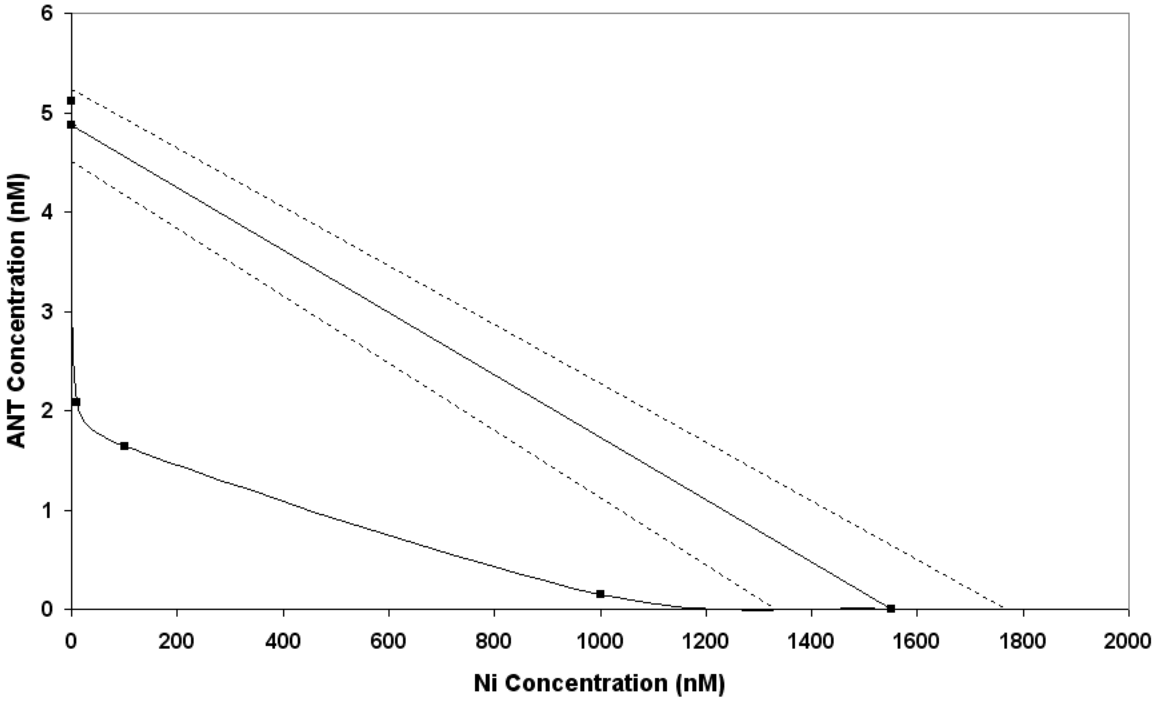

Figure 4.17 Isobologram for EC50s of binary mixtures of ANT + Ni under SSR. Dotted lines represent 95% confidence intervals. EC50s of the varying mixtures of ANT + Ni were plotted on the isobologram with their 95% confidence limits. Within the 95% confidence intervals simple additive toxicity is observed. Points residing above, on, and under the lines indicate antagonistic, additive and synergistic toxicity respectively.

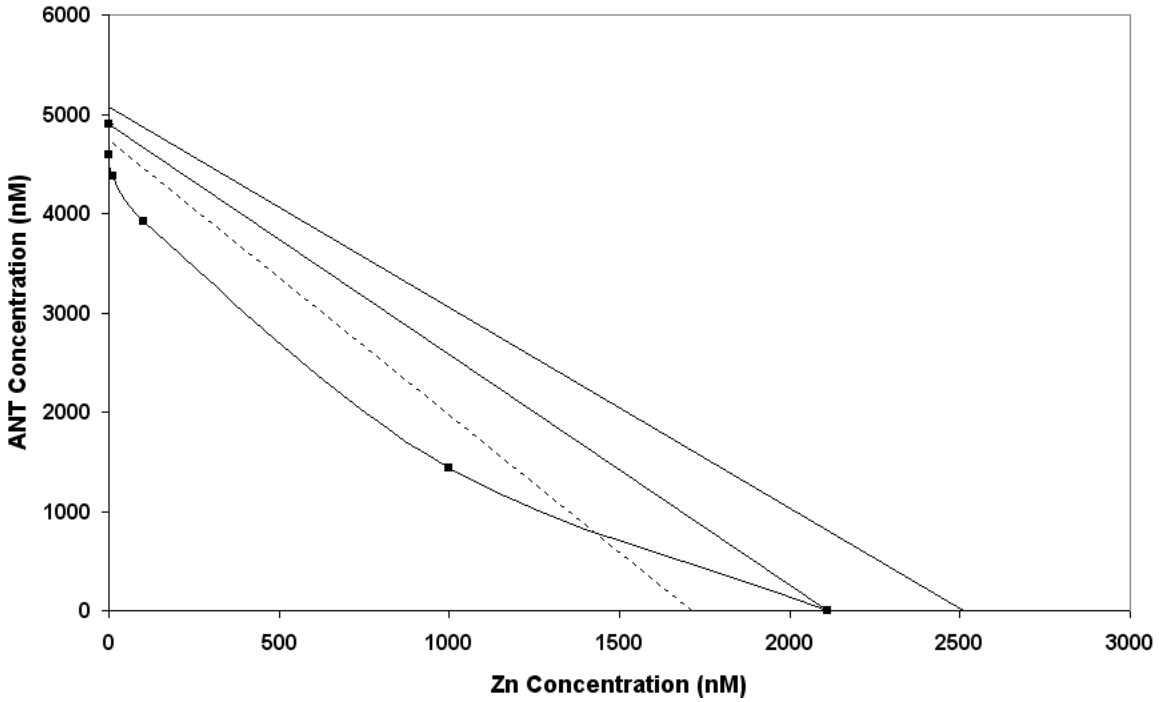

Figure 4.18 Isobologram for EC50s of binary mixtures of ANT + Zn under dark. Dotted lines represent 95% confidence intervals. EC50s of the varying mixtures of ANT + Zn were plotted on the isobologram with their 95% confidence limits. Within the 95% confidence intervals simple additive toxicity is observed. Points residing above, on, and under the lines indicate antagonistic, additive and synergistic toxicity respectively.

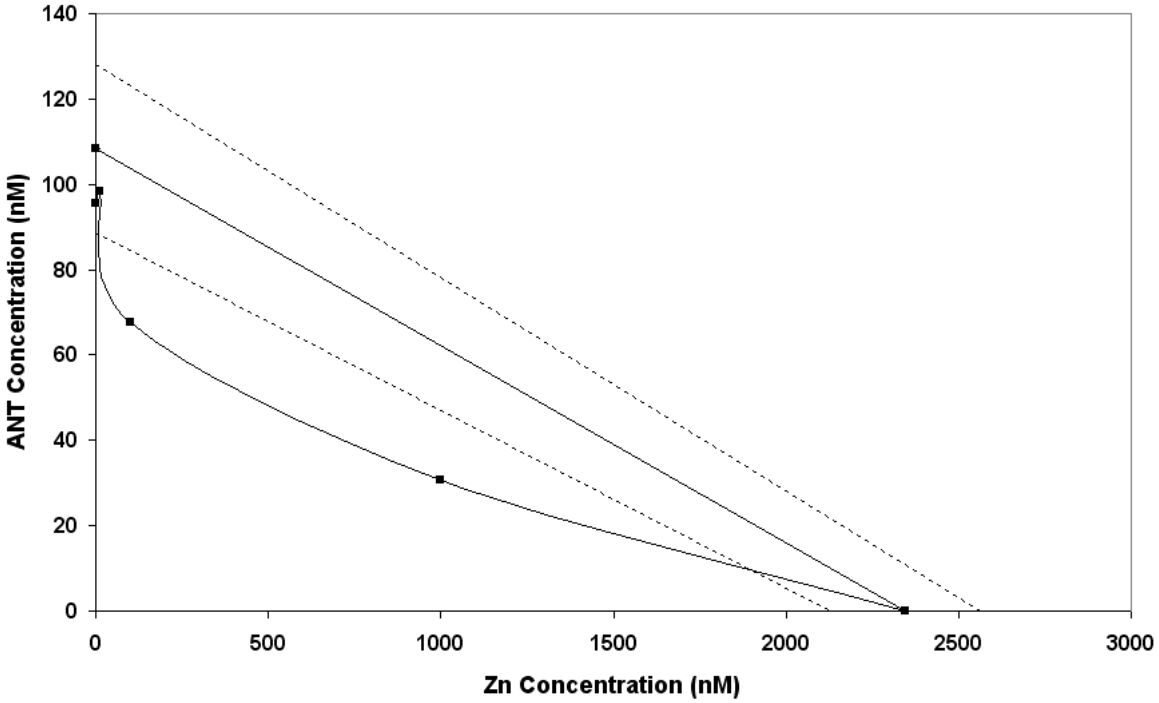

Figure 4.19 Isobologram for EC50s of binary mixtures of ANT + Zn under PAR. Dotted lines represent 95% confidence intervals. EC50s of the varying mixtures of ANT + Zn were plotted on the isobologram with their 95% confidence limits. Within the 95% confidence intervals simple additive toxicity is observed. Points residing above, on, and under the lines indicate antagonistic, additive and synergistic toxicity respectively.

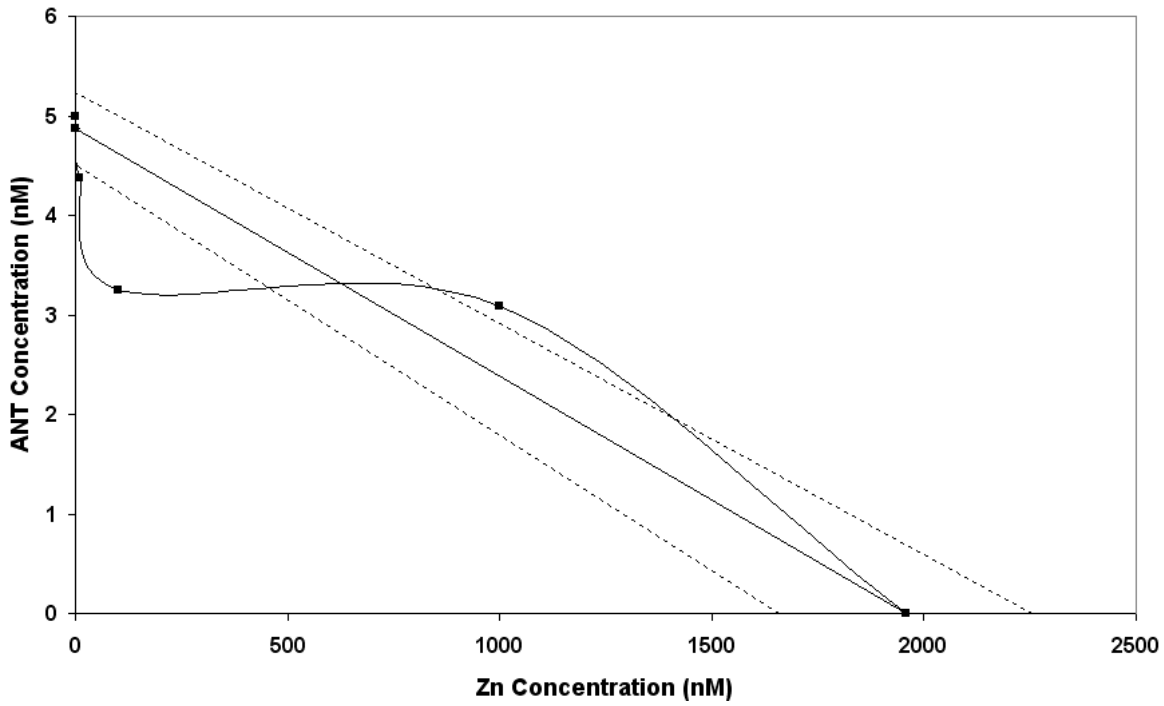

Figure 4.20 Isobologram for EC50s of binary mixtures of ANT + Zn under SSR. Dotted lines represent 95% confidence intervals. EC50s of the varying mixtures of ANT + Zn were plotted on the isobologram with their 95% confidence limits. Within the 95% confidence intervals simple additive toxicity is observed. Points residing above, on, and under the lines indicate antagonistic, additive and synergistic toxicity respectively.

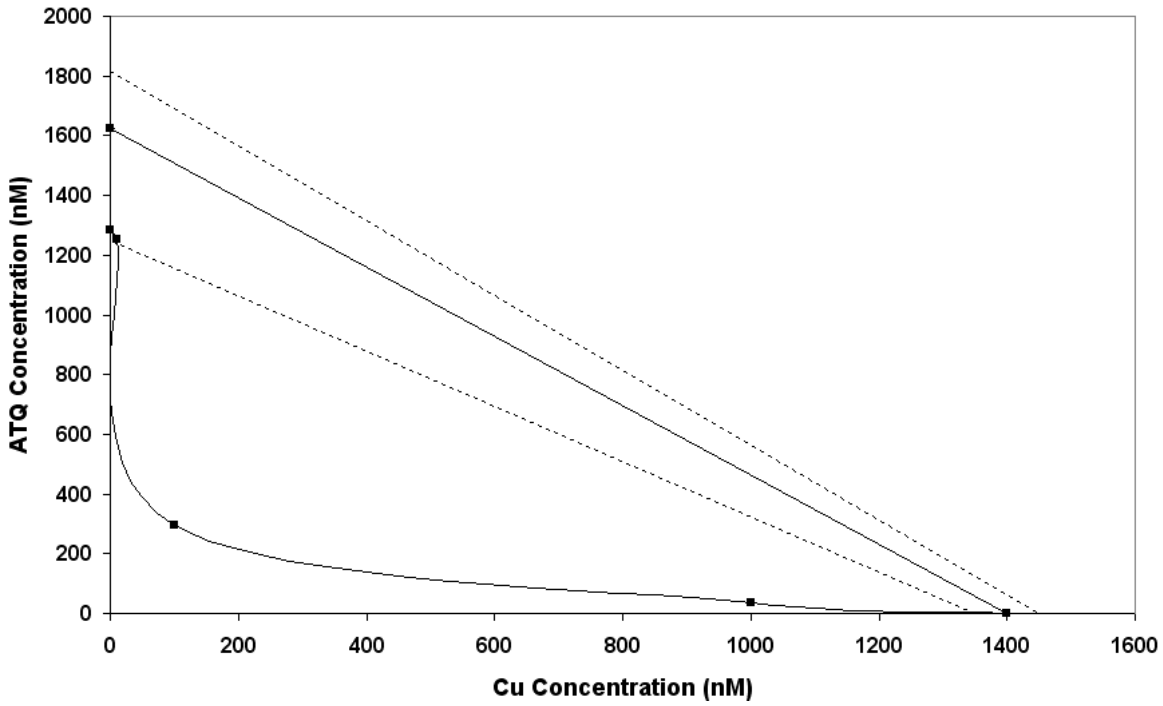

Figure 4.21 Isobologram for EC50s of binary mixtures of ATQ + Cu under dark. Dotted lines represent 95% confidence intervals. EC50s of the varying mixtures of ATQ + Cu were plotted on the isobologram with their 95% confidence limits. Within the 95% confidence intervals simple additive toxicity is observed. Points residing above, on, and under the lines indicate antagonistic, additive and synergistic toxicity respectively.

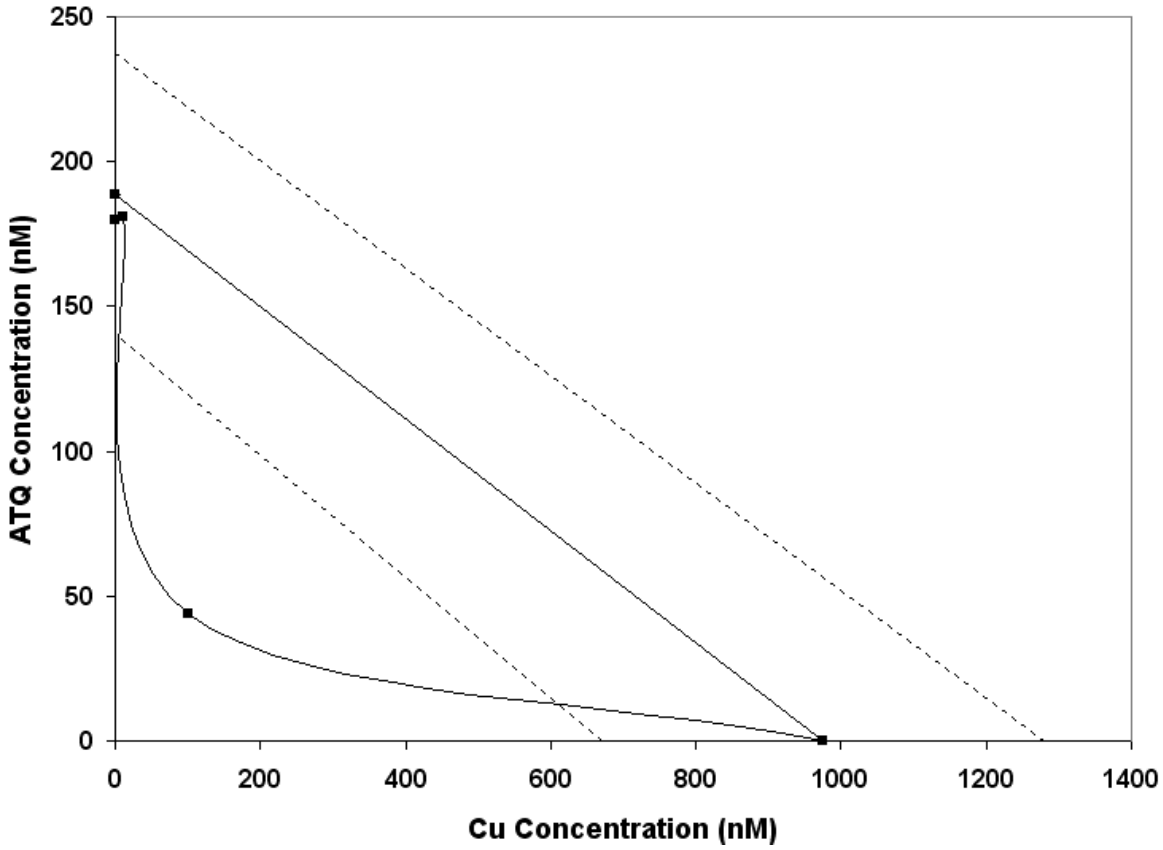

Figure 4.22 Isobologram for EC50s of binary mixtures of ATQ + Cu under PAR. Dotted lines represent 95% confidence intervals. EC50s of the varying mixtures of ATQ + Cu were plotted on the isobologram with their 95% confidence limits. Within the 95% confidence intervals simple additive toxicity is observed. Points residing above, on, and under the lines indicate antagonistic, additive and synergistic toxicity respectively.

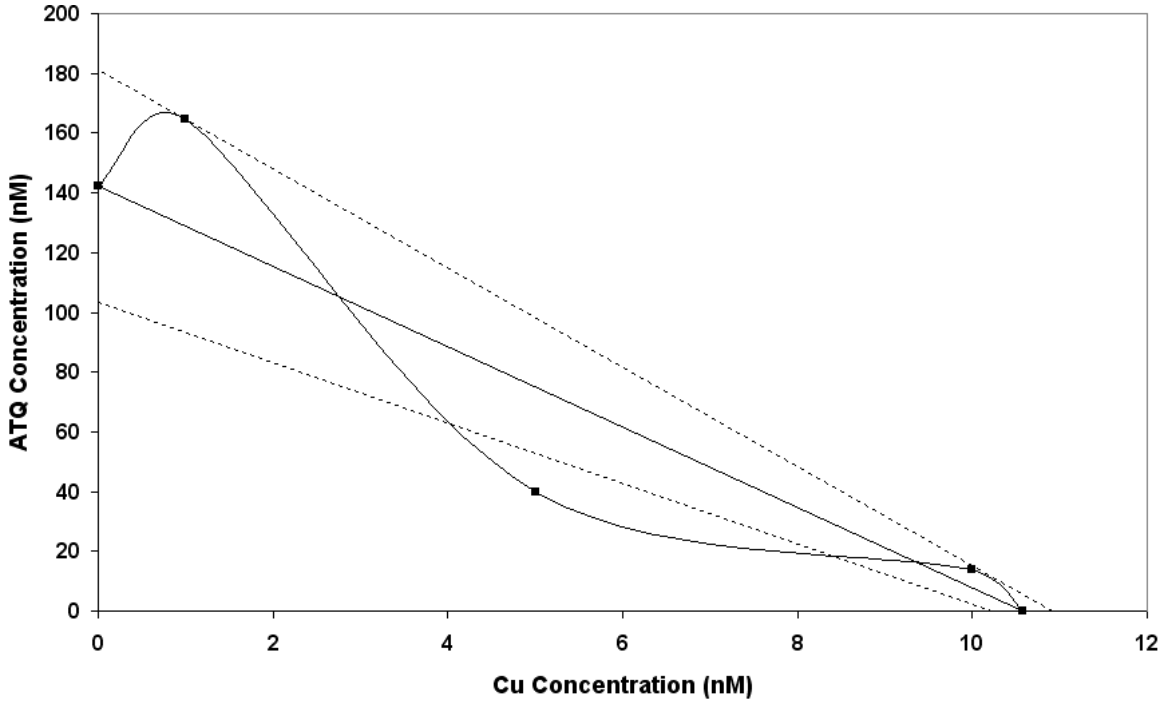

Figure 4.23 Isobologram for EC50s of binary mixtures of ATQ + Cu under SSR. Dotted lines represent 95% confidence intervals. EC50s of the varying mixtures of ATQ + Cu were plotted on the isobologram with their 95% confidence limits. Within the 95% confidence intervals simple additive toxicity is observed. Points residing above, on, and under the lines indicate antagonistic, additive and synergistic toxicity respectively.

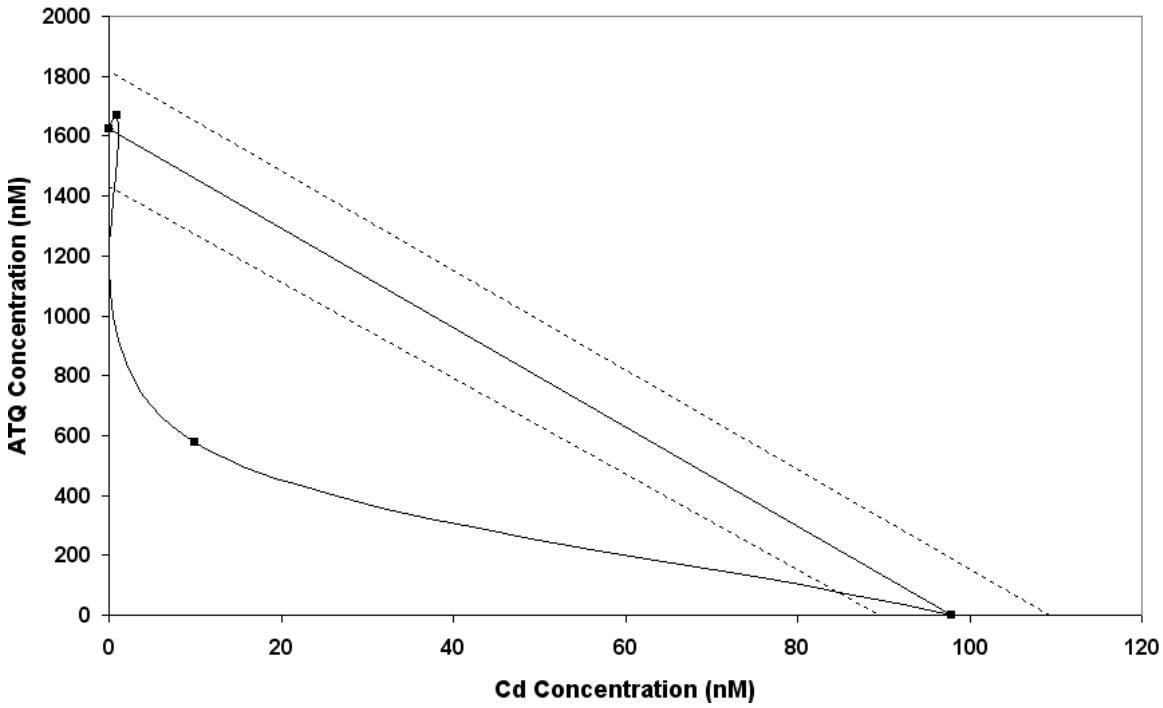

Figure 4.24 Isobologram for EC50s of binary mixtures of ATQ + Cd under dark. Dotted lines represent 95% confidence intervals. EC50s of the varying mixtures of ATQ + Cd were plotted on the isobologram with their 95% confidence limits. Within the 95% confidence intervals simple additive toxicity is observed. Points residing above, on, and under the lines indicate antagonistic, additive and synergistic toxicity respectively.

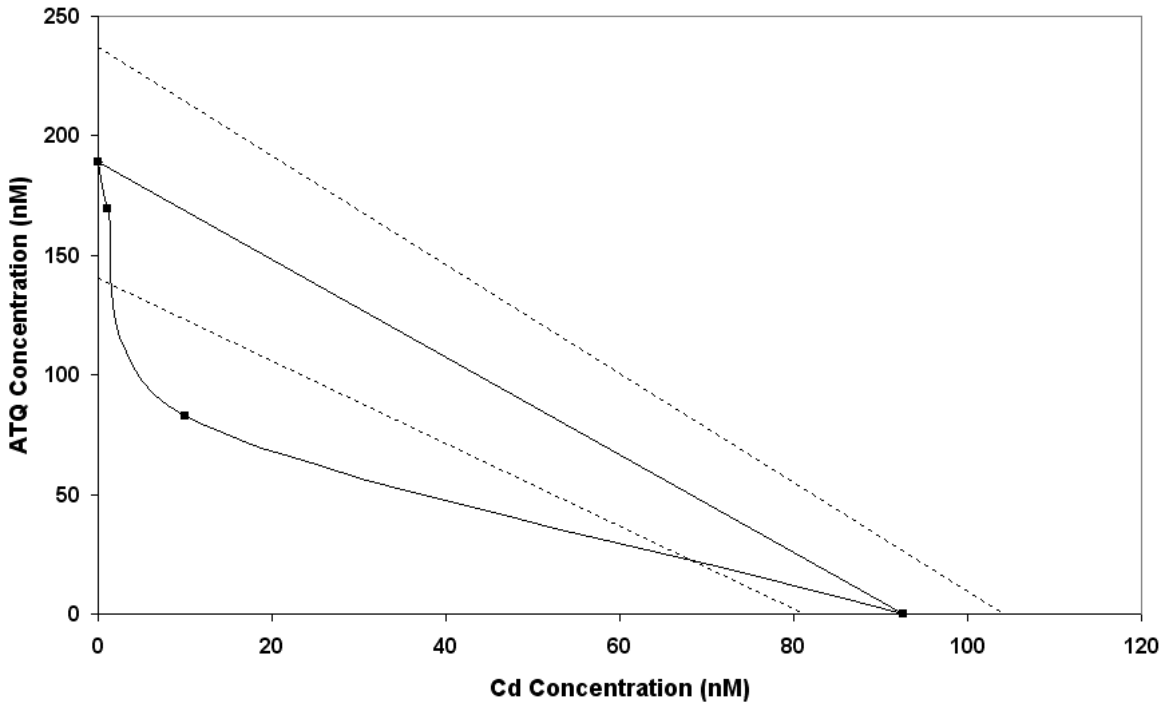

Figure 4.25 Isobologram for EC50s of binary mixtures of ATQ + Cd under PAR. Dotted lines represent 95% confidence intervals. EC50s of the varying mixtures of ATQ + Cd were plotted on the isobologram with their 95% confidence limits. Within the 95% confidence intervals simple additive toxicity is observed. Points residing above, on, and under the lines indicate antagonistic, additive and synergistic toxicity respectively.

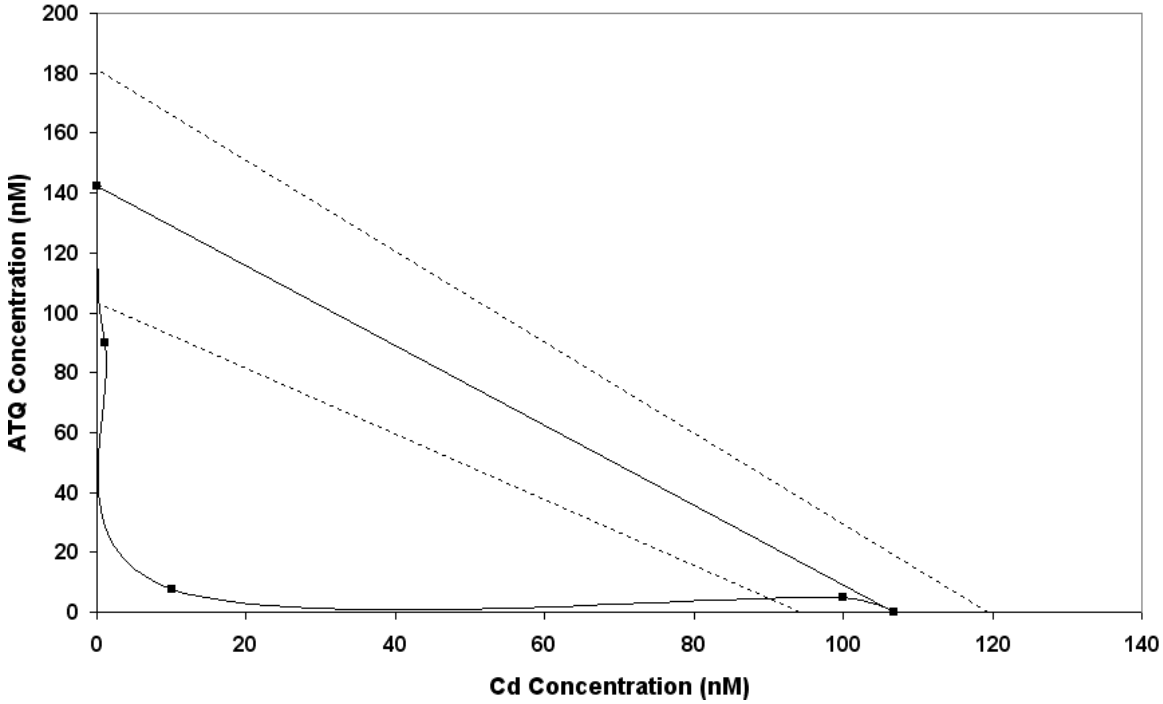

Figure 4.26 Isobologram for EC50s of binary mixtures of ATQ + Cd under SSR. Dotted lines represent 95% confidence intervals. EC50s of the varying mixtures of ATQ + Cd were plotted on the isobologram with their 95% confidence limits. Within the 95% confidence intervals simple additive toxicity is observed. Points residing above, on, and under the lines indicate antagonistic, additive and synergistic toxicity respectively.

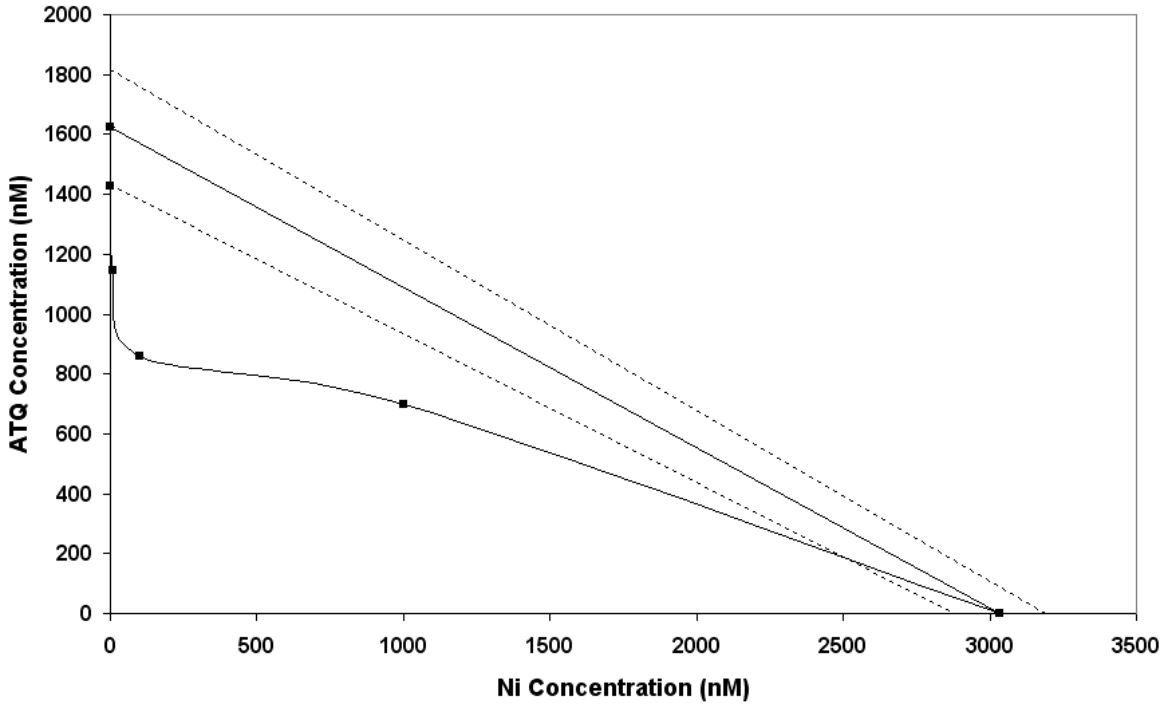

Figure 4.27 Isobologram for EC50s of binary mixtures of ATQ + Ni under dark. Dotted lines represent 95% confidence intervals. EC50s of the varying mixtures of ATQ + Ni were plotted on the isobologram with their 95% confidence limits. Within the 95% confidence intervals simple additive toxicity is observed. Points residing above, on, and under the lines indicate antagonistic, additive and synergistic toxicity respectively.

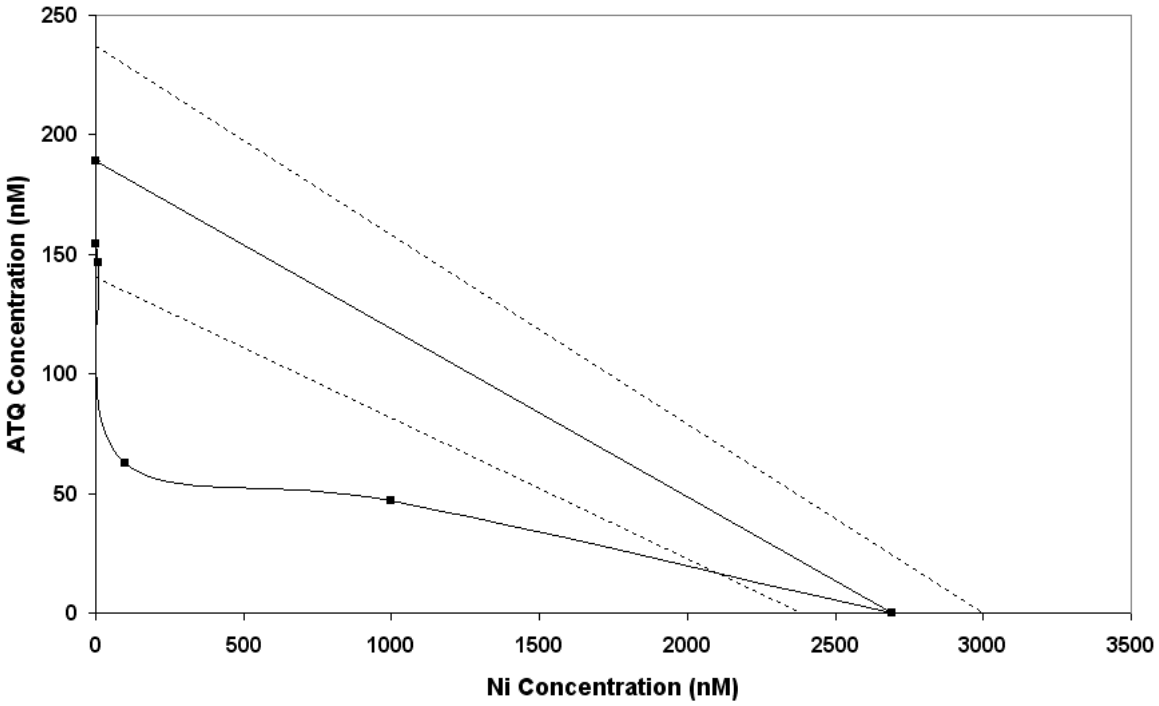

Figure 4.28 Isobologram for EC50s of binary mixtures of ATQ + Ni under PAR. Dotted lines represent 95% confidence intervals. EC50s of the varying mixtures of ATQ + Ni were plotted on the isobologram with their 95% confidence limits. Within the 95% confidence intervals simple additive toxicity is observed. Points residing above, on, and under the lines indicate antagonistic, additive and synergistic toxicity respectively.

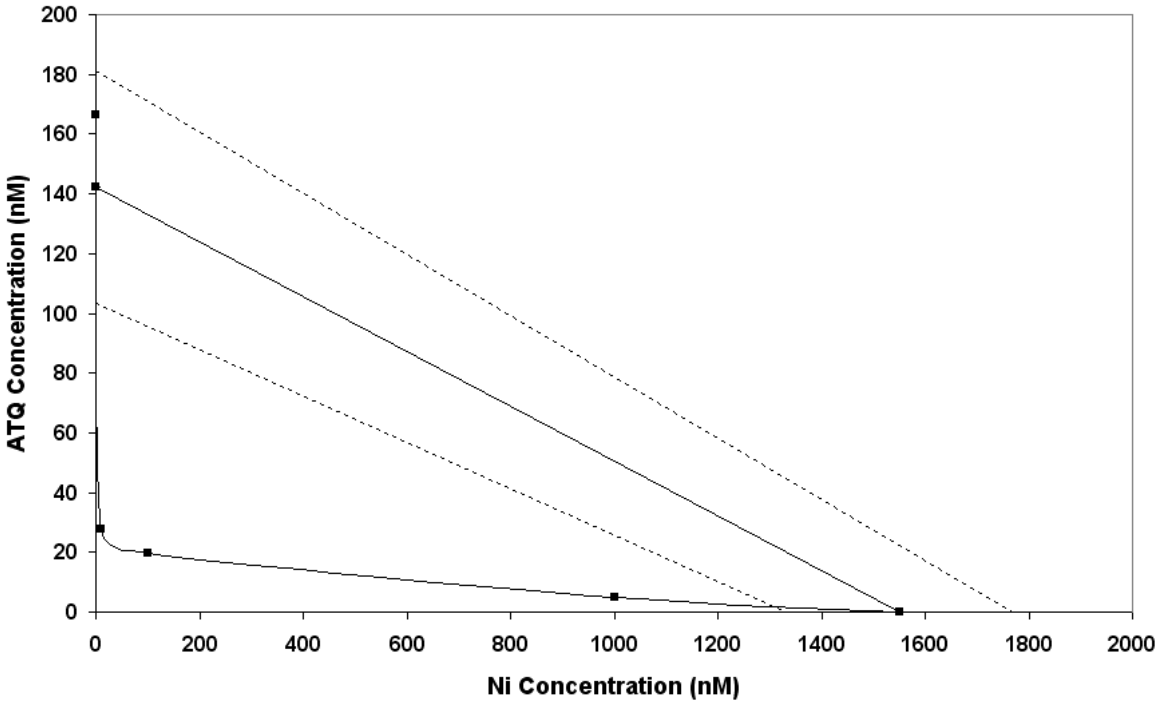

Figure 4.29 Isobologram for EC50s of binary mixtures of ATQ + Ni under SSR. Dotted lines represent 95% confidence intervals. EC50s of the varying mixtures of ATQ + Ni were plotted on the isobologram with their 95% confidence limits. Within the 95% confidence intervals simple additive toxicity is observed. Points residing above, on, and under the lines indicate antagonistic, additive and synergistic toxicity respectively.

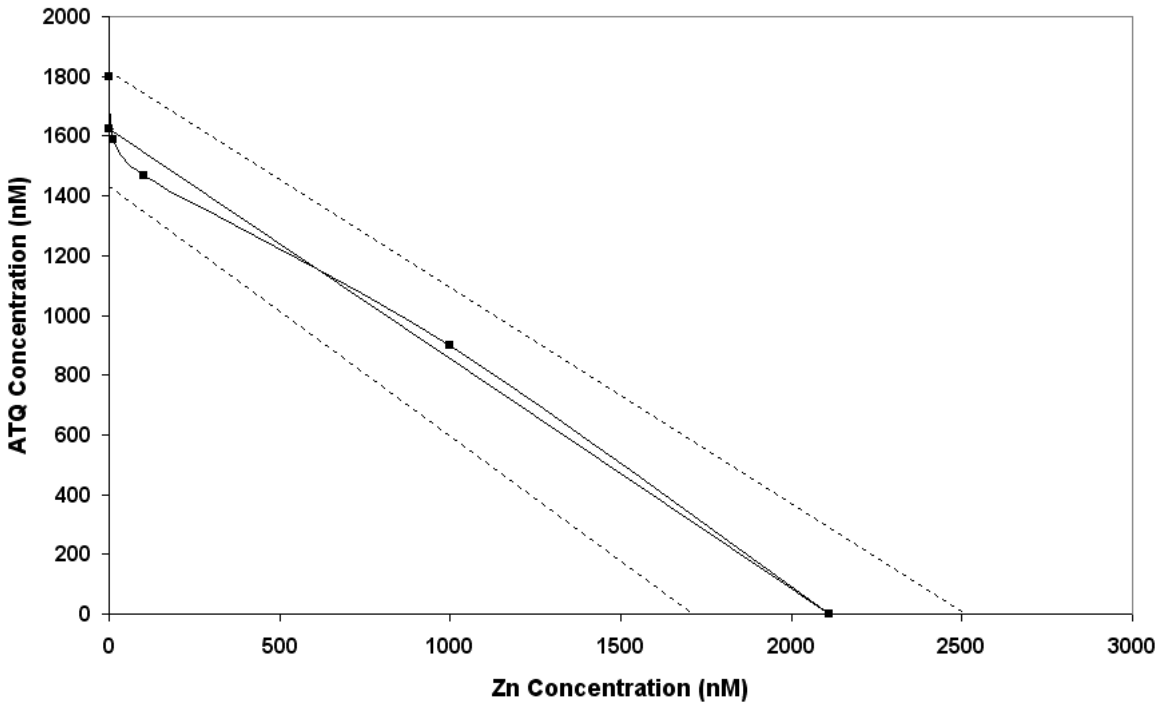

Figure 4.30 Isobologram for EC50s of binary mixtures of ATQ + Zn under dark. Dotted lines represent 95% confidence intervals. EC50s of the varying mixtures of ATQ + Zn were plotted on the isobologram with their 95% confidence limits. Within the 95% confidence intervals simple additive toxicity is observed. Points residing above, on, and under the lines indicate antagonistic, additive and synergistic toxicity respectively.

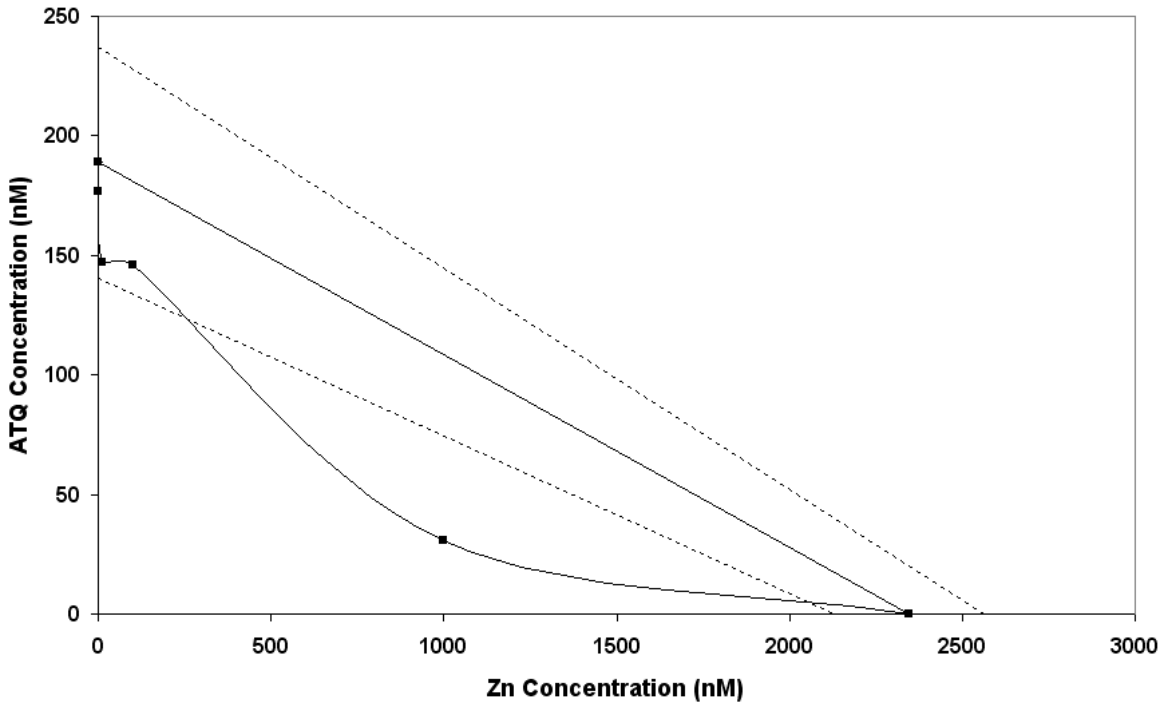

Figure 4.31 Isobologram for EC50s of binary mixtures of ATQ + Zn under PAR. Dotted lines represent 95% confidence intervals. EC50s of the varying mixtures of ATQ + Zn were plotted on the isobologram with their 95% confidence limits. Within the 95% confidence intervals simple additive toxicity is observed. Points residing above, on, and under the lines indicate antagonistic, additive and synergistic toxicity respectively.

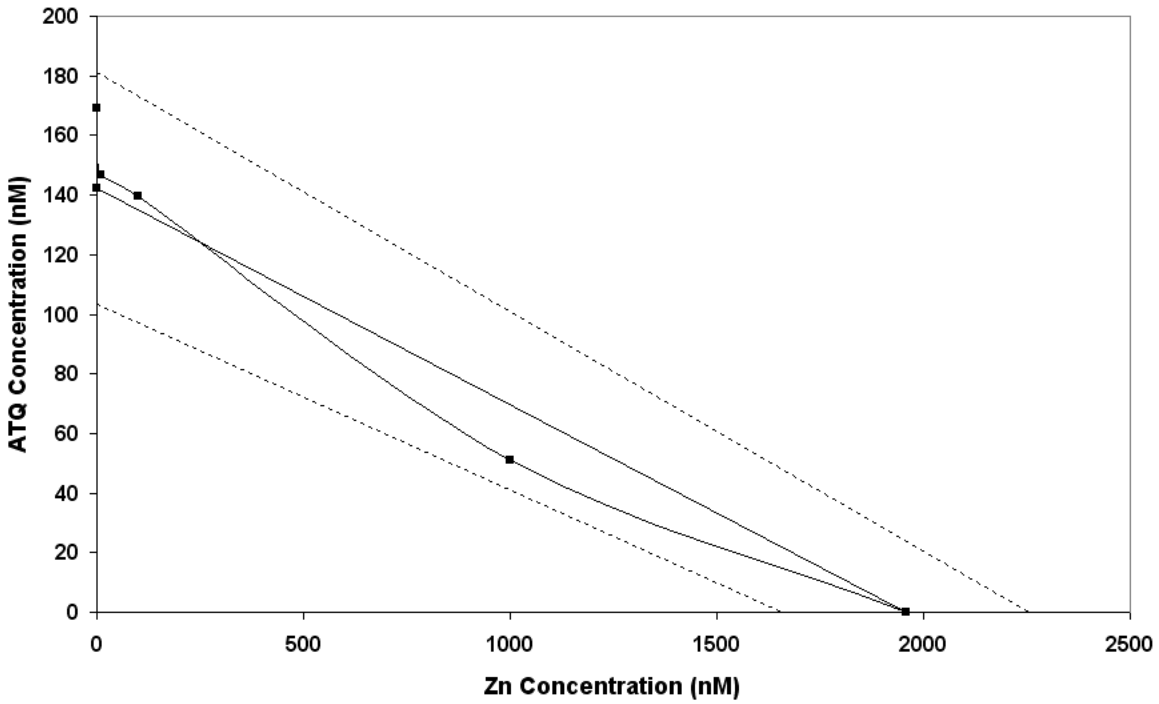

Figure 4.32 Isobologram for EC50s of binary mixtures of ATQ + Zn under SSR. Dotted lines represent 95% confidence intervals. EC50s of the varying mixtures of ATQ + Zn were plotted on the isobologram with their 95% confidence limits. Within the 95% confidence intervals simple additive toxicity is observed. Points residing above, on, and under the lines indicate antagonistic, additive and synergistic toxicity respectively.

response curves for ATQ + metals are shown in figures 4.57 - 4.80. The 1-hATQ concentration response curves were determined to be very similar to those of ATQ and were not analyzed in this thesis. These curves appear in appendix A figures 6.1 - 6.24.

4.2.1 ANT + Metals

The PAH + metal mixtures generally showed a drastic increase in toxicity across all three lighting regimes. Generally the dark PAH + metal EC50s were not statistically different from the predicted values for the mixtures, indicating additive toxicity. In all of the mixtures the highest concentration of metal present was always the most toxic for a given PAH + metal mixture. For the ANT + metal dark treatments it was found that the most toxic mixture was ANT + 1000 nM Cd, which was found to be acutely toxic at all concentrations of ANT. Mixtures of ANT + 1000 nM Cu were also found to be exceedingly toxic with an EC50 of 537 nM ANT in the dark (Figure 4.1). Mixtures of ANT with Ni and Zn showed that both were only minimally toxic in the Dark 1000 nM treatments, with ANT EC50s of 1259 nM (Ni) (Figure 4.3) and 1433 nM (Zn) (Figure 4.4). The ANT + Ni and ANT+ Zn treatments in the dark were not found to be statistically different. For Cu, Ni, and Zn, the 1 and 10 nM concentrations did not appear to have any affect on the toxicity of ANT. Cd appeared to have a small affect the toxicity of ANT at 1 nM and at 10 nM had a large effect on ANT with EC50s of 3904 nM and 491 nM respectively. The results of the dark treatments all matched the predicted values for each of the mixtures, with the exception of ANT + 100 nM Cd which was slightly less toxic than predicted (Figure 4.2).

The results of the ANT + metal PAR treatments showed varying degrees of toxicity (Table 4.2). The PAR treatments were 4 fold more toxic than the dark treatments for each of the mixtures. The most toxic ANT mixture was ANT + 100 nM Cd, which was found to be acutely toxic. ANT + 1000 nM Cu was found less toxic in the dark, with an EC50 of 2.58 nM (Figure 4.1). The least toxic mixture at 1000 nM was found to be ANT + 1000 nM Ni which had an EC50 of 102.2 nM. ANT + Zn mixtures were found to be slightly more toxic than ANT + Ni mixtures with an EC50 of 30.6 nM. In the PAR treatments concentrations of 1 nM and 10 nM of any of the four metals did not seem to have any affect on the toxicity of ANT (Table 4.2).

The ANT + metal mixtures under SSR showed a marked increase in toxicity over that of the PAR treatments by 2-6 fold. The ANT + metal mixture that was the most toxic was ANT + 10 nM Cd which was acutely toxic under SSR (Figure 4.2). The least toxic of the 1000 nM mixtures was ANT + Zn, with an EC50, at 1.09 nM. Interestingly ANT + 1 nM Zn seemed to become less toxic than ANT on its own with an EC50 of 8.72 nM compared to that of ANT on its own at 4.87 nM under SSR (Table 2.2, Chapter 2). For the SSR treatments the 1 nM metal mixtures with ANT seemed to have no effect on the toxicity of ANT. However at 10 nM or greater concentrations the metals showed a synergistic effect on the toxicity of ANT.

The concentration response curves for ANT + Cu across all three lighting regimes ranged over three orders of magnitude. The EC50s for ANT varied according to the concentration of Cu. In the dark, it was found that 1 nM and 10 nM concentrations of Cu had no impact on the EC50 of ANT. However, the ANT + 100 nM Cu mixture showed a 60% increase in the EC50 of ANT (2056 nM) compared to ANT (4902 nM) on its own.

The ANT + 1000 nM Cu (537 nM) mixture showed a 10 fold increase in EC50 over that of the ANT (4902 nM) alone. The slopes of the ANT + Cu concentration response curves under the dark treatment show varying slopes. The dark ANT + 1 nM Cu, ANT + 10 nM Cu, and ANT + 100 nM Cu show similar slopes (Figure 4.33-4.34), that are very similar to that of ANT on its own (Figure 2.1, Chapter 2). However the slope of the ANT + 1000 nM Cu treatment was shallower than that of the other three. This shallower slope was very similar to that of the predicted slope for ANT + 1000 nM Cu (Figure 4.33).

The ANT + Cu treatments under PAR lighting showed a 10 fold increase in toxicity over those in the Dark treatment. The ANT + 1 nM Cu and ANT + 10 nM Cu mixtures showed no affect on the toxicity of ANT and were not statistically different from the single toxicant data for ANT. The 100 nM Cu mixture showed a 5 fold increase in toxicity over that of ANT alone, at 23.6 nM and 108 nM respectively. The 1000 nM ANT + Cu mixture showed a 50 fold increase in EC50 (2.58 nM) compared to ANT (108 nM) alone. The slopes of the concentration response curves for ANT + 1 nM, and ANT + 10 nM Cu under PAR lighting were both very similar to each other and were almost identical to the slope of ANT on its own. The 100 nM and 1000 nM ANT + Cu mixtures had very similar slopes to each other, and were unlike the predicted slopes. Also these slopes did not match the ANT slope or Cu slope (Figures 4.35- 4.36).

The ANT + Cu treatment under SSR lighting showed an increase in toxicity of 25-100 fold over that of the PAR assay. Under SSR Cu concentrations of 10 nM and greater were found to have an affect on the EC50 of ANT. 1 nM Concentrations of Cu did not show any statistically significant effect on the EC50 of ANT. Higher concentrations of Cu were acutely lethal under SSR conditions at all concentrations of

ANT. The slopes of the concentration response curve for ANT + 10 nM Cu under SSR (Figure 4.35) was very steep and was much steeper than that of either ANT (Figure 2.2, Chapter 2) or Cu (Figure 3.1, Chapter 3) alone.

The EC50s of ANT + Cd mixtures ranged over two orders of magnitude. The Cd mixtures were usually very toxic at low concentrations of Cd. The ANT + Cd mixtures in the dark were found to be extremely toxic at 100 nM concentration of Cd, with an EC50 of 5.78 nM (Figure 4.2). Cd was the only metal that showed a large affect on ANT concentration at 1 nM and 10 nM concentrations, with an increase of 25% and 1000% in EC50 respectively. Concentration response curves for ANT + Cd in the dark showed similar slopes across all of the concentrations (Figures 4.39- 4.40).

Under PAR lighting mixtures of ANT + Cd showed a slight increase in toxicity over that of the dark treatment (Figure 4.2). At 100 nM Cd, ANT became acutely toxic to *Hyalella azteca*. At 1 nM and 10 nM concentrations Cd under PAR lighting did not seem to have an affect on ANT toxicity, with the EC50s for both treatments showing no statistical difference from that of ANT on its own. The slopes of the ANT + Cd concentration response curves were almost identical to those found in the dark treatments (Figures 4.9). Treatment of ANT + Cd mixtures with SSR showed an increase in toxicity over that of the PAR treatment (Figure 4.2). The toxicity of the 1 nM ANT + Cd increased 50 fold from 142 nM to 2.21 nM (Table 4.2). At concentrations of 10 nM Cd and above ANT became acutely toxic. The slope of the concentration response curve for the 1 nM ANT + Cd was identical to that of ANT on its own (Figure 4.43).

The concentration response curves for mixtures of ANT + Ni under the Dark treatment, showed a four fold increase in toxicity as the concentration of Ni increased

from 1 nM to 1000 nM. The 1 nM and 10 nM Ni + ANT mixtures were not found to be statistically different from those of ANT on its own. The 100 nM ANT + Ni (3894 nM) showed a 20% increase in toxicity over that of ANT alone (4902 nM) (Figure 4.3). The 1000 nM ANT + Ni treatment in the dark (1259 nM) showed a 75% increase in toxicity over that of ANT alone (4902 nM). The concentration response curves for ANT + Ni in the dark showed a similar slope for all concentrations of Ni, which was very similar to that of ANT alone (Figures 4.44 - 4.45).

Mixtures of ANT + Ni under PAR treatment (Table 4.2) showed a 10-20 fold increase in toxicity compared to that of the dark treatment (Table 4.1). The 1 nM ANT + Ni treatment was not found to be statistically different from that of ANT alone. The 10 nM ANT + Ni mixture was found to be 15 % more toxic than that of ANT alone, with EC50s of 84.2 nM and 108 nM respectively. The 1000 nM ANT + Ni treatment under PAR showed a 50% increase in toxicity over that of ANT alone. The slopes of the concentration response curves for ANT + Ni were almost identical across all of the concentrations of Ni (Figures 4.46-4.47).

The EC50s for mixtures of ANT + Ni under SSR were found to be 10-20 fold more toxic than those of the PAR ANT + Ni treatments. Mixtures of ANT and 1000 nM Ni were found to be acutely toxic under SSR. The toxicity of the ANT + 1 nM Ni mixture was found to be statistically the same as ANT alone, with EC50 values of 5.12 nM and 4.87 nM, respectively. The concentration response curves for ANT + Ni showed two distinct slopes (Figure 4.49 – 4.50). The first slope was found in the ANT + 1 nM Ni and ANT + 10 nM Ni concentration response curves (Figure 4.49), and were found to be similar to that of ANT alone (Figure 2.1, Chapter 2). The second slope shared by ANT +

100 nM Ni and ANT + 1000 nM Ni was found to be steeper than that of the ANT + 1 nM Ni and ANT + 10 nM Ni concentration response curves (Figure 4.50).

The concentration response curves for ANT + Zn in the dark treatment showed an increase in toxicity as the concentration of Zn increased. The slopes for all four concentrations of ANT + Zn in the dark were identical to each other (Figure 4.51 – 4.52). These slopes were slightly steeper than the slope of ANT alone and shallower than that of Zn alone. The 1 nM and 10 nM concentrations of Zn were not found to have any affect on the toxicity of ANT. The 100 nM ANT + Zn mixture was found to be 8% more toxic than that of ANT on its own.

When exposed to PAR, mixtures of ANT + Zn increased in toxicity 10 fold compared to that of the dark treatment. The 1 nM and 10 nM Zn treatments showed no effect on the toxicity of ANT. The EC50 of the ANT + 100 nM Zn (67.5 nM) treatment showed an increase of 40% over that of ANT alone (108 nM). The EC50 of the ANT + 1000 nM Zn (30.6 nM) treatment showed a 70% increase in toxicity over that of ANT alone (108 nM). The concentration response curves for ANT + Zn under PAR showed similar slopes for all four of the Zn concentrations (Figure 4.53- 4.54).

The toxicity of ANT + Zn mixtures under SSR increased in toxicity over that of the PAR treatment by 10-15 fold. The ANT + 1 nM Zn treatment showed a slight increase in toxicity over that of ANT alone. The 10, 100, and 1000 nM treatments all showed an increase in toxicity over that of ANT alone ranging from an 11 % increase to and 80% increase. The slopes of the four ANT + Zn concentration response curves had nearly identical slope across the four different metal concentrations (Figure 4.55 – 4.56).

4.2.2 ATQ + Metals

Mixtures of ATQ + metals generally showed an increase in toxicity as the lighting sources were changed, from dark to SSR (290-700 nm). The mixtures of ATQ + 1 nM Cu (1284 nM) and ATQ + 10 nM Cu (1251 nM) in the dark treatment increased the toxicity of ATQ by 40% over that of the ATQ (1624 nM) mixture alone. Mixtures of ATQ + 100 nM Cu showed 8 fold increase in toxicity compared to ATQ alone, with EC50s of 203 nM and 1624 nM respectively. The ATQ + 1000 nM Cu treatment under dark was 50 fold more toxic than ATQ alone, with an EC50 of 37.7 nM. The slopes of the concentration response curves for ATQ + Cu showed a characteristic slope across all of the different concentration of Cu (Figure 4.57-4.58). This slope was slightly steeper that that of ATQ.

Under PAR, ATQ + 1000 nM Cu was found to be toxic at all concentrations of ATQ. The toxicity of ATQ + 1 nM Cu (179 nM) and ATQ + 10 nM Cu (181 nM) were found not to be statistically different from the EC50 of ATQ alone (188 nM). The EC50 for mixtures of ATQ + 100 nM Cu was found to be 10 fold more toxic than that of ATQ alone under PAR lighting. The slopes of the concentration response curves for ATQ + 1 nM Cu and ATQ + 10 nM Cu were very similar to those of ATQ on its own (Figure 4.59). The slopes of the concentration response curves for ATQ + 100 Cu and ATQ + 1000 nM Cu were almost identical to each other but were steeper than those of ATQ or Cu alone (Figure 4.60).

Mixtures of ATQ + 1000 nM Cu under SSR were found to be toxic at all concentrations of ATQ. Mixtures of ATQ + 1 nM Cu (1284 nM) were found to be statistically the same as ATQ (1624 nM) alone under SSR. Mixtures of ATQ + 10 nM

Cu (13.7 nM) showed a 10 fold increase in toxicity under SSR compared to that of the PAR treatment (181 nM). Under SSR lighting mixtures of ATQ + 100 nM Cu increased 25 fold over that of the PAR treatment. The concentration response curves for ATQ + 1 nM Cu was very similar to that of ATQ alone under SSR. The concentration response curve for ATQ + 10 nM Cu and ATQ+ 100 nM Cu were both very similar and were steeper than that of ATQ alone (Figure 4.61 - 4.62).

ATQ + 100 nM Cd mixtures were found to be acutely toxic at all concentrations of ATQ under dark conditions. Mixtures of ATQ + 1 nM Cd (1671 nM) were found not to be statistically different from ATQ on its own (1624 nM). The toxicity of ATQ + 10 nM Cd in the dark treatment (577 nM) was found to be 3 times more toxic than ATQ alone (1625 nM). The slopes of the concentration response curves for ATQ + Cd were all found to be identical (Figure 4.63).

When exposed to PAR light mixtures of ATQ + 100 Cd was found to be acutely toxic at all concentrations of ATQ. ATQ + 1 nM Cd was found not to have an effect on the toxicity of ATQ, with EC50s of 169.7 and 188 nM, respectively. Mixtures of ATQ + 10 nM Cd were found to be 2 fold more toxic than that of ATQ on its own and 10 fold more toxic than ATQ + 10 nM Cd in the Dark treatment. The slopes of the concentration-response-curves for ATQ + 1 nM Cd and ATQ + 10 nM Cd showed a very similar slope to each other (Figure 4.65).

Mixtures of ATQ + 100 nM Cd were found to be acutely toxic when exposed to SSR at all concentrations of ATQ. ATQ + 10 nM Cd (7.62 nM) mixtures were found to be 10 fold more toxic under SSR than under PAR (82.8 nM). Mixtures of ATQ + 1 nM Cd (89.8 nM) were found to be 2 fold more toxic than that of the ATQ alone. The

concentration response curves for ATQ + 1 nM Cd was found to be very similar to that of ATQ alone under SSR (Figure 4.67). The slope of ATQ + 10 nM Cd was found to be different from that of the ATQ + 1 nM Cd slope being slightly steeper.

The EC50 of ATQ + 1 nM Ni (1428 nM) was not found to be statistically different from that of ATQ alone (1625 nM). Mixtures of ATQ + 100 nM Ni (859 nM) were found to be 2 fold more toxic than that of ATQ (1625 nM). Mixtures of ATQ + 1000 nM Ni were found to be 10 fold more toxic than ATQ, with an EC50 of 109 nM. The concentration response curves for ATQ + 1 nM Ni and ATQ + 10 nM Ni were found to be very similar to that of ATQ alone (Figure 4.69). The concentration response curves for ATQ + 100 nM Ni and ATQ + 1000nM Ni were found to be very similar to each other (Figure 4.70).

The slopes of the PAR concentration response curves for ATQ + 1 nM Ni and ATQ + 10 nM Ni were found to be very similar to that of ATQ (Figure 4.71). The slopes of ATQ + 100 nM Ni and ATQ + 1000 nM Ni were both very similar but were much steeper than those of ATQ alone (figure 4.72). Mixtures of ATQ + 1 nM Ni (154 nM) and ATQ + 10 nM Ni (146 nM) were both found to have no impact on the toxicity of ATQ (188 nM), with EC50s that were not statistically different from that of ATQ. The toxicity of ATQ + 100 nM Ni was found to be 2 times greater than that of ATQ on its own under PAR. This was also found to be 10 times greater than that of ATQ + 100 nM Ni in the dark treatment.

Under the SSR treatment the EC50 for ATQ + 1 nM Ni (166) was not found to be statistically different from that of ATQ (142 nM). The mixture of ATQ + 10 nM Ni (27.7 nM) and ATQ + 100 nM Ni (19.6 nM) was found to be 10 fold more toxic than ATQ.

The greatest effect under SSR was observed with the ATQ + 1000 nM Ni, which increased the toxicity of ATQ by 70 fold, with EC50s of 4.81 nM and 142 nM respectively. The slopes of the concentration response curves for ATQ + Ni under SSR were all found to be very similar (Figure 4.73 – 4.74). The slopes of these concentration response curves were steeper than that of ATQ or Ni alone.

Mixtures of ATQ + Zn were found to have very little effect on ATQ toxicity in the dark. The EC50s of ATQ + 1 nM Zn (1798 nM), ATQ + 10 nM Zn (1588 nM) and ATQ + 100 nM Zn (1467 nM) mixtures were all found to be statistically the same as ATQ (1625 nM). The toxicity of ATQ + 1000 nM Zn (899 nM) was found to be 2 fold more toxic than ATQ (1625 nM). The slopes of the concentration response curves for ATQ + 1 nM Zn, ATQ + 10 nM Zn, and ATQ + 1000 nM Zn, were all found to be very similar in shape to ATQ (Figure 4.43 – 4.44). The slope of the concentration response curve for ATQ + 1000 nM Zn was found to be unique among the dark treatments, being steeper than the other curves (Figure 4.76).

Treatments of ATQ with concentrations of 1, 10, and 100 nM Zn under PAR resulted in EC50s that were not statistically different from those of ATQ (188 nM). Treatments of ATQ with 1000 nM Zn resulted in an increase in EC50 of 5 fold from 188 nM (ATQ) to 30.7 nM (ATQ + 1000 nM Zn). The slopes of the concentration response curves for ATQ + 1 nM Zn, ATQ + 10 nM Zn, and ATQ + 100 nM Zn were all very similar, and resembled that of ATQ (Figure 4.77 – 4.78). The slope of the ATQ + 1000 nM Zn concentration response curve under PAR was similar to that of the ATQ + 1000 nM curve under dark conditions (Figure 4.78).

When exposed to SSR light, ATQ with concentrations of 1, 10 and 100 nM Zn, produced EC50s that were not statistically different form that of ATQ. Mixtures of ATQ + 1000 nM Zn (26.8 nM) were found to be 6 fold more toxic under SSR than ATQ on its own (142). The slope of the concentration response curves for ATQ + 1000 nM Zn was unique among the SSR ATQ + Zn treatments (Figure 4.79); but was similar to that of the ATQ + 1000 nM Zn treatments under PAR (Figure 4.78). The slopes of the concentration response curves for ATQ + 1 nM Zn, ATQ + 10 nM Zn, and ATQ + 100 nM Zn were all found to be similar to ATQ (Figure 4.79 – 4.80).

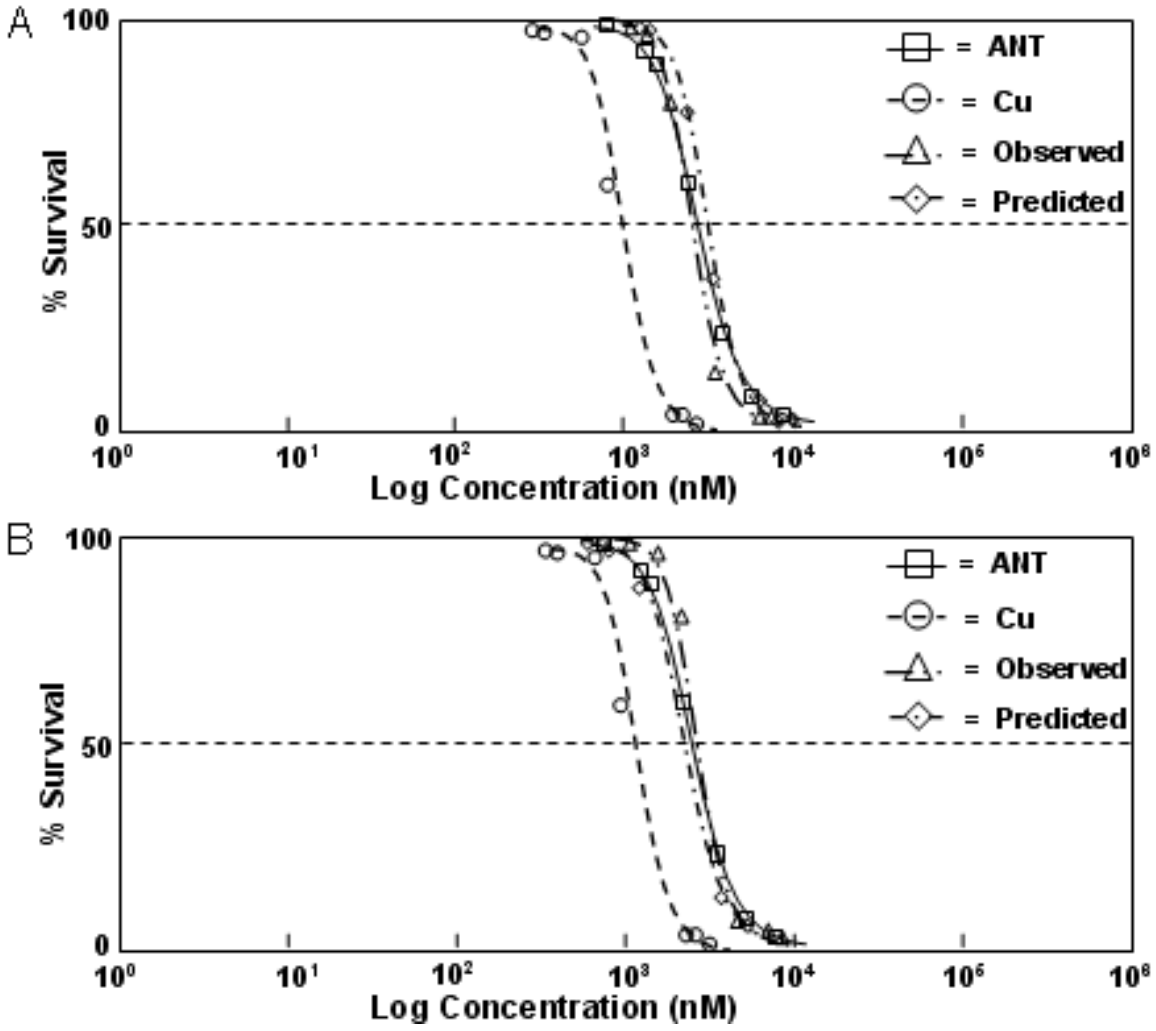

Figure 4.33 Concentration response curves for ANT + 1 nM Cu and ANT + 10 nM Cu to *Hyalella azteca* under dark conditions. ANT concentrations were varied while Cu was kept at a constant concentration. A. ANT + 1 nM Cu B. ANT + 10 nM Cu.

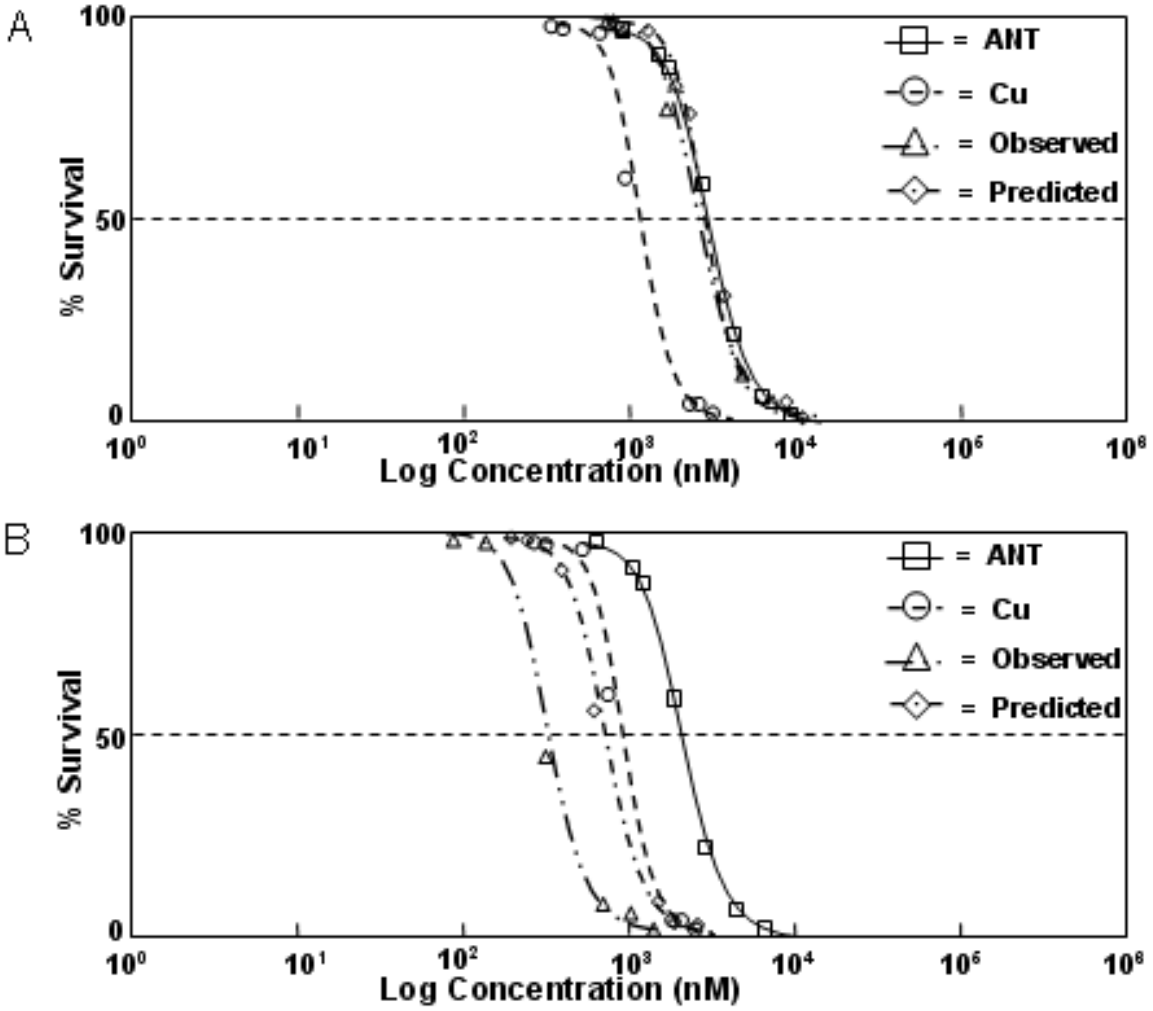

Figure 4.34 Concentration response curves for ANT + 100 nM Cu and ANT + 1000 nM Cu to *Hyalella azteca* under dark conditions. ANT concentrations were varied while Cu was kept at a constant concentration. A. ANT + 100 nM Cu B. ANT + 1000 nM Cu.

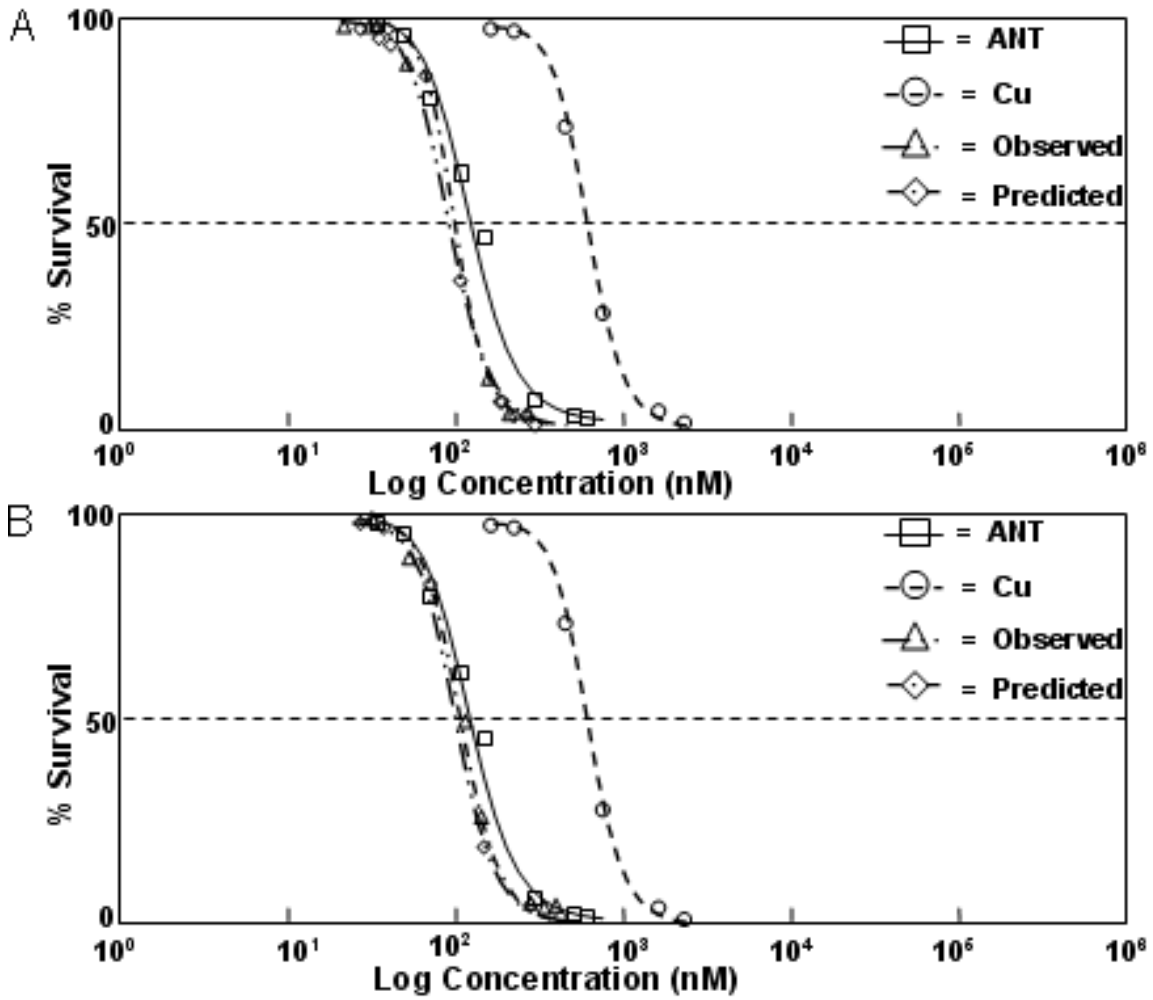

Figure 4.35 Concentration response curves for ANT + 1 nM Cu and ANT + 10 nM Cu to *Hyalella azteca* under PAR conditions. ANT concentrations were varied while Cu was kept at a constant concentration. A. ANT + 1 nM Cu B. ANT + 10 nM Cu.

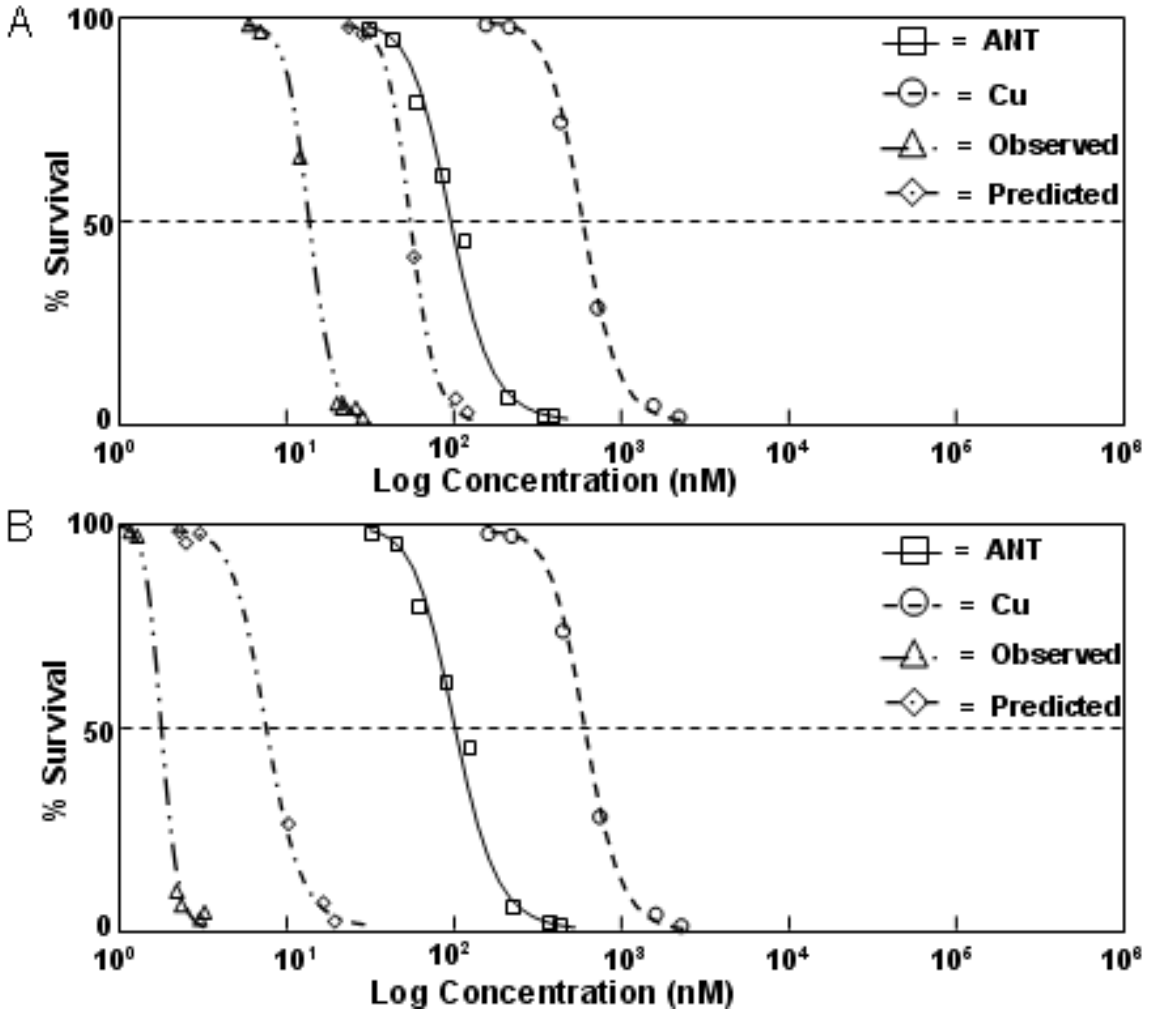

Figure 4.36 Concentration response curves for ANT + 100 nM Cu and ANT + 1000 nM Cu to *Hyalella azteca* under PAR conditions. ANT concentrations were varied while Cu was kept at a constant concentration. A. ANT + 100 nM Cu B. ANT + 1000 nM Cu.

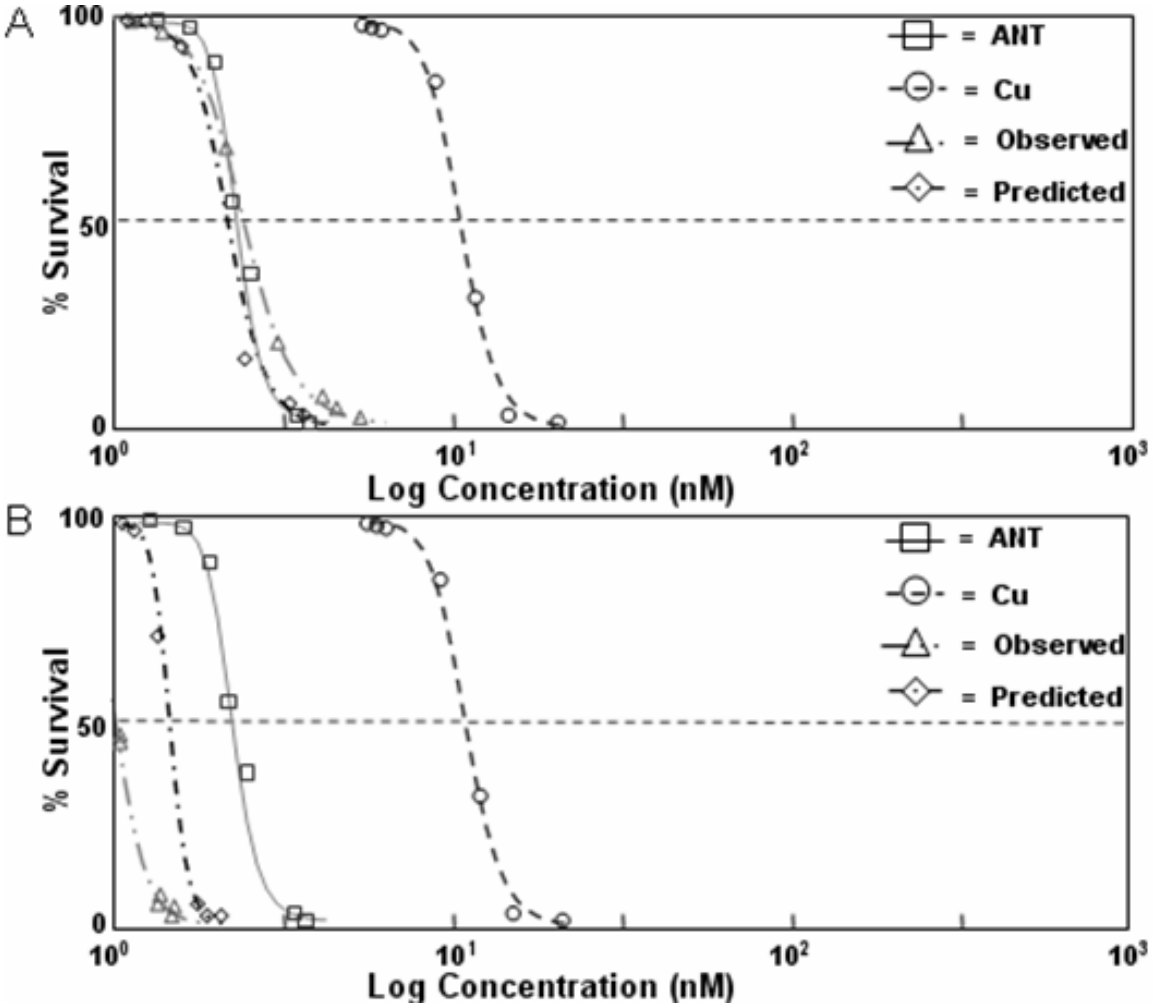

Figure 4.37 Concentration response curves for ANT + 1 nM Cu and ANT + 10 nM Cu to *Hyalella azteca* under SSR conditions. ANT concentrations were varied while Cu was kept at a constant concentration. A. ANT + 1 nM Cu B. ANT + 10 nM Cu.

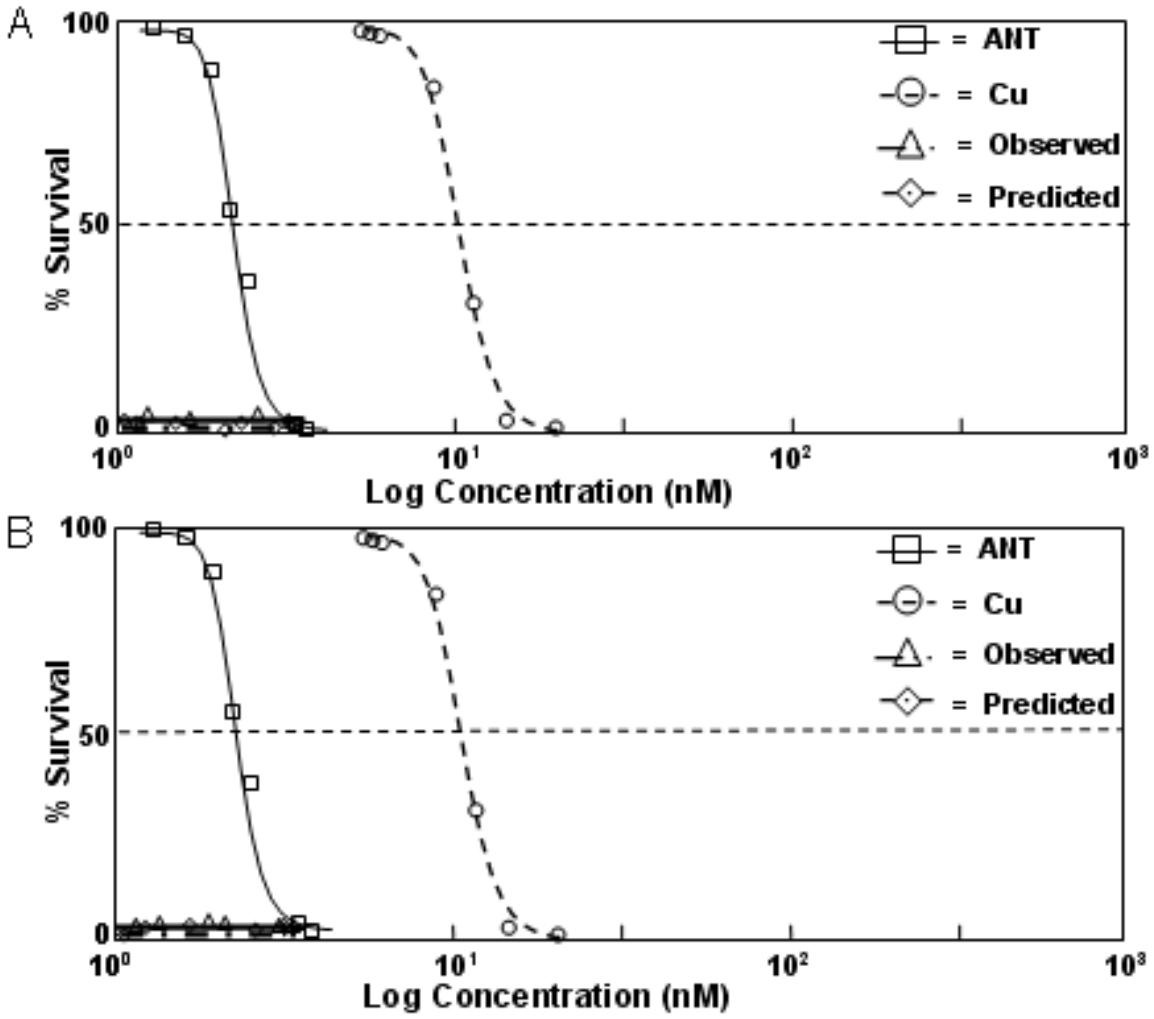

Figure 4.38 Concentration response curves for ANT + 100 nM Cu and ANT + 1000 nM Cu to *Hyalella azteca* under SSR conditions. ANT concentrations were varied while Cu was kept at a constant concentration. A. ANT + 100 nM Cu B. ANT + 1000 nM Cu

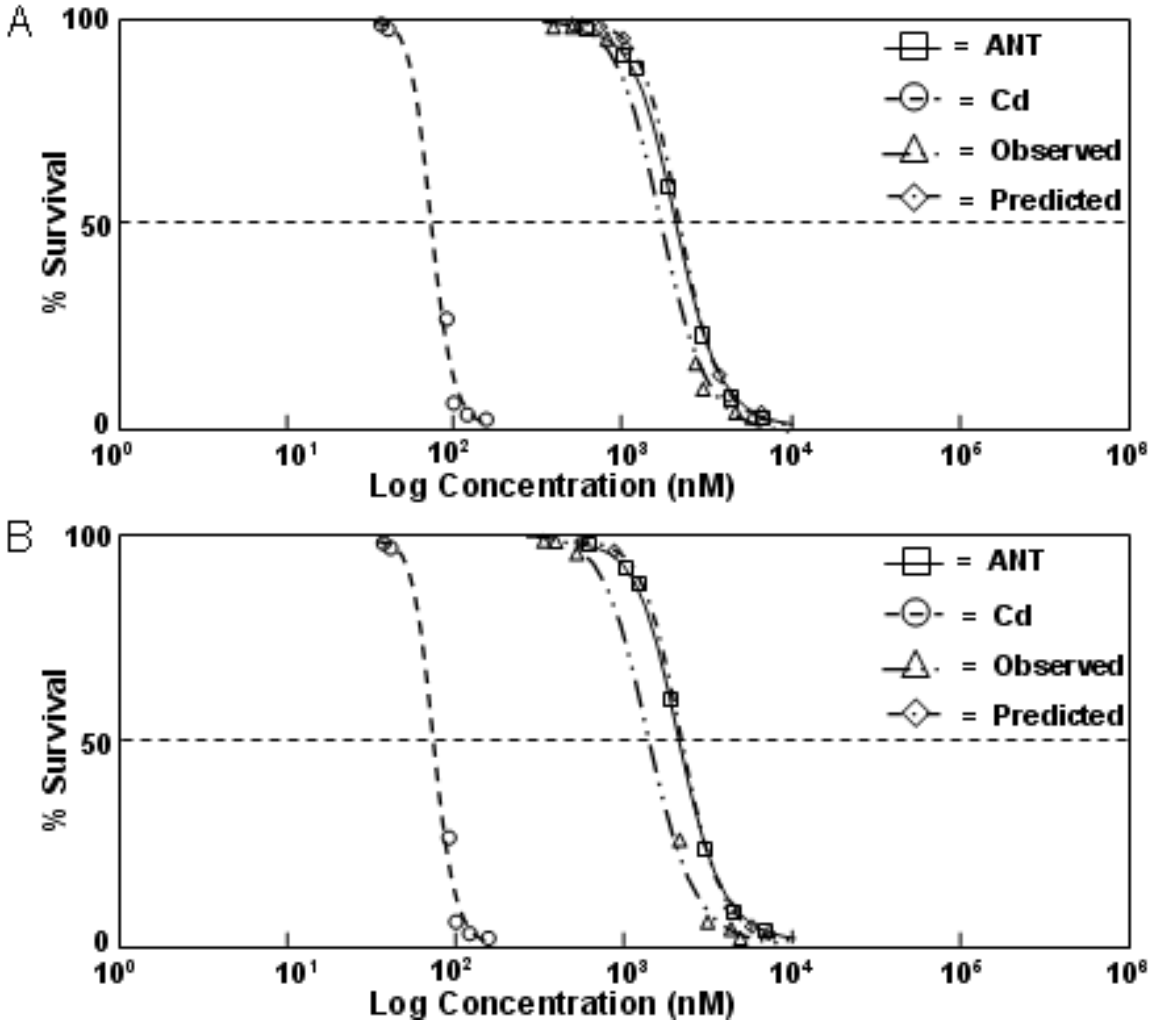

Figure 4.39 Concentration response curves for ANT + 1 nM Cd and ANT + 10 nM Cd to *Hyalella azteca* under dark conditions. ANT concentrations were varied while Cd was kept at a constant concentration. A. ANT + 1 nM Cd B. ANT + 10 nM Cd.

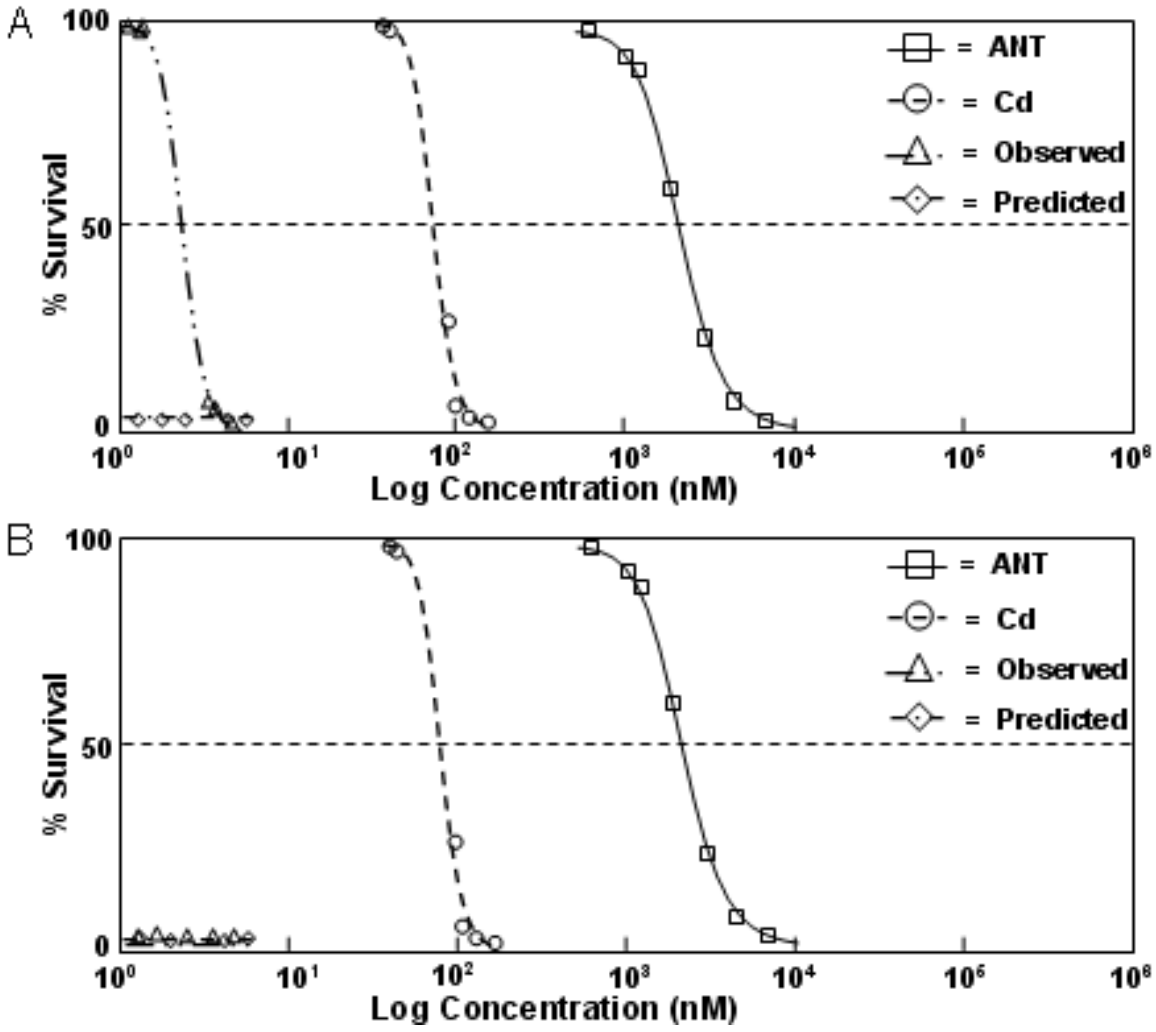

Figure 4.40 Concentration response curves for ANT + 100 nM Cd and ANT + 1000 nM Cd to *Hyalella azteca* under dark conditions. ANT concentrations were varied while Cd was kept at a constant concentration. A. ANT + 100 nM Cd B. ANT + 1000 nM Cd.

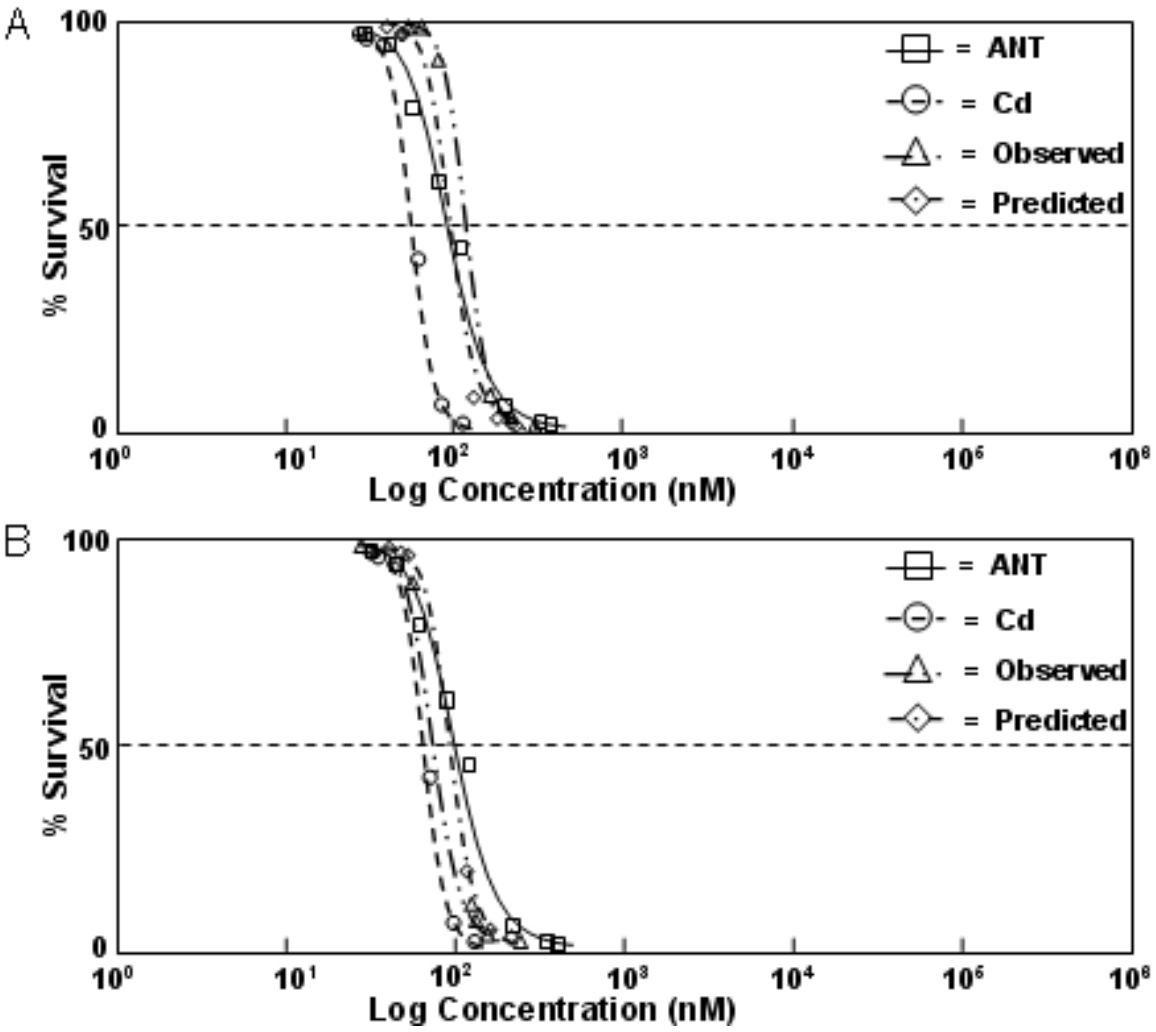

Figure 4.41 Concentration response curves for ANT + 1 nM Cd and ANT + 10 nM Cd to *Hyalella azteca* under PAR conditions. ANT concentrations were varied while Cd was kept at a constant concentration. A. ANT + 1 nM Cd B. ANT + 10 nM Cd.

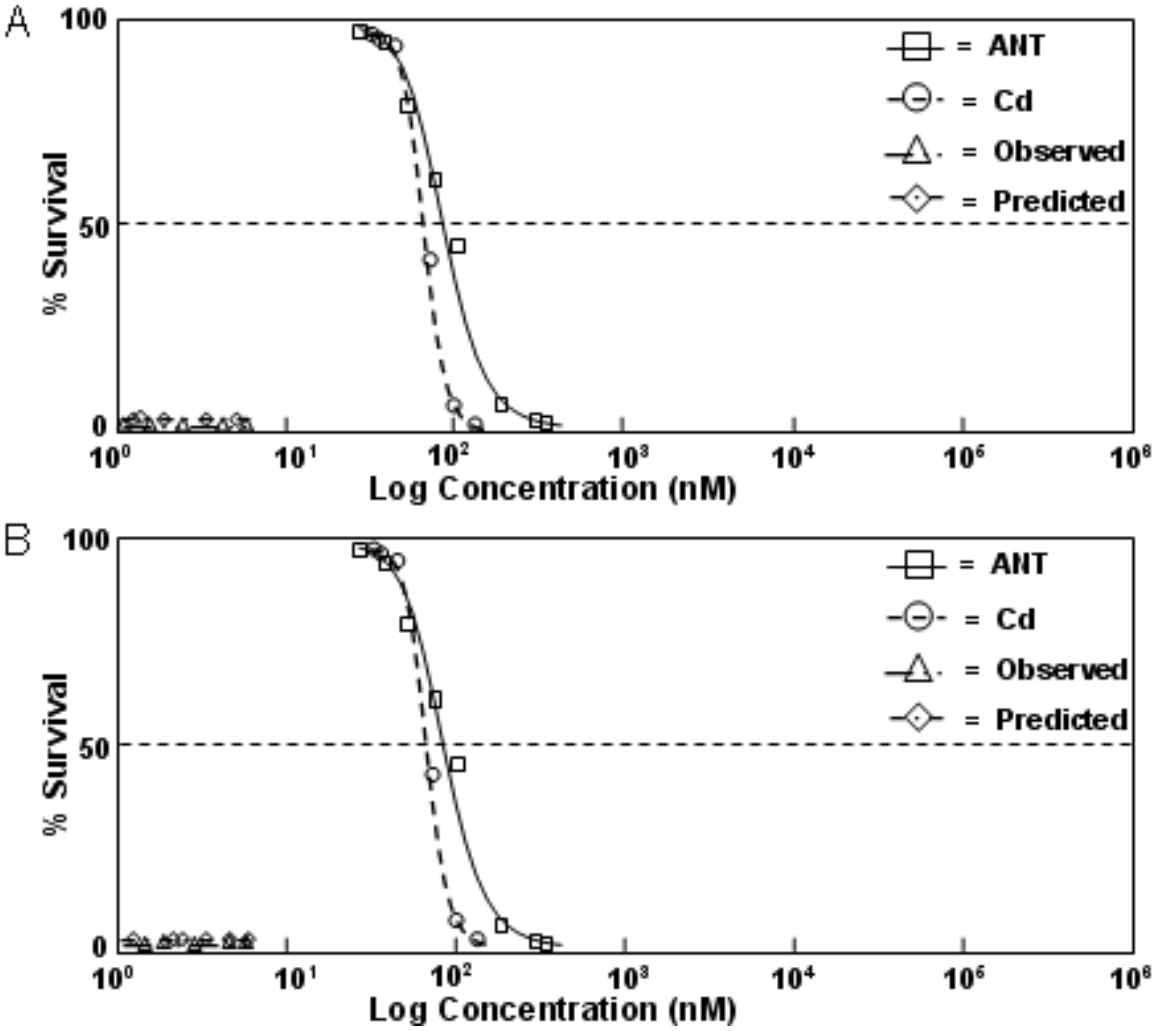

Figure 4.42 Concentration response curves for ANT + 100 nM Cd and ANT + 1000 nM Cd to *Hyalella azteca* under PAR conditions. ANT concentrations were varied while Cd was kept at a constant concentration. A. ANT+ 100 nM Cd B. ANT+ 1000 nM Cd.

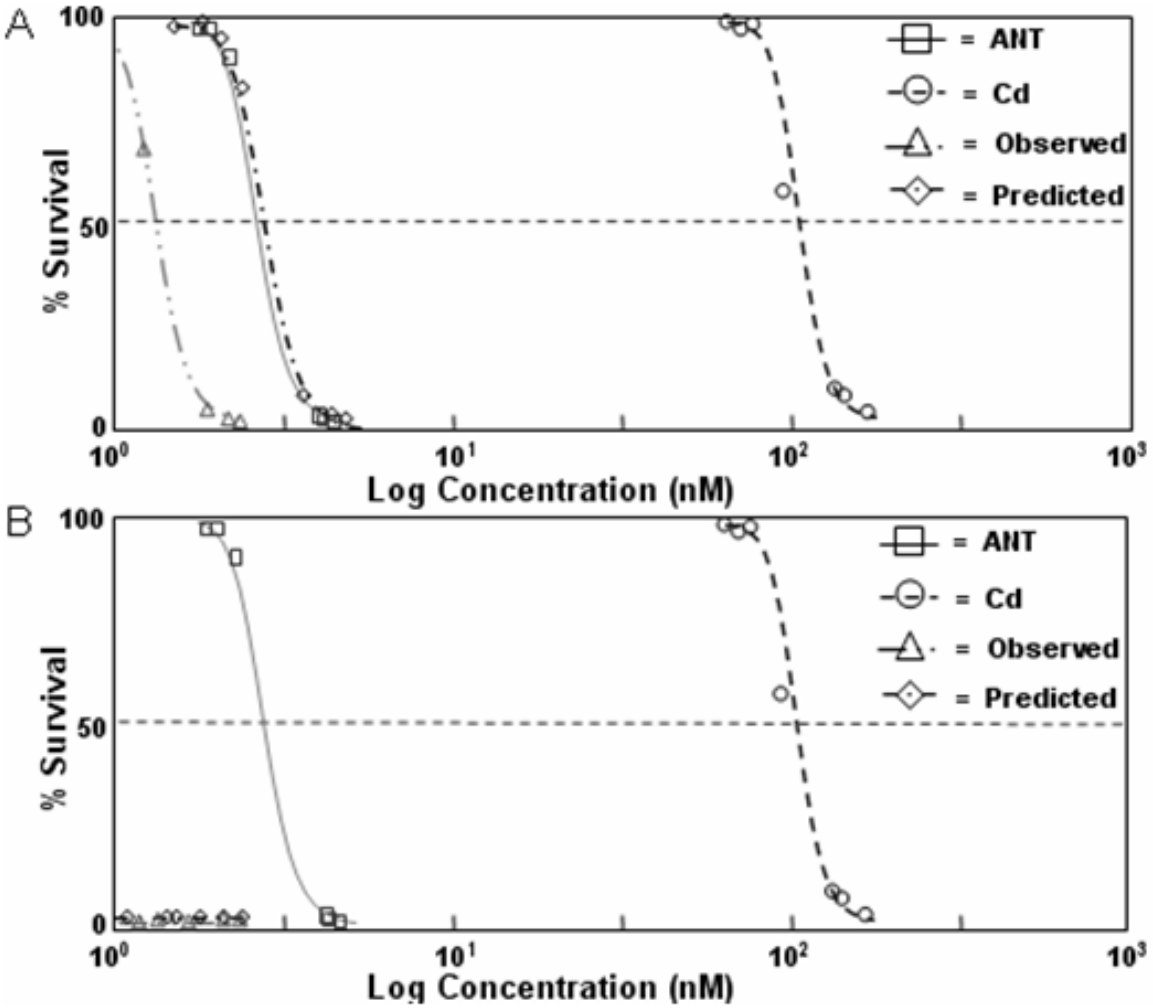

Figure 4.43 Concentration response curves for ANT + 1 nM Cd and ANT + 10 nM Cd to *Hyalella azteca* under SSR conditions. ANT concentrations were varied while Cd was kept at a constant concentration. A. ANT + 1 nM Cd B. ANT + 10 nM Cd.

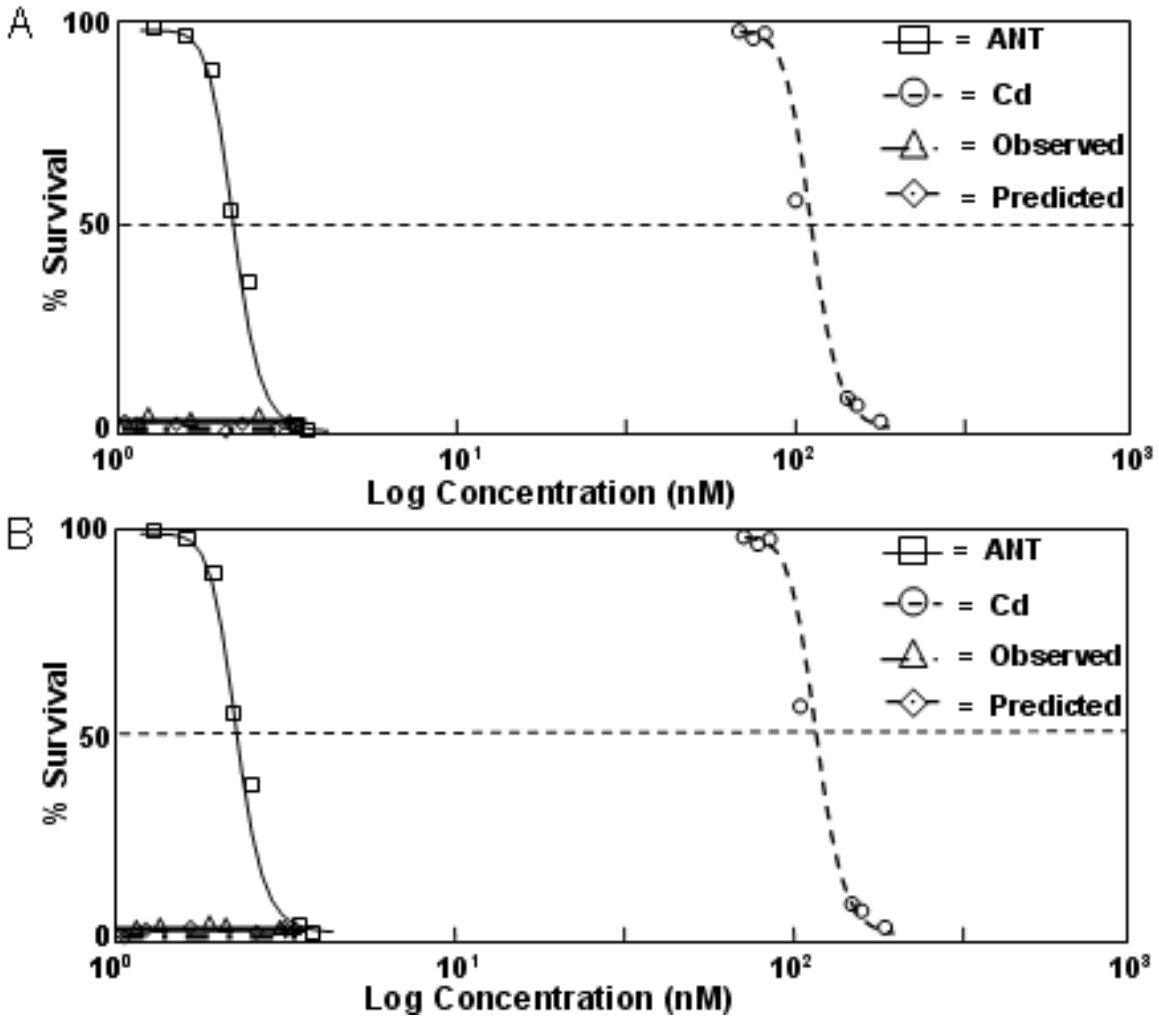

Figure 4.44 Concentration response curves for ANT + 100 nM Cd and ANT + 1000 nM Cd to *Hyalella azteca* under SSR conditions. ANT concentrations were varied while Cd was kept at a constant concentration. A. ANT + 100 nM Cd B. ANT + 1000 nM Cd

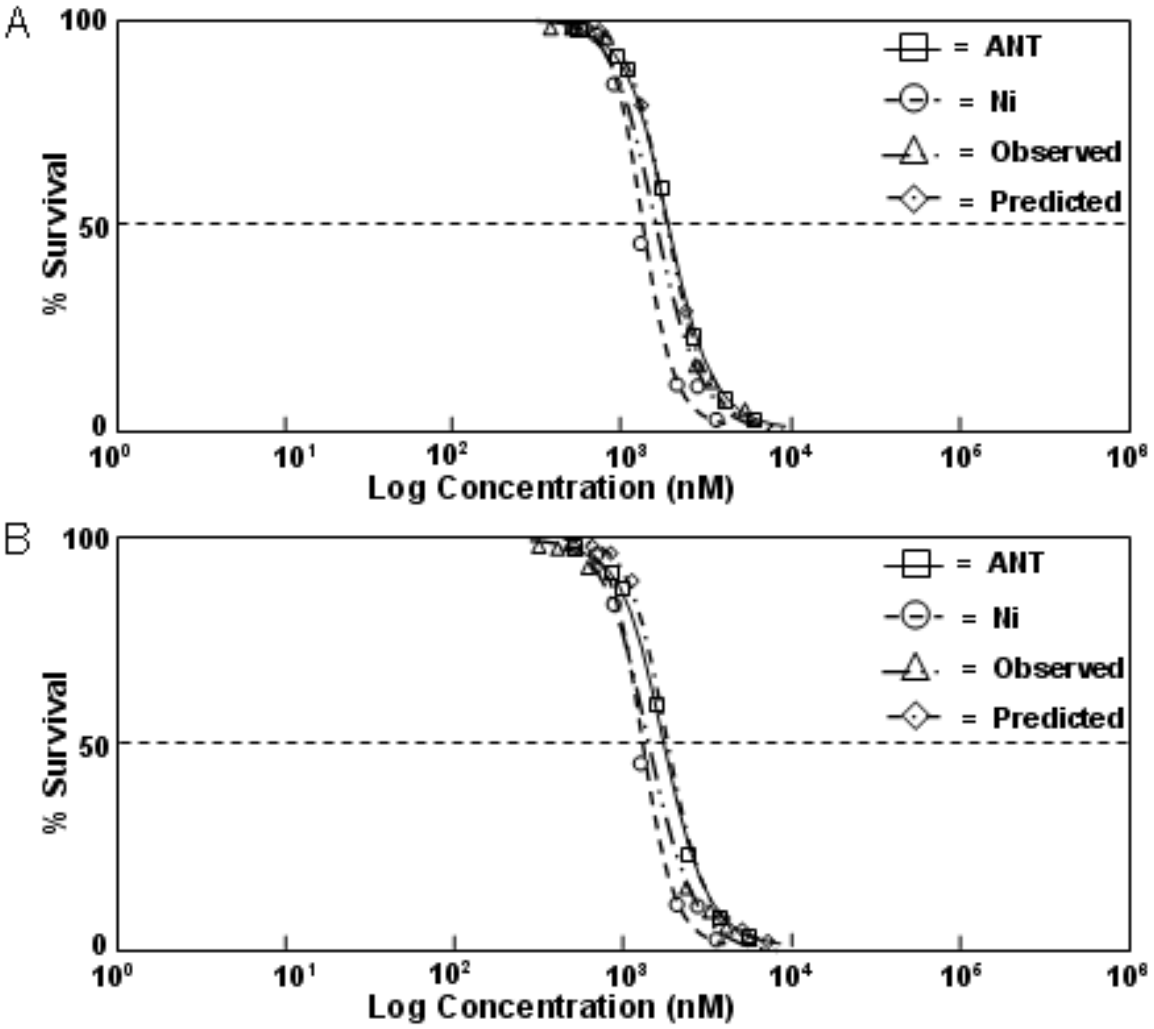

Figure 4.45 Concentration response curves for ANT + 1 nM Ni and ANT + 10 nM Ni to *Hyalella azteca* under dark conditions. ANT concentrations were varied while Ni was kept at a constant concentration. A. ANT + 1 nM Ni B. ANT + 10 nM Ni.

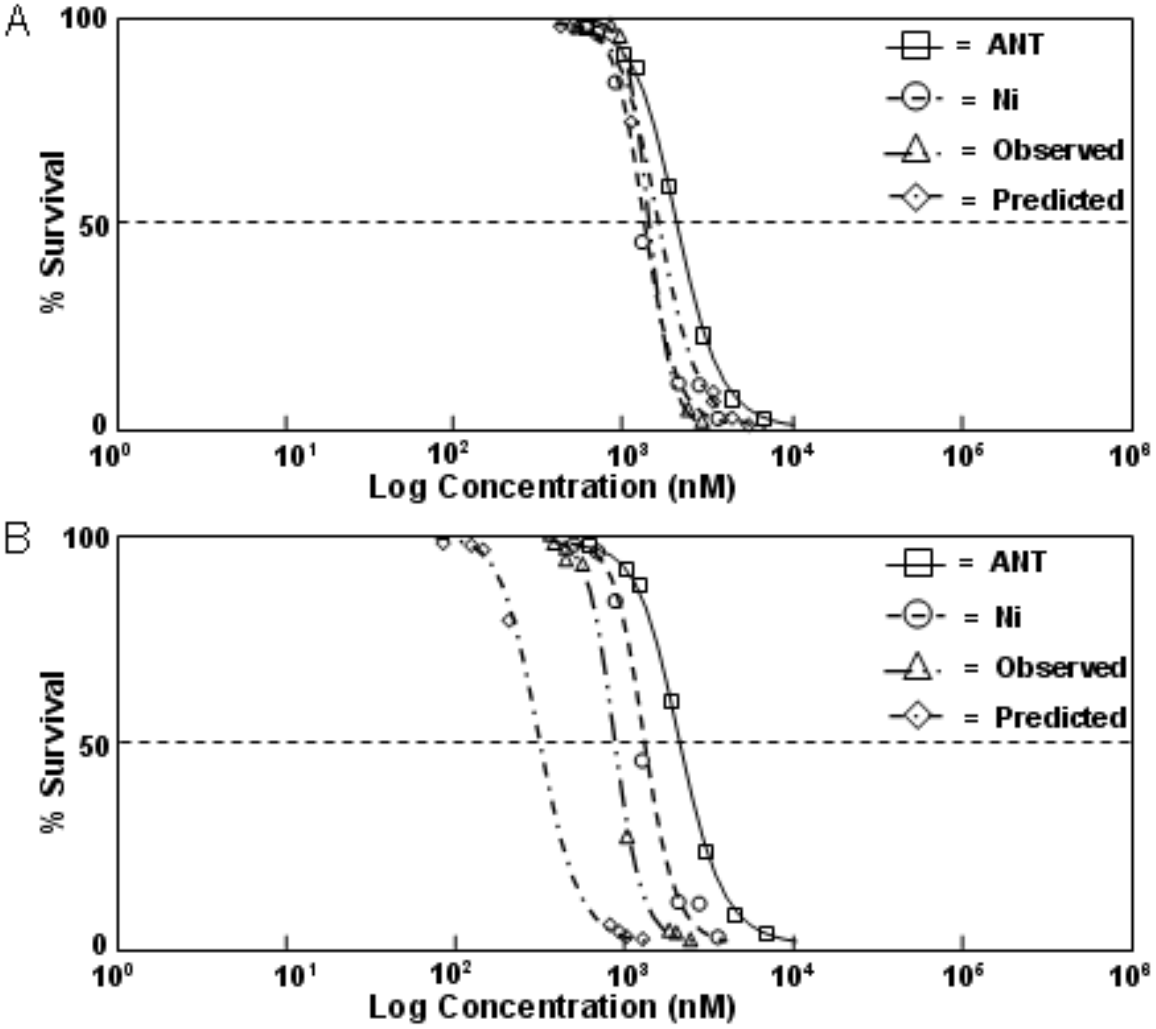

Figure 4.46 Concentration response curves for ANT + 100 nM Ni and ANT + 1000 nM Ni to *Hyalella azteca* under dark conditions. ANT concentrations were varied while Ni was kept at a constant concentration. A. ANT + 100 nM Ni B. ANT + 1000 nM Ni.

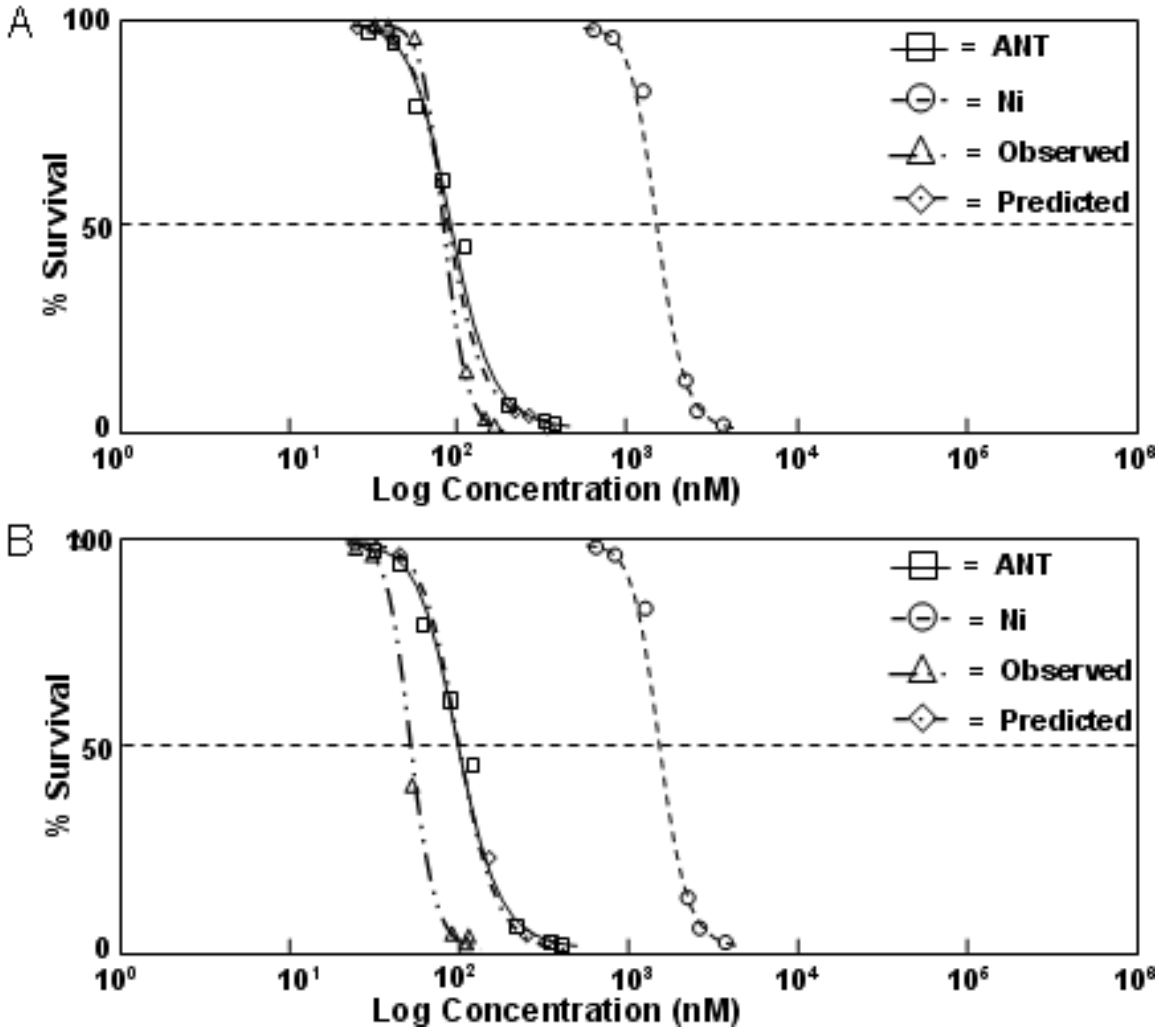

Figure 4.47 Concentration response curves for ANT + 1 nM Ni and ANT + 10 nM Ni to *Hyalella azteca* under PAR conditions. ANT concentrations were varied while Ni was kept at a constant concentration. A. ANT + 1 nM Ni B. ANT + 10 nM Ni.

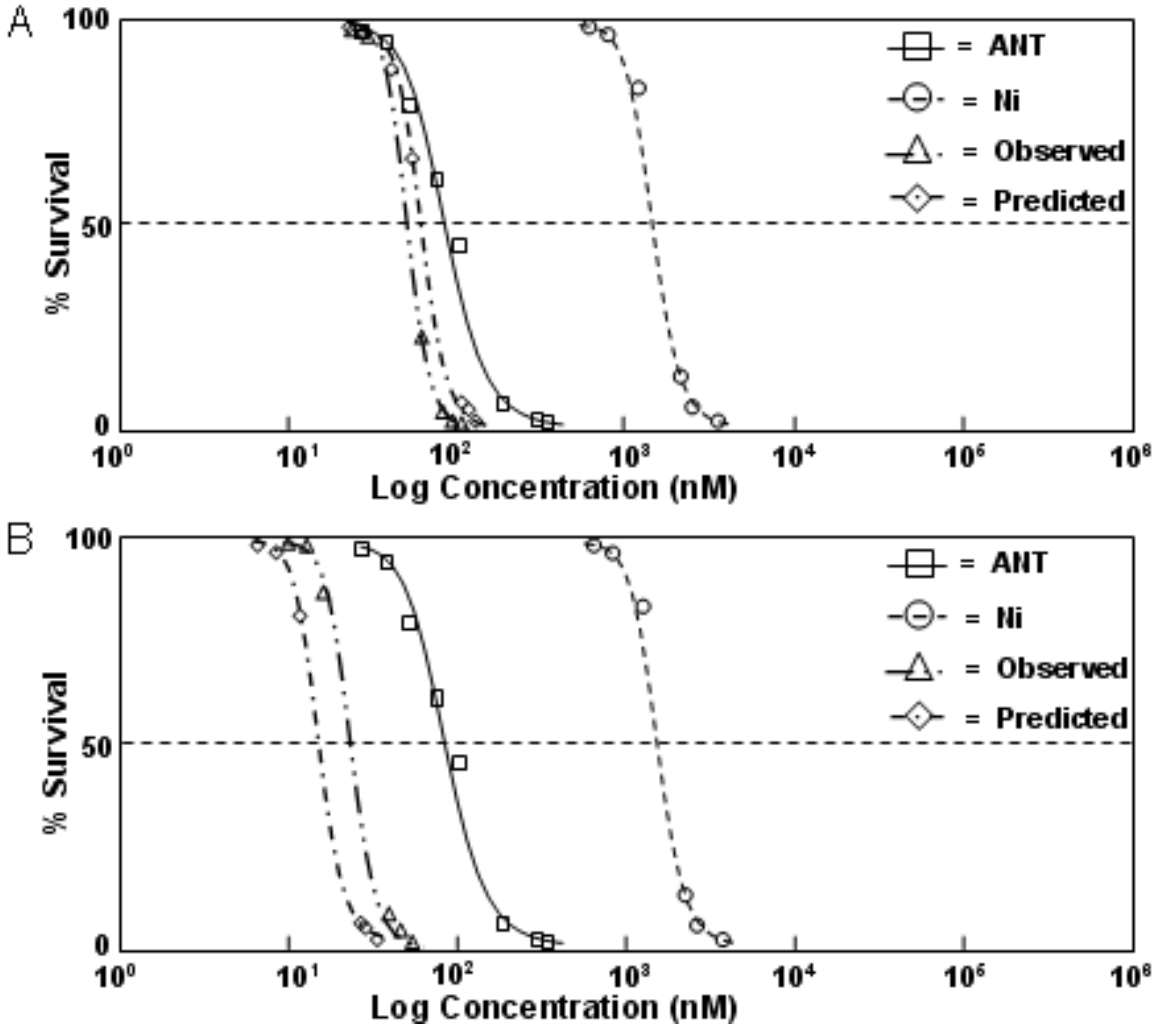

Figure 4.48 Concentration response curves for ANT + 100 nM Ni and ANT + 1000 nM Ni to *Hyalella azteca* under PAR conditions. ANT concentrations were varied while Ni was kept at a constant concentration. A. ANT+ 100 nM Ni B. ANT+ 1000 nM Ni.

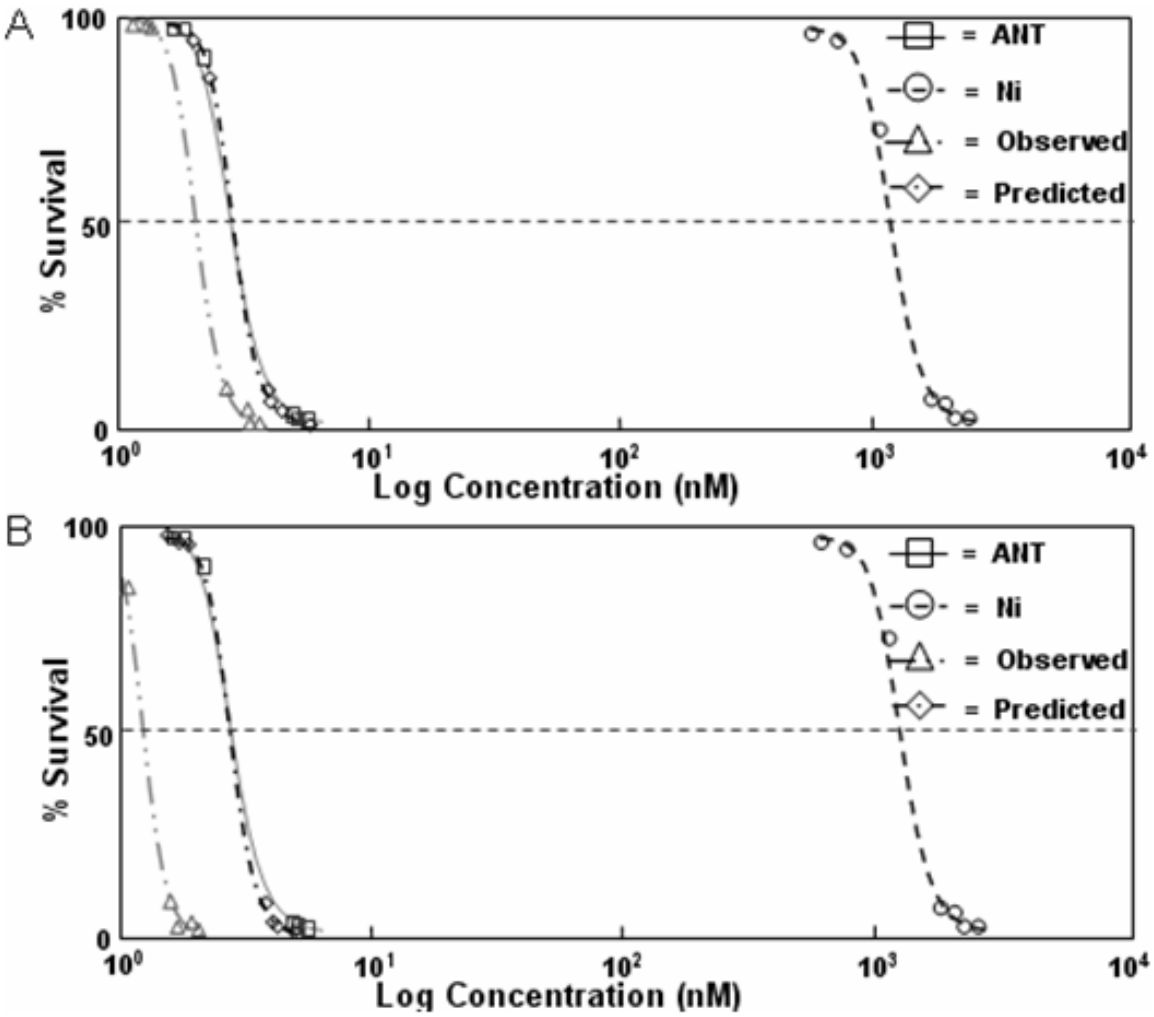

Figure 4.49 Concentration response curves for ANT + 1 nM Ni and ANT + 10 nM Ni to *Hyalella azteca* under SSR conditions. ANT concentrations were varied while Ni was kept at a constant concentration. A. ANT + 1 nM Ni B. ANT + 10 nM Ni.

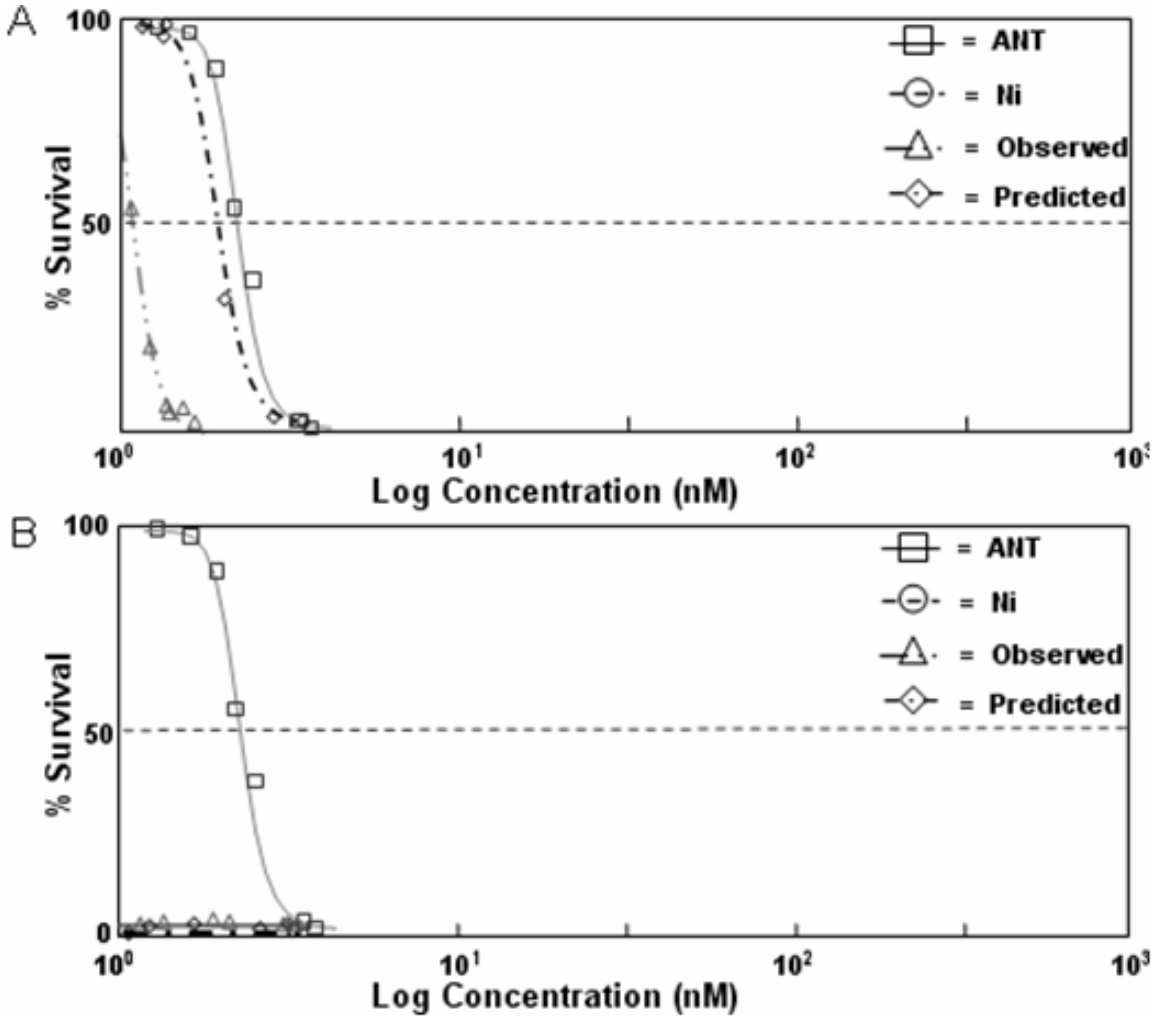

Figure 4.50 Concentration response curves for ANT + 100 nM Ni and ANT + 1000 nM Ni to *Hyalella azteca* under SSR conditions. ANT concentrations were varied while Ni was kept at a constant concentration. A. ANT + 100 nM Ni B. ANT + 1000 nM Ni

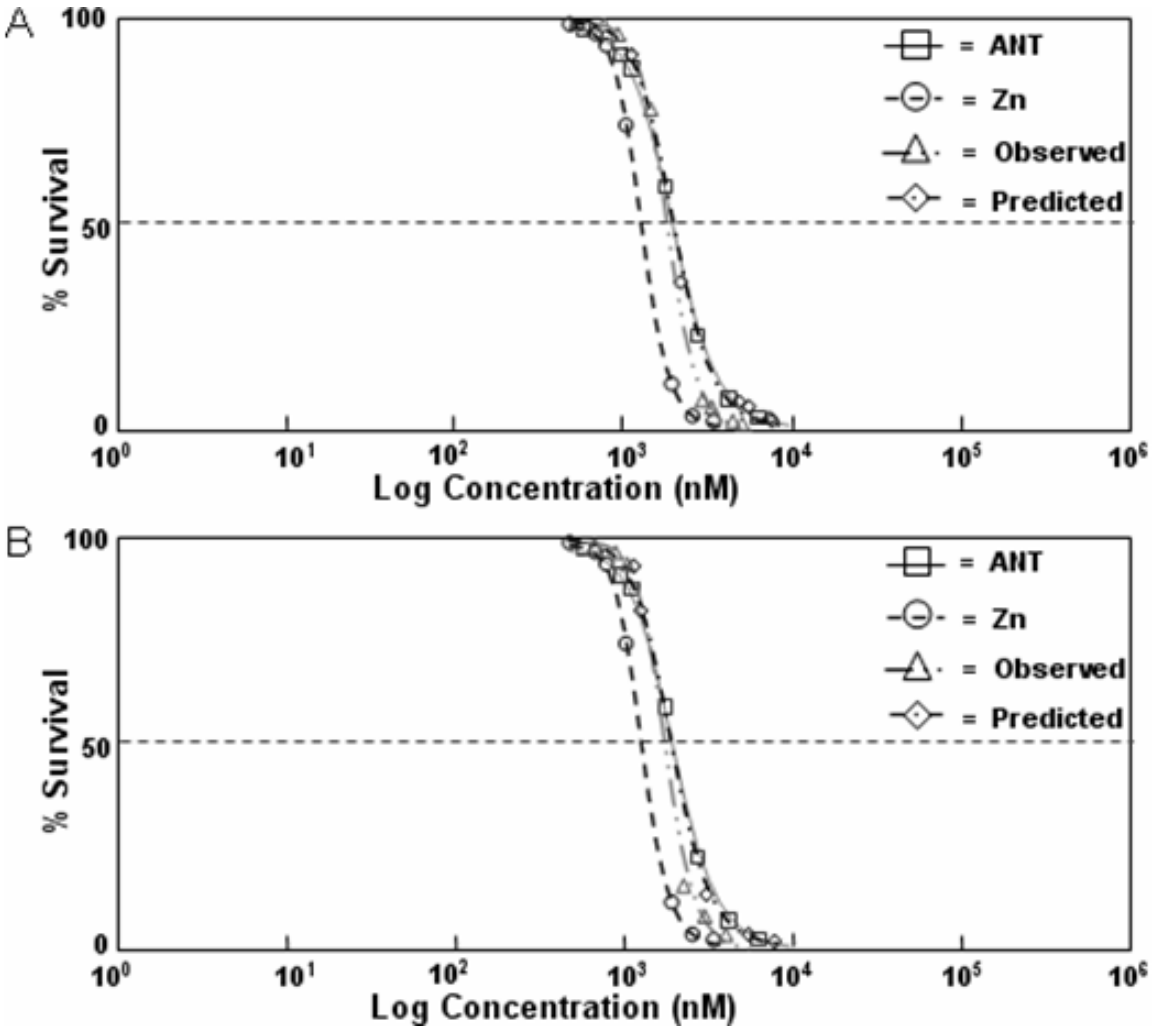

Figure 4.51 Concentration response curves for ANT + 1 nM Zn and ANT + 10 nM Zn to *Hyalella azteca* under dark conditions. ANT concentrations were varied while Zn was kept at a constant concentration. A. ANT + 1 nM Zn B. ANT + 10 nM Zn.

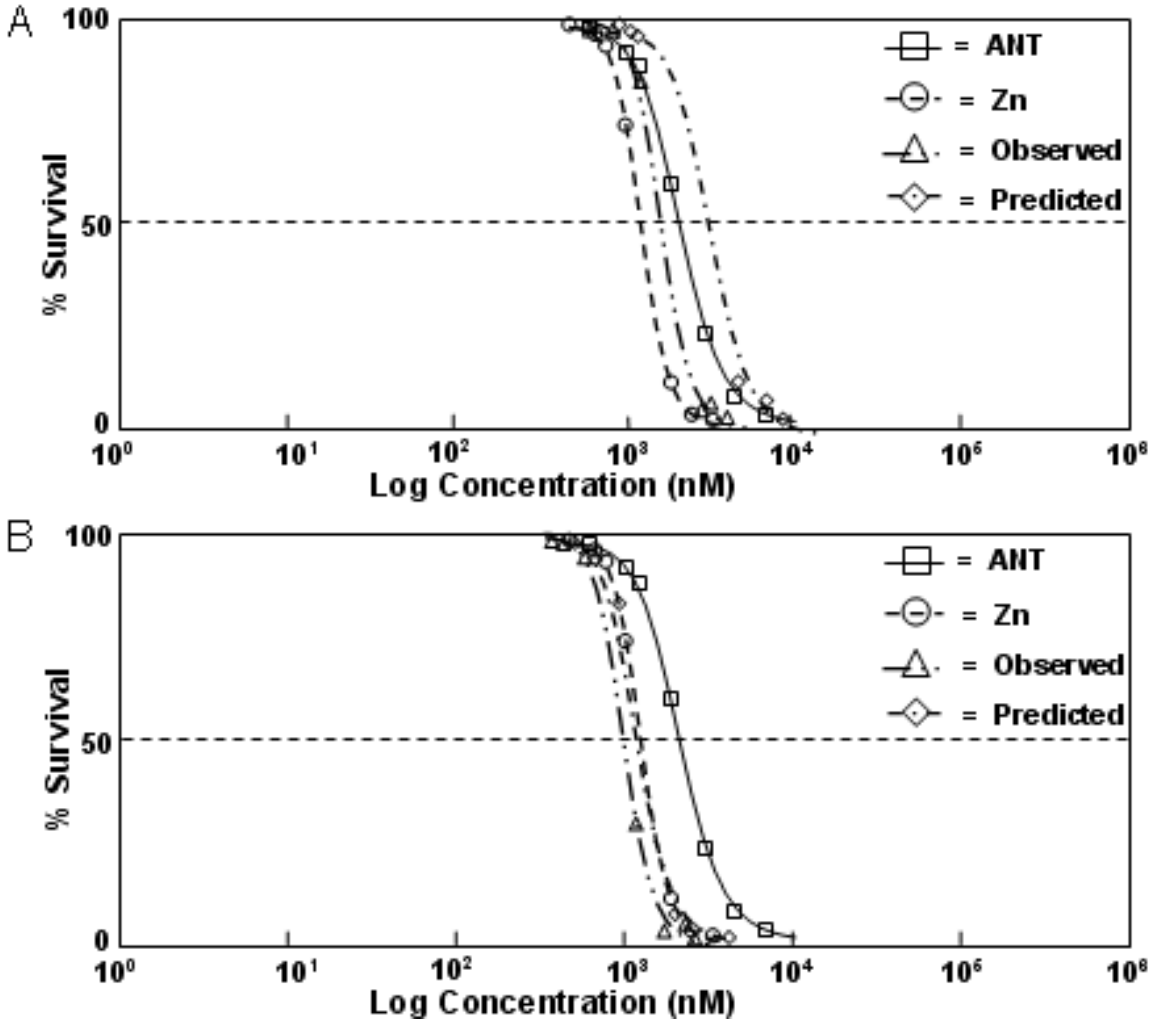

Figure 4.52 Concentration response curves for ANT + 100 nM Zn and ANT + 1000 nM Zn to *Hyalella azteca* under dark conditions. ANT concentrations were varied while Zn was kept at a constant concentration. A. ANT + 100 nM Zn B. ANT + 1000 nM Zn.

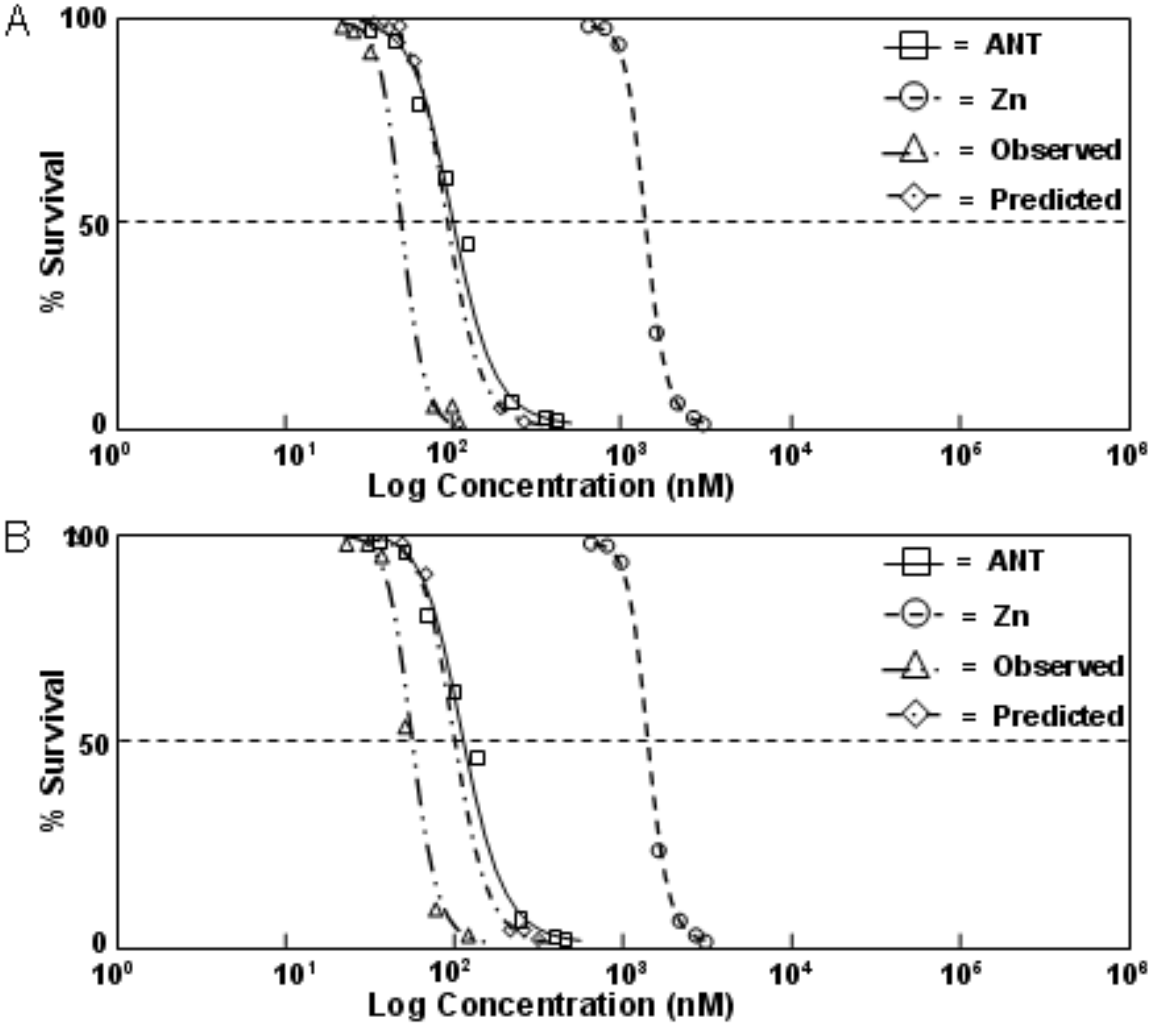

Figure 4.53 Concentration response curves for ANT + 1 nM Zn and ANT + 10 nM Zn to *Hyalella azteca* under PAR conditions. ANT concentrations were varied while Zn was kept at a constant concentration. A. ANT + 1 nM Zn B. ANT + 10 nM Zn.

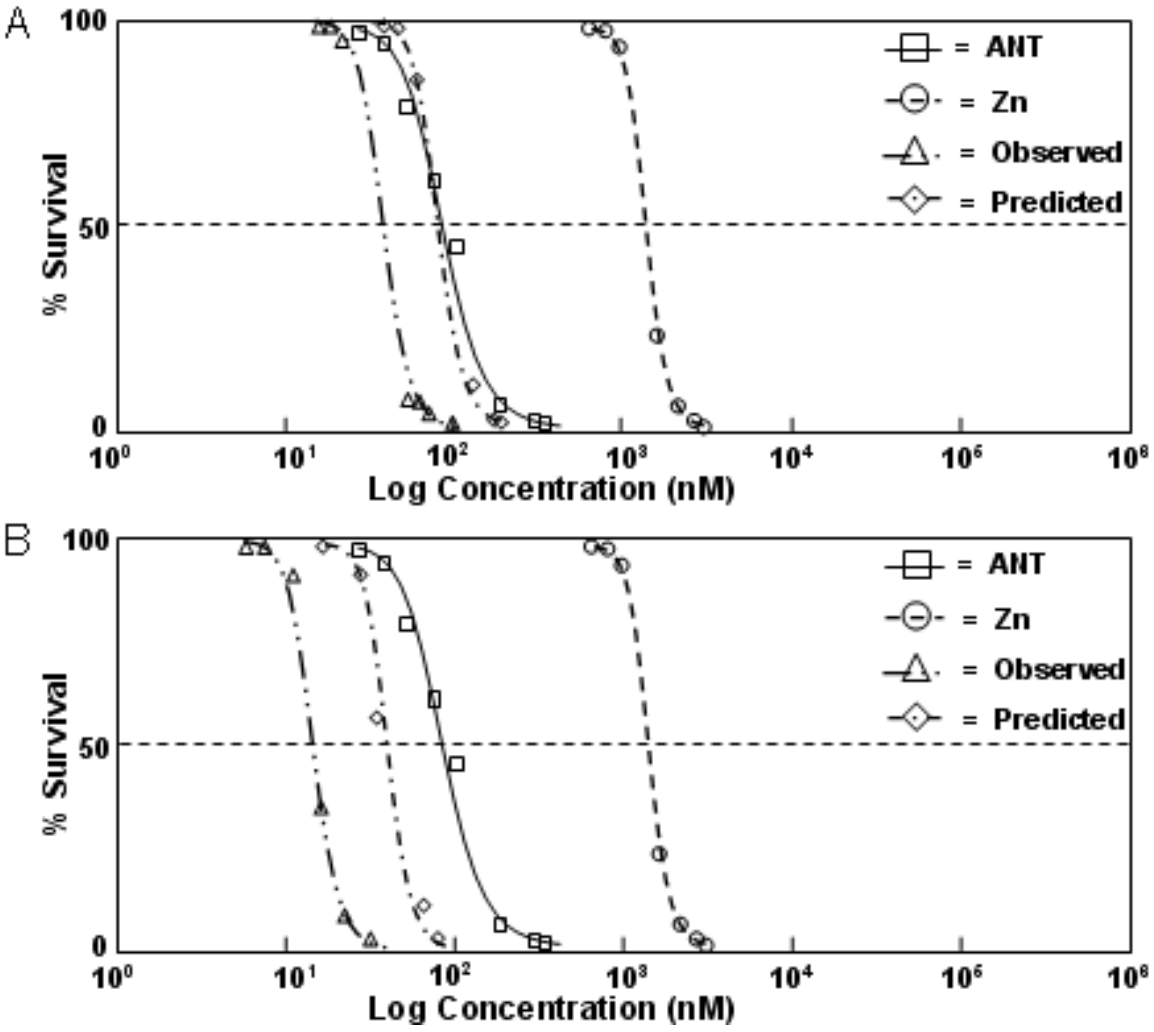

Figure 4.54 Concentration response curves for ANT + 100 nM Zn and ANT + 1000 nM Zn to *Hyalella azteca* under PAR conditions. ANT concentrations were varied while Zn was kept at a constant concentration. A. ANT+ 100 nM Zn B. ANT+ 1000 nM Zn.

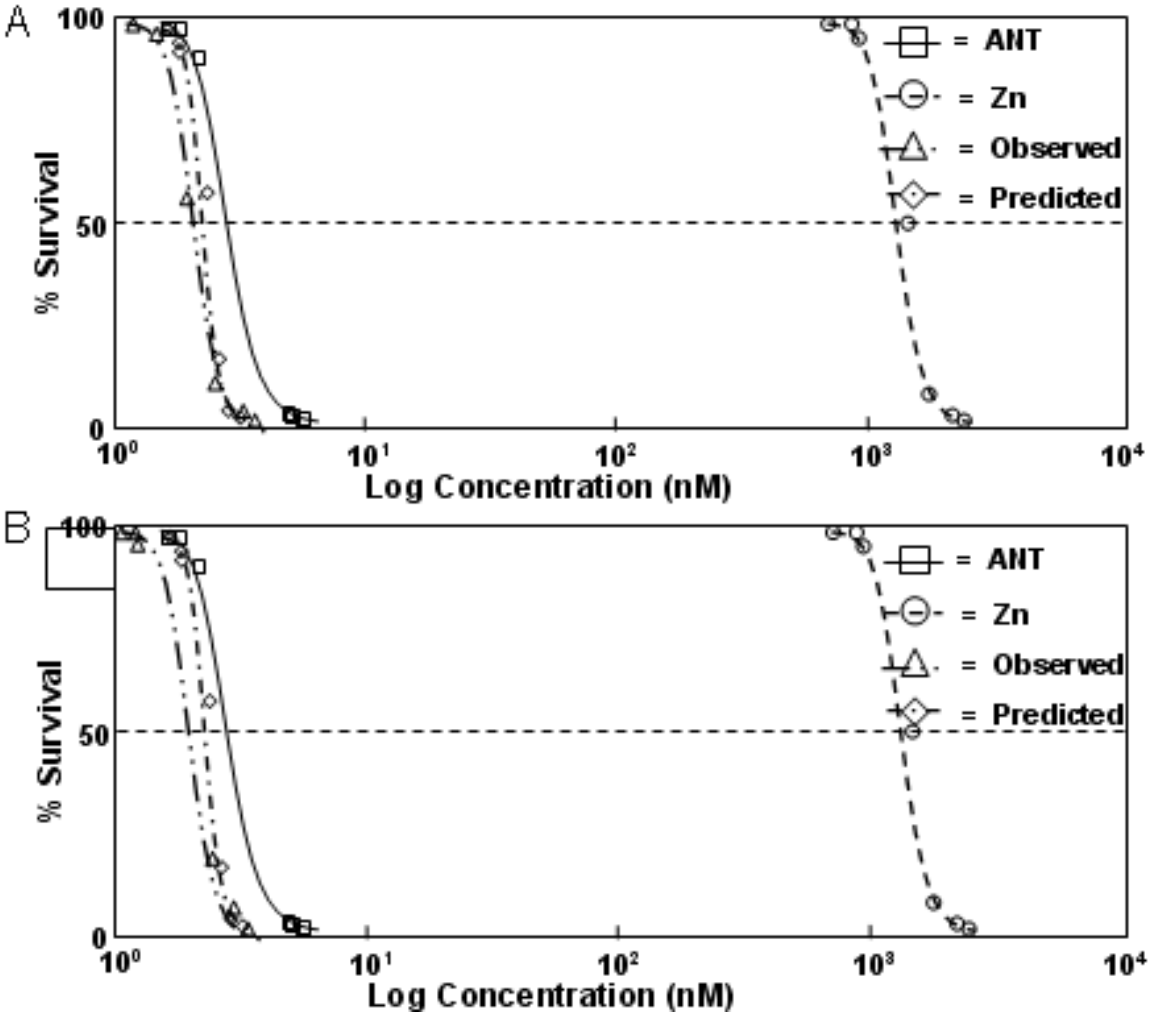

Figure 4.55 Concentration response curves for ANT + 1 nM Zn and ANT + 10 nM Zn to *Hyalella azteca* under SSR conditions. ANT concentrations were varied while Zn was kept at a constant concentration. A. ANT + 1 nM Zn B. ANT + 10 nM Zn.

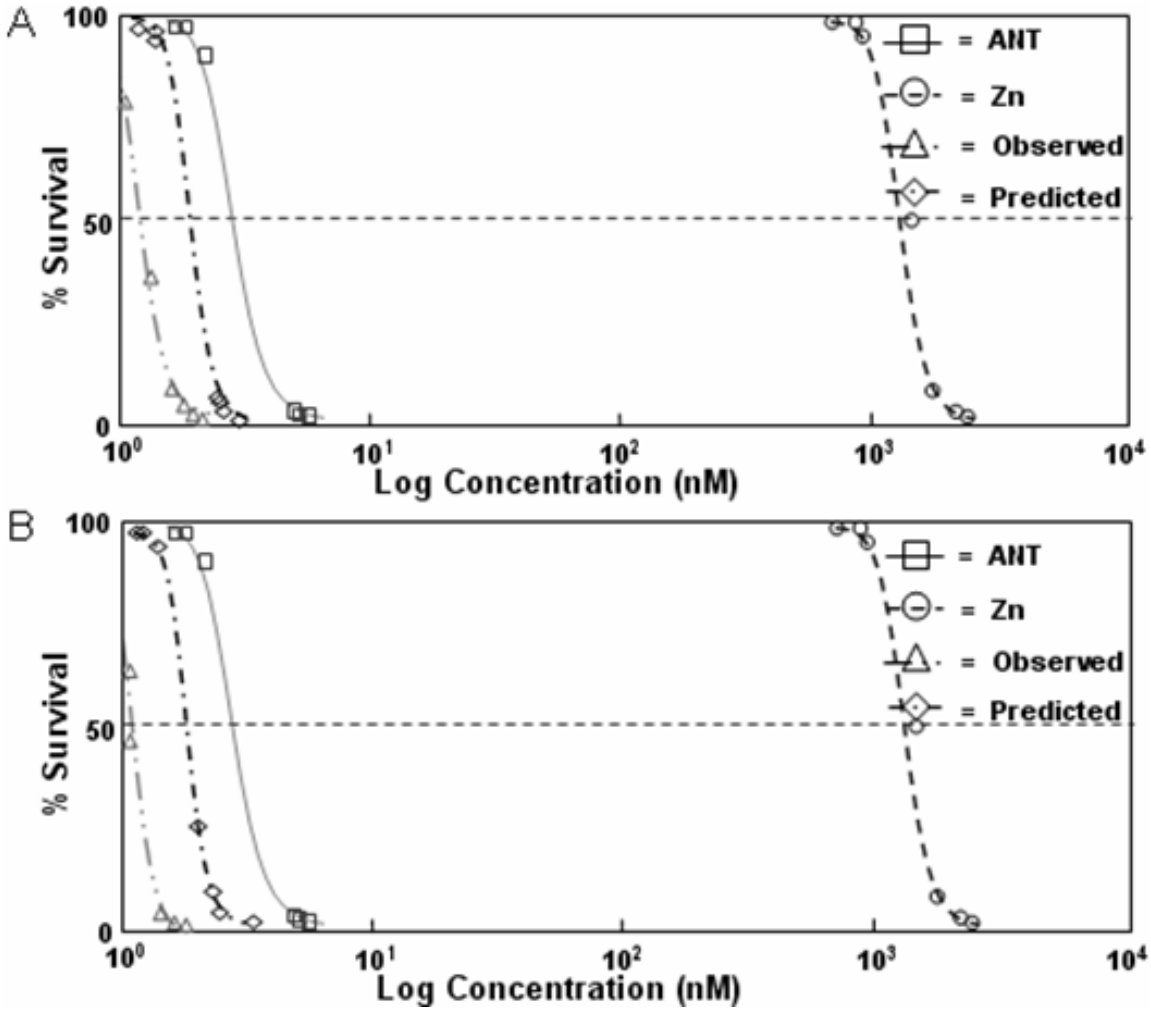

Figure 4.56 Concentration response curves for ANT + 100 nM Zn and ANT + 1000 nM Zn to *Hyalella azteca* under SSR conditions. ANT concentrations were varied while Zn was kept at a constant concentration. A. ANT + 100 nM Zn B. ANT + 1000 nM Zn.

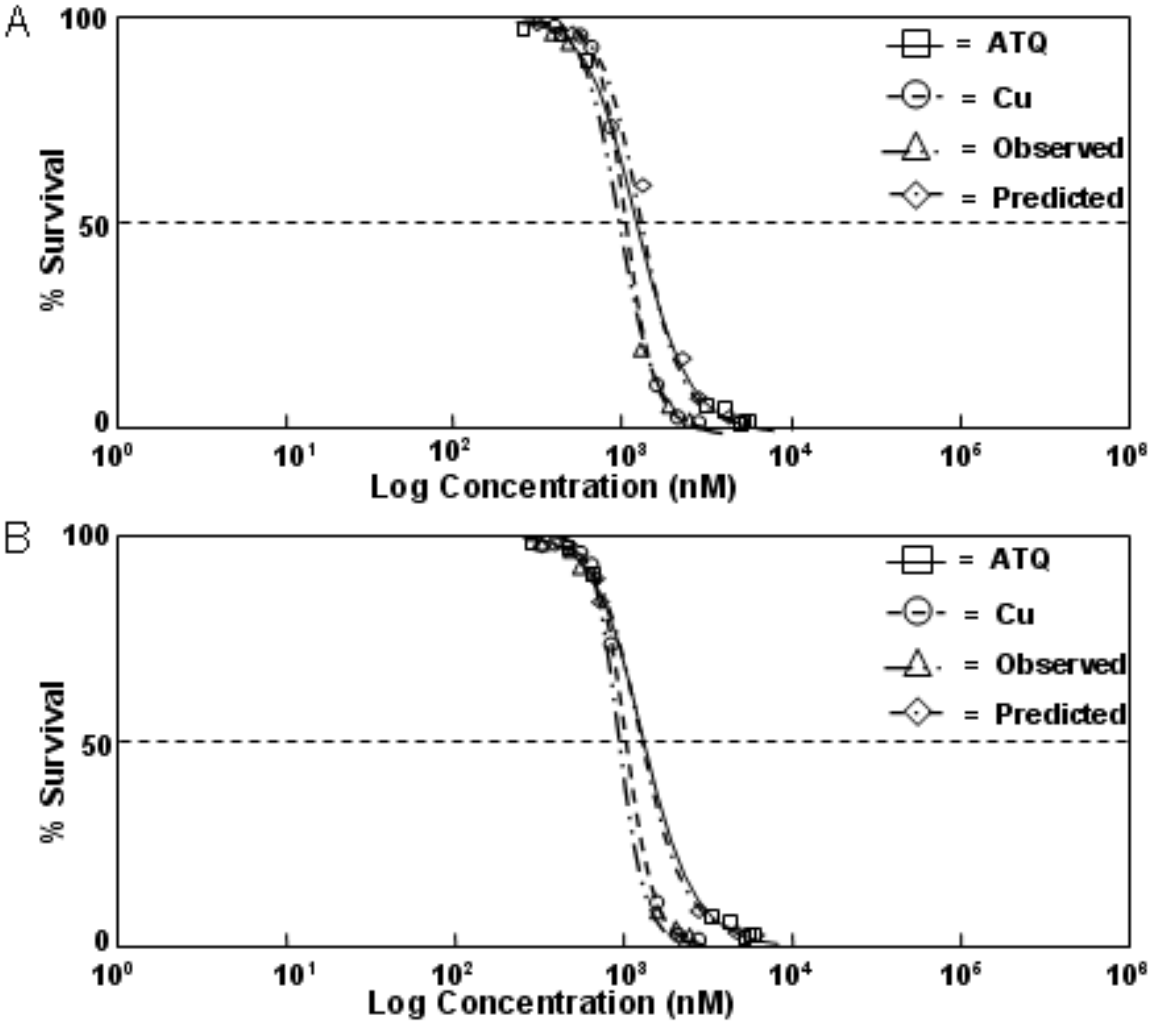

Figure 4.57 Concentration response curves for ATQ + 1 nM Cu and ATQ + 10 nM Cu to *Hyalella azteca* under dark conditions. ATQ concentrations were varied while Cu was kept at a constant concentration. A. ATQ + 1 nM Cu B. ATQ + 10 nM Cu.

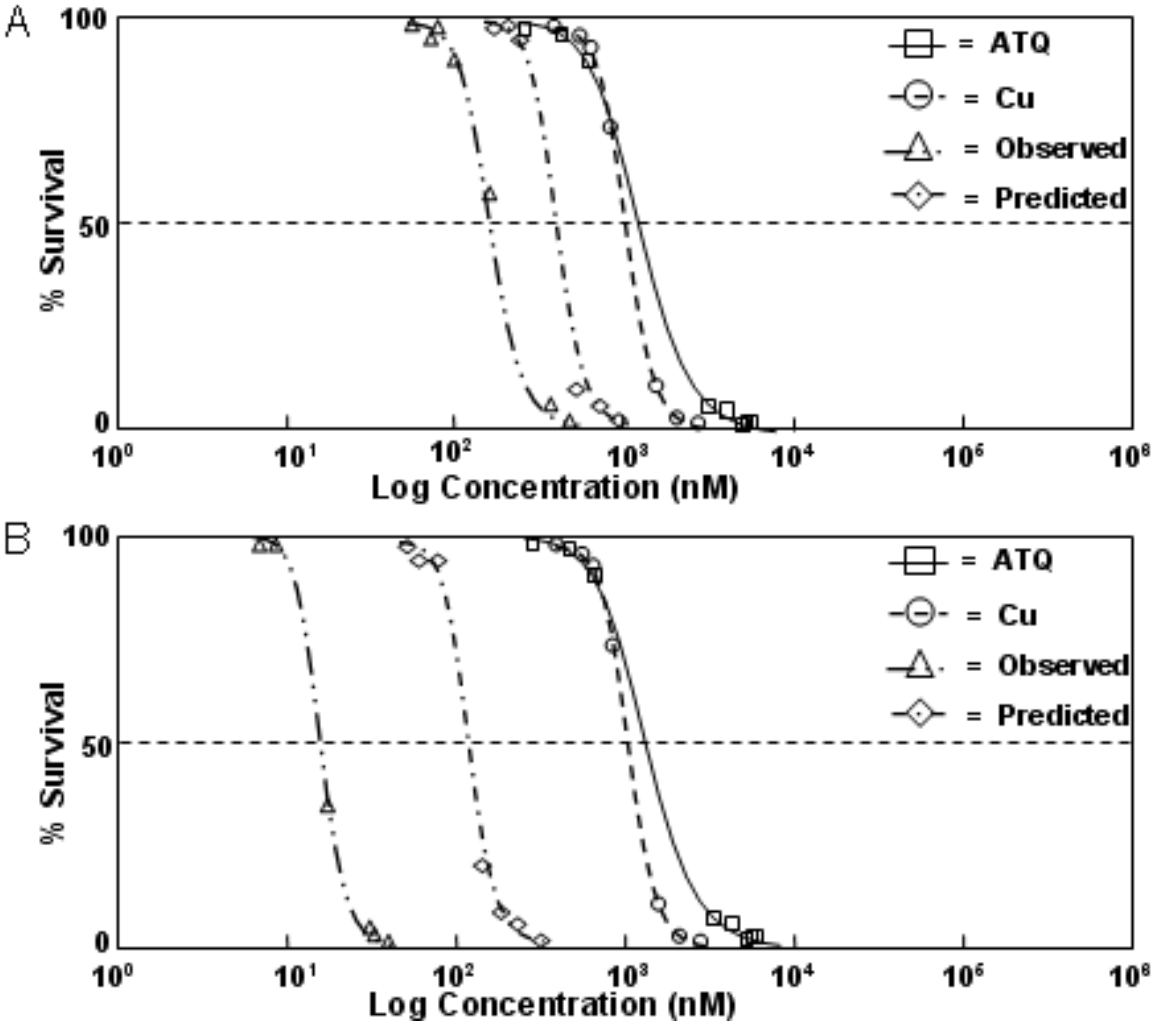

Figure 4.58 Concentration response curves for ATQ + 100 nM Cu and ATQ + 1000 nM Cu to *Hyalella azteca* under dark conditions. ATQ concentrations were varied while Cu was kept at a constant concentration. A. ATQ + 100 nM Cu B. ATQ + 1000 nM Cu.

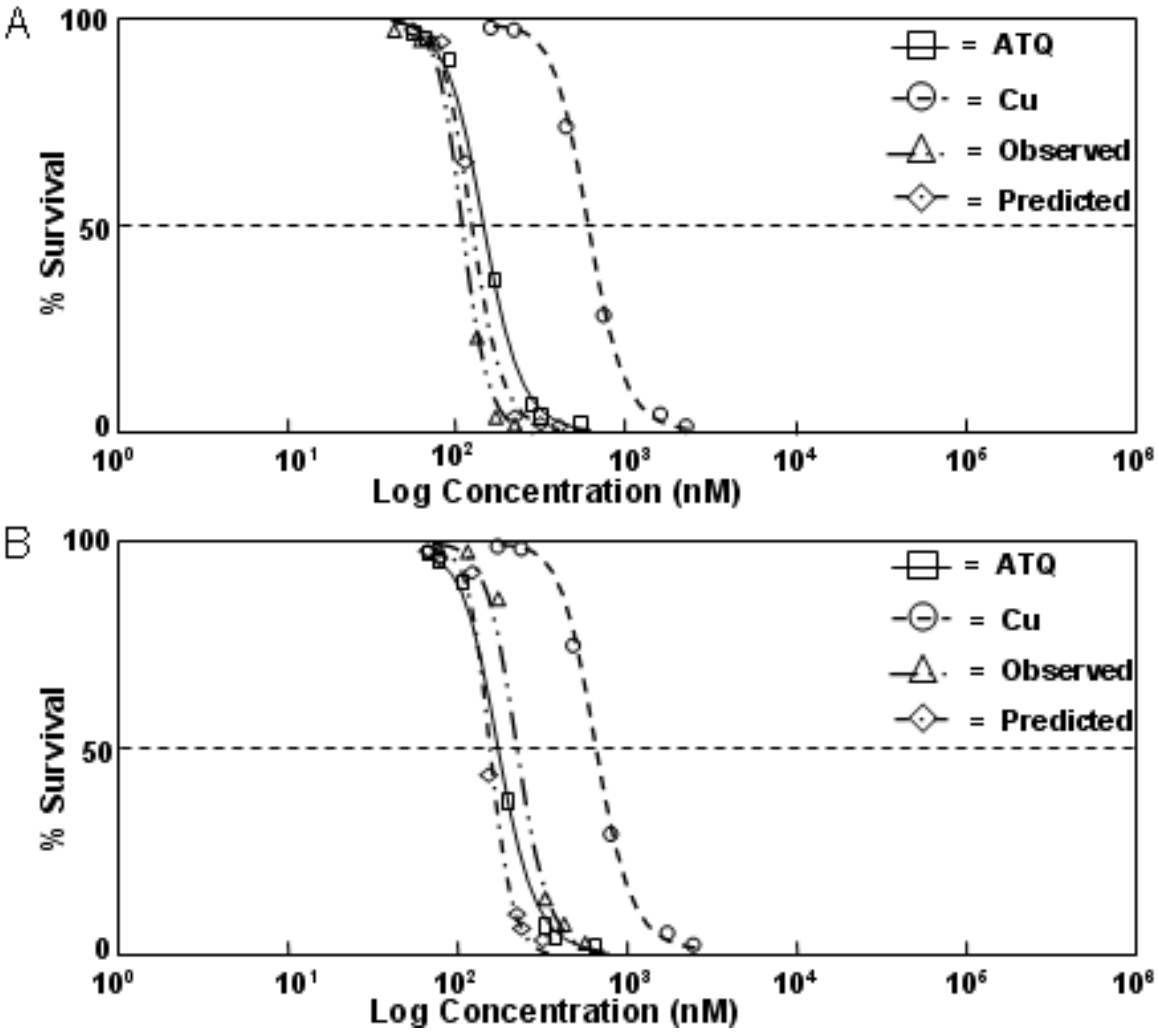

Figure 4.59 Concentration response curves for ATQ + 1 nM Cu and ATQ + 10 nM Cu to *Hyalella azteca* under PAR conditions. ATQ concentrations were varied while Cu was kept at a constant concentration. A. ATQ + 1 nM Cu B. ATQ T + 10 nM Cu.

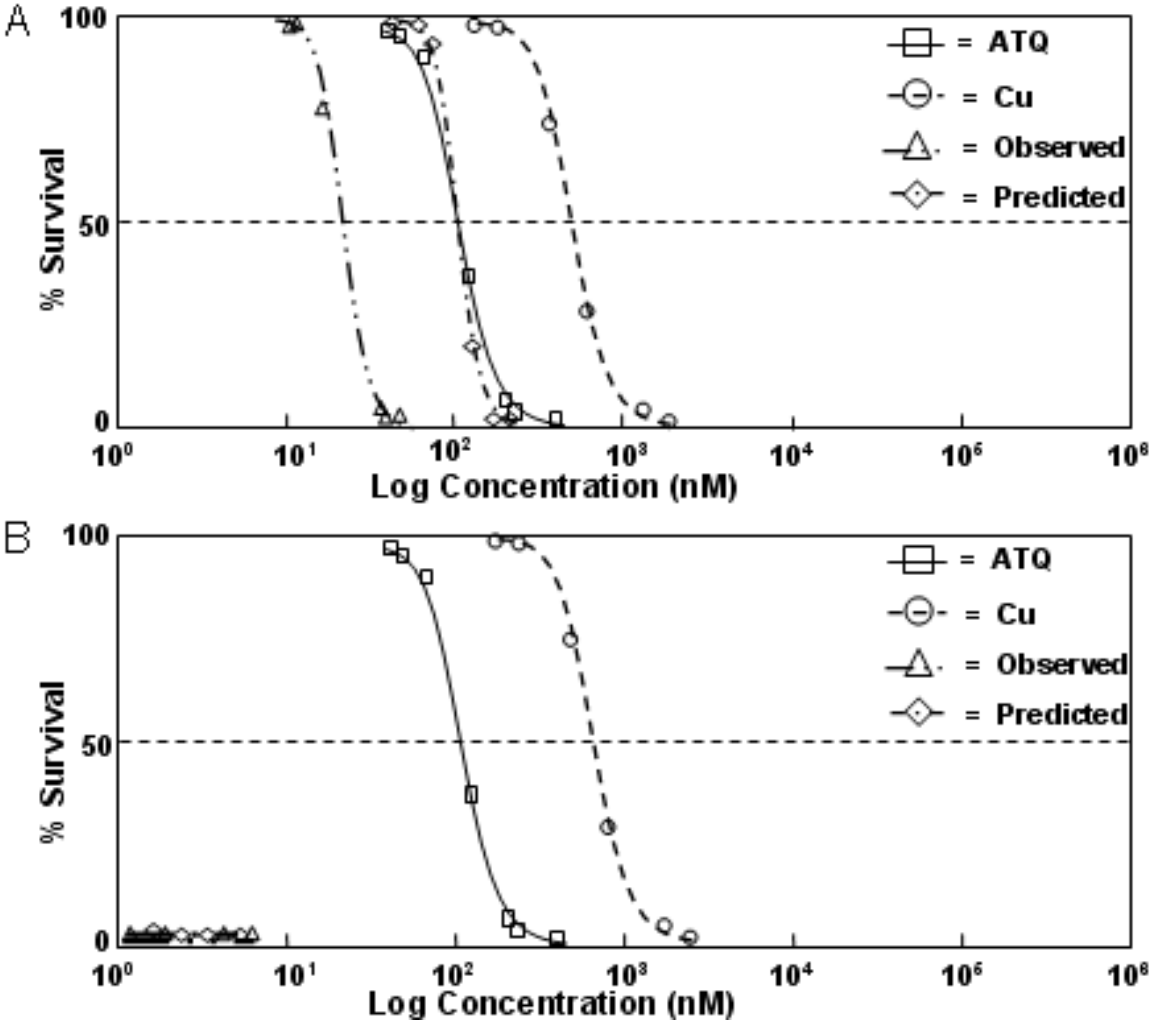

Figure 4.60 Concentration response curves for ATQ + 100 nM Cu and ATQ + 1000 nM Cu to *Hyalella azteca* under PAR conditions. ATQ concentrations were varied while Cu was kept at a constant concentration. A. ATQ + 100 nM Cu B. ATQ + 1000 nM Cu.

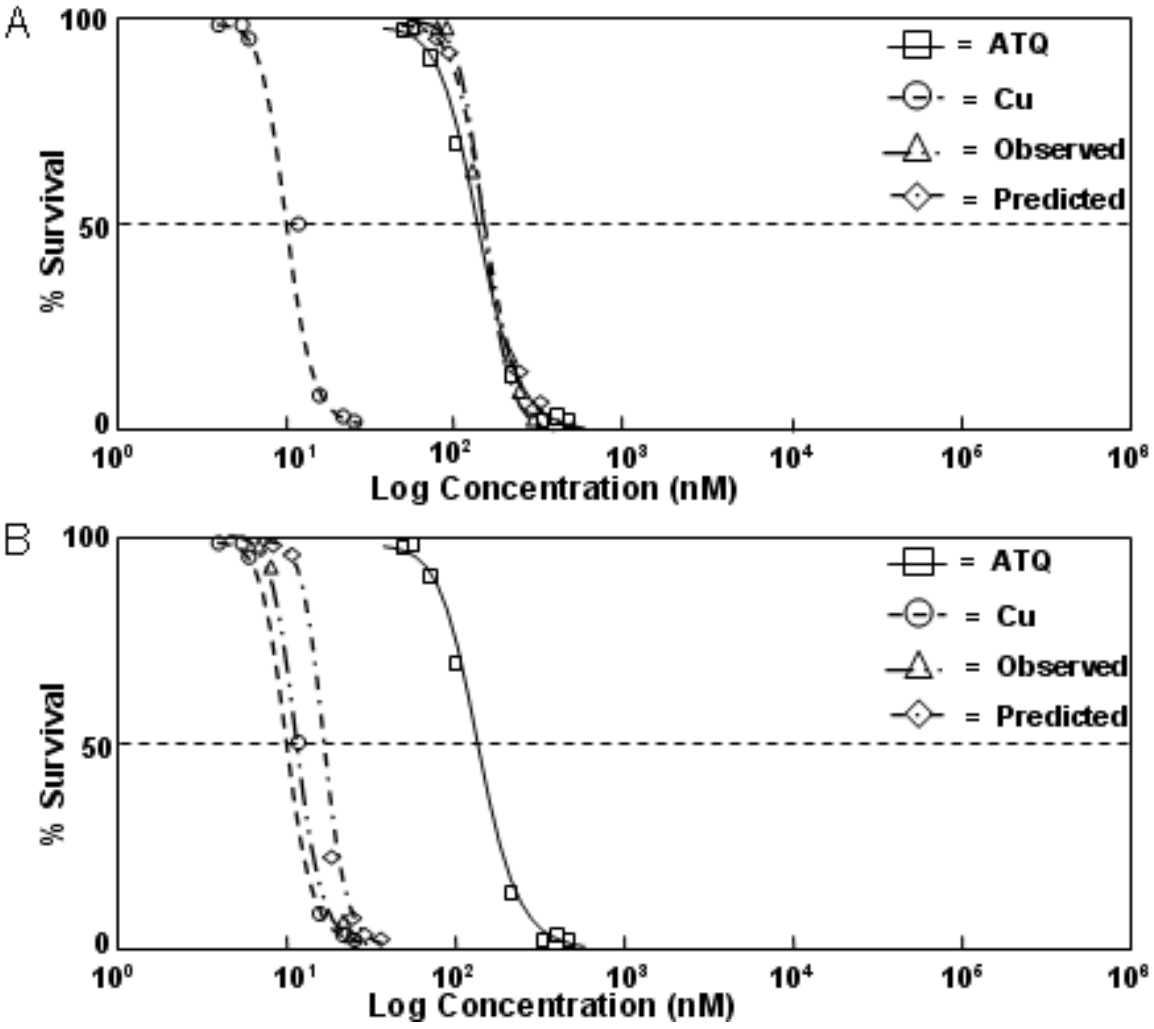

Figure 4.61 Concentration response curves for ATQ + 1 nM Cu and ATQ + 10 nM Cu to *Hyalella azteca* under SSR conditions. ATQ concentrations were varied while Cu was kept at a constant concentration. A. ATQ + 1 nM Cu B. ATQ + 10 nM Cu.

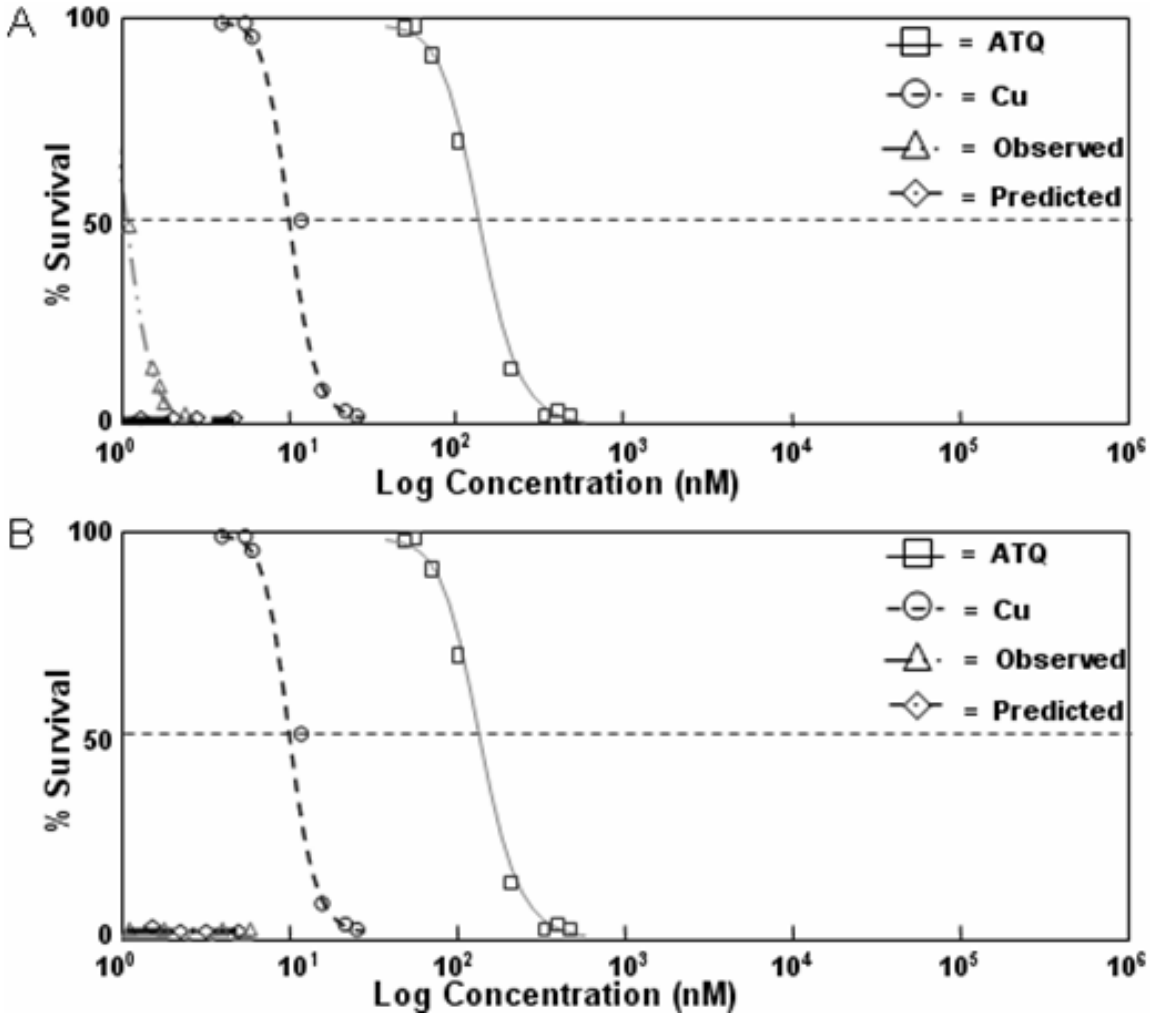

Figure 4.62 Concentration response curves for ATQ + 100 nM Cu and ATQ + 1000 nM Cu to *Hyalella azteca* under SSR conditions. ATQ concentrations were varied while Cu was kept at a constant concentration. A. ATQ + 100 nM Cu B. ATQ + 1000 nM Cu

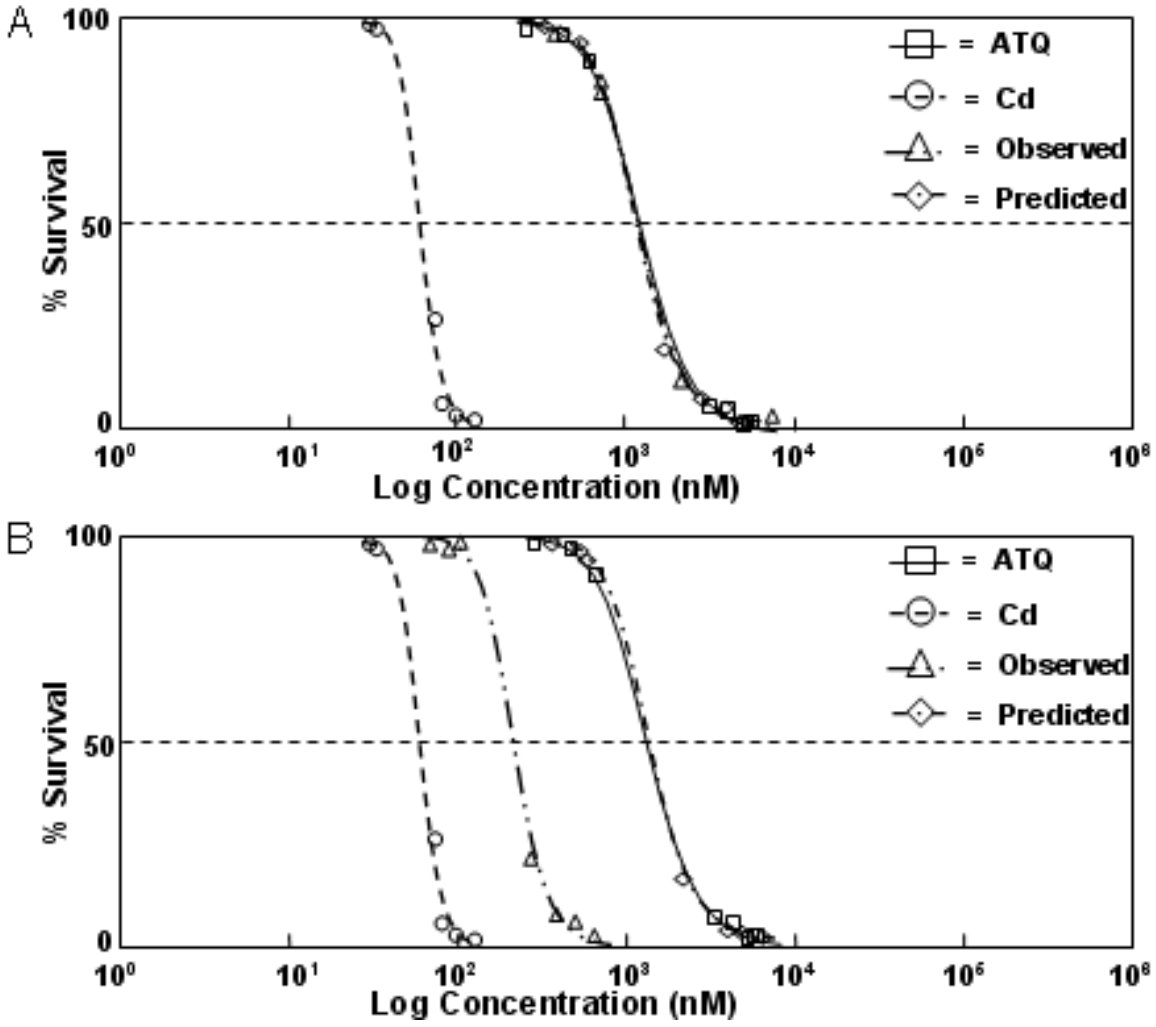

Figure 4.63 Concentration response curves for ATQ + 1 nM Cd and ATQ + 10 nM Cd to *Hyalella azteca* under dark conditions. ATQ concentrations were varied while Cd was kept at a constant concentration. A. ATQ + 1 nM Cd B. ATQ + 10 nM Cd.

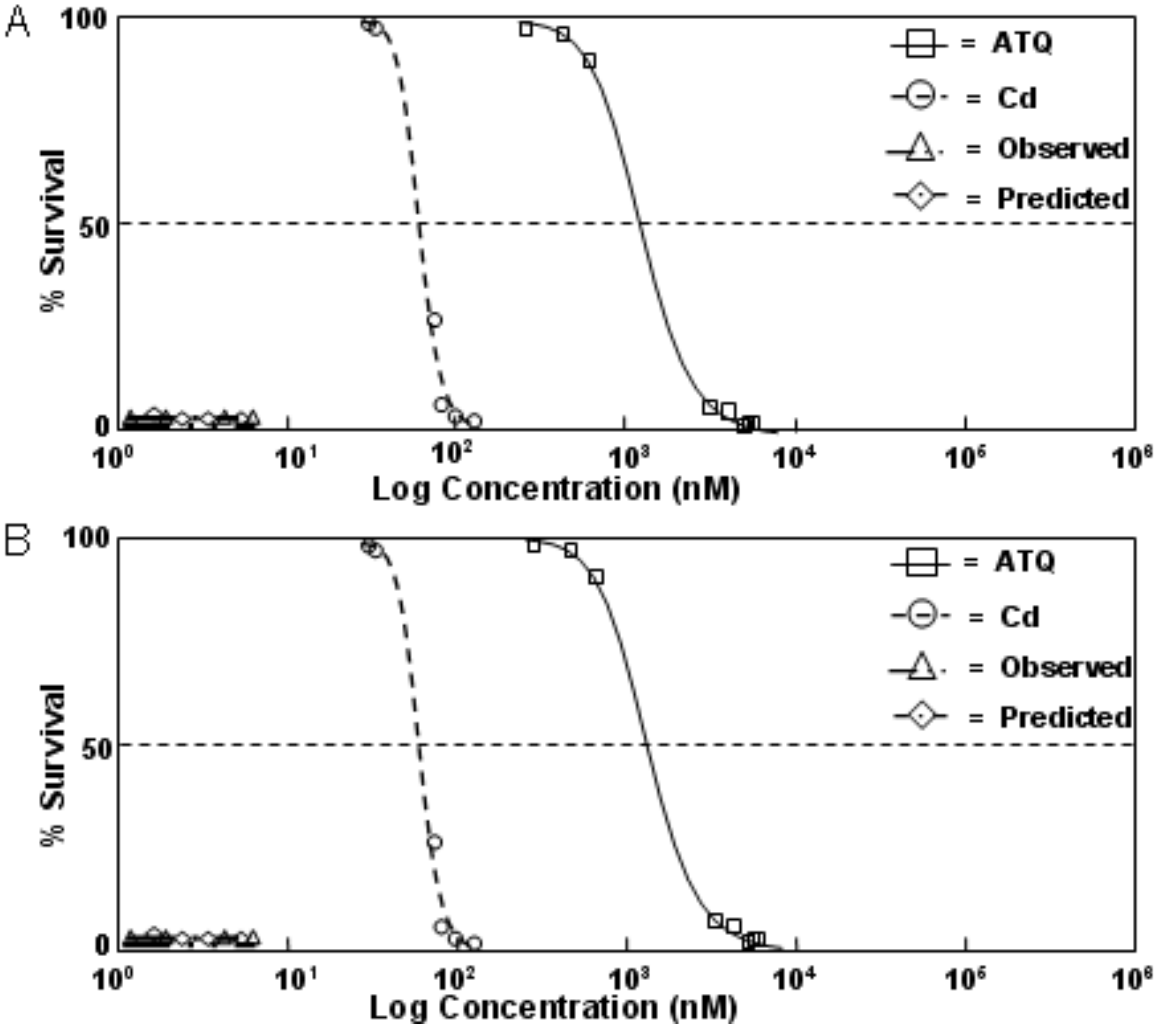

Figure 4.64 Concentration response curves for ATQ + 100 nM Cd and ATQ + 1000 nM Cd to *Hyalella azteca* under dark conditions. ATQ concentrations were varied while Cd was kept at a constant concentration. A. ATQ + 100 nM Cd B. ATQ + 1000 nM Cd.

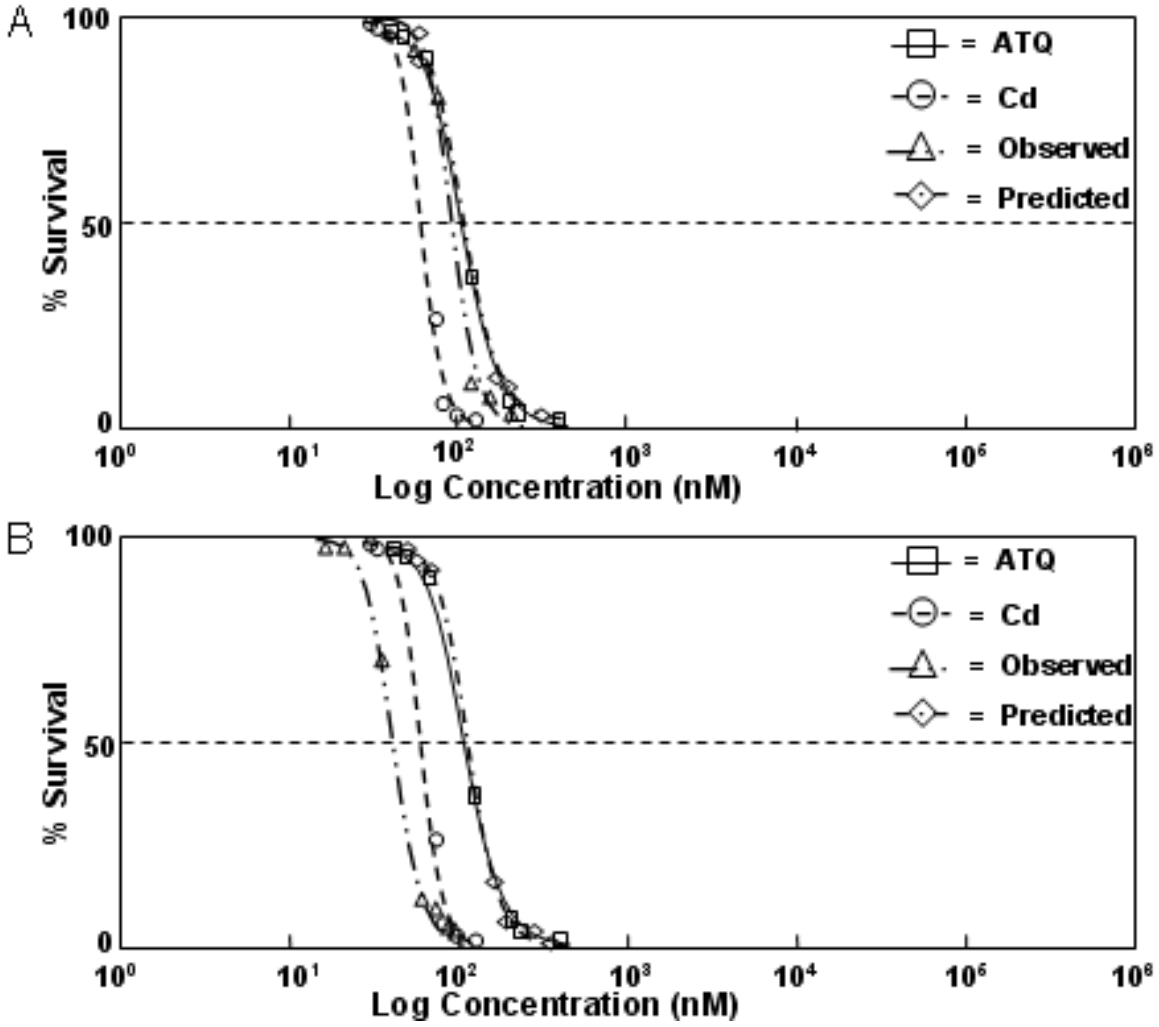

Figure 4.65 Concentration response curves for ATQ + 1 nM Cd and ATQ + 10 nM Cd to *Hyalella azteca* under PAR conditions. ATQ concentrations were varied while Cd was kept at a constant concentration. A. ATQ + 1 nM Cd B. ATQ T + 10 nM Cd.

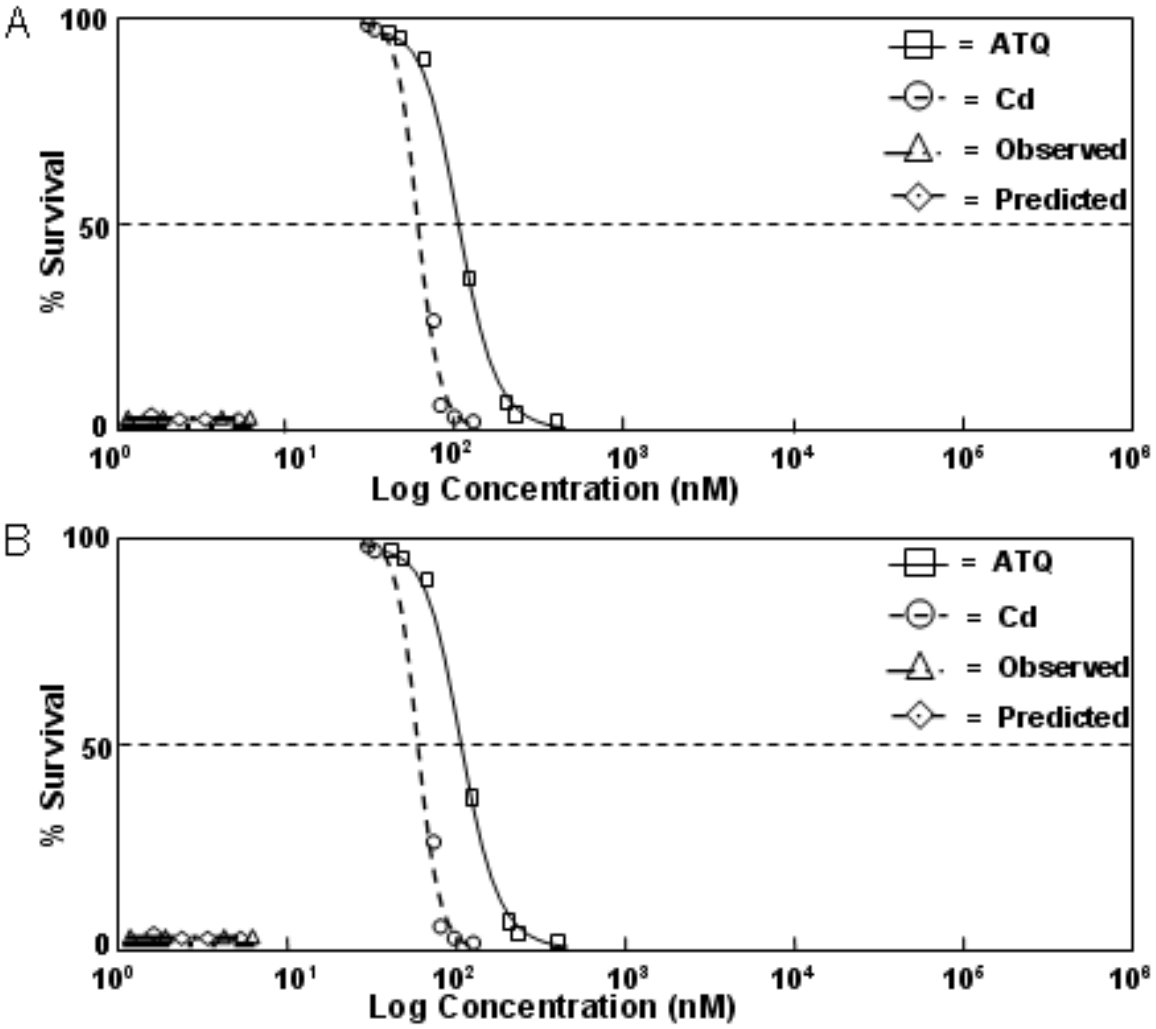

Figure 4.66 Concentration response curves for ATQ + 100 nM Cd and ATQ + 1000 nM Cd to *Hyalella azteca* under PAR conditions. ATQ concentrations were varied while Cd was kept at a constant concentration. A. ATQ + 100 nM Cd B. ATQ + 1000 nM Cd.

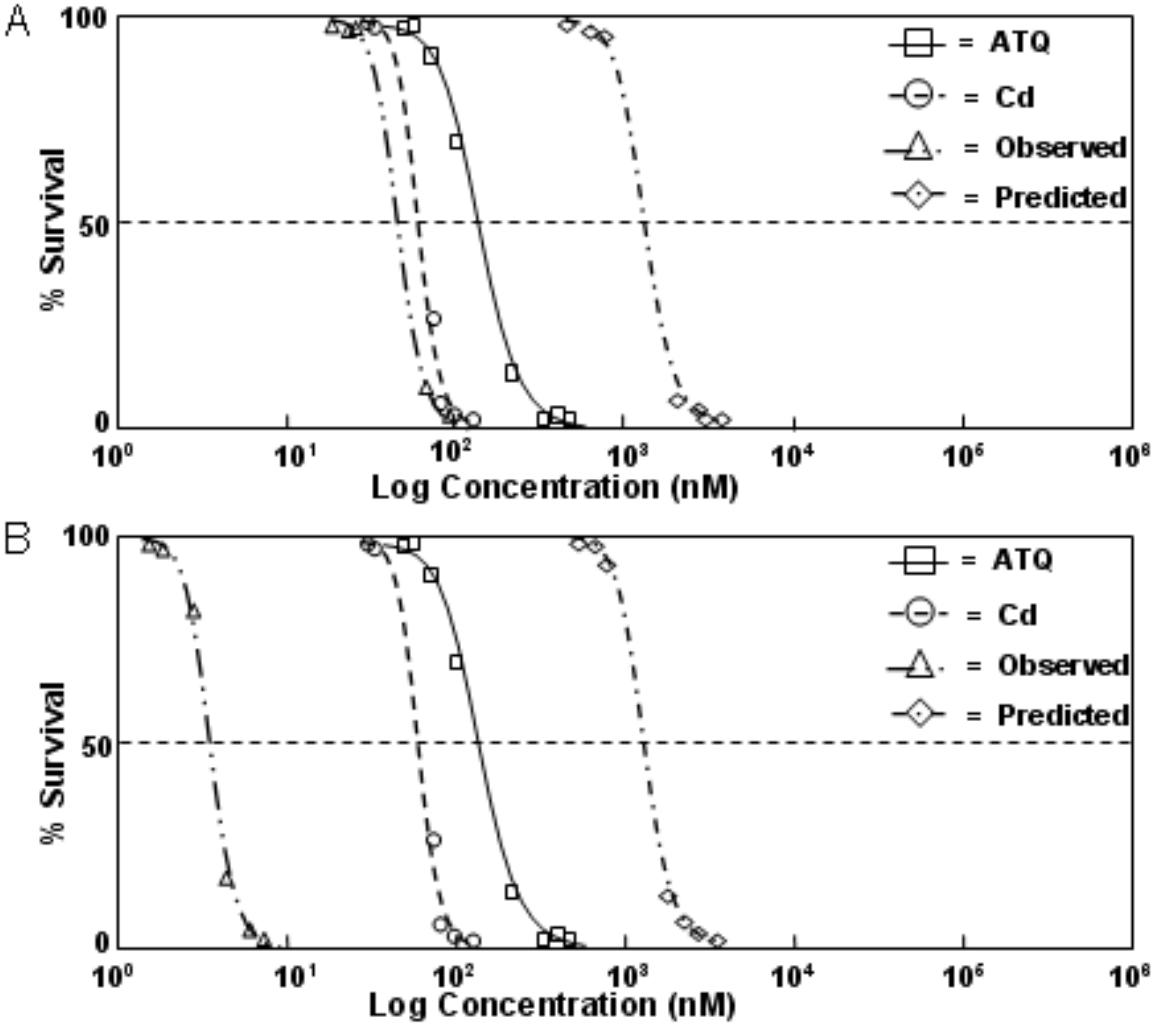

Figure 4.67 Concentration response curves for ATQ + 1 nM Cd and ATQ + 10 nM Cd to *Hyalella azteca* under SSR conditions. ATQ concentrations were varied while Cd was kept at a constant concentration. A. ATQ + 1 nM Cd B. ATQ + 10 nM Cd.

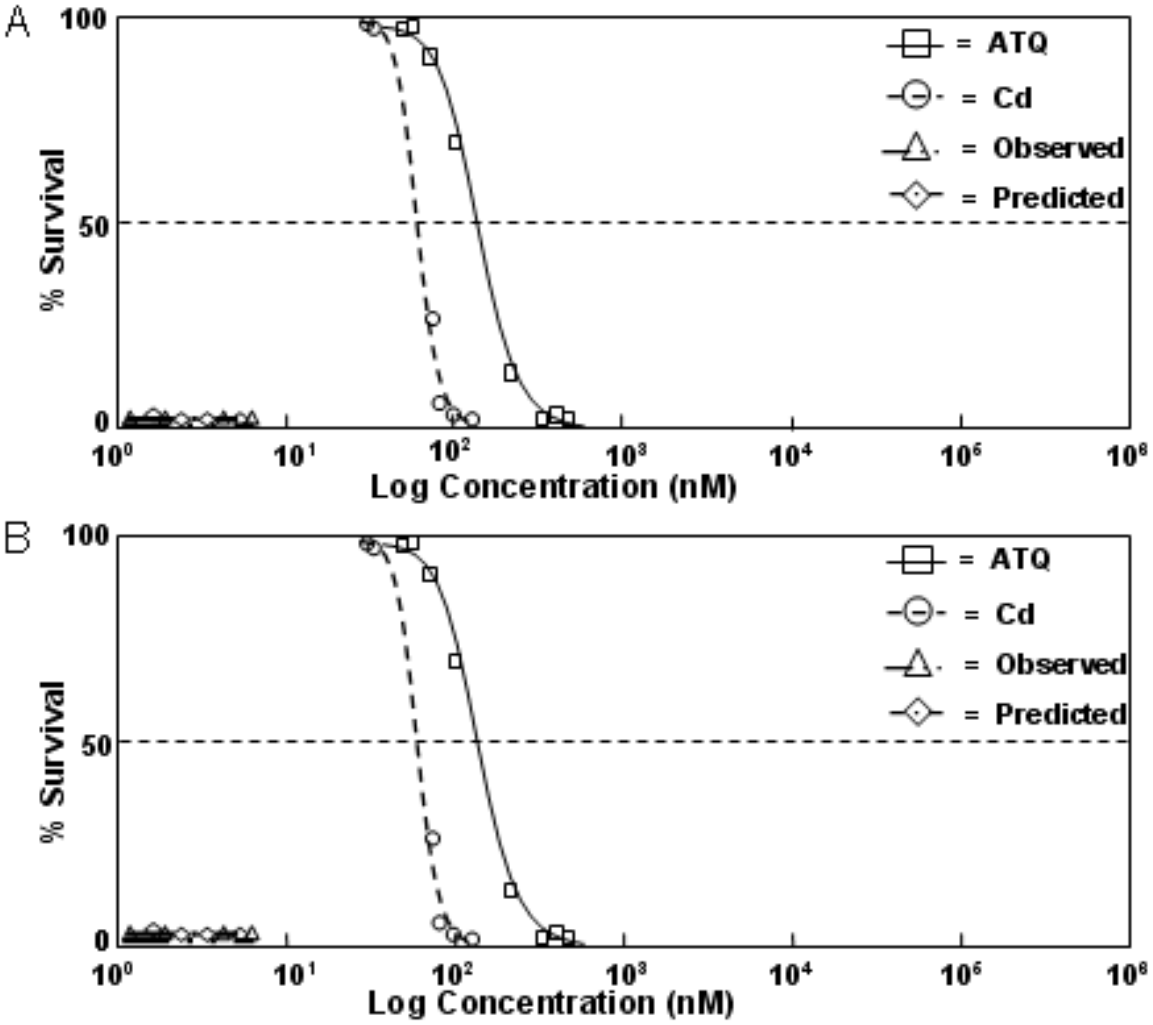

Figure 4.68 Concentration response curves for ATQ + 100 nM Cd and ATQ + 1000 nM Cd to *Hyalella azteca* under SSR conditions. ATQ concentrations were varied while Cd was kept at a constant concentration. A. ATQ + 100 nM Cd B. ATQ + 1000 nM Cd.

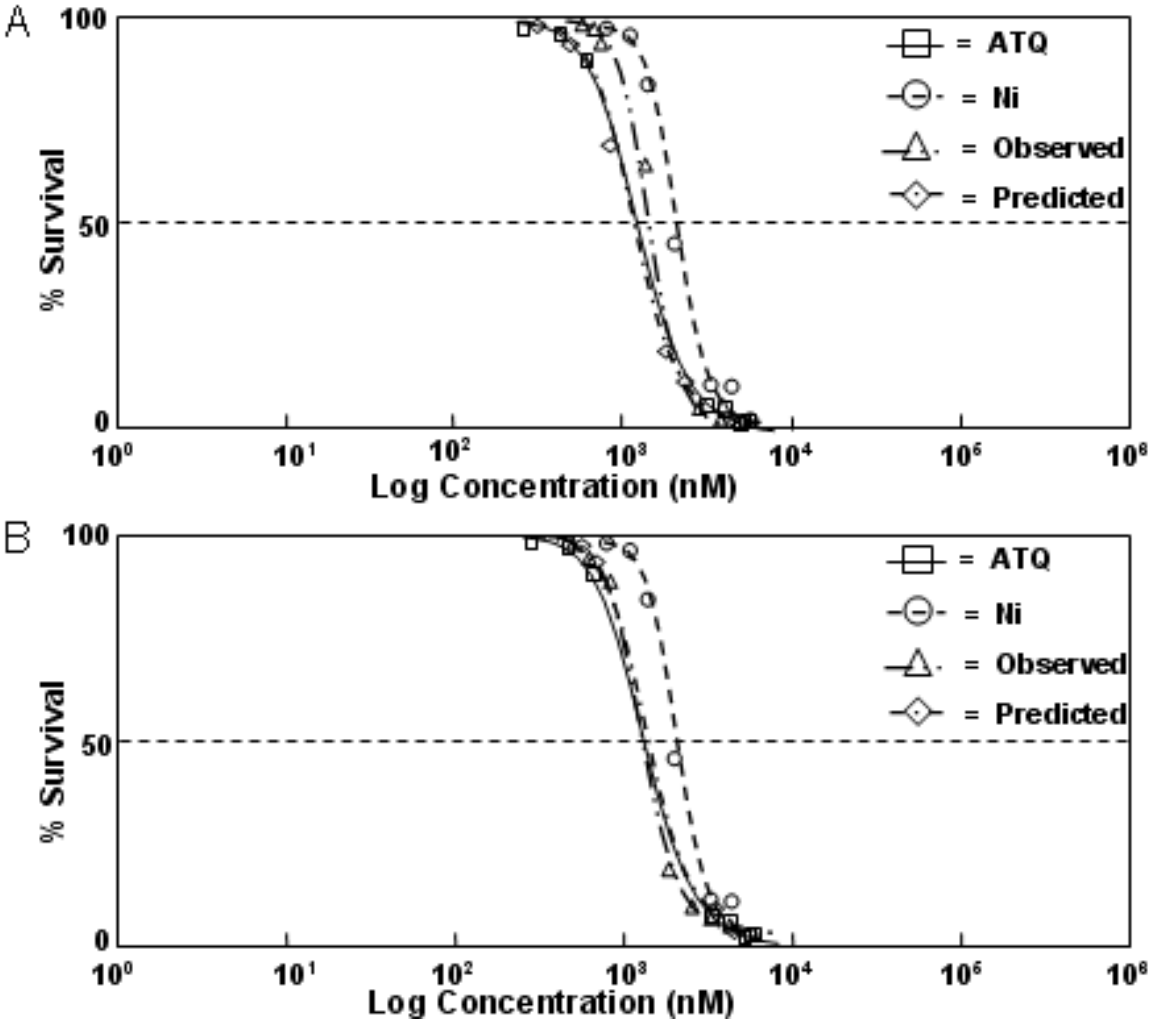

Figure 4.69 Concentration response curves for ATQ + 1 nM Ni and ATQ + 10 nM Ni to *Hyalella azteca* under dark conditions. ATQ concentrations were varied while Ni was kept at a constant concentration. A. ATQ + 1 nM Ni B. ATQ + 10 nM Ni.

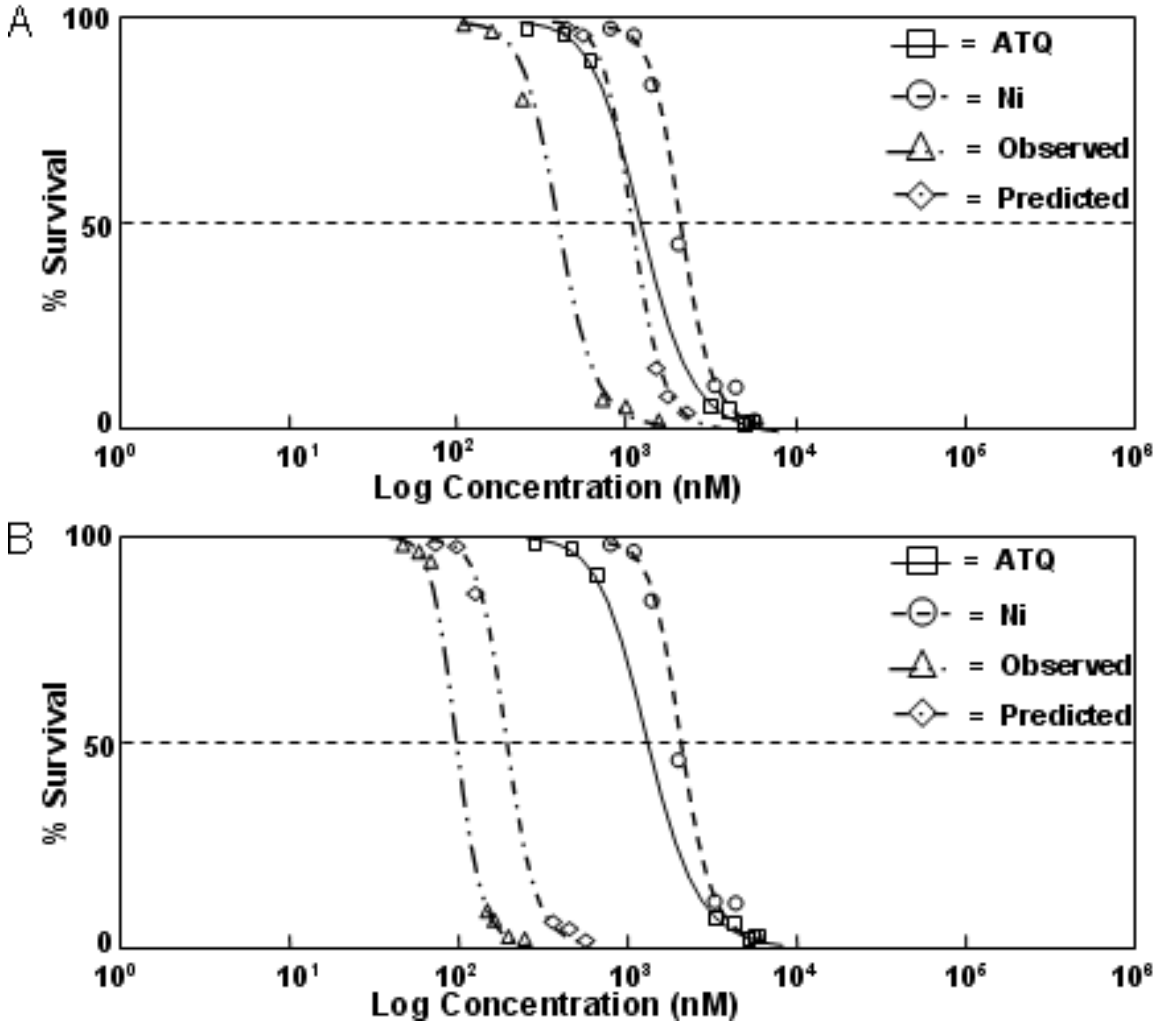

Figure 4.70 Concentration response curves for ATQ + 100 nM Ni and ATQ + 1000 nM Ni to *Hyalella azteca* under dark conditions. ATQ concentrations were varied while Ni was kept at a constant concentration. A. ATQ + 100 nM Ni B. ATQ + 1000 nM Ni.

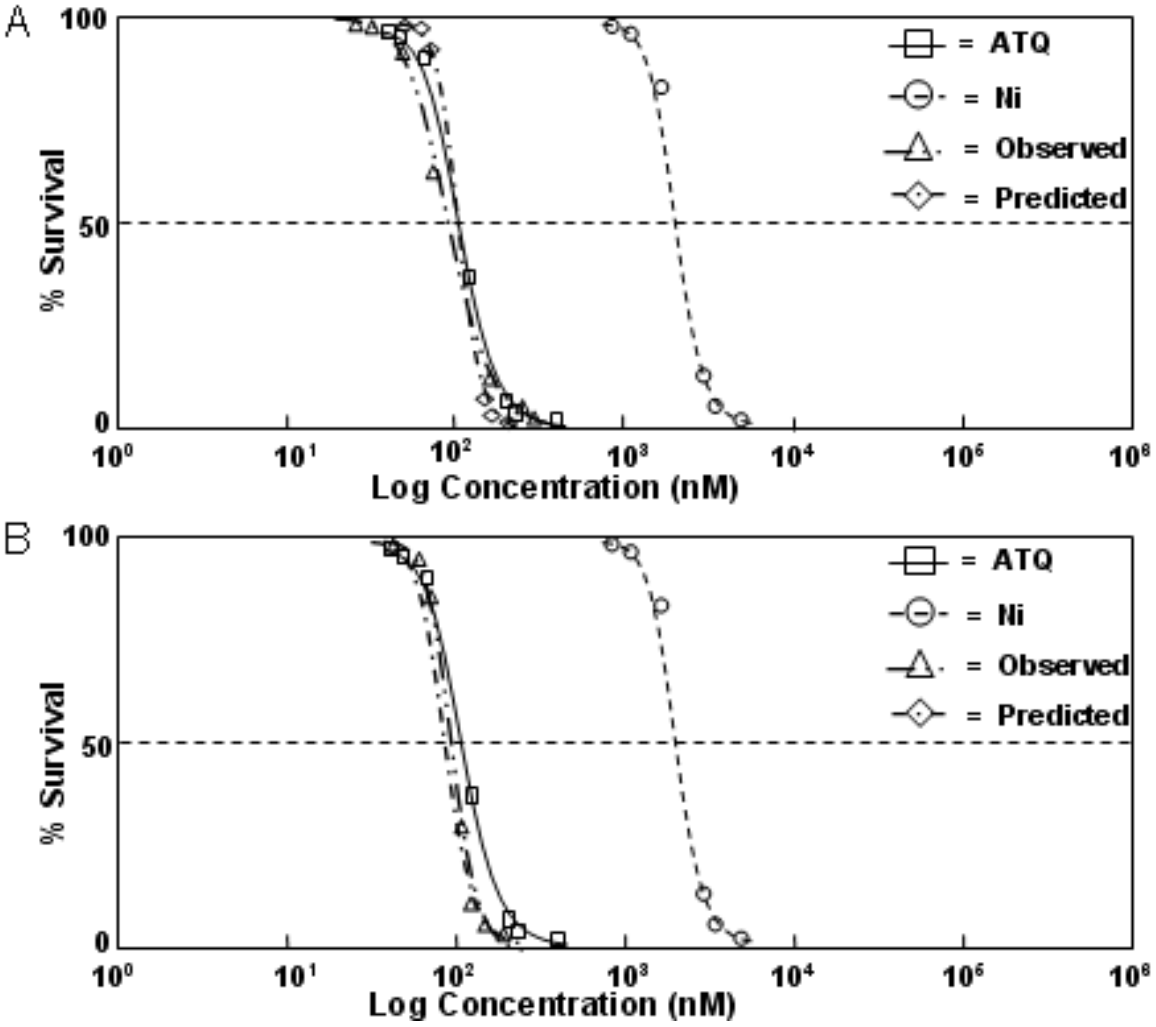

Figure 4.71 Concentration response curves for ATQ + 1 nM Ni and ATQ + 10 nM Ni to *Hyalella azteca* under PAR conditions. ATQ concentrations were varied while Ni was kept at a constant concentration. A. ATQ + 1 nM Ni B. ATQ T + 10 nM Ni.

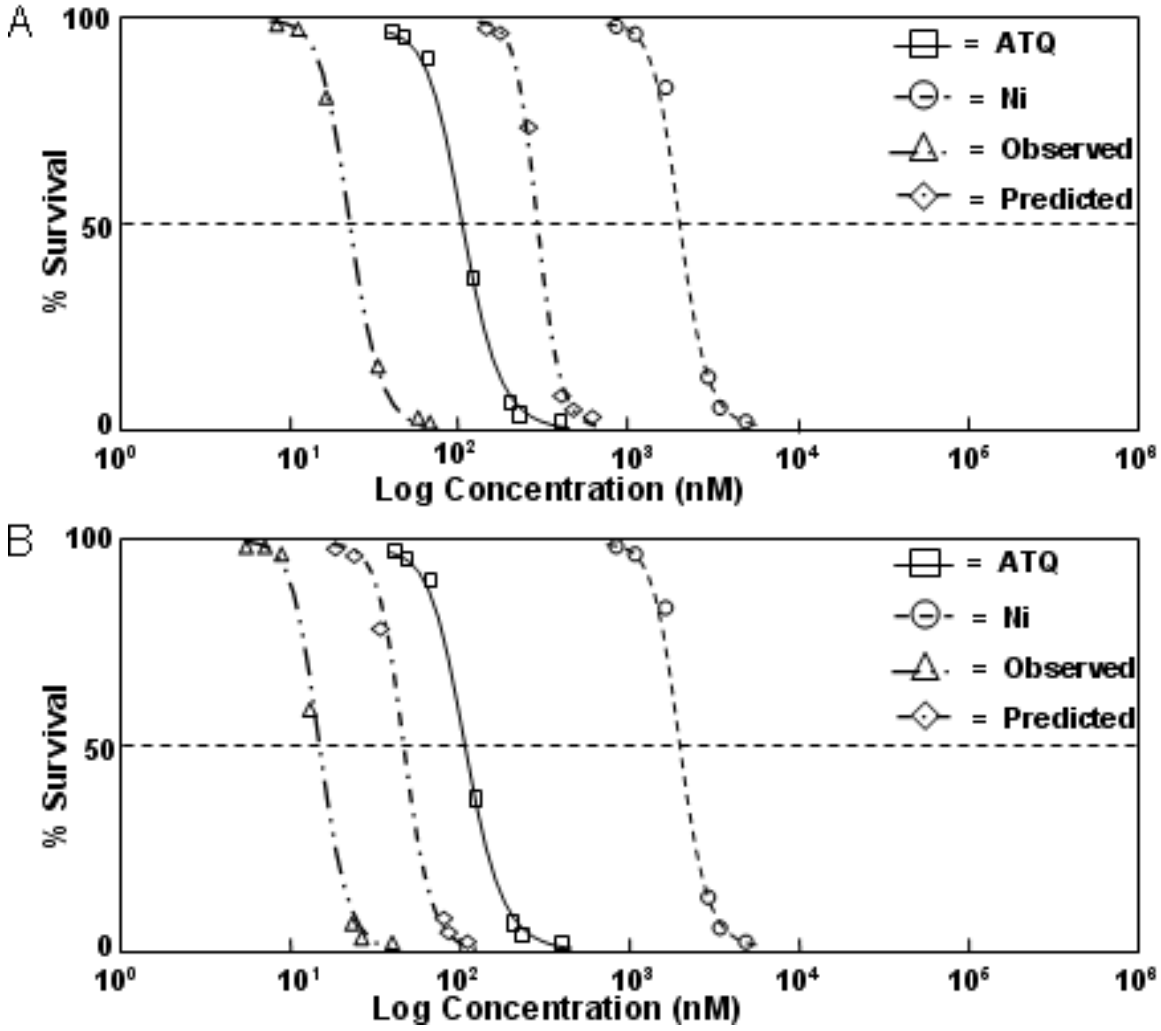

Figure 4.72 Concentration response curves for ATQ + 100 nM Ni and ATQ + 1000 nM Ni to *Hyalella azteca* under PAR conditions. ATQ concentrations were varied while Ni was kept at a constant concentration. A. ATQ + 100 nM Ni B. ATQ + 1000 nM Ni.

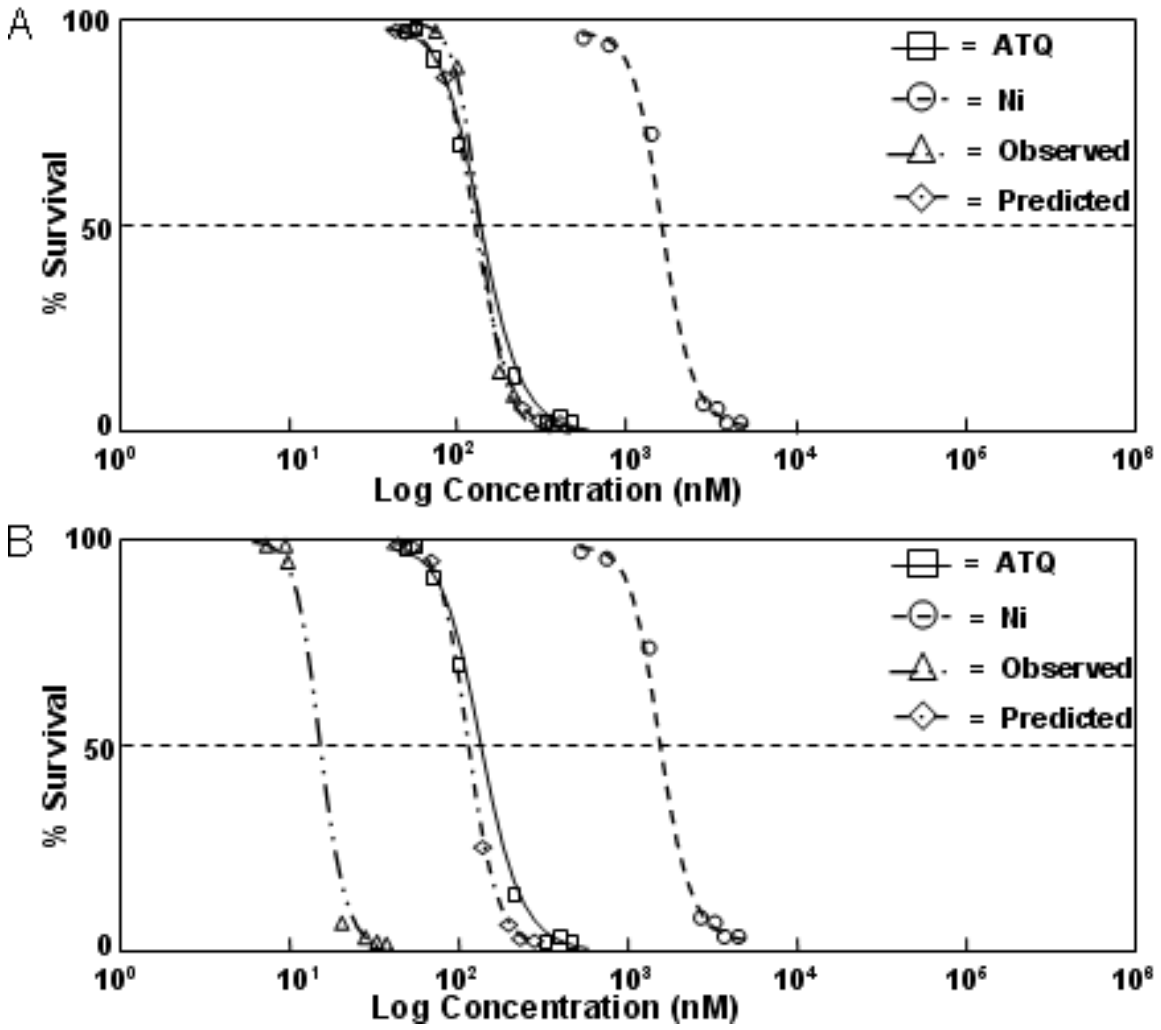

Figure 4.73 Concentration response curves for ATQ + 1 nM Ni and ATQ + 10 nM Ni to *Hyalella azteca* under SSR conditions. ATQ concentrations were varied while Ni was kept at a constant concentration. A. ATQ + 1 nM Ni B. ATQ + 10 nM Ni.

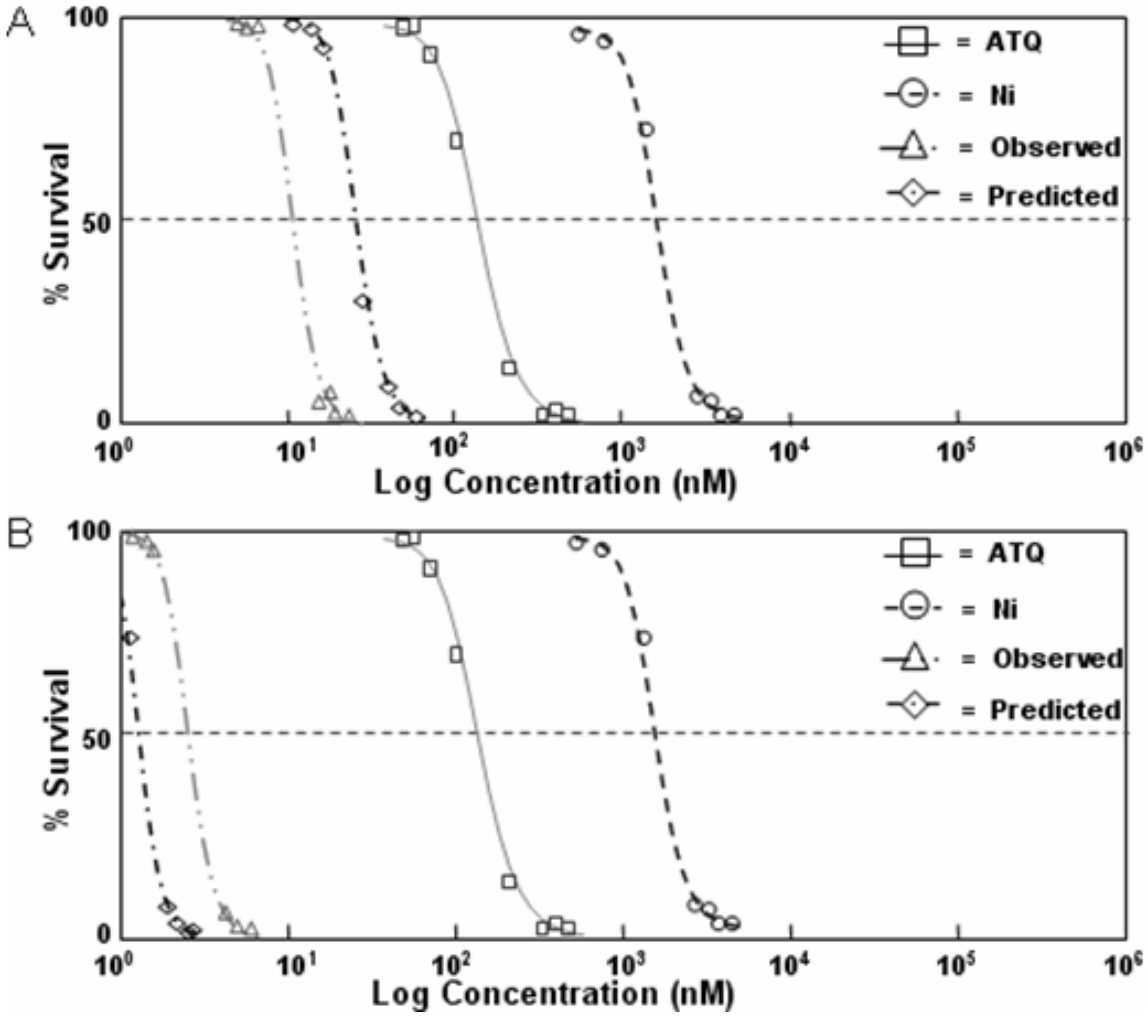

Figure 4.74 Concentration response curves for ATQ + 100 nM Ni and ATQ + 1000 nM Ni to *Hyalella azteca* under SSR conditions. ATQ concentrations were varied while Ni was kept at a constant concentration. A. ATQ + 100 nM Ni B. ATQ + 1000 nM Ni.

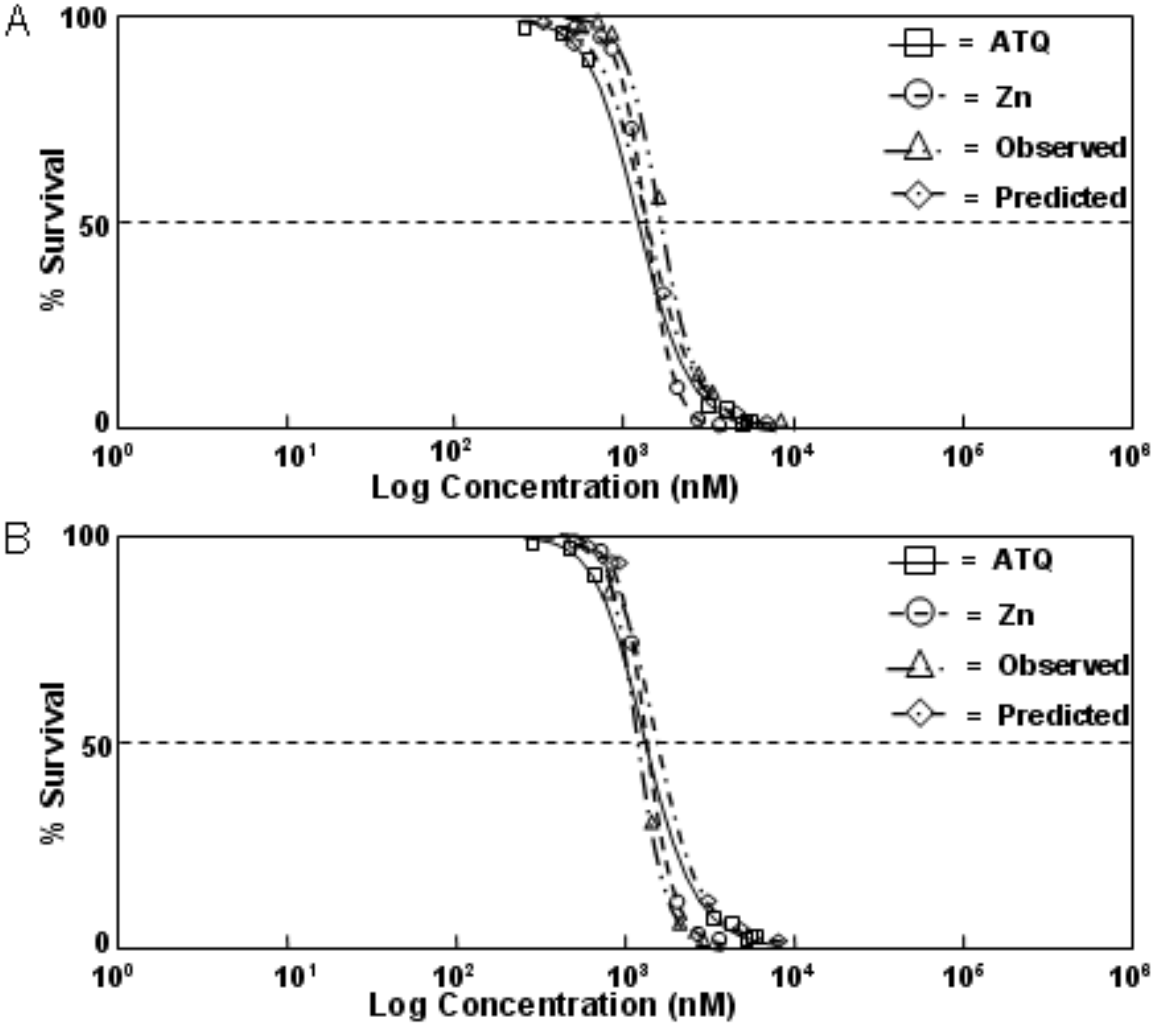

Figure 4.75 Concentration response curves for ATQ + 1 nM Zn and ATQ + 10 nM Zn to *Hyalella azteca* under dark conditions. ATQ concentrations were varied while Zn was kept at a constant concentration. A. ATQ + 1 nM Zn B. ATQ + 10 nM Zn.

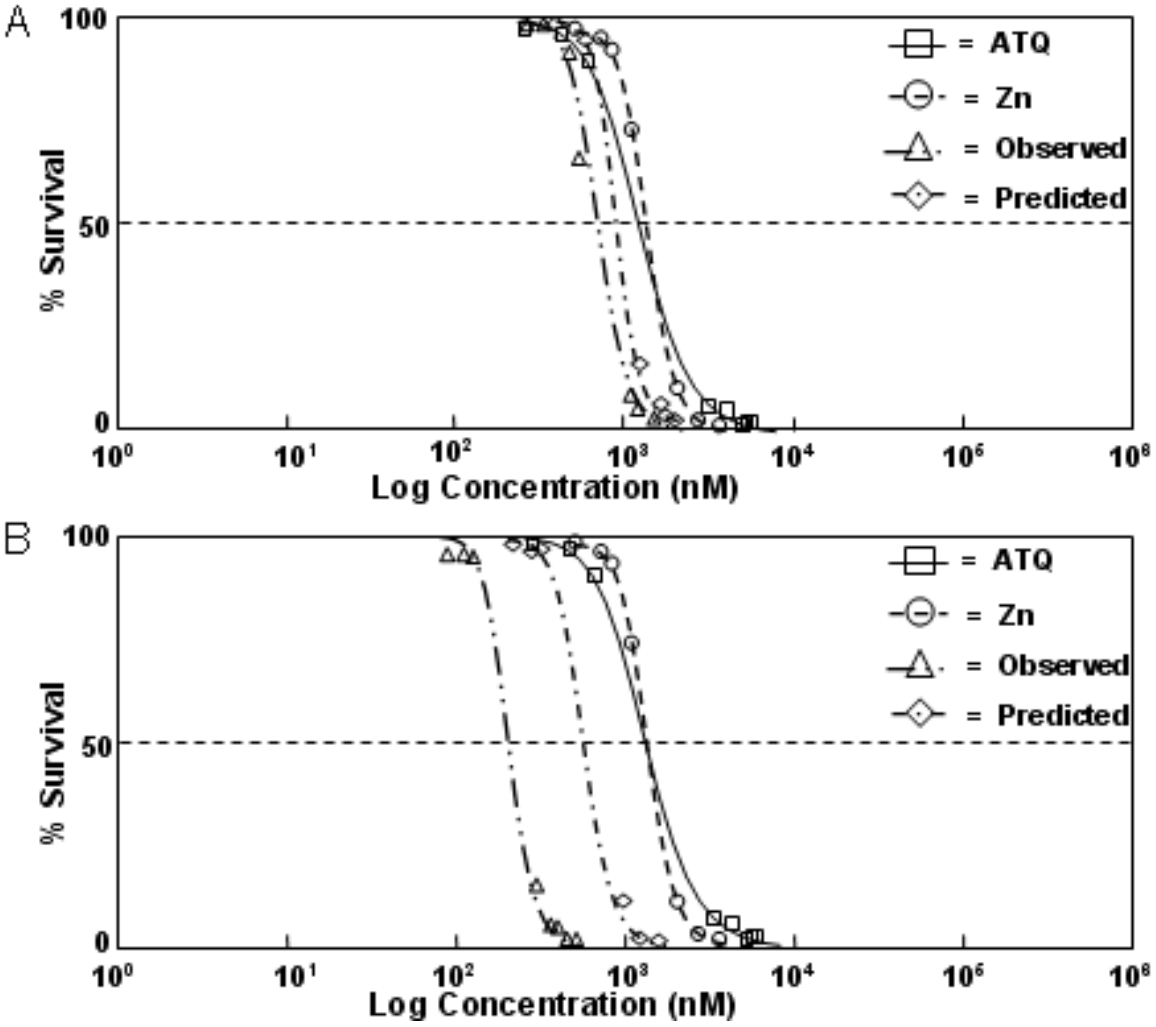

Figure 4.76 Concentration response curves for ATQ + 100 nM Zn and ATQ + 1000 nM Zn to *Hyalella azteca* under dark conditions. ATQ concentrations were varied while Zn was kept at a constant concentration. A. ATQ + 100 nM Zn B. ATQ + 1000 nM Zn.

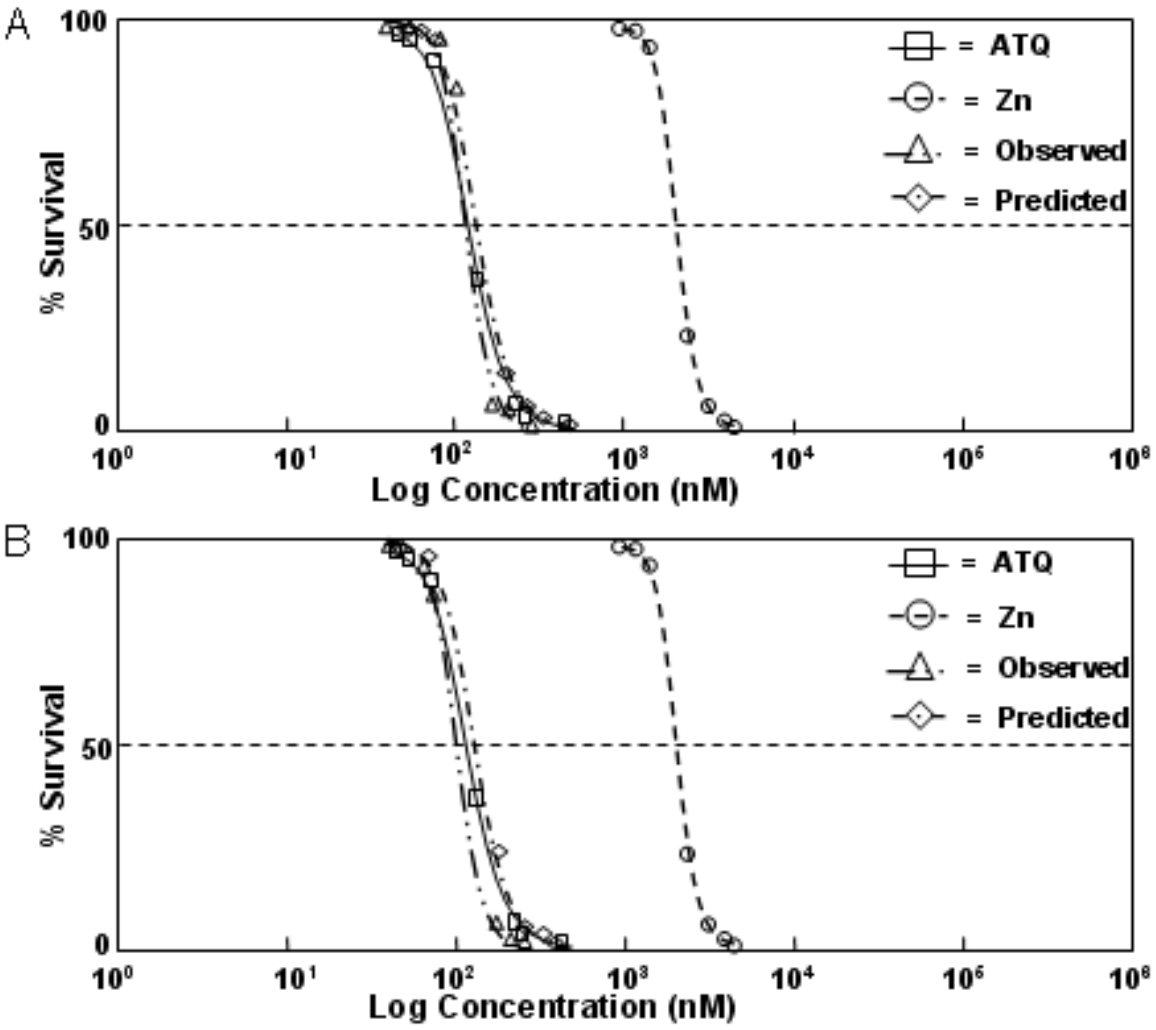

Figure 4.77 Concentration response curves for ATQ + 1 nM Zn and ATQ + 10 nM Zn to *Hyalella azteca* under PAR conditions. ATQ concentrations were varied while Zn was kept at a constant concentration. A. ATQ + 1 nM Zn B. ATQ T + 10 nM Zn.

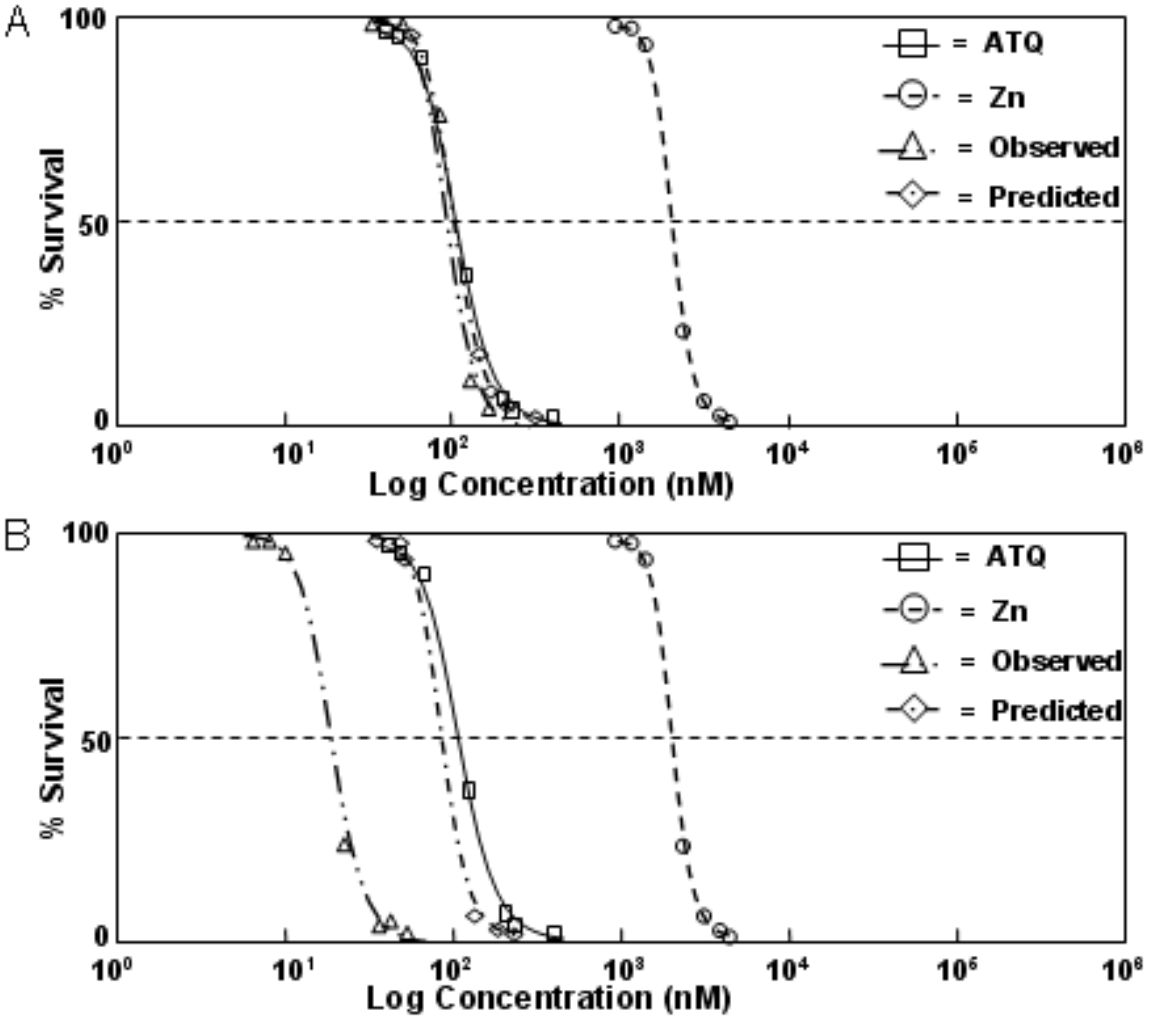

Figure 4.78 Concentration response curves for ATQ + 100 nM Zn and ATQ + 1000 nM Zn to *Hyalella azteca* under PAR conditions. ATQ concentrations were varied while Zn was kept at a constant concentration. A. ATQ + 100 nM Zn B. ATQ + 1000 nM Zn.

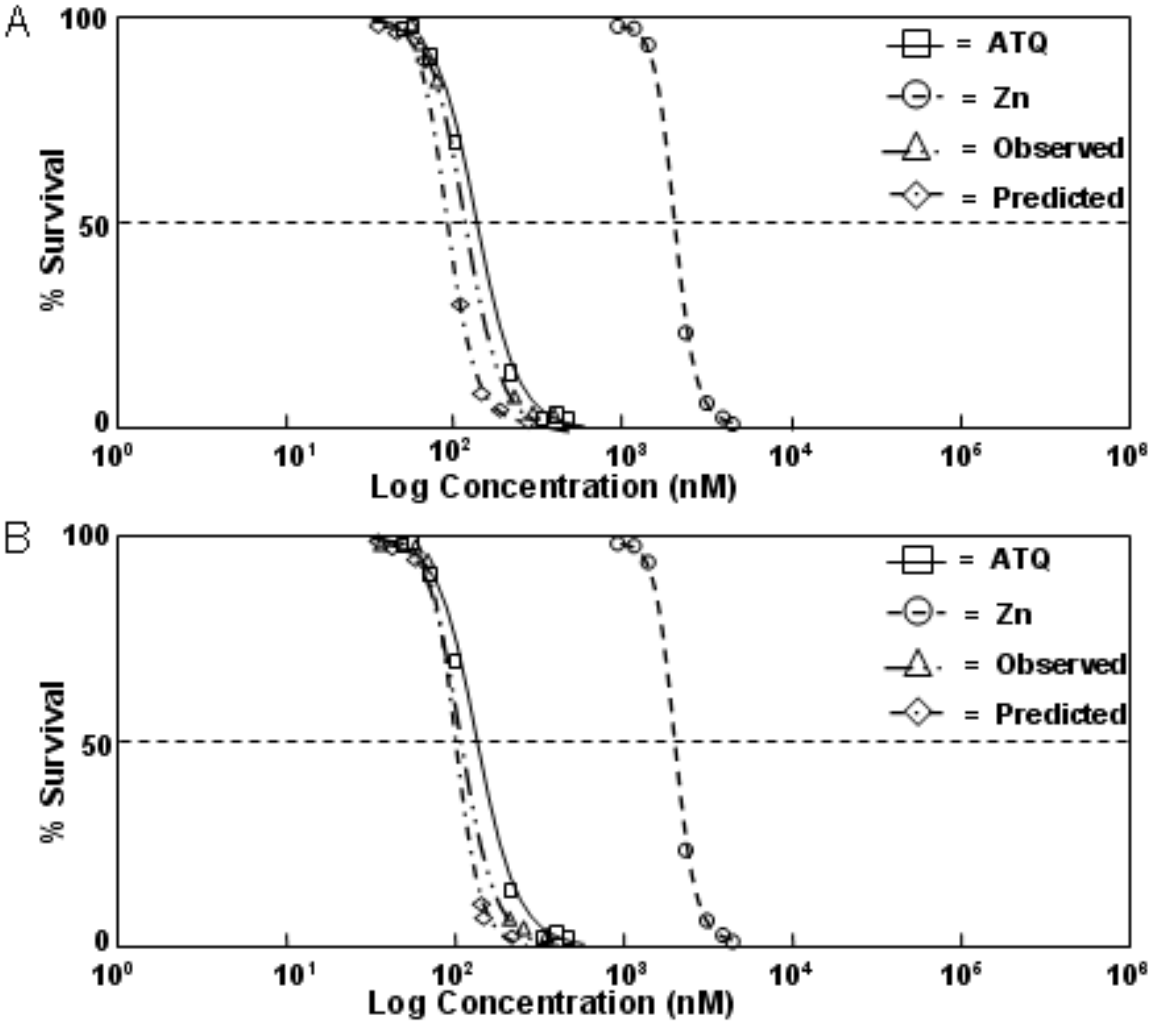

Figure 4.79 Concentration response curves for ATQ + 1 nM Zn and ATQ + 10 nM Zn to *Hyalella azteca* under SSR conditions. ATQ concentrations were varied while Zn was kept at a constant concentration. A. ATQ + 1 nM Zn B. ATQ + 10 nM Zn.

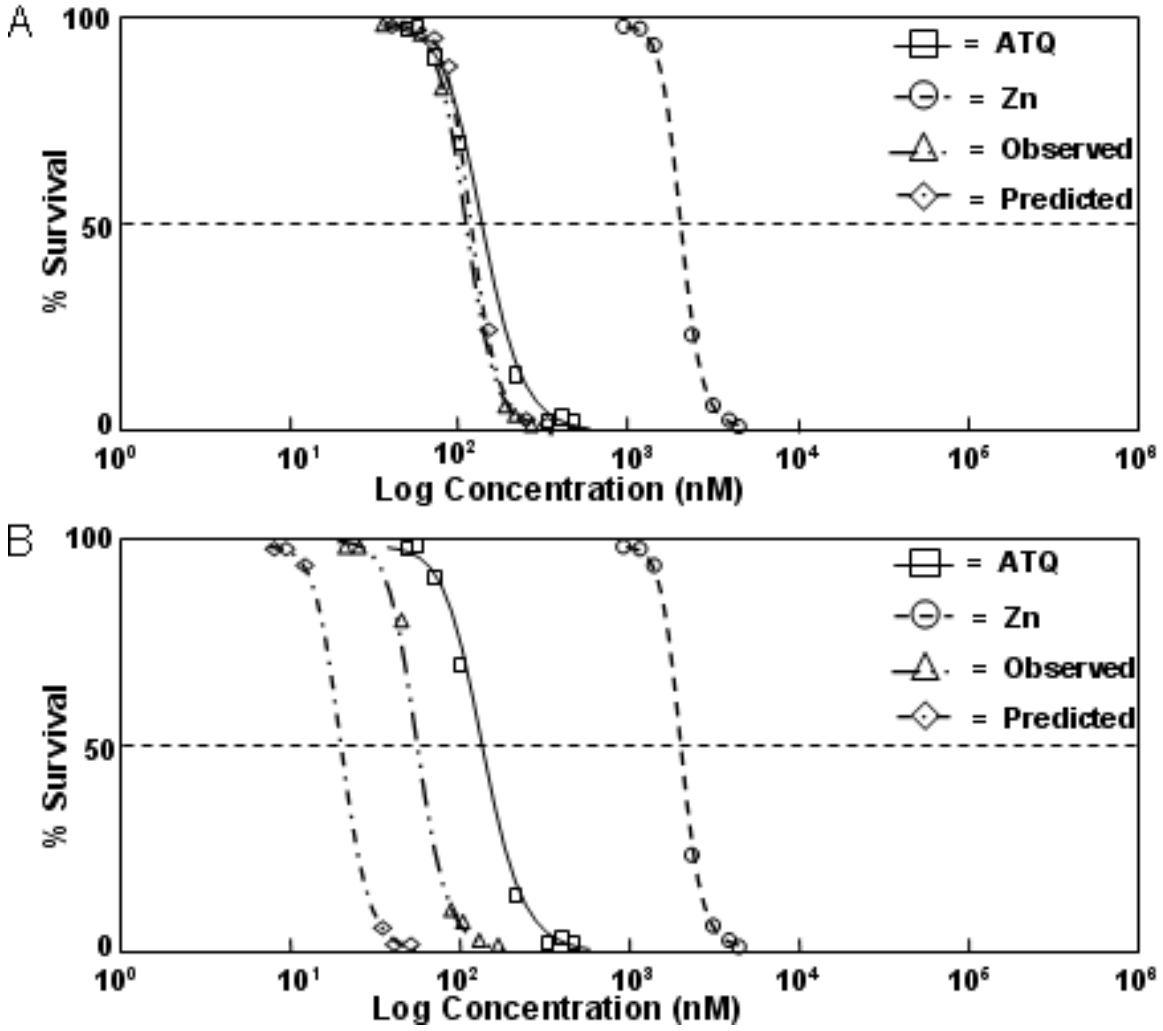

Figure 4.80 Concentration response curves for ATQ + 1 nM Zn and ATQ + 10 nM Zn to *Hyalella azteca* under SSR conditions. ATQ concentrations were varied while Zn was kept at a constant concentration. A. ATQ + 100 nM Zn B. ATQ + 1000 nM Zn.

4.3 Discussion

PAHs and metals are persistent environmental co-contaminants. Their interactions when present as co-contaminants often cause unexpected interactions and as a result the toxicities of these mixtures are often underestimated. Previous studies have demonstrated how metals and PAHs can become toxic in the presence of actinic radiation. The results of this study will help to address the issue of metal and PAH mixture toxicity under varying lighting conditions.

The toxicity of different mixtures of 3 PAHs (ANT, ATQ, 1-hATQ) and one of four metals (Cu, Cd, Ni, Zn) was assessed under three lighting regimes: dark, PAR, and SSR. The resulting data was then plotted to produce concentration response curves. From these concentration response curves, EC50s for the mixtures were determined (Table 4.1- 4.9). The data was analyzed using two models, the first being a concentration response model based on response addition, and the second being a concentration addition model based on isobolic concentration addition. In the first model predicted concentration response curves for ANT + metals, ATQ + metals, and 1-hATQ + metals were also made to determine how predictable PAH + metal mixture toxicity can be based on work done by Norwood et al. (2003) (Figure 4.33- 4.80). From these predicted curves, predicted EC50s were obtained for comparison (Tables 4.4-4.65). The concentration response curves for 1-hATQ + metals can be found in appendix A (Figures 6.1 - 6.24), as most of the 1-hATQ results mirrored those of ATQ + metal results. The isobolic concentration addition model was then compared to the concentration response model.

The results of the dark trials generally followed the predicted values for mixture toxicity and were thus generally concluded to be additive in nature. In the PAR treatments the observed values seemed to deviate from those of the predicted values often showing a synergistic toxic effect. In the SSR trials the results were almost always synergistic compared to the predicted values.

4.3.1 ANT + Cu

. In this experiment mixtures of ANT + Cu were tested under 3 lighting conditions. Mixtures of ANT + Cu were found to be toxic under all three lighting conditions. As the wavelengths of light increased (dark to SSR), the toxicity of the ANT + Cu mixture increased. Interestingly, the ANT + Cu mixtures under PAR and SSR lighting almost always interacted in a synergistic way, the results of which are displayed in Figures 4.3-4.6.

Dark treatments of ANT + Cu followed the predicted values and were additive in toxicity. The ANT + 1 nM Cu and ANT + 10 nM Cu matched the predicted values well; with the predicted toxicity for both of these mixtures being no change in toxicity compared to ANT. The slopes of the ANT + 1 nM Cu and ANT + 10 nM Cu concentration response curves were identical to ANT alone. Figure 4.1 and 4.2 illustrate the effects of ANT + Cu under dark conditions. In the dark, ANT + 100 nM Cu and ANT + 1000 nM Cu exhibited synergistic toxicity compared to their predicted values. The concentration response curves for ANT + 100 nM and ANT + 1000 nM Cu were very similar to each other and much steeper than those of ANT or Cu alone. This suggests that these two mixtures share a similar toxicity mechanism that is different from the

mechanisms of either Cu or ANT. One proven mechanisms is redox cycling and disruption of the mitochondrial electron transport chain (ETC). Babu et al (2001) and Xie et al. (2006) independently demonstrated that PAHs (ATQ, PHE and PHQ) in the presence of Cu or other redox metals cause increased ROS production and inhibit the ETC (Babu et al 2001, Xie et al. 2005, Wang et al. 2008).

Mixtures of ANT + 1 nM Cu and ANT + 10 nM Cu under PAR, were not statistically different from the values predicted, indicating additive toxicity. However the 100 nM and 1000 nM treatments of ANT + Cu (23.6 nM and 2.58 nM) (Table 4.1) under PAR light exhibited a 3 fold increase in toxicity over the predicted values (77.94 nM and 8.68 nM) (Table 4.2), showing a synergistic toxic effect. This is because Cu has aa chromophore and absorbs PAR, however ANT does not absorb PAR light well and therefore the mixture should only be additive or slightly synergistic in toxicity. One possible reason for this synergism, is that Cu is able to redox cycle with quinolated compounds in the organism (Weckx and Clijsters 1996). It is also possible that the organism's detoxification mechanisms (Cytochrome P450s and other mixed function oxygenases) modified ANT to ATQ and other ATQ derivatives, which in turn could lead to absorption of PAR, light (Huang et al. 1997).

The mixtures of ANT + 100 nM Cu and ANT + 1000 nM Cu under SSR were acutely toxic at all concentrations of ANT. These findings match the predicted values which predicted that at both ANT + 100 nM and ANT + 1000 nM Cu would be acutely toxic. The 1 nM ANT + Cu treatment matched the predicted values, showing additive toxicity under these conditions. ANT + 10 nM Cu however was found to be more toxic (0.89 nM) than the predicted value of 4.87 nM showing synergistic toxicity. This result

is not surprising as ANT is known to undergo photomodification in the presence of SSR radiation, leading to the formation of photoproducts including many ATQ's (Mallakin et al. 1999). Several studies have shown that in the presence of SSR light Cu and 1,2-dhATQ can redox cycle with each other leading to ROS formation and cellular damage (Huang et al. 1995:1997, Babu et al. 2003:2005). These studies also showed synergistic toxicity to *Lemna gibba* in the presence of SSR radiation. The concentration response curves for ANT + 1 nM Cu and ANT + 10 nM Cu were both very similar. However, ANT + 1 nM Cu was found to show additive in toxicity and ANT + 10 nM Cu was found to exhibit synergistic toxicity. Therefore even with similar slopes it is unlikely that these two mixtures share a similar mechanism of toxicity..

4.3.2 ANT + Cd

The ANT + Cd mixtures in the dark all had EC50 values similar to that published by Zbigniew et al (2006). Mixtures of ANT + Cd were all found to be toxic, and were generally more toxic than the predicted EC50. Among all four metals, Cd was found to have the greatest effect on PAH toxicity, regardless of the presence of actinic radiation. Even at low levels (10 nM), cadmium had a significant impact on the toxicity of the PAHs tested, whereas the other metals did not become toxic in the dark until they were at a concentration of at least 100 nM. This is likely due to the intrinsic toxicity of Cd to benthic invertebrates and is consistent with data published by Borgmann et al. (2005). The toxicity of the ANT + 1 nM Cd mixture seemed to follow the lighting toxicity pattern for ANT with a 10-25% increase in toxicity, likely stemming from the added

burden of Cd. A possible mechanism for this is Cd membrane depolarization via a Cd induced membrane disruption (Bolduc et al 2004).

The treatments of ANT + 100 nM Cd and ANT + 1000 nM Cd were found to be acutely toxic when mixed with any concentration of ANT except for the dark 100 nM treatment. Zbigniew and Wojcieh (2006) found similar results in green algae. These results were expected, as preliminary results of Cd toxicity show an EC50 in the dark regime of 97.8 nM, and 106 nM under SSR. However, the dark treatment of 100 nM ANT + Cd resulted in a measurable EC50, with an EC50 of 5.78 nM which was much higher than that of the predicted value (Acutely toxic). This result indicates that the interaction for 100 nM ANT + Cd in the Dark might be slightly antagonistic. However this might also be due to the small number of animals used in these treatments, as it is unlikely that the toxicity of either Cd or ANT decreases when the two are present as a mixture. Zbigniew and Wojcieh found similar results in green algae. They also suggested that Cd toxicity is likely due to the disruption of Cu/Zn SOD, likely by competing with either the Zn or the Cu (Zbigniew and Wojcieh 2006).

The ANT + Cd PAR EC50 observed values correlated very well with the predicted values. The ANT + 1 nM Cd and ANT + 10 nM Cd treatments were not statistically different from the predicted values and were said to be additive in toxicity. The ANT + 100 nM Cd and ANT + 1000 nM Cd treatments were found to be acutely toxic to *Hyalella azteca* and were not found to be statistically different from the predicted values. This suggests that ANT + Cd under PAR lighting are additive in toxicity.

The ANT + Cd SSR treatments were found to be acutely toxic at all concentrations except for ANT + 1 nM Cd. These results are unexpected as the predicted

EC50 for 10 nM ANT + Cd showed that the mixture of ANT + Cd should have an EC50 around 4.87 nM. These results show that ANT + 10 nM Cd exhibits synergistic toxicity to *Hyalella azteca* under SSR. ANT, like other PAHs, can undergoe photooxidation in the presence of actinic radiation, leading the formation of oxyPAHs and other photoproducts (Foote 1991, Mallakin et al 1999). The slopes of the concentration response curves for all of the ANT + Cd treatments (dark, PAR and SSR) are all very similar. This indicates that ANT + Cd mixtures regardless of lighting conditions likely share a similar toxicity mechanism. One proposed mechanism is ROS production which has been shown in Daphnia magna and *Vibrio fischeri* to be a key contributor to PAH and Metal mixture toxicity (Xie et al. 2006, Wang et al. 2008).

4.3.3 ANT + Ni

The mixtures of ANT + Ni were all moderately toxic and showed a similar pattern of toxicity to the ANT + Cu treatments. The ANT + Ni however generally showed a slightly synergistic toxic affect as lighting was increased, compared to ANT + Cu which showed a large synergistic toxic effect as lighting increased. The similar pattern to ANT + Cu toxicity is likely because both Cu and Ni are redox active metals and should therefore act in a similar fashion (Xie et al. 2006)

The dark treatments of ANT + 10 nM Ni and ANT + 100 nM ANT + Ni were not statistically different from the predicted values and were additive in toxicity. The ANT + 1 nM Ni was found not to have an effect on the toxicity of ANT. However the dark treatments of 1000 nM ANT + Ni showed a different result. In the dark 1000 nM ANT + Ni the observed EC50 of 1259 nM was 2 fold less than the predicted EC50 of 723 nM.

This antagonistic toxicity is unexpected, as at 1000 nM Ni is approaching its EC50 and the mixture should be becoming much more toxic than it is. One possible explanation for this is several studies have shown Ni's bioavailability to *Hyalella azteca*, in the presence of dissolved organics to be greatly reduced. The threshold concentration for this depends on the organic but effects were not usually seen below 500 nM concentrations of Ni (Doig and Liber 2006:2007, Jaouen 2006).

Of the PAR ANT + Ni treatments the 10 nM, 100 nM and 1000 nM showed synergistic toxicity. The ANT + 1 nM Ni treatment was found to be statistically similar to that of ANT on its own. Therefore it can be said that Ni at 1 nM concentration has no effect on ANT toxicity. The ANT + 100 nM Ni treatment showed a 20% increase in toxicity over that of the predicted value, and were said to be synergistic in toxicity. The 1000 nM ANT + Ni had an EC50 of 48.4 nM which was 30% less toxic than the predicted value of 34.1 nM. This antagonistic toxicity observation is surprising, and might be explained by Ni speciation with other dissolved organics (ANT, *Hyalella azteca* excrement), which can sometimes limit the toxicity of Ni (Doig et al. 2006).

The toxicity of the SSR ANT + Ni treatments was all synergistic in their toxicity except for the ANT + 1 nM Ni treatment which showed no statistical difference to that of the predicted value. ANT + 10 nM Ni, ANT + 100 nM Ni and ANT + 1000 nM Ni were found to exhibit synergistic toxicity, being much more toxic than predicted. Also the slopes of the concentration response curves for ANT + 10 nM Ni, ANT + 100 nM Ni and ANT + 1000 nM Ni were all very similar, which suggests that they all share a similar mechanism of toxicity. One possible mechanism is redox cycling via a photoproduct. ANT, in the presence of SSR has been shown to undergo photomodification, into over 20

photoproducts (Mallakin et al. 1999). These photoproducts are more soluble and many are able to interfere with the mitochondrial ETC via redox cycling (Tripuranthakam et al. 1999, Lampi et al 2005). Ni is also redox active metal and toxicity has been shown to redox cycle with quinolated PAHs such as PHQ as well as with ubiquinone in the mitochondrial ETC (Xie et al. 2006, Wang et al. 2008).

4.3.4 ANT + Zn

The ANT + Zn mixtures were all moderately toxic to *Hyalella azteca*. However the ANT + Zn mixtures were the least toxic of all four of the ANT + metal mixtures tested. The toxicity pattern across the three lighting regimes was unique and the slopes of the dose response curves indicated that ANT + Zn had a distinct mechanism of toxicity compared to the other metals tested (Figures 4.19-4.24). It is also important to note that mixtures of ANT + 1 nM Zn and ANT + 10 nM Zn was not found to increase the toxicity of ANT under any of the lighting conditions.

The dark ANT + 100 nM Zn and ANT + 1000 nM Zn treatments were not statistically different from the predicted values. This additive toxicity for these ANT + Zn trials was expected. The ANT + 1 nM Zn and ANT + 10 nM Zn trials found that these concentrations of Zn had no impact on the toxicity of ANT. This data set matches published data for single toxicant testing (Timmermans 1993, Borgmann and Norwood 1997, Lee et al 2001) and shows that Zn and ANT in the absence of actinic radiation likely do not have any effect on one and others toxicity.

The results of the ANT + 1 nM Zn and ANT + 10 nM Zn treatments under PAR lighting matched the predicted values, and were found to be additive in toxicity. The

ANT + 100 nM Zn and ANT + 1000 nM Zn treatments however showed synergistic toxicity, with 35% and 65% increase over predicted toxicity respectively. These results are surprising as Zn is not known to be photoactive and is not redox active either. Also ANT does not absorb PAR light. However above 80 nM concentrations, Zn has been shown in *Daphnia magna* to compete with other divalent ions (Cu^{2+}, Fe^{2+}, Mn^{2+}). This can lead to membrane instabilities and narcosis on an acute scale. It can also lead to increased sensitivity to other contaminants, thought to be a result of Zn replacing divalent cations (Cu^{2+}, Fe^{2+}, Ca^{2+}) in many enzymes including Cytochrome C oxidases (Muyssen et al. 2006, Clifford and McGeer, 2008). Therefore the increased toxicity under PAR lighting is likely due to the decrease in cellular defenses (by Zn) as well as the increase in ROS production from ANT and PAR.

Mixtures of ANT + 1 nM Zn and ANT + 10 nM Zn when exposed to SSR were not statistically different from the predicted toxicity values, and were said to be additive in toxicity. The 100 nM ANT + Zn treatment however showed synergistic toxicity; with 30% lower EC50 than the predicted value. The 1000 nM treatment also exhibited synergistic toxicity, with a 3 fold increase in toxicity over the predicted values. These results are likely due to ANT undergoing photomodification into other photoproducts, with increased water solubility (Mallakin et al. 1999). Across all of the lighting conditions the slopes of the concentration response curves for ANT + 100 nM Zn and ANT + 1000 nM Zn were found to be nearly identical; making it highly likely they all share a similar toxicity mechanism. This mechanism is likely due to the ability of Zn ions to compete with other divalent ions uptake, resulting in interference with enzymes and biological pathways (Muyssen et al. 2006, Clifford and McGeer. 2008).

4.3.5 ATQ + Cu

Treatments of ATQ + Cu under the dark were all found to be synergistic, being more toxic than predicted. Mixtures of ATQ + 1 nM Cu and ATQ + 10 nM Cu were found to increase the toxicity of ATQ by 25 % and 30 % respectively. This result differs from other studies, as previous studies have shown that low nM amounts of Cu have no noticeable affect on the EC50 of ANT (Babu et al. 2003). The slopes of the concentration response curves for ATQ + 1 nM Cu and ATQ + 10 nM Cu (Figure 4.25), were found to be very similar to those of ATQ + 100 nM Cu and ATQ + 1000 nM Cu (Figure 4.26). This likely indicates that these mixtures all share a similar mechanism of toxicity. Previous studies have shown that mixtures of PAHs and Cu often interact in a synergistic way. The mechanism that has been proposed to explain this is redox cycling, which has been shown to occur in mixtures of redox Cu and quinolated PAHs (Babu et al. 2003:2005, Xie et al. 2006:2007).

When exposed to PAR lighting mixtures of ATQ + 1 nM Cu and ATQ + 10 nM Cu were found to be additive in toxicity, with EC50 values that were not statistically different from the predicted values. Mixtures of ATQ + 100 nM Cu were found to be synergistically toxic to Hyalella azteca with an EC50 five fold greater than that of the predicted value. This increase in toxicity is likely due to ATQs absorption of PAR light which leads to the formation of ROS (Mallakin et al. 1999). This ROS production coupled with Cu leads to an increase in redox cycling, which in turn causes necrosis and death (Babu et al. 2005). The concentration response curves for ATQ + 1 nM Cu and ATQ + 10 nM Cu were identical and were very similar to that of ATQ (Figure 4.27).

Thus it is likely that these two mixtures share a similar mechanism of toxicity to that of ATQ.

The results of the ATQ + Cu mixtures when exposed to SSR showed a marked increase in toxicity over that of the PAR treatments. Notably ATQ + 1 nM Cu was found to be additive in toxicity, being statistically similar to that of the predicted value. The concentration response curve for ATQ + 1 nM Cu was found to be almost identical to that of ATQ, indicating that both share a similar toxicity mechanism. Under the SSR treatment ATQ + 10 nM Cu (13.7 nM) was found to be 2 fold more toxic than predicted (23.5 nM) and 10 fold more toxic than ATQ (142 nM) on its own. The ATQ + 100 nM Cu was found to be slightly less toxic than predicted; however this might be due to the EC50 value approaching the lower bound of our measurements. The lowest concentration used in this thesis was 0.5 nM Cu, which might not allow for proper EC50 determination, if the EC50 is in the pM range. The concentration response curves for ATQ + 10 nM Cu and ATQ + 100 nM Cu under SSR showed similar slopes (Figure 4.29 – 4.30). This indicates that these two mixtures likely have similar toxicity mechanisms.

4.3.6 ATQ + Cd

Mixtures of ATQ + 100 nM Cd and 1000 nM Cd were found to be acutely toxic at all concentrations of ATQ across all of the lighting conditions. This is not surprising as toxicity testing of Cd on its own has shown that 100 nM concentrations are usually acutely lethal to *Hyalella azteca* regardless of lighting conditions (Table 3.2) (Borgmann et al. 2005). The EC50 of mixtures of ATQ + 1 nM Cd (1671 nM) under dark lighting showed no statistical difference from the EC50 of ATQ (1625 nM). The dark

concentration response curves for ATQ + 1 nM Cd shared a similar slope to that of ATQ, which suggests that they share similar toxicity mechanisms. Mixtures of ATQ + 10 nM Cd (577 nM) in the dark showed a three fold increase in toxicity over that of the predicted value (1625 nM). One possible explanation for this is that Cd *in vitro* has been shown to produce ROS in the presence of free sulfur containing amino acids (Cysteine, Methionine). This along with ATQs known redox cycling capabilities might explain this increase in toxicity (Bolduc et al 2004, Xie et al. 2006). The slope of the concentration response curve for ATQ + 10 nM Cd was found to be much steeper than that of ATQ or Cu concentration response curve.

Under PAR lighting ATQ + 1 nM Cd was found to match the predicted value and was said to be additive in toxicity. The slope of the ATQ + 1 nM Cu concentration response curve was found to be very similar to that of ATQ on its own, and is therefore likely that they both share a similar toxicity mechanism (Figure 4.33). The toxicity of ATQ + 10 nM Cd was found to be synergistic, being 2 fold more toxic than that of the predicted value, with EC50s of 82.8 nM and 188 nM respectively. The slope of the ATQ + 10 nM Cd under PAR lighting was very similar to that of ATQ + 10 nM Cd under dark lighting. This suggests that both the toxicity mechanism for both of these treatments of ATQ + 10 nM Cd is very similar (Figure 4.31 and 4.33).

The mixtures of ATQ + 1 nM Cd (89.8 nM) when exposed to SSR, was found to exhibit synergistic toxicity, being more toxic than predicted (142 nM). Mixtures of ATQ + 10 nM Cd (7.62 nM) were also found to be synergistic in toxicity, being 15 fold more toxic than the predicted value (142 nM). These values were not expected and are likely due to the ability of Cd to produce ROS. The mechanism for Cd ROS production is not

fully understood, but is thought to involve sulfahydryl functional groups in proteins (Doig et al. 2005). ATQs in the presence of metals and ROS have been known to redox cycle, disrupting electron transport (Huang et al. 1997). Therefore a mixture of Cd and ATQ would likely redox cycle, which in turn would be responsible for the toxicity of the mixture (Bolduc et al. 2004, Babu et al. 2005, Xie et al. 2007).

4.3.7 ATQ + Ni

Mixtures of ATQ + 1 nM Ni in the Dark treatment were found to be statistically the same as predicted values and were said to be additive in toxicity. Mixtures of ATQ + 10 nM Ni, ATQ + 100 nM Ni and ATQ + 1000 nM Ni all exhibited synergistic toxicity, being more toxic than predicted. Interestingly the ATQ + Ni treatments in the dark followed a pattern of toxicity very similar to that of ATQ + Cu in the dark. This toxicity trend was slightly less than that of Cu but was still comparable. The slopes of the concentration response curves for ATQ + 10 nM Ni, ATQ + 100 nM Ni and ATQ + 1000 nM Ni were all similar (Figure 4.37 – 4.38) and were very similar in shape to those of the ATQ + Cu in the Dark (4.25 – 4.26). This likely indicates that they share a similar toxicity mechanism. One mechanism that has been proposed is mitochondrial disruption via redox cycling between Ni and quinolated PAHs (Xie et al. 2006, Wang et al. 2008)

Mixtures of ATQ + 1 nM Ni (154 nM) and ATQ + 10 nM Ni (146 nM) in the dark treatments were not found to be statistically different from the predicted values (188 nM) and were said to be additive in toxicity. ATQ + 100 nM Ni mixtures were found to be synergistically toxic being 3 fold more toxic than predicted. ATQ + 1000 nM Ni mixtures were also found to be synergistically toxic, being two fold more toxic than

predicted. This increases in toxicity is likely due the weak ATQ absorption of PAR light, which increases the amount of ROS produced (Mallakin et al. 1999).

When mixtures of ATQ + 1 nM Ni (166 nM) were treated with SSR, it was found that the mixtures were additive in toxicity as the EC50s were not statistically different from the predicted value (142 nM). The mixtures of ATQ + 10 nM Ni were found to be 10 fold more toxic than predicted. ATQ + 100 nM Ni was found to be only 20% more toxic than predicted. The slopes of the concentration response curves for ATQ + 10 nM Ni and ATQ + 100 nM Ni were very similar. Thus it is likely that both of these mixtures exhibit similar mechanisms of toxicity. This mechanism is likely redox cycling in the mitochondrial electron transport chain (Xie et al. 2007)

4.3.8 ATQ + Zn

Mixtures of ATQ + 1 nM Zn, ATQ + 10 nM Zn and ATQ + 100 nM Zn across all three lighting regimes matched the predicted values, and were said to be additive in toxicity. The slopes of all of the concentration response curves for ATQ + 1 nM Zn, ATQ + 10 nM Zn and ATQ + 100 nM Zn were all very similar. Thus it is likely that regardless of the lighting conditions these mixtures share a similar toxicity mechanism (Figure 4.43 - 4.47). Mixtures of ATQ + 1000 nM Zn (899 nM) in the dark treatment were found not to be statistically different from the predicted value (903 nM). However the concentration response curve for ATQ + 1000 nM Zn was found to be steeper than that of ATQ, which likely means it has a different mechanism of toxicity.

Mixtures of ATQ + 1000 nM Zn (30.7 nM) when exposed to PAR lighting, showed synergistic toxicity, with a 3 fold increase in toxicity over that of the predicted

value (102 nM). ATQ + 1000 nM Zn (26.8 nM) under SSR lighting also showed synergistic toxicity, with EC50s that were 25% more toxic than predicted (40.2 nM). The concentration response curves for both of these mixtures had slopes that were very similar to each other and different from that of ATQ alone. Thus in all likelihood ATQ + 1000 nM Zn under PAR and SSR lighting shares a similar toxicity mechanism (Figure 4.48). One possible reason for this toxicity is that Zn can often replace other divalent ions (Ca^{2+}, Cu^{2+}, Ni^{2+} etc…) which are often the reaction centers of many ROS scavenging proteins. It is possible that high concentrations of Zn could disrupt these proteins leading to an increase in ROS, and mortality (Fitzgerald et al. 1998, Szilagyi et al. 2004).

The results of this study demonstrated the toxicity of one of three PAHs (ANT, ATQ, and 1-hATQ) mixed with one of four metals (Cu, Cd, Ni, Zn). Most of the PAH + metal mixtures exhibited additive toxicity in the absence of light and low concentrations of metals. However as the concentration of metal was increased and as actinic radiation was added the mixtures began to exhibit synergistic toxicity. The most toxic mixture was Cd/ANT mixtures which were toxic at all concentrations except 1 nM concentrations and was found to be acutely toxic at levels above 10 nM. The results of the mixture assays showed that redox active metals (Cu, Ni) + PAH become toxic when exposed to actinic radiation.

4.3.9 PAH and metal mixture toxicity: A comparison between a concentration addition model and response addition model.

Isobolic analysis is used in toxicology to examine dose combinations of two toxicants that yield the same effect. In this case analysis of mixture toxicity to *Hyalella azteca* based on EC50s was performed. The data sets were analyzed and compared to those of the response addition model previously discussed. The results of the comparison showed that most of the mixtures of PAHs and metals responded in a similar fashion, even when the model used for the prediction was different; however, there were several exceptions. In this section isobolograms were analyzed and compared to the response addition model previously described.

When looking at the isobologram for mixture toxicity of ANT + Cu under dark (Figures 4.9) it is clear that the concentration addition model depicts synergistic toxicity for mixtures of ANT + Cu below 1000 nM Cu. This toxicity does not match that of the response addition model, however mixtures of ANT + 1000 nM Cu in the dark are shown in Figure 4.9 to be additive in toxicity, which is consistent with that of the response addition model. The isobologram for mixtures of ANT + Cu under PAR showed additive toxicity for mixtures of ANT + 1, 10 and 1000 nM Cu (Figure 4.10). Additive toxicity was also observed in the response addition model for the PAR treatments of ANT + 1 nM Cu and ANT + 10 nM Cu. However, for mixtures of ANT + 100 nM Cu under PAR the response addition model showed synergistic toxicity for this mixture. The isobologram for ANT + Cu under SSR showed additive toxicity for all four concentrations of Cu (Figure 4.11). The response addition model showed additive toxicity at all concentrations

of Cu except for ANT + 100 nM Cu which exhibited synergistic toxicity (Figure 4.1). Based on these two models it can be concluded that the toxic effects observed are usually in agreement for mixtures of ANT + Cu.

Analysis of isobolograms of mixtures of ATQ + Cu in the dark, showed additive toxicity for ANT + 1 nM Cu and ATQ + 10 nM Cu (Figure 4.21). Synergistic toxicity was observed for mixtures of ATQ + 100 nM and ATQ + 1000 nM Cu (Figure 4.21). The response addition model agreed with the isobolograms for mixtures of ATQ + Cu in the dark (Figure 4.5). In the isobologram for ATQ + Cu under PAR showed additive toxicity for ATQ + 1 nM Cu and ATQ + 10 nM Cu (Figure 4.22) which was also seen in the response addition model (Figure 4.5). The isobologram for mixtures of ATQ + 100 nM Cu under PAR (Figure 4.22) revealed synergistic toxicity to *Hyalella azteca,* which matched that of the response addition model (Figure 4.5). The isobologram for ATQ + Cu under SSR showed additive toxicity for ATQ + 1 nM Cu and synergistic toxicity for ATQ + 10 nM Cu (Figure 4.23). The response addition model also showed additive toxicity for ATQ + 1 nM Cu and synergistic toxicity for ATQ + 10 nM Cu.

Based on analysis of this data set using both concentration addition and response addition, it can be concluded that mixtures of ANT or ATQ and Cu generally exhibit synergistic interactions under Dark, PAR and SSR.

From the isobologram data the mixture toxicity for ANT + Cd in the dark showed synergistic toxicity for all four treatments (Figure 4.12). The response addition model mated the isobologram data showing additive toxicity for all four treatments (Figure 4.2).

The isobolograms for ANT + Cd mixtures under PAR were found to exhibit additive toxicity at all concentrations of Cd (Figure 4.13). The response addition model

agreed with this predicting additive toxicity for ANT + 1 nM Cd and ANT + 10 nM Cd. However, the response addition model for ANT + 100 nM Cd and ANT + 1000 nM Cd showed synergistic toxicity for these two mixtures. When looking at the isobologram for ANT + Cd under SSR, acute toxicity was observed at levels above 1 nM Cd. For ANT + 1 nM Cd synergistic toxicity is observed (Figure 4.14). This is in agreement with the response addition model which also shows synergistic toxicity (Figure 4.2). When looking at ANT + Cd interactions the two models correlated very well in predicted interactions.

The isobolograms for toxicity mixtures of ATQ + Cd in the dark showed additive toxicity for ATQ + 1 nM Cd and synergistic toxicity for ATQ + 10 nM Cd (Figure 4.24). The response addition model also showed additive toxicity for ATQ + 1 nM Cd and synergistic toxicity for ATQ + 10 nM Cd (Figure 4.6). For the ATQ + 1 nM Cd PAR isobolograms additive toxicity was observed and for ATQ + 10 nM Cd PAR treatments synergistic toxicity was observed (Figure 4.25); both of these agree with the response addition model (Figure 4.6). The isobolograms for mixtures of ATQ + Cd under SSR showed synergistic toxicity for ATQ + 1 nM Cd and ATQ + 10 nM Cd (Figure 4.26). The response addition model also showed synergistic toxicity for both of these treatments (Figure 4.6). Thus both response addition and concentration addition showed identical results for mixtures of ATQ + Cd under all three treatments.

Isobolograms for the mixture toxicity of ANT + Ni in the dark showed synergistic toxicity for all four concentrations of Ni (Figure 4.15). This data is not consistent with the response addition model data. The response addition model shows additive toxicity for ANT + 1, 10 and 100 nM Ni treatments and antagonistic toxicity for ANT + 1000 nM

Ni in the dark (Figure 4.3). Isobolograms of mixture toxicity for ANT + Ni PAR showed synergistic toxicity for ANT + 1, 10, 100 nM Ni, and additive toxicity for ANT + 1000 nM Ni (Figure 4.16). The response addition model shows that the interactions for ANT + 1, 10, 100 nM Ni all exhibit additive toxicity, and the ANT + 1000 nM Ni treatment shows antagonistic toxicity (Figure 4.3). The isobologram for mixture toxicity ANT + Ni under SSR showed synergistic toxicity for mixtures of ANT + 1, 10, 100 nM Ni (Figure 4.17). The response addition model showed additive toxicity for ANT + 1 nM Ni and synergistic toxicity for ANT + 10 nM Ni and ANT + 100 nM Ni (Figure 4.3). For mixtures of ANT + Ni under dark, both the concentration addition and response addition models showed different interactions for the dark and the PAR treatment. For the SSR treatment the interactions were similar for ANT + 10 nM Ni, and ANT + 100 nM Ni. Thus both the response addition and the concentration addition models showed different toxic effects for mixtures of ANT + Ni under the three lighting conditions.

The isobolograms for mixture toxicity for ATQ + Ni showed synergistic toxicity for all four concentrations of Ni (Figure 4.27). The response addition model showed additive toxicity for mixtures of ATQ + 1, 10, 100 nM Ni, and synergistic toxicity for ATQ + 1000 nM Ni (Figure 4.7). For the ATQ + Ni PAR treatment isobolograms the ATQ + 1 nM Ni treatment showed additive toxicity. Synergistic toxicity was observed in the isobolograms for ATQ + 10, 100, 1000 nM Ni treatments (Figure 4.28). The response addition model showed additive toxicity for ATQ + 1 nM Ni and ATQ + 10 nM Ni (Figure 4.7). In the ATQ + 100 nM Ni and ATQ + 1000 nM Ni PAR treatments the response addition model showed synergistic toxicity (Figure 4.7). When looking at the ATQ + Ni SSR isobolograms we see synergistic toxicity for all four concentrations of Ni

(Figure 4.29). The response addition model shows synergistic toxicity for ATQ + 10 nM Ni and ATQ + 100 nM Ni (Figure 4.7). However for ATQ + 1 nM Ni the response addition model shows additive toxicity and for ATQ + 1000 nM Ni the model shows antagonistic toxicity (Figure 4.7).

The mixture toxicity isobologram for ANT + Zn under dark showed synergistic toxicity for all four concentrations of Zn (Figure 4.18). The response addition model showed additive toxicity for all four concentrations of Zn (Figure 4.8). Additive toxicity was observed in the ANT + 1 nM Zn and ANT + 10 nM Zn isobolograms under PAR (Figure 4.19). Synergistic toxicity was observed in the isobologram of ANT + 100 nM Zn and ANT + 1000 nM Zn (Figure 4.19). The response addition model for ANT + Zn under PAR shows additive toxicity for ANT + 1, 10, 100 nM Zn and synergistic toxicity for mixtures of ANT + 1000 nM Zn (Figure 4.8). The isobologram for mixtures of ANT + Zn under SSR showed additive toxicity for ANT + 1, 10 and 1000 nM Zn and synergistic toxicity for ANT + 100 nM Zn. (Figure 4.20). The response addition model showed additive toxicity for mixtures of ANT + 1 nM Zn and ANT + 10 nM Zn. The response addition model showed synergistic toxicity for ANT + 100 nM Zn and ANT + 1000 nM Zn (Figure 4.4). Thus the interactions of ANT + Zn were almost always found to be the same using both the response addition model and the concentration addition model.

The mixture toxicity isobologram for ATQ + Zn under dark showed additive toxicity for all four concentrations of Zn (Figure 4.30). The response addition model also showed additive toxicity for all four mixtures of ATQ + Zn (Figure 4.4). The isobologram for ATQ + Zn under PAR showed additive toxicity for ATQ + 1, 10, 100

nM Zn and synergistic toxicity for ATQ + 1000 nM Zn (Figure 4.31). The response addition model also showed additive toxicity for ATQ + 1, 10, 100 nM Zn and synergistic toxicity for ATQ + 1000 nM Zn under PAR (Figure 4.4). For mixtures of ATQ + Zn under SSR the isobolograms showed additive toxicity for all four concentrations of Zn (Figure 4.32). The response addition model showed additive toxicity for ATQ + 1, 10, 100 nM Zn and synergistic toxicity for ATQ + 1000 nM Zn (Figure 4.4). Both statistical models used in this study show very similar results in the interactions between ATQ and Zn under dark, PAR and SSR.

The two methods used in this study are both useful instruments in understanding toxic interactions. The first model response addition assumes that the toxicants in question both act independently from each other (Sorensen et al. 2007). The second model, concentration addition (isobolic analysis) assumes that the toxicants in question both act on similar biological systems, producing a similar response. Based on these ideas, if it is known that two toxicants share a similar mechanism of toxicity the model of concentration addition should be used to gauge the interactions. If the toxicants do not likely share a similar mechanism of toxicity then response addition should be used. Furthermore if the mechanism is completely unknown then concentration addition is usually a better model to use as it allows us to test whether an observed deviation from the concentration addition model reflects a true deviation or weather it is just due to random sampling error (Sorensen et al. 2007).

In the literature it has been shown in several studies that mixtures of redox active metals and PAHs, generally share a similar mechanism of toxicity, that being the production of ROS (Babu et al. 2003; 2007, Xie et al 2006; 2007). For the mixtures of

PAHs (ANT, ATQ) and redox active metals (Cu, Ni) it was found that the toxicity models did not match up well. The mixtures of PAHs (ANT, ATQ) and non-redox active metals (Cd, Zn) however showed almost identical mixture interactions across the three lighting treatments in both the concentration addition model and the response addition model.

Metals and PAHs likely have many shared toxicity mechanisms and many distinct toxicity mechanisms (Babu et al 2001, Timmermans et al 1993, Gurst et al. 2005, Xie et al. 2006, Clifford and McGeer 2008). This is likely the reason that in non-redox active metal + PAH mixtures we see the models predicting similar interactions. It is also the reason why when we see redox active metals + PAHs we see dissimilar interaction predictions.

Chapter 5

General Conclusions

PAHs and metals are common environmental contaminants that are produced both naturally and anthropogenically. They are both priority contaminants due to their prevalence and known toxicity. One aspect of both PAH and metal toxicity that has not been extensively addressed is the interactions of these chemicals under different parts of the solar spectrum.

The toxicities of all of the PAHs increased as more of the solar spectrum was added from dark to SSR. Toxicity however was observed in the absence as well as presence of light. Therefore it is not a requirement of PAH toxicity to have actinic radiation present. This has been shown in many previous studies in both plants (Babu et al. 2001) and animals (Lampi et al. 2005). The results presented here also suggest that compounds that are only minimally toxic in the absence of light can become highly toxic in the presence of light, likely through photochemical processes. Many of the oxyPAHs were far more toxic than their parent compounds, which suggest that photomodification of parent PAHs likely plays a key role in the increase of toxicity under actinic radiation. Thus it is likely that the toxicity of parent PAHs is due to photomodification and to photosensitization.

The metal assays showed an increase in toxicity as more of the solar spectrum was added to redox active metals (Cu, Ni). However, no change in toxicity over the four treatments to the non redox active metals (Cd, Zn). Cd was found to be toxic to *Hyalella azteca* under all four radiation treatments at environmentally relevant levels, suggesting that Cd is intrinsically toxic to *Hyalella azteca*. Zn was found to be relatively non-toxic

to *Hyalella azteca,* with acute toxicity levels much higher than those found in the environment. Based on this study the order of metal toxicity for Dark, PAR and PAR/UV-A treatments can be said Cd > Cu > Ni > Zn, and the order of metal toxicity under SSR was found to be Cu > Cd > Ni > Zn.

The metal/ANT assays showed varying results depending on the metal, the PAH and the type of radiation it was exposed to. Most of the metal/ANT mixtures exhibited additive toxicity in the absence of light and at low concentrations of metals (1 nM and 10 nM). However as the concentration of metal was increased and as actinic radiation was added the mixtures began to exhibit synergistic toxicity. The most toxic by far was Cd/ANT mixtures which were toxic at all concentrations except 1 nM, and was found to be acutely toxic at levels above 10 nM. The mixture assays showed that redox active metals/ANT mixtures toxicity increased exponentially when exposed to actinic radiation. The redox active metal/PAH mixtures exhibited synergistic toxicity under dark as well as PAR and SSR treatments. Whereas the non-redox active metal mixtures did increase in toxicity but usually at a much lower level than that of the redox active metals.

Based on comparison of the response addition model and the concentration addition model several things can be concluded. The first is that redox active metal (Cu, Ni) + PAH mixtures differ in toxic interactions depending on which model is used for prediction. However, the non-redox active metals (Cd, Zn) showed similar toxic interactions when using both models. Based on these models it is hoped that experiments will be designed to test the toxicity mechanisms for these mixtures to help with future environmental risk assessment.

References

Abel PD. 1989. Water Pollution Biology. Toronto, Canada: John Wiley & Sons. Canada Ltd.

A-H-Mackerness S, Surplus SL, Blake P, John CF, Buchanan-Wollaston V, Jordan BR, Thomas B.1999. Ultraviolet-B-Induced stress and changes in gene expression in Arabidopsis thaliana: Role of signaling pathways controlled by jasmonic acid, ethylene and reactive oxygen species.

Akhtar, TA. 2004. Identification of similar stress responses elicited by copper and ultraviolet radiation on the aquatic plant *Lemna gibba*. University of Waterloo: Waterloo, Ontario, Canada.

Amiard-Triquet C, Amiad J, Robert J, Metayer C, Marchand J, Martin J. 1983. Comparative accumulation of oligo-metallic elements in estuary, marine and freshwater habitats (Bay of Bourgneuf). *J Biol Marine.* 24:105-118.

Anderson A. 1992. Recent follow-up of nickel refining workers in Norway and respiratory cancer. In Nickel and Human Health: current Perspectives, Nieboer E and Niragu J. Eds. 621-627. John Wiley and Sons Ltd. New York. NY

Ankley G, Collyard S, Monson P, Kosian P. 1994. Influence of Ultraviolet Light on the Toxicity of Sediments Contaminated with Polycyclic Aromatic Hydrocarbons. *Environ Toxicol Chem.* 13:1791-1796

Babu TS, Marder JB, Tripuranthakam S, Dixon DG, Greenberg BM. 2001. Synergistic Effects of a Photooxidized Polycyclic Aromatic Hydrocarbon and Copper on Photosynthesis and Plant Growth: Evidence that *In Vivo* Formation of Reactive Oxygen Species is a Mechanism of Copper Toxicity. *Environ Toxicol Chem.* 20:1351-1358.

Babu TS, Akhtar T, Lampi M, Tripuranthakam S, Dixon G, Greenberg BM. 2003. Similar Stress Responses are elicited by Copper and Ultraviolet Radiation in the Aquatic Plant *Lemna gibba*: Implication of Reactive Oxygen Species as Common Signals. *Plant Cell Physiol* 44: 1320-1329.

Babu TS, Tripuranthakam S, Greenberg BM. 2005. Biochemical responses of the aquatic higher plant Lemna gibba to a mixture of copper and 1,2-dihydroxyanthraquinone: synergistic toxicity via reactive oxygen species. *Environ Toxicol Chem* 24:3030-3036.

Barbosa M, De Almeida M, Mariz D, de Almeida J. 2004. Studies of channel sediments contaminated with organics and heavy metals. *J Hazard Mat* 110:29-38.

Boese BL, Ozretich R, Lamberson J, Swartz R, Cole F, Pelletier J, Jones J.1999. Toxicity and Phototoxicity of Mixtures of Highly Lipophillic PAH compounds in Marine

Sediments: Can the PAH Model Be Extrapolated?. *Environ Contam Toixcol* 36:270-280.

Bolduc JS, Denizeau F, Jumarie C. 2004. Cadmium-induced mitochondrial membrane potential dissipation does not necessarily require cytosolic oxidative stress: Studies using rhodamine-123 fluorescence unquenching. *Toxicol Sci* 77:299-306.

Bondy GS, Armstrong CL, Dawson BA, Heroux-Metcalf C, Neville GA, Rogers CG.1994. Toxicity of structurally related anthraquinones and anthrones to mammalian cells in vitro. *Toxicol In Vitro* 8:329-335.

Borgmann U, Norwood W. 1997. Toxicity and Accumulation of Zinc and Copper in *Hyalella azteca* exposed to metal-spiked sediments. *Can J Fish Aquat*. Sci.54:1046-1054.

Borgmann U, Couillard Y, Doyle P, Dixon DG. 2005. Toxicity of Sixty-Three Metals and Metalloids to *Hyalella azteca* at Two Levels of Water Hardeness. *Environ Toxicol Chem.* 24:641-652.

Borgmann U, Norwood W, Dixon DG. 2004. Re-evaluation of metal bioaccumulation and chronic toxicity in *Hyalella azteca* using saturation curves and the Biotic Ligand Model. *Environ Poll.* 131:469-484.

Brack W, Altenburger R, Küster E, Messiner B, Wenzel KD, Schüürman G. 2003. Identification of Toxic Products of Anthracene Photomodification in Simulated Sunlight. *Environ Toxicol Chem*. 22:2228-2237.

Brasseur C, Widart S, Muller M, Maghuin-Rogister G, Scippo ML.2007.Alteration of the estrogen hormone pathway in hepatic cells after exposure to polycyclic aromatic hydrocarbons. *Toxicol Lett.* 172:38-49.

Brennan L, Kantorow M. 2008. Mitochondrial Function and Redox Control in the Aging Eye: Role of MsrA and Other Repair Systems in Cataract and Macular Degenerations. *Experimental Eye Research*. In Press

Briggs MK, Desavis E, MAzzer PA, Sunoj RB, Hatcher SA, Hadad CM, Hatcher PG.2003. A new approach to evaluating the extent of Michael Adduct formation to PAH quinones: Tetramethyl-ammonium hydroxide (TMAH) thermochemolysis with GC/MS. *Chem Res Toxicol* 16:1484-1492.

Burgess RM, Ahrens MJ, Hickey CW. 2003. An Ecotoxicological Perspective. Toronto, Canada: John Wiley & Sons Canada Ltd. 218-315

Christian P, West KP, Jr. 1998. Interactions between zinc and vitamin A: an update. *Am J Clin Nutr*. 68:435S-441S.

Clifford M, McGeer J. 2008. Development of a biotic ligand model for the acute toxicity of zinc to *Daphnia pluex* in soft waters. *Aquatic Toxicol* 91:26-32.

Collyard SA, Ankley GT, Hoke RA, Goldstein T. 1994. Influence of age on the relative sensitivity of *Hyalella azteca* to diazinon, alkylphenyl ethoxylates, copper, cadmium, and zinc. *Arch Environ Contam Toxicol* 26:110-113.

Dabestani R, Ivanov IN. 1999. A compilation of physical, spectroscopic and photophysical properties of polycyclic aromatic hydrocarbons. *Photochem Photobiol* 70:10-34.

Diamond S, Mount D, Burkhard L, Ankley G, Makyen E, Leonard E. 2000. Effect of Irradiance Spectra on the Photoinduced Toxicity of Three Polycyclic Aromatic Hydrocarbons. *Environ Toxicol Chem.* 19:1389-1396.

Diamond SA, Milroy NJ, Mattson VR, Heinis LJ, Mount DR. 2003. Photoactivated Toxicity in Amphipods Collected from Polycyclic Aromatic Hydrocarbon-Contaminated Sites. *Environ Tox Chem*. 22:2752-2760.

Doig L, Liber K. 2006. Influence of dissolved organic matter on nickel bioavailability and toxicity to *Hyalella azteca* in water-only exposures. *Aquatic Tox.* 76:203-216.

Doig L, Liber K. 2007. Nickel speciation in the presence of different sources of dissolved organic matter. *Ecotox Environ saf.* 66:169-177.
Dong S, Fu P, Shisat RN, Hwang H-M, Leszczynski J, Yu H. 2002. UV-A light-induced DNA cleavage by isomeric methyl benz(a)anthracenes. *Chem Res Toxicol* 15:400-407.

Environment Canada. 2003. Guidance manual for the categorization of organic and inorganic substances on Canada's domestic substances list. Existing Substances Branch, Environment Canada, PQ.

Eisler R. 1998. Nickel hazards to fish wildlife, and invertebrates: a synoptic review. *Biological Science Report*. USGS/BRD/BSR-1998-0001.

Eide DJ. 2003. Multiple Regulatory Mechanisms Maintain Zinc Homeostasis is *Saccharomyces cerevisiae*. *J Nutri* 133:1532S-1535.

El-Alawi Y, Huang XD, Dixon DG, Greenberg BM. 2002. Quantitative Structure-Activity Relationship for the Photoinduced Toxicity of Polycyclic Aromatic Hydrocarbons to the Luminescent Bacteria *Vibrio fischeri*. *Eviron Toxicol Chem*. 21:2225-2232.

Feldmannova´ M, Hilscherova´ K , Marsˇ a´ lek B, Bla´ ha L. 2006.Effects of N-Heterocyclic Polyaromatic Hydrocarbons on Survival, Reproduction, and biochemical parameters in *Daphnia magna*. *Environ Toxicol* 21:425-431.

Fernandez M, L'Haridon J. 1992.Influence of lighting conditions on toxicity and genotoxicity of various PAH in the newt in vivo. *Mutant Res* 288:31-41.

Fitzgerald DJ. 1998. Safety guidelines for Copper in water. *AM J Clin Nutr.* 67:1098S-1102S.

Flowers-Geary L, Bleczinski W, Harbey RG, Penning TM. 1996. Cytotoxicity and mutagenicity of polycyclic aromatic hydrocarbon *0*-quinones produced by dihydrodiol dehydrogenase. *Chem Biol Interact* 99:55-72.

Foote CS. 1968. Mechanisms of Photosensitized Oxidation. *Science*. 162:963-970.

Foote CS. 1976. Photosensitized Oxidation and Singlet Oxygen: Consequences in Biological Systems. In: Pryor WA, editor. Free Radicals in Biology. New York, NY. USA: Academic Press. 85-133.

Foote CS. 1991. Definition of Type 1 and Type 2 Photosensitized Oxidation. *Photochem Photobiol*. 54:659

Fox MA, Olive S. 1979. Photooxidation of Anthracene on atmospheric particulate matter. *Science* 205:582-583.

Goldstein S, Meyerstein D, Czapski G. 1993. "The Fenton reagents". *Free Radical Biology and Medicine* 15:435-445.

Gouvea S, Boyer G, Twiss M. 2008. Influence of ultraviolet radiation, copper, and zinc on microcystin content in Microcystis aeruginosa (Cyanobacteria). *Harm Algae* 7:194-205.

Guthrie J, Mandal R, Salam M, Hassan N, Murimboh J, Chakrabarti C, Back, M, Gregoire D. 2003. Kinetic studies of nickel speciation in model solution of a well-characterized humic acid using the competing ligand exchange method. *Anal Chem Acta.* 480:157-169.

Gurst K, Fleeger J. 2005. Exposure-Related Effects on Cd Bioaccumulation Explain Toxicity of Cd-Phenanthrene Mixtures in *Hyalella Azteca*. *Environ Toxicol Chem.* 24: 2918-2926.

Gurst K. 2005. Joint Toxicity of Cadmium and Phenanthrene in the Freshwater Amphipod *Hyalella azteca*. *Arch Environ Contam Toxicol.* 50:7-13.

Hamblin MR, Demidova-Rice T. 2007. Cellular chromophores and signaling in low level light therapy. *Proc SPIE* 6284: 642802

Hatch A, Burton A. 1999. Phototoxicity of Fluoranthene to two Freshwater Crustaceans, *Hyalella azteca* and *Daphnia magna*: Measures of Feeding inhibition as a Toxicological Endpoint. *Hydrobiologia.* 400:243-248.

Health Canada. CEPA Priority Substance List Assessment Report - Polycyclic Aromatic Hydrocarbons. National Printers. Ottawa, Canada. 1999. Health Canada. CEPA Priority Substance List Assessment Report –Cadmium and its Compounds. National Printers. Ottawa, Canada. 1999.

Hershfinkel M, Silverman W, and Sekler I. 2007. The Zinc Sensing Receptor, a Link Between Zinc and Cell Signaling. *Mol Med* 13 (7-8):331-336.

Huang XD, Dixon DG, Greenberg BM. 1993. Impacts of UV Radiation and Photomodification on the toxicity of PAHs to the higher plant *Lemna gibba* (Duckweed). *Environ Toxicol Chem.* 12:1067-1077

Huang XD, Dixon DG, Greenberg BM. 1995. Increased Polycyclic Aromatic Hydrocarbon Toxicity Following Their Photomodification in Natural Sunlight; Impacts of the Duckweed *Lemna gibba* L. G-3. *Ecotoxicol Environ Saf.* 32:194-200.

Huang, XD. McConkey BJ., Babu TB., Greenberg, BM. 1997a. Mechanisms of Photoinduced Toxicity of Photomodified Anthracene To Plants: Inhibition of Photosynthesis in the Aquatic Higher Plant *Lemna gibba* (Duckweed). *Environ Toxicol Chem.* 16:1707-1715.

Huang XD, Krylov SN., Ren L, McConkey BJ. Dixon DG., Greenberg BM. 1997b. Mechanistic Quantitative Structure-Activity Relationship Model for the Photoinduced Toxicity of Polycyclic Aromatic Hydrocarbons: II. An Empirical Model for the toxicity of 16 Polycyclic Aromatic Hydrocarbons to the Duckweed *Lemna gibba* L. G-3 *Environ Toxicol Chem.* 16:2296-2303

Huang C, Li J, Ding M, Leonard S, Wang L, Castranova V, Vallyathan V, Shi X. 2001. UV induces phosphorylation of protein kinase B (Akt) at Ser473 and Thr308 in mouse epidermal Cl 41 cells through hydrogen peroxide. J. Biol. Chem. 276:40234–40240.

Jaouen G. 2006. Bioorganometallics: Biomolecules, Labeling, Medicine; Wiley-VCH: Weinheim.

Kang J, Zhang Y, Chen J, Chen H, Lin C, Wang Q, Ou Y. 2003. Nickel-indusced histone hypoacetylation: the role of reactive oxygen species. *Toxicol Scien*. 74:279-286.

Kasprzak K. 1989. Enhancement of Hydroxylation and Deglycosylation of 2-deoxyguanosine by Carcinogenic Nickel Compounds. *Cance Res* 49:5964-5968.

Kasprzak K. 1991. The role of Oxidative damage in metal carcinogenicity. *Chem Res Toxicol* 4:604-615.

Kasprzak K, Sunderman F, Salnikow K.2003. Nickel Carcinogenisis. *Mutat Res*. 533:67-97.

Keithly J, Brooker J, Deforest D, Wu BK, Brix KV. 2004. Acute and chronic toxicity of nickel to a cladoceran (*Ceriodaphnia dubia*) and an amphipod (*Hyalella azteca*). *Environ Toxicol Chem* 23:691-696.

Kelly M.1988. Mining and the Freshwater Environment. Elsevier Applied Science, London. 231-234

King M, Lai E, McCay P. 1975. Singlet oxygen production associated with enzyme-catalyzed lipid peroxidation in liver microsomes. *J Biol Chem*. 250:6496-6502.

King J, Cousins R. Zinc. In: Shils M, Shike M, Ross A, Caballero B, Cousins R, eds. Modern Nutrition in Health and Disease. 10th ed. Baltimore: Lippincott Williams & Wilkins; 2006:271-285.

Klaassen C. 2001. Casarett and Doull's Toxicology: The Basic Science of Poisons. 6th Edition. New York. NY McGraw-Hill publications.

Kramer KJ, Jak RG, Van Hattum B, Hooftman RN, Zwolsman JJ. 2004. Copper toxicity in relation to surface water-dissolved organic matter: biological effects to Daphnia magna. *Enviro Toxicol Chem* 23:2971-80.

Kruschwitz L.G. 1978. Environmental Factors Controlling the Reproduction of the Amphipod *Hyalella azteca*. Proc. Okla. Acad. Sci. 58:16-21

Kurihara R, Shiraishi F, Tanaka N, Hashimoto S. 2005. Presence and estrogenicity of anthracene derivatives in coastal Japanese waters. *Environ Toxicol Chem.* 24:1984-1993.

Landis WG, Yu MH. 1995. Introduction to Environmental Toxicology: Impacts of Chemicals upon Ecosystems. New York, NY, Lewis Publishers.

Landrum P, Giesy J. Oris J, Allred P. 1986. Photoinduced toxicity of polycyclic aromatic hydrocarbons to aquatic organisms. Oil in fresh water: Chemistry, biology, technology. J.H Vandermeulen and S. Hrudy. Elmsford, NY, Permagon Press

Lampi MA, Huang XD, El-Alawi Y, McConkey B, Dixon DG, Greenberg BM. 2001. Occurance and toxicity of photomodified polycyclic aromatic hydrocarbon mixtures present in contaminated sediments. In Greenberg BM, Roberts RN, Gensmer RW (eds). *Environemtnal Toxicology and Risk Assesment*. Vol 10 m ASTM STP 1403, American Society for Testing Materials, West Conshocken, PA, 211-221.

Lampi MA, Gurska J, McDonald K, Xie F, Huang XD, Dixon DG, Greenberg BM. 2005. Photoinduced Toxicity of Polycyclic Aromatic Hydrocarbons to *Daphnia magna*:

Ultraviolet-Mediated Effects and the Toxicity of Polycyclic Aromatic Hydrocarbon photoproducts. *Environ Toxicol Chem*. 25:278-286.

Lampi M, Gurska J, Huang XD, Dixon DG, Greenberg BM. 2007.A predictive quantitative structure-activity relationship model for the photoinduced toxicity of polycyclic aromatic hydrocarbons to *Daphnia magna* with the use of factors for photosensitization and photomodification. *Environ Toxicol Chem.* 26:406-15

Lazzaro A, Montserrat C, Marti C, Flors C, Izquierdo L, Grillo Teresa, Louis J, Santi N. 2004. Light and singlet oxygen-mediated antifungal activity of phenylphenalenone phytoalexins. *Photochem Photobiol Sci.* 3:706-710.

Lee JH, Landrum PF, Field LJ, Koh CH. 2001. Application for a ΣPolycyclic Aromatic Hydrocarbon Model and a Logistic Regression Model to Sediment Toxicity Data Based on a Species-Specific, Water-Only LC50 Toxic Unit for *Hyalella azteca*. *Environ Toxicol Chem.* 20:2102-2113.

Legzdins AE, McCarry BE, Marvin CH, Bryant DW.1995. Methodology for assay-directed fractionation studies of air particulate material and other complex environmental matrices. *Int J Environ Anal Chem.* 60:79-94.

Lehto K-M, Puhakka JA, Lemmetyinen H. 2003. Photodegredation products of polycyclic aromatic hydrocarbons in water and their amenability to biodegradation. *Polycyclic Aromatic Compounds* 23:401-416.

Li Y, Trush MA. 1993. Oxidation of Hydroquinone by Copper: Chemical Mechanism and Biological Effects. *Arch Biochem Biophys* 300:346-355.

Li W, Zhao Y, Chou IN, 1994. Alterations in cytoskeletal organization and homeostasis of cellular thiols in cadmium-resistant cells. *Toxicol Appl Pharmacol.* 126:114-123.

Lynn S, Yew FH, Chen KS, Jan KY. 1997. Reactive oxygen species are involved in nickel inhibition of DNA repair. *Environ Mol Mutagen* 29:208-216.

MacDonald RW, Barrie LA, Bidleman TF, Diamond ML, Gregor DJ, Semkin RG, Strachan WM, Li YF, Wania F, Alaee M , Alexeeva LB, Backus SM, Bailey R, Bewers JM, Gobeil C, Halsall CJ, Harner T, Hoff JT, Jantunen LM, Lockhart WL, Mackay D, Muir DC, Pudykiewicz J, Reimer KJ, Smith JN, Stern GA, Schroeder WH, Wagemann R, Yunker MB. 2000. Contaminants in the Canadian Arctic: 5 years of progress in understanding sources occurrence and pathways. *The Science of the Total Environment* 254:93-234.

Mallakin A, McConkey BJ, Miao G, McKibben B, Snieckus V, Dixon DG, Greenberg BM. 1999. Impacts of Structural Photomodification on the toxicity of environmental contaminants: Anthracene photooxidation products. *Ecotoxicol Environ Saf*. 43:204-212.

Mallakin A, Dixon DG, Greenberg BM. 2000. Pathway of Anthracene Modification under Simulated Solar Radiation. *Chemosphere*. 40:1435-1441.

Maliszewska-Kordybach B. 2000. Polycyclic aromatic hydrocarbons in agro-ecosystems-example of Poland. *Polycycl Aromat Comp.* 21:287-295.

McConkey BJ, Duxbury CL, Dixon DG, Greenberg BM. 1997. Toxicity of PAH photooxidation product to the bacteria *Photobacterium phosphoreum* and the duckweed Lemna gibba: effects of phenanthrene and its primary photoproduct, Phenanthraquinone. *Environ Toxicol Chem*. 16:892-899.

McKinney R, Pruell R, Burgess R. 1999. Ratio of the Concentration of Anthraquinone to Anthracene in Costal Marine Sediments. *Chemosphere.* 38:2415-2430

McLusky D, Bryant V, Cambell R. 1986. The effect of temperature and salinity on the toxicity of heavy metals to marine and estuarine invertebrates. *Oceang Mar Biol Ann Rev.* 24:481-520.

Miller JA .1998. The metabolism of Xenobiotics to reactive electrophiles in chemical carcinogenesis and mutagenesis: a collaboration with Elizabeth Cavert Miller and our associates. *Drug Metab Rev* 30**:**645–674.

Muyssen BT, DeSchamphelaere KA, Janssen CR. 2006. Mechanisms of chronic waterborne Zn toxicity in Daphnia magna. *Aquat Toxicol* 77:393-401.

Nriagu JO. 1979. Copper in the Environment. Canadian Centre for Inland Waters, Toronto, Canada: John Wiley & Sons Canada Ltd.

Neff JM. 1985. Polycyclic Aromatic Hydrocarbons. Fundamentals of Aquatic Toxicology. Toronto, Canada: Hemisphere Publishing Corporation. P.335-454

Newsted JL, Giesy JP. 1987. Predictive Models for Photoinduced Acute Toxicity of Polycyclic Aromatic Hydrocarbons to *Daphnia magna* Strauss (Cladocera, Crustacea). *Environ Toxicol Chem.* 6:455-461.

Norwood WP, Borgmann U, Dixon DG, Wallace A. 2003. Effects of metal mixtures on aquatic biota: A review of observations and methods. *Human and Ecological Risk Assessment* 9:795-811.

NRCC, "Polycyclic Aromatic Hydrocarbons in the Aquatic Environment: Formation, Sources Fate and Effects on Aquatic Biota". NRC Associate committee on Scientific Criteria for Environmental Quality, Publication No. NRCC 18981, Ottawa, Ont., 209 p. 1983.

Nuutinen S, Landrum P, Schuler L, Kukkonen J, Lydy M. 2003. Toxicokinetics of Organic Contaminants in *Hyalella azteca*. *Arch Environ Contam Toxicol.* 44:467-475.

Nykamp J, Bols NC, Calson JC. 2001. Phenanthrenequinone Disrupts Progesterone Production in Rat Luteal Cells. Reprod Toxicol 15:393-398.
Oehme FW. 1979. Toxicology is a Bastard. *Vet Hum Toxicol.* 21:164-165.

Oris J, Giesy J. 1985. "The Photoinduced Toxicity of Anthracene to Juvenile Sunfish (*Lepomis Spp*)". *Aquatic Toxicol* 6:133-146.

Parkerton TF, Stone MA, Letinski DJ. 2000. Assessing the aquatic toxicity of complex hydrocarbon mixtures using solid phase micro-extraction. *Toxic Lett.* 112-113:273-282.

Perceval O, Pinel-Alloul B, Methot G, Couillard Y, Giguere A, Campbell PG, Hare L. 2002. Cadmium accumulation and metallothionein synthesis in freshwater bivalves (*Pyganodon randis*); relative influence of the metal exposure gradient versus limnological variability. *Environ Pollut.* 118:5-17.

Peterson S, Kusk KO. 2000. Photosynthesis tests as an alternative to growth tests for hazard assessment of toxicant. *Arch Envron Contam Tox* 38:152-157.

Pourahmad J, O'Brian PJ. 2000. A Comparison of Hepatocyte Cytotoxic Mechanisms for Cu^{2+} and Cd^{2+}. *Toxicology.* 143:263-273.

Pourahmad J, O'Brian PJ. 2003. Contrasting Role of Na^{+} Ions in Modulating Cu^{2+} or Cd^{2+} Induced Hepatocyte Toxicity. *Chem Biol Interact.* 126:159-169

Sadiq M. 1992. Toxic Metal Chemistry in Marine Environments. Marecl Dekker Inc. NewYork, NY, USA. 106-154.

Sanders M. 1995. Distribution of polycyclic aromatic hydrocarbons in Oyster (Crassostrea virginica) and surface sediment from two estuaries in South Carolina. Arch *Environ Contam Toxicol.* 28:397-405.

Schuler LJ, Wheeler M, Bailer J, Lydy M. 2003. Toxicokinetics of Sediment-Sorbed Benzo[a]Pyrene and Hexacholobiphenyl Using the Freshwater Invertebrates *Hyalella Azteca*, Chironomus Tentans, and Lumbriculus Variegatus. *Environ Toxicol Chem.* 22:439-449.

Shou M, Gonzalez FJ, Gelboin HV.1996. Stereoselective epoxidation and hydration at the K-region of polycyclic aromatic hydrocarbons by cDNA-expressed cytochromes P450 1A1, 1A2, and epoxide hydrolase. *Biochemistry* 10;35(49):15807-13

Snyder R. 1988. Role of Active oxygen Species in Meta Induced DNA strand breakage in Human Diploid Fribroblasts. *Mutat Res.* 193:237-246.

Sorensen H, Cedergreen N, Skovgaard I, Streibig J. 2007. An Isobole-based statistical model and test for synergisim/antagonism in binary mixture toxicity experiments. *Environ Ecol Stat* 14:383-397.

Stacy N, Cantilena L, Klaassen C. 1980. Cadmium toxicity and lipid peroxidation in isolated rat hepatocytes. *Toxicol Appl Pharmacol.* 53:470-480.

Stephenson GL, Kooper N, Atkinson GF, Solomon KR, Scroggins RP. 2000. Use of non-linear regression techniques for describing concentration response relationships of plant species exposed to contaminated site soils. *Environ Toxicol Chem.* 19:2968-2981.

Stowe C, Nelson R, Werdin R. 1978. Zinc phosphate poisoning in dogs. *J Amer Vet Med.* 173:270-276

Strong D. 1972. Life History Variation among Populations of an Amphipod (*Hyalella azteca*). *Ecology*. 53:1103.

Szilagyi R, Bryngelson P, Maroney M, Hedman B, Hodgson K, Solomon E. 2004. S K-Edge X-ray Absorption Spectroscopic Investigation of the Ni-Containing Superoxide Dismutase Active Site: New Structural Insight into the Mechanism. *J Amer Chem Soc.* 126:3018-3019.

Tabershaw I. 1977. "Chemical Hazards. Copper." In Occupational Diseases: A Guide to Their Recognition. U.S. Public Health Serv. Publ. (NIOSH)77-181, U.S. Government Printing Office, Washington, D.C.

Tabak HH, Lazorchak JM, Khodadoust AP, Antia JE, Bagchi R, Suidan MT. 2003. Studies on Bioremediation of Polycyclic Aromatic Hydrocarbon-Contaminated Sediments: Bioavailability, Biodegradability, and Toxicity Issues. *Environ Toxicol Chem.* 22:473-482

Takamure Y, Shimada H, Kiyozumi M, Yasutake A, Imamura Y. 2005. A possible mechanism of resistance to cadmium toxicity in male Long-Evan rats. *Environ Toxic Pharma.* 21:231-234.

Timmermans K. 1993. Accumulation and Effects of Trace Metals in Freshwater invertebrates. In: Dallinger R and Rainbow P (eds) *Ecotoxicology of Metals in Invertibrates.* Lewis Publishers, Florida. 133-145.

Tanaka T, Suzui M, Kojima T, Okamoto K, Wang A, Mori H. 1995. Chemoprevention of the naturally occurring carcinogen 1-hydroxyanthraquinone-induced carcinogenesis by the nonsteroidal anti-inflammatory drug indomethacin in rats. *Cancer Detect Prev* 19:418-425.

Tripuranthakam S, Duxbury CL, Babu TS, Greenberg BM. 1999. Development of a Mitochondrial Respiratory Electron Transport Bioindicator fof Assesment of Aromatic Hydrocarbon Toxicity. In: Henshel DS, Black, M.C. and M.C. Harrass, editor. Environmental Toxicology and Risk Assessment: Standardization of Biomarkers for Endocrine Disruption and Environmental Assessment: Eighth Volume, ASTM STP 1364. West Conshohocken, PA: American Society for Testing and Materials.

USEPA (2000) Methods for measuring the toxicity and bioaccumulation of sediment-associated contaminants with freshwater invertebrates, Second[ed], EPA 600/R-99/064. Office of Research and Development, U.S. Environmental Protection Agency, Duluth, MN.

Van Assche F, Clijsters H. 1990. Effects of metals on enzyme activity in plants. *Plant Cell Environ.* 13:195-206.

Verrhiest G, Clement B, Blake G. 2001. Single and Combined Effects of Sediment-Associated PAHs on Three Species of Freshwater Macroinvertebrates. *Ecotox.* 10: 363-372

Vondracek J, Kozubik A, Machala M. 2002.Modulation of Estrogen Receptor-Dependent Reporter Construct Activation and G_0/G_1–S-Phase Transition by Polycyclic Aromatic Hydrocarbons in Human Breast Carcinoma MCF-7 Cells. *Toxicol Sci.* 70:193-201.

Wang W, Lampi M, Huang XD, Gerhardt K, Dixon DG, Greenberg BM. 2008. Assessment of Mixture Toxicity of Copper, Cadmium and Phenanthrenequinone to the Marine Bacterium *Vibrio fischeri*. *Environ Toxicol*. In press.

Weckx JE, Clijsters HM. 1996. Oxidative damage and defense mechanisms in primary leaves of *Phaseolus vulgaris* as a result of root assimilation of toxic amounts of copper. *Physiol Plant* 96:506-512.

Watanabe M, Suzuki T. 2001. Cadmium-induced abnormality in strains of *Euglena gracilis*: Morphological alteration and its prevention by zinc and cyanocobalmin. *Comp Biochem Physiol C* 130:29-39.

Wilcoxen S, Meier P, Landrum P. 2003. The Toxicity of Fluoranthrene to *Hyalella azteca* in sediment and Water-Only exposures under varying light spectra. *Excotox and Environ Saf.* 54:105-117.

Xia T, Korge P, Weiss JN, Li N, Venkatesen MI, Sioutas C, Nel A. 2004. Quinones and Aromatic Chemical Compounds in Particulate Matter Induce Mitochondrial Dysfunction: Implications for Ultra-fine Particle Toxicity. *Environ Health Perspect.* 112:1347-1358.

Xie F, Kozar S, Lampi MA., Dixon DG, Norwood W, Borgmann U, Greenberg BM. 2006. Assessment of the Toxicity of Copper, 9,10-Phenanthrenequinone and Phenanthrene to *D.magna*. *Environ Toxicol Chem.* 25:613-622.

Xie F, Lampi MA, Dixon DG, Greenberg BM. 2007. Assessment of the Toxicity of Mixtures of Nickel or Cadmium with 9,10-Phenanthrenequinone to *Daphnia magna*: Impact of a Reactive Oxygen-Mediated Mechanism with Different Redox-Active Metals. *Environ Toxicol Chem.* 26:1425-1432.

Yamagata N. 1979. Industrial Emission of Cadmium in Japan. *Environ Health Perspect.* 28:17-22.

Yang JL, Chao JI, Lin JG.1996 Reactive oxygen species may participate in the mutagenicity and mutational spectrum of cadmium in Chinese Hamster Ovary-K1 cells. *Chem Res Toxicol* 9:1360-1367.

Younglai EV, Foster WG, Hughes EG, Trim K, Jarrel JF. 2002. Levels of environmental contaminants in human follicular fluid, serum, and seminal plasma of couples undergoing in vitro fertilization. *Arch Environ Contam Toxico.* 43:121-126.

Zbigniew T, Wojciech P. 2006. Individual and combined effect of anthracene, cadmium, and chloridazone on growth and activity of SOD izoformes in three *Scenedesmus* species. *Ecotox Environ Saf* 65 323-331.

Appendix

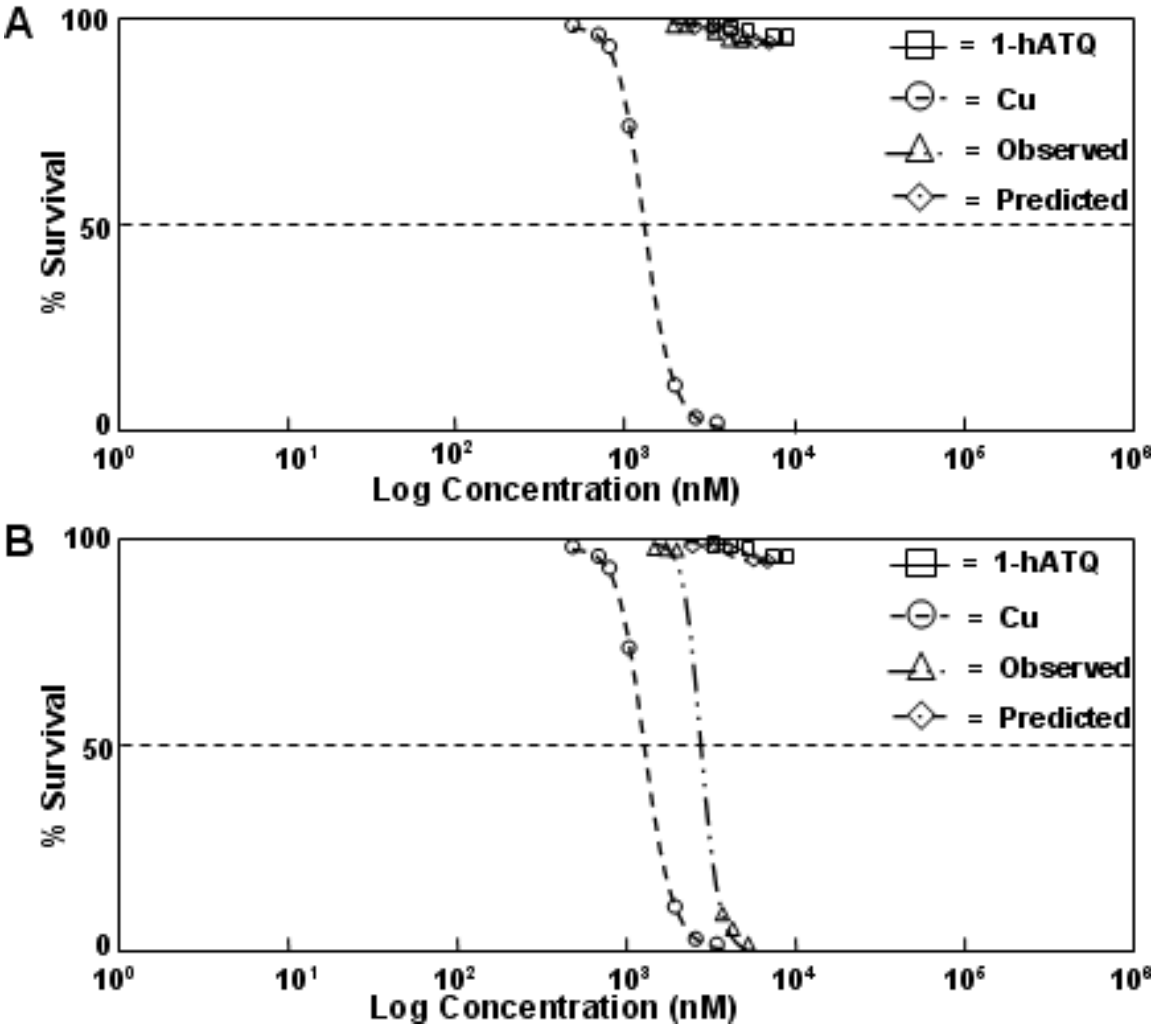

Figure 7.1 Concentration response curves of mixtures to *Hyalella azteca* under dark conditions. 1-hATQ concentrations were varied while Cu was kept at a constant concentration. A. 1-hATQ + 1 nM Cu B. 1-hATQ + 10 nM Cu.

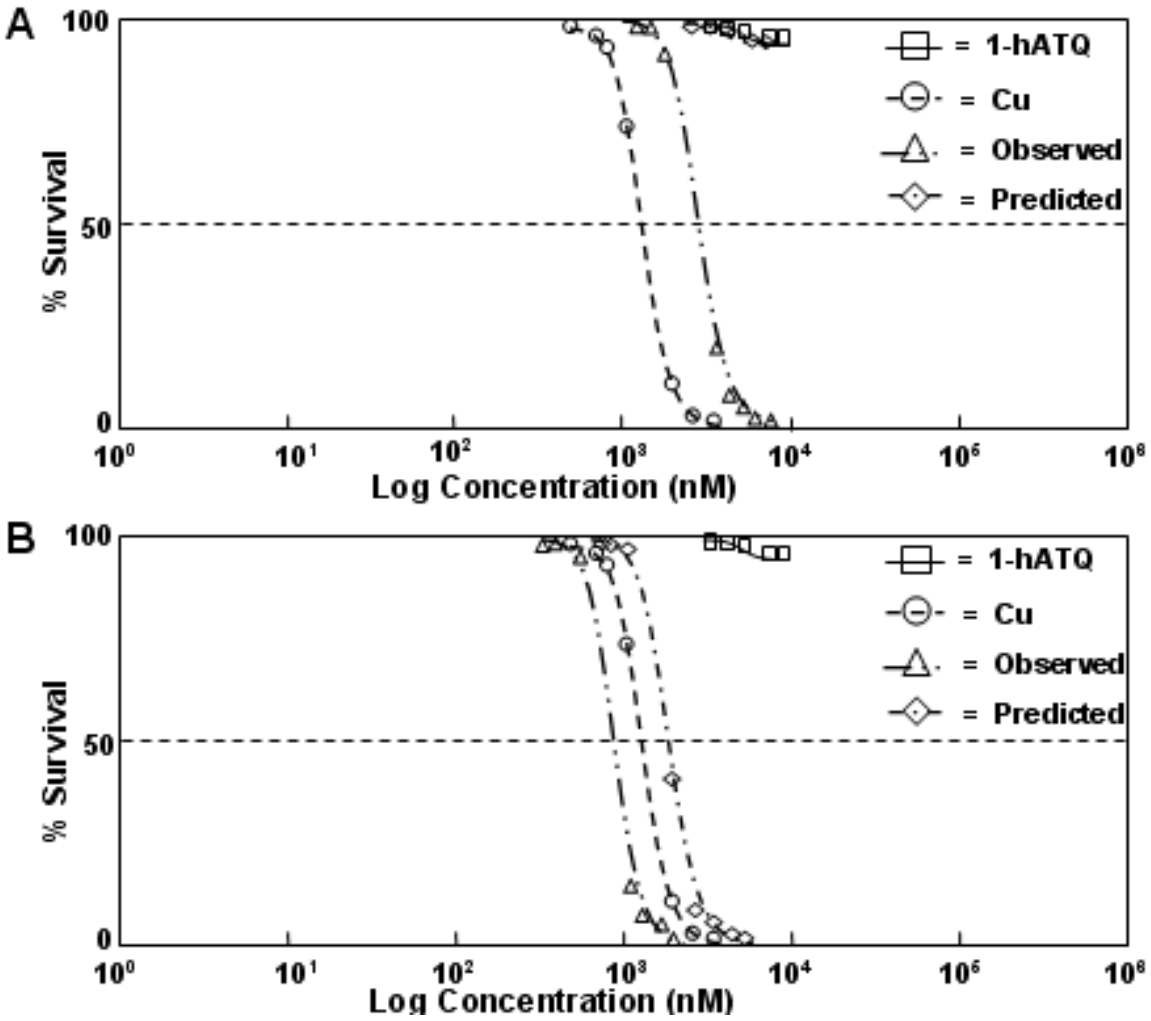

Figure 7.2 Concentration response curves of mixtures to *Hyalella azteca* under dark conditions. 1-hATQ concentrations were varied while Cu was kept at a constant concentration. A. 1-hATQ + 100 nM Cu B. 1-hATQ + 1000 nM Cu.

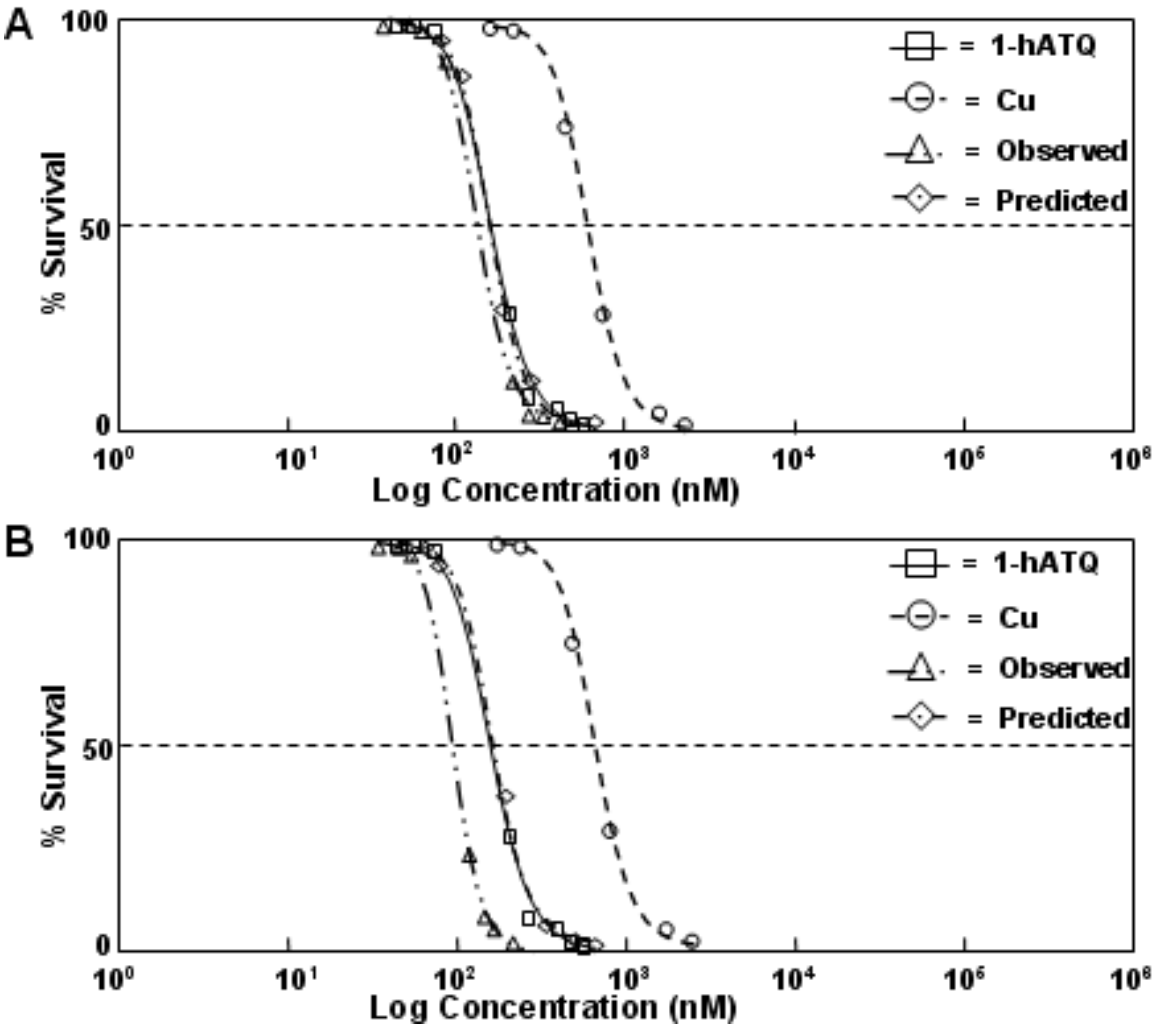

Figure 7.3 Concentration response curves of mixtures to *Hyalella azteca* under PAR conditions. 1-hATQ concentrations were varied while Cu was kept at a constant concentration. A. 1-hATQ + 1 nM Cu B. 1-hATQ + 10 nM Cu.

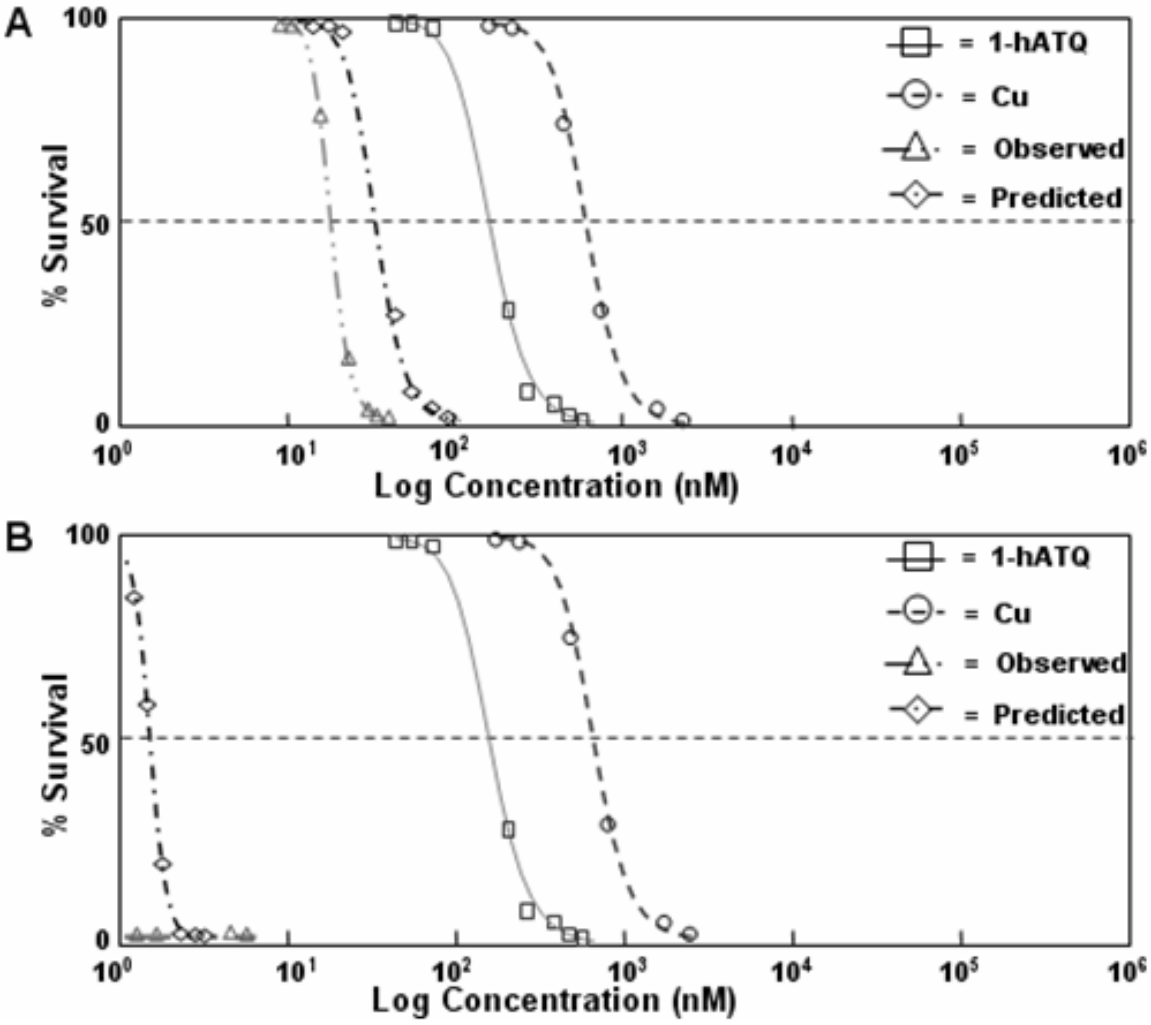

Figure 7.4 Concentration response curves of mixtures to *Hyalella azteca* under PAR conditions. 1-hATQ concentrations were varied while Cu was kept at a constant concentration. A. 1-hATQ + 100 nM Cu B. 1-hATQ + 1000 nM Cu.

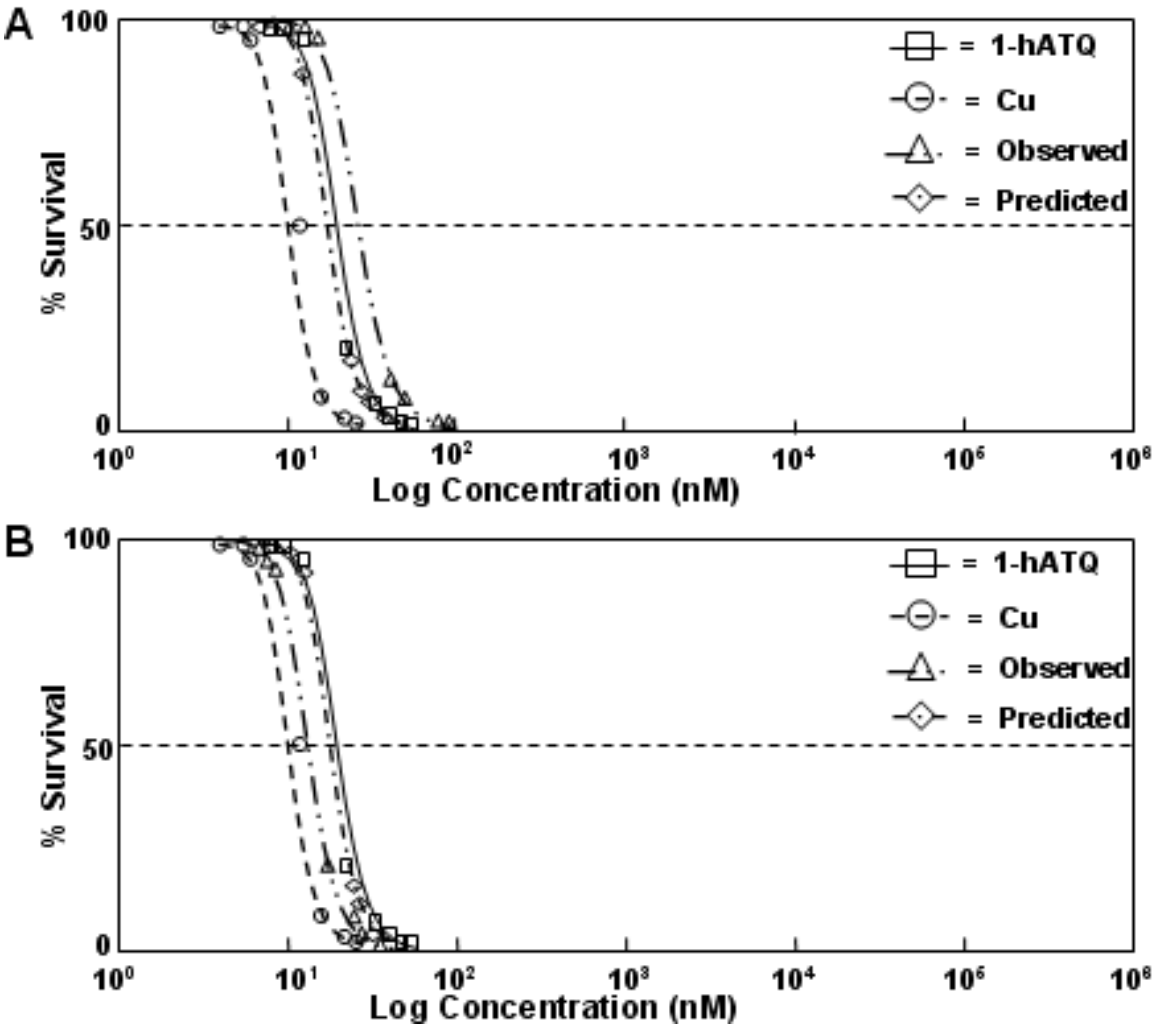

Figure 7.5 Concentration response curves of mixtures to *Hyalella azteca* under SSR conditions. 1-hATQ was varied while Cu was kept at a constant concentration. A. 1-hATQ + 1 nM Cu B. 1-hATQ + 10 nM Cu.

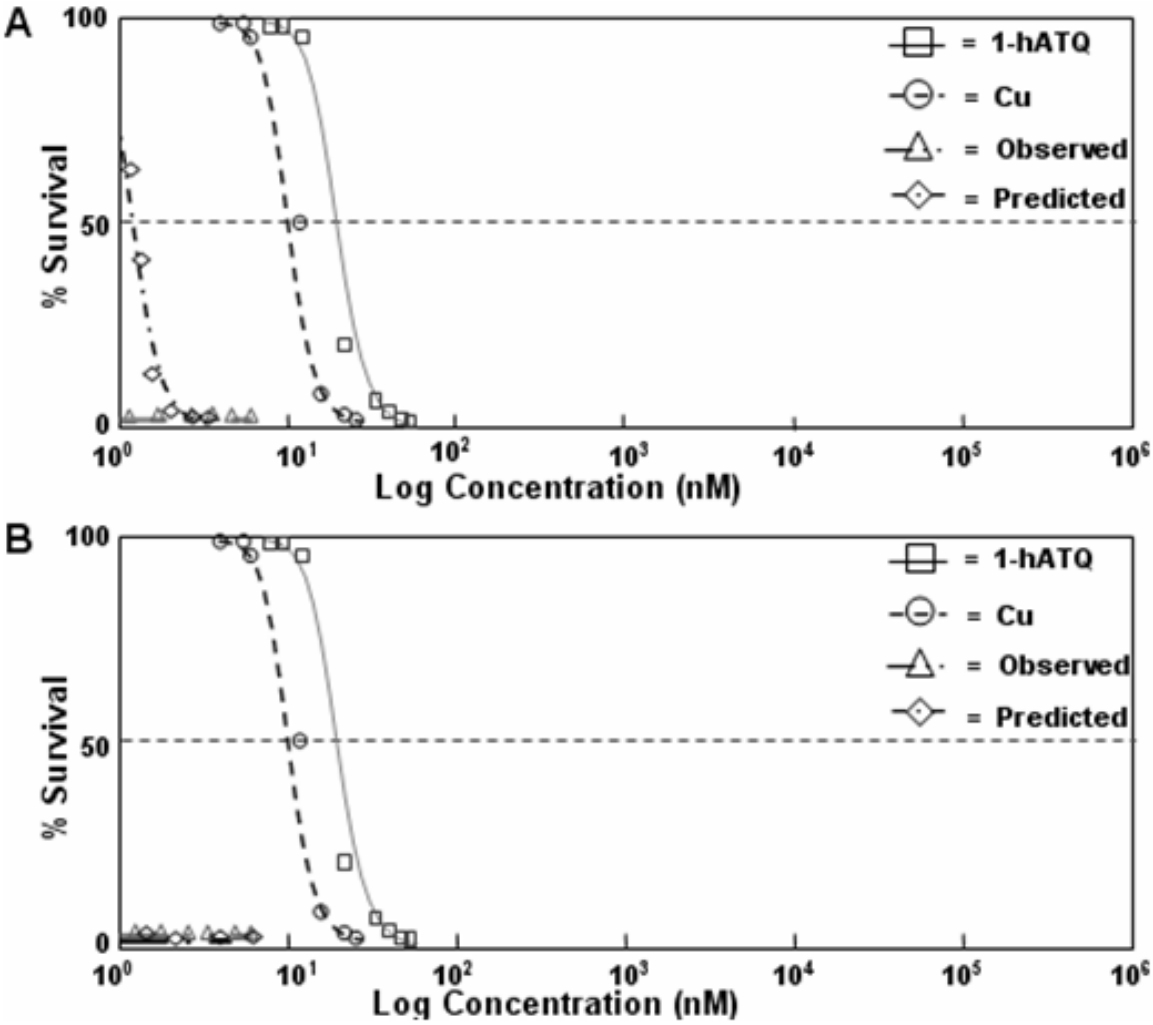

Figure 7.6 Concentration response curves of mixtures to *Hyalella azteca* under SSR conditions. 1-hATQ was varied while Cu was kept at a constant concentration. A. 1-hATQ + 100 nM Cu B. 1-hATQ + 1000 nM Cu.

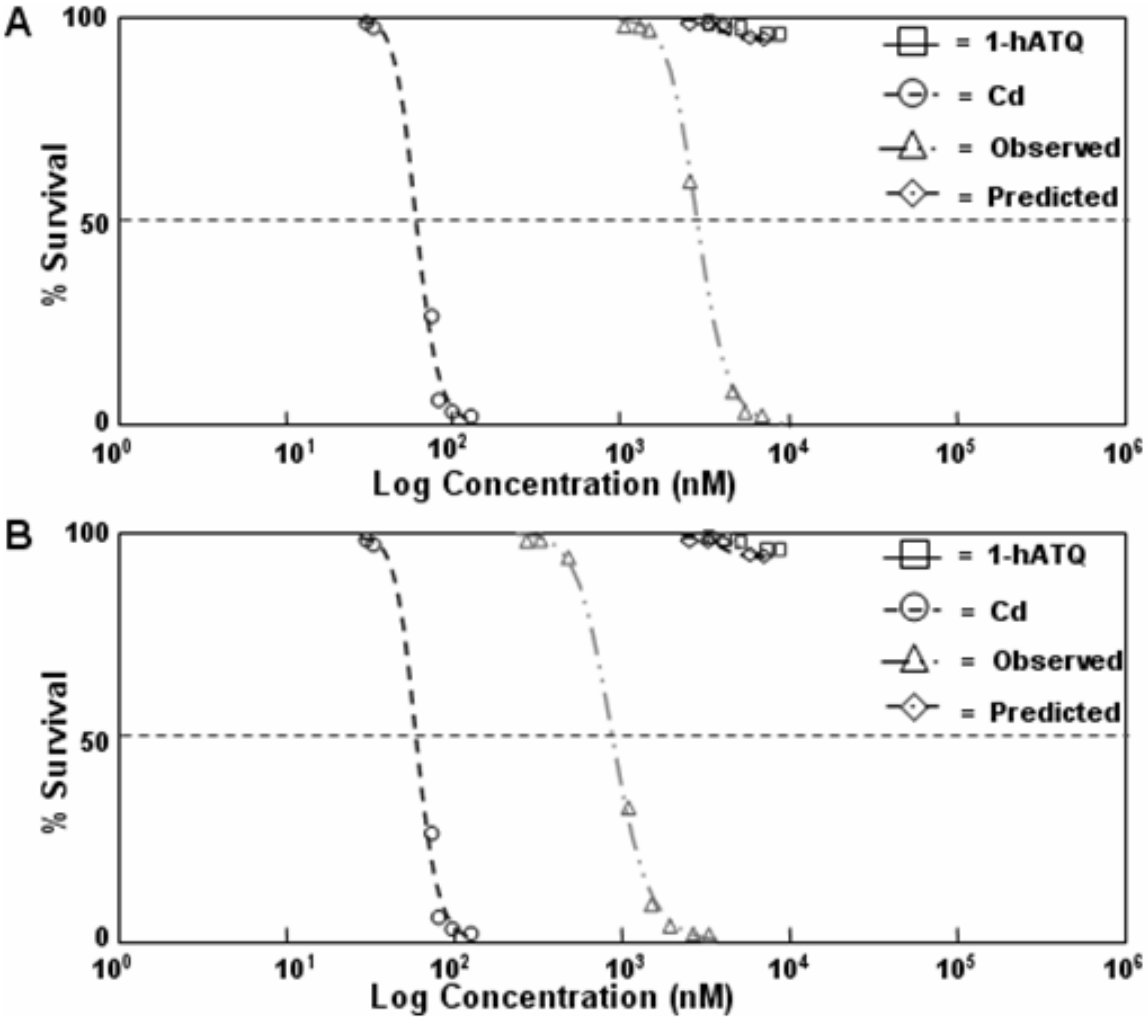

Figure 7.7 Concentration response curves of mixtures to *Hyalella azteca* under dark conditions. 1-hATQ was varied while Cd was kept at a constant concentration. A. 1-hATQ + 1 nM Cd B. 1-hATQ + 10 nM Cd.

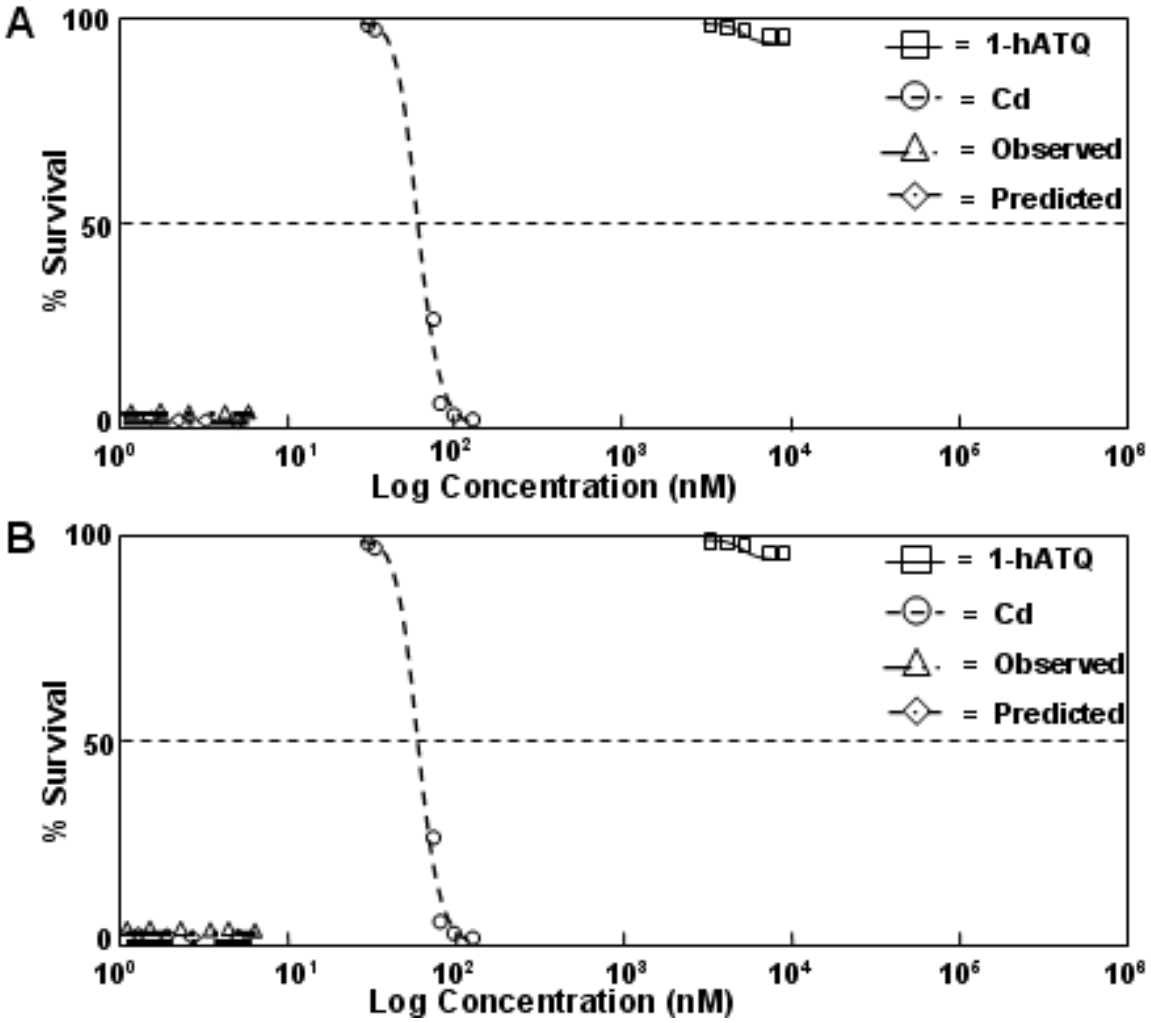

Figure 7.8 Concentration response curves of mixtures to *Hyalella azteca* under dark conditions. 1-hATQ was varied while Cd was kept at a constant concentration. A. 1-hATQ + 100 nM Cd B. 1-hATQ + 1000 nM Cd.

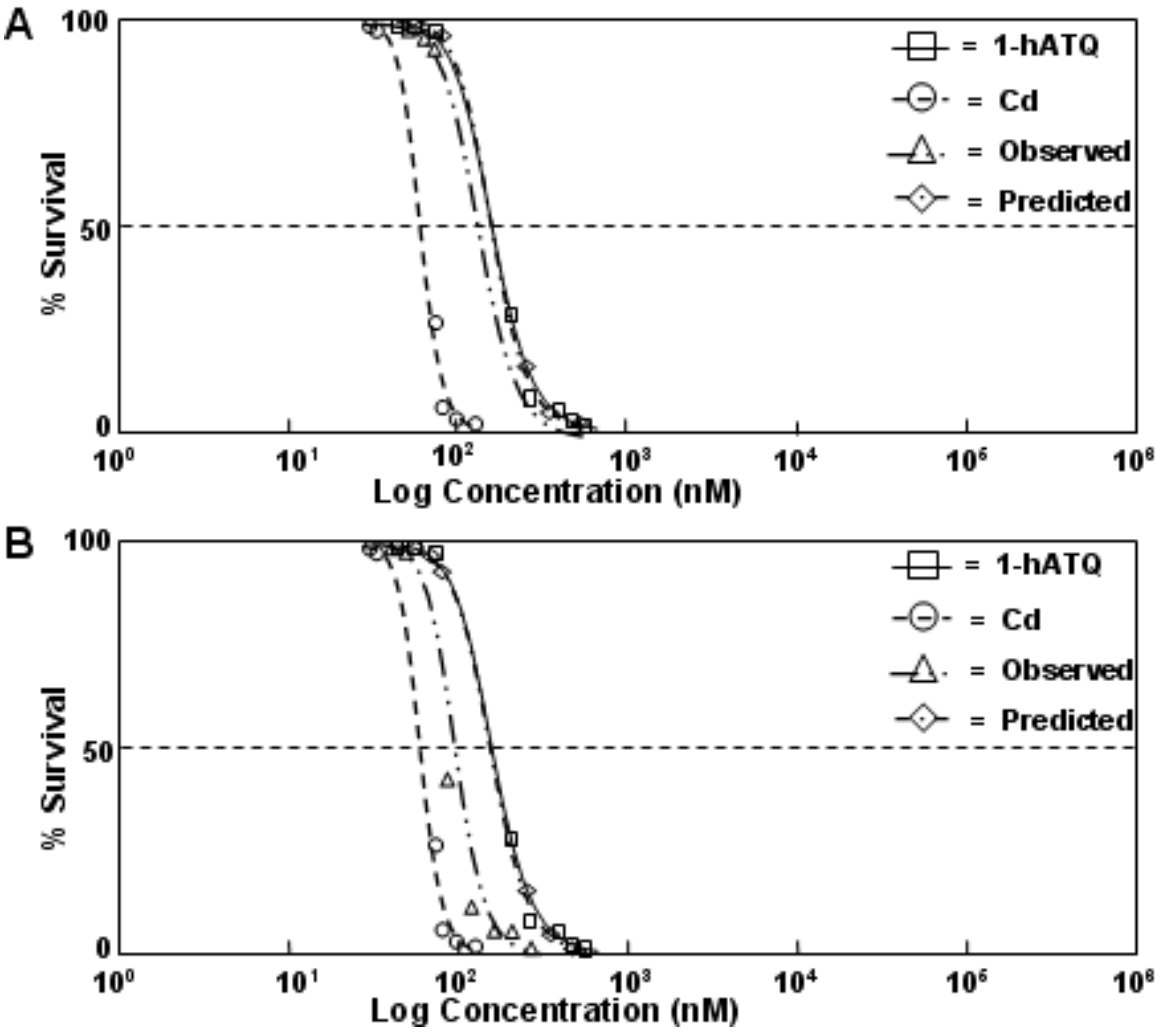

Figure 7.9 Concentration response curves of mixtures to *Hyalella azteca* under PAR conditions. 1-hATQ was varied while Cd was kept at a constant concentration. A. 1-hATQ + 1 nM Cd B. 1-hATQ + 10 nM Cd.

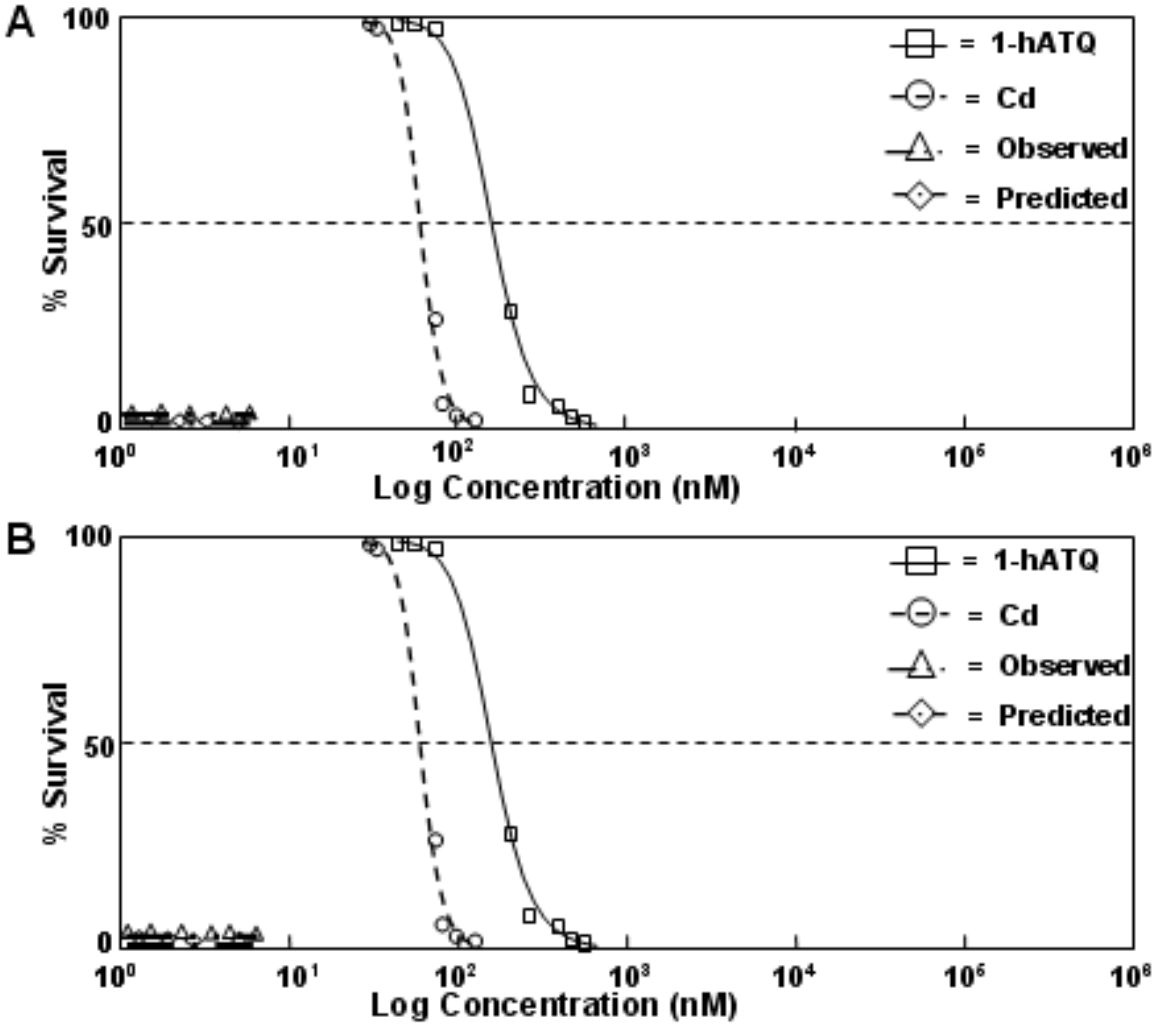

Figure 7.10 Concentration response curves of mixtures to *Hyalella azteca* under PAR conditions. 1-hATQ was varied while Cd was kept at a constant concentration. A. 1-hATQ + 100 nM Cd B. 1-hATQ + 1000 nM Cd.

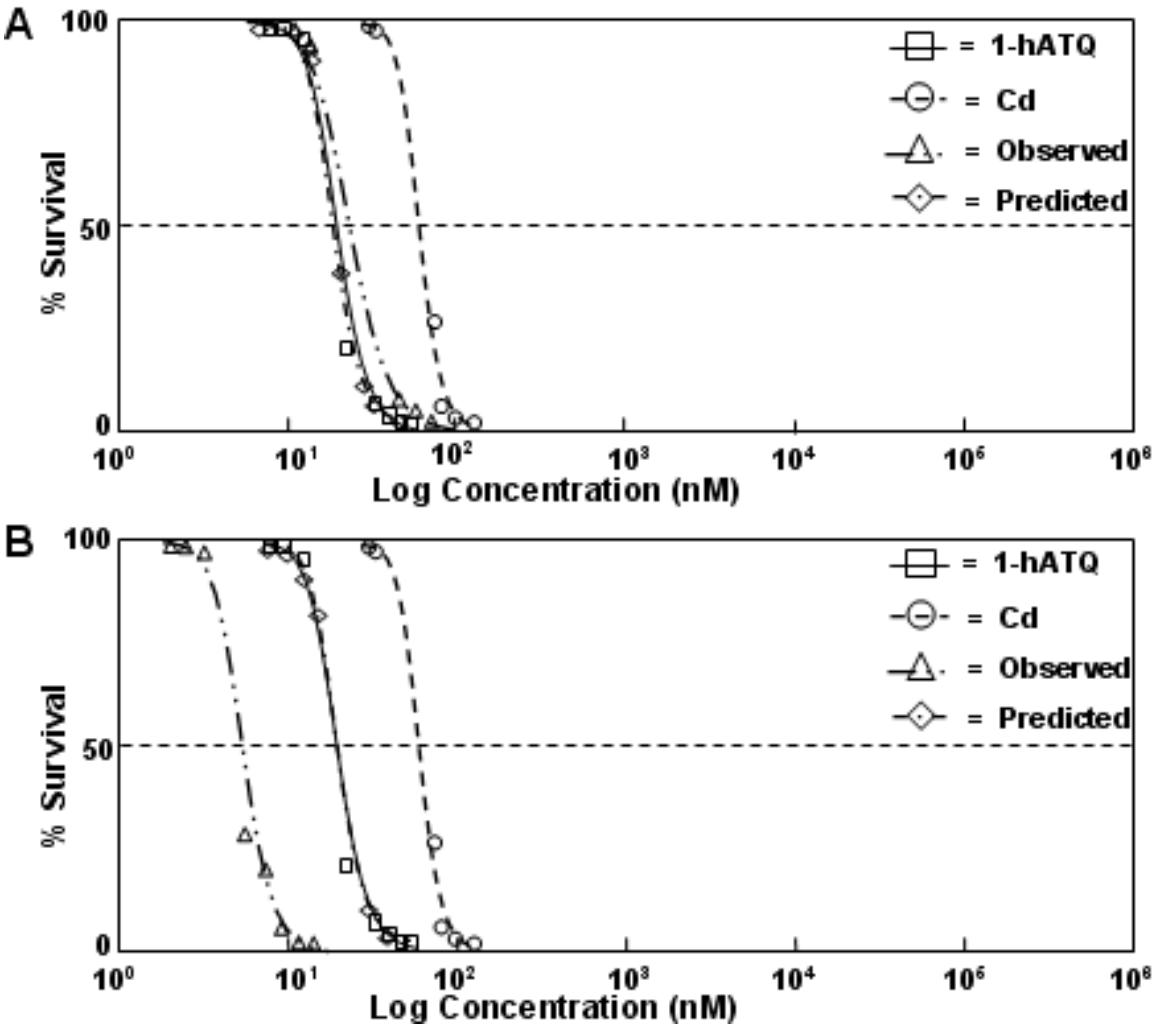

Figure 7.11 Concentration response curves of mixtures to *Hyalella azteca* under SSR conditions. 1-hATQ was varied while Cd was kept at a constant concentration. A. 1-hATQ + 1 nM Cd B. 1-hATQ + 10 nM Cd.

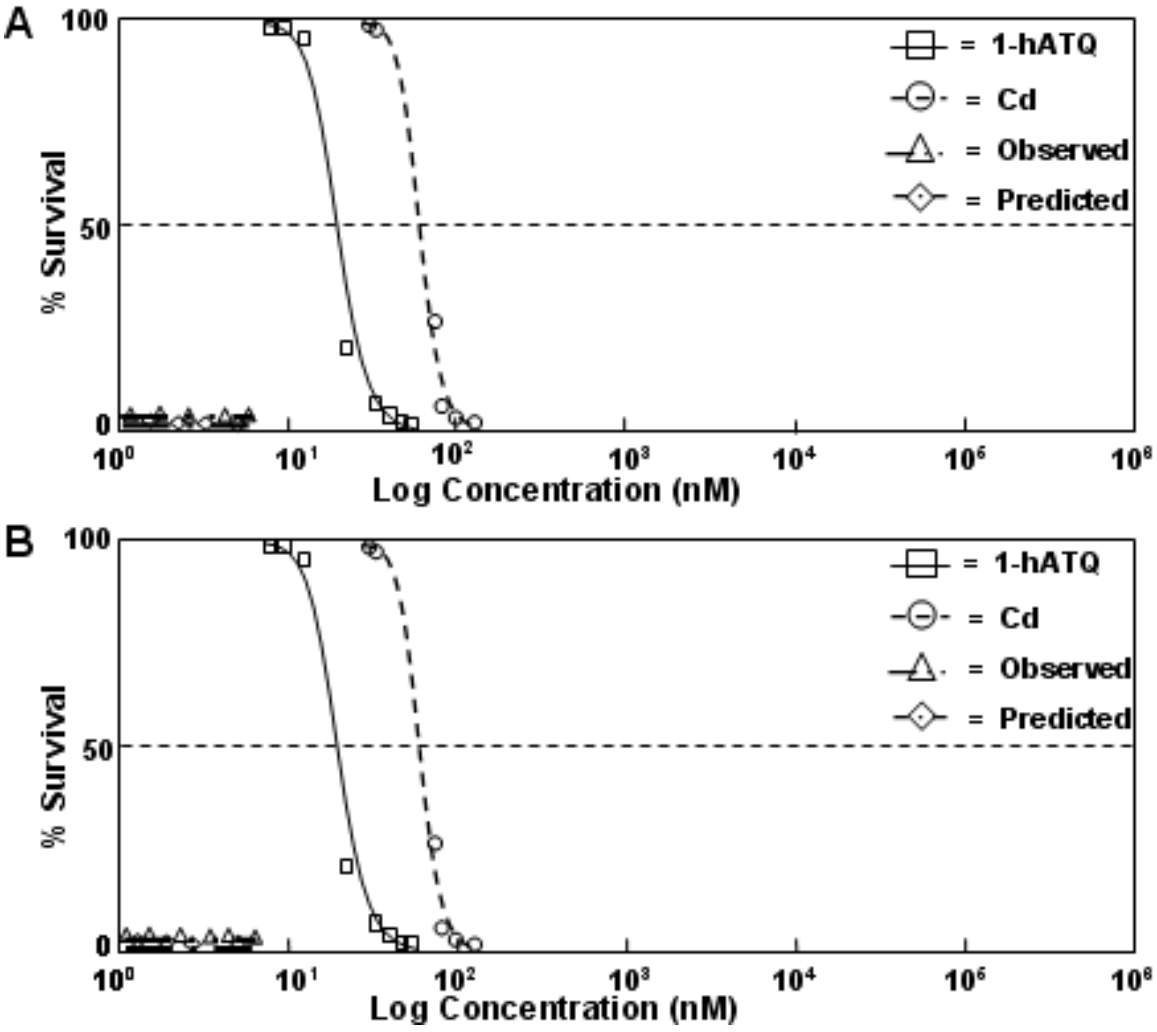

Figure 7.12 Concentration response curves of mixtures to *Hyalella azteca* under SSR conditions. 1-hATQ was varied while Cd was kept at a constant concentration. A. 1-hATQ + 100 nM Cd B. 1-hATQ + 1000 nM Cd.

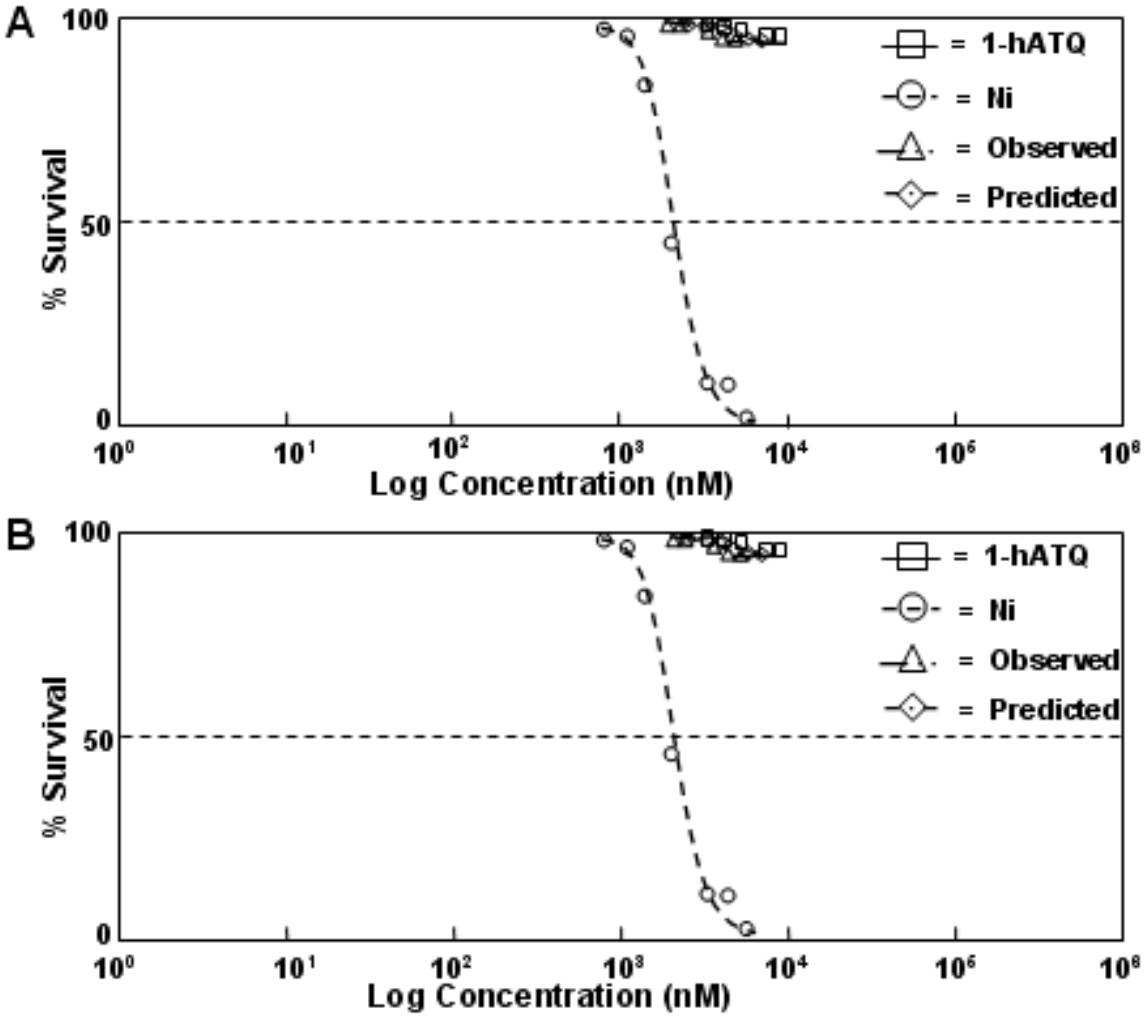

Figure 7.13 Concentration response curves of mixtures to *Hyalella azteca* under dark conditions. 1-hATQ was varied while Ni was kept at a constant concentration. A. 1-hATQ + 1 nM Ni B. 1-hATQ + 10 nM Ni.

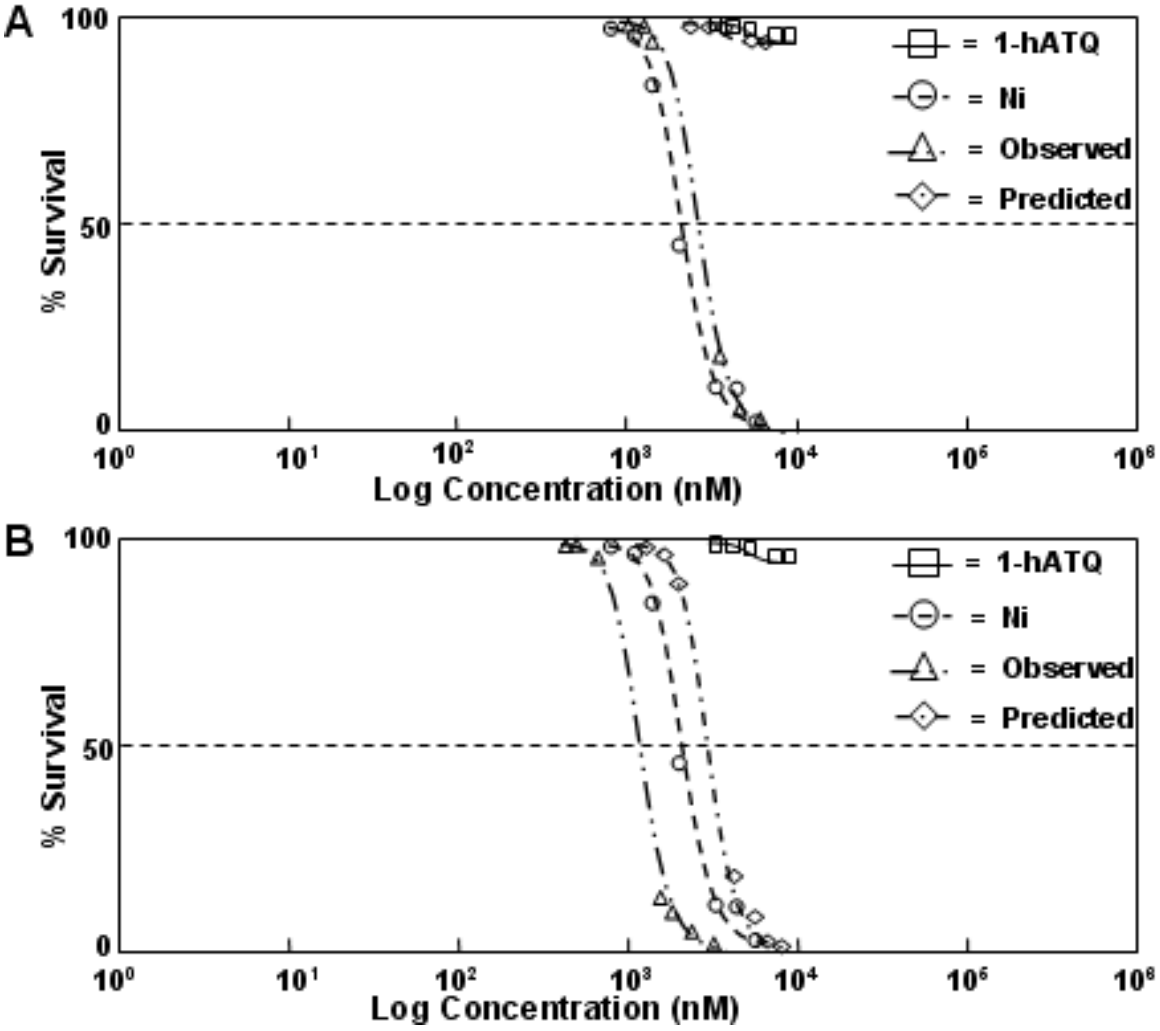

Figure 7.14 Concentration response curves of mixtures to *Hyalella azteca* under dark conditions. 1-hATQ was varied while Ni was kept at a constant concentration. A. 1-hATQ + 100 nM Ni B. 1-hATQ + 1000 nM Ni.

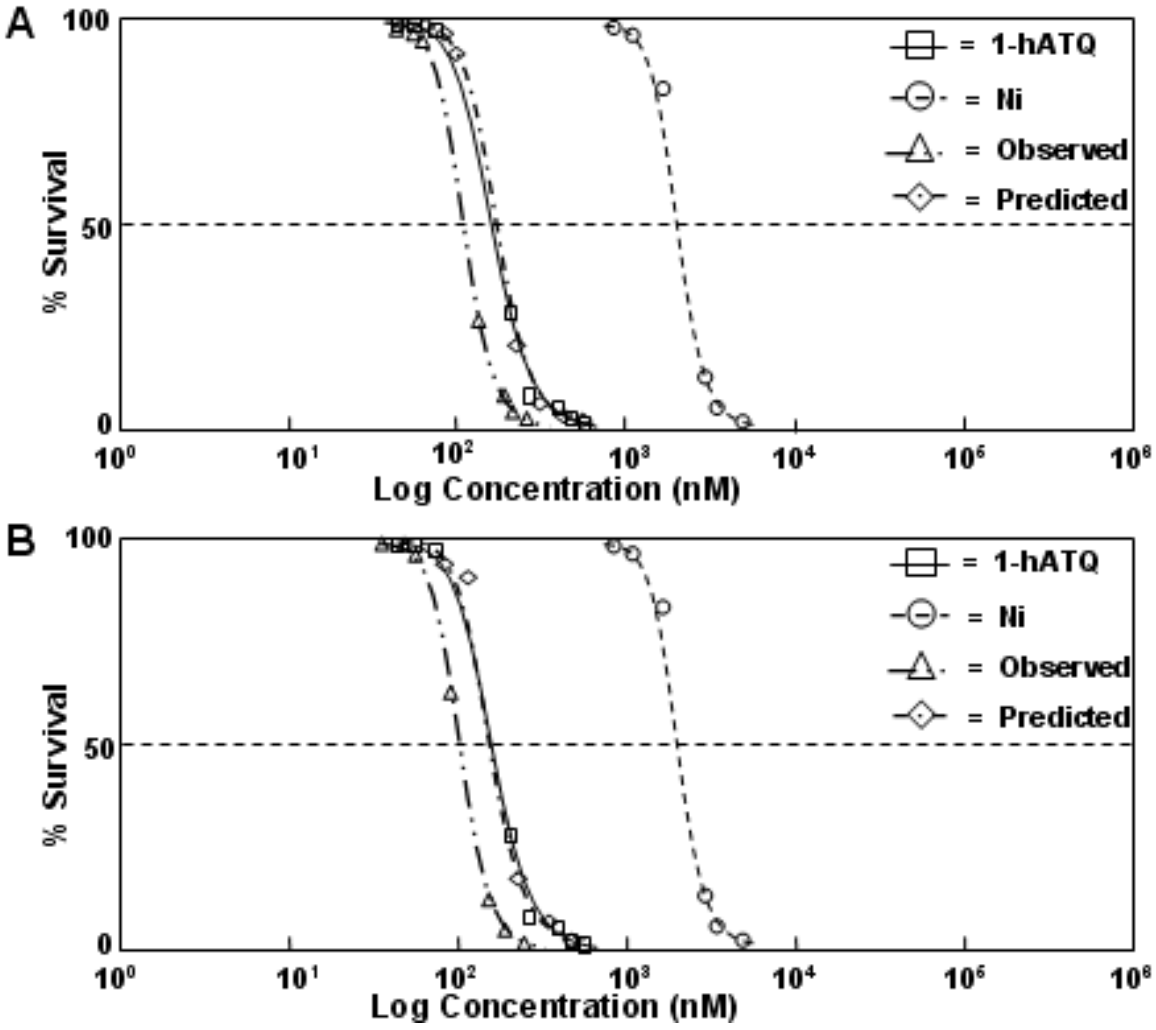

Figure 7.15 Concentration response curves of mixtures to *Hyalella azteca* under PAR conditions. 1-hATQ was varied while Ni was kept at a constant concentration. A. 1-hATQ + 1 nM Ni B. 1-hATQ + 10 nM Ni.

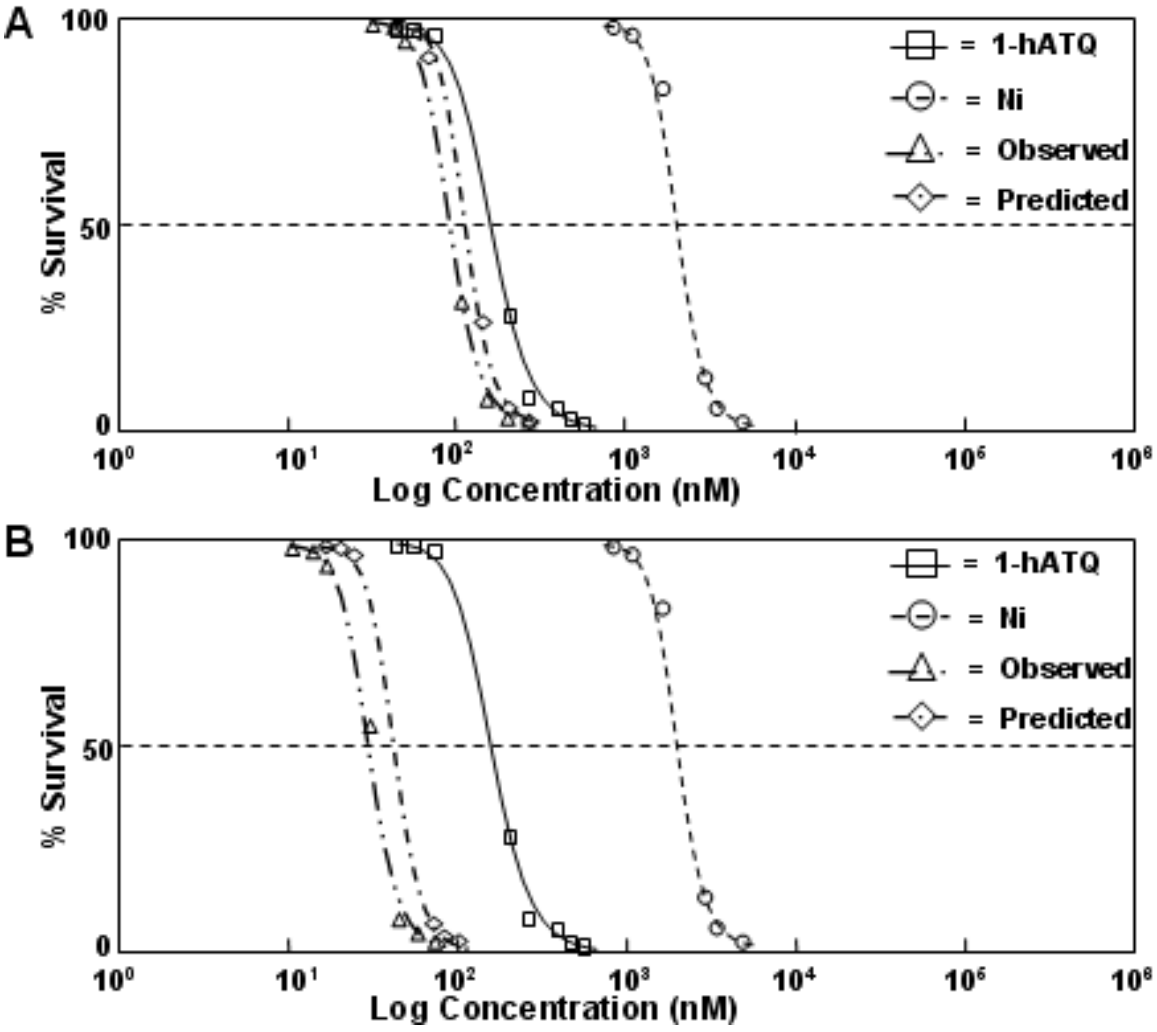

Figure 7.16 Concentration response curves of mixtures to *Hyalella azteca* under PAR conditions. 1-hATQ was varied while Ni was kept at a constant concentration. A. 1-hATQ + 100 nM Ni B. 1-hATQ + 1000 nM Ni.

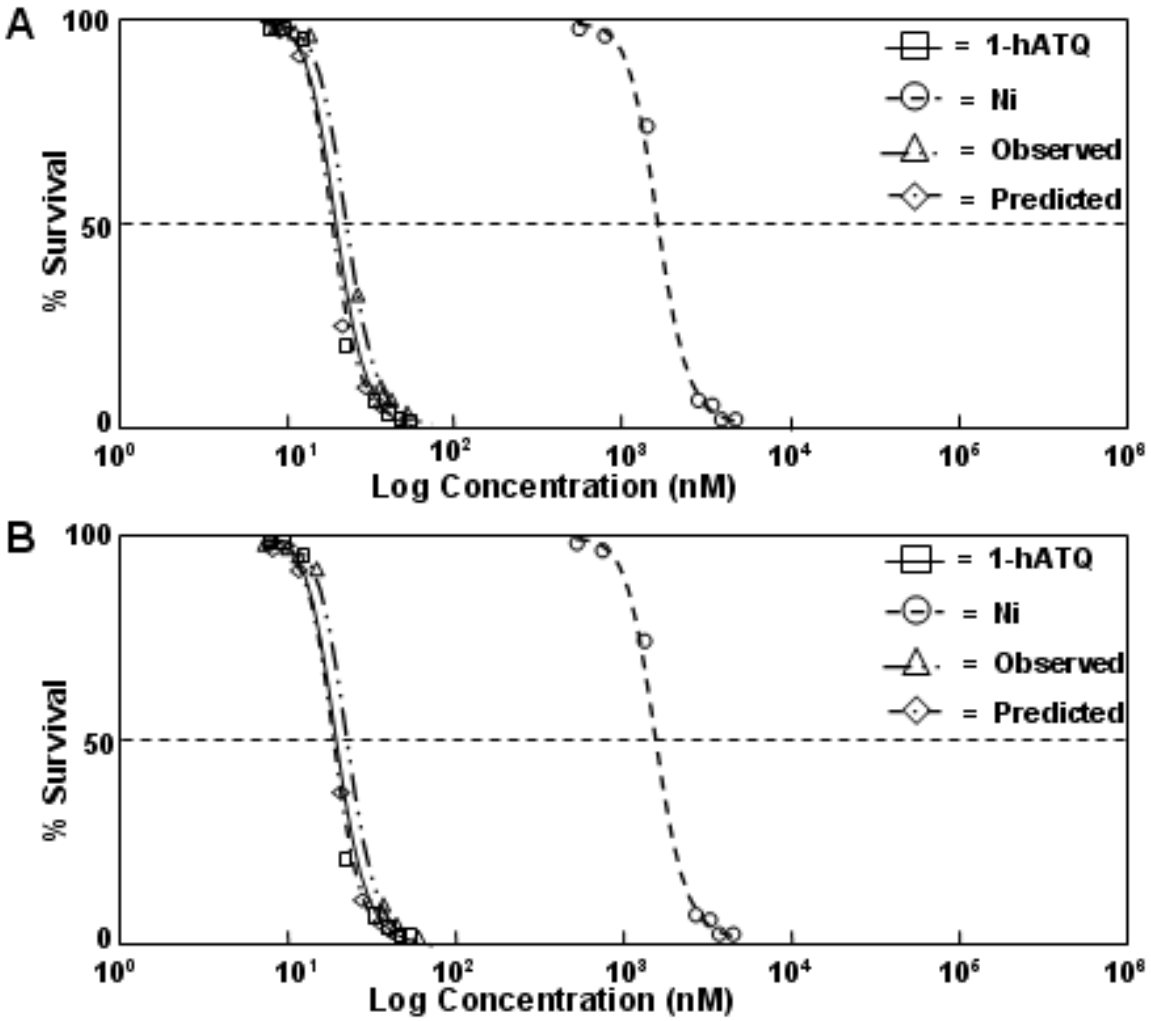

Figure 7.17 Concentration response curves of mixtures to *Hyalella azteca* under SSR conditions. 1-hATQ was varied while Ni was kept at a constant concentration. A. 1-hATQ + 1 nM Ni B. 1-hATQ + 10 nM Ni.

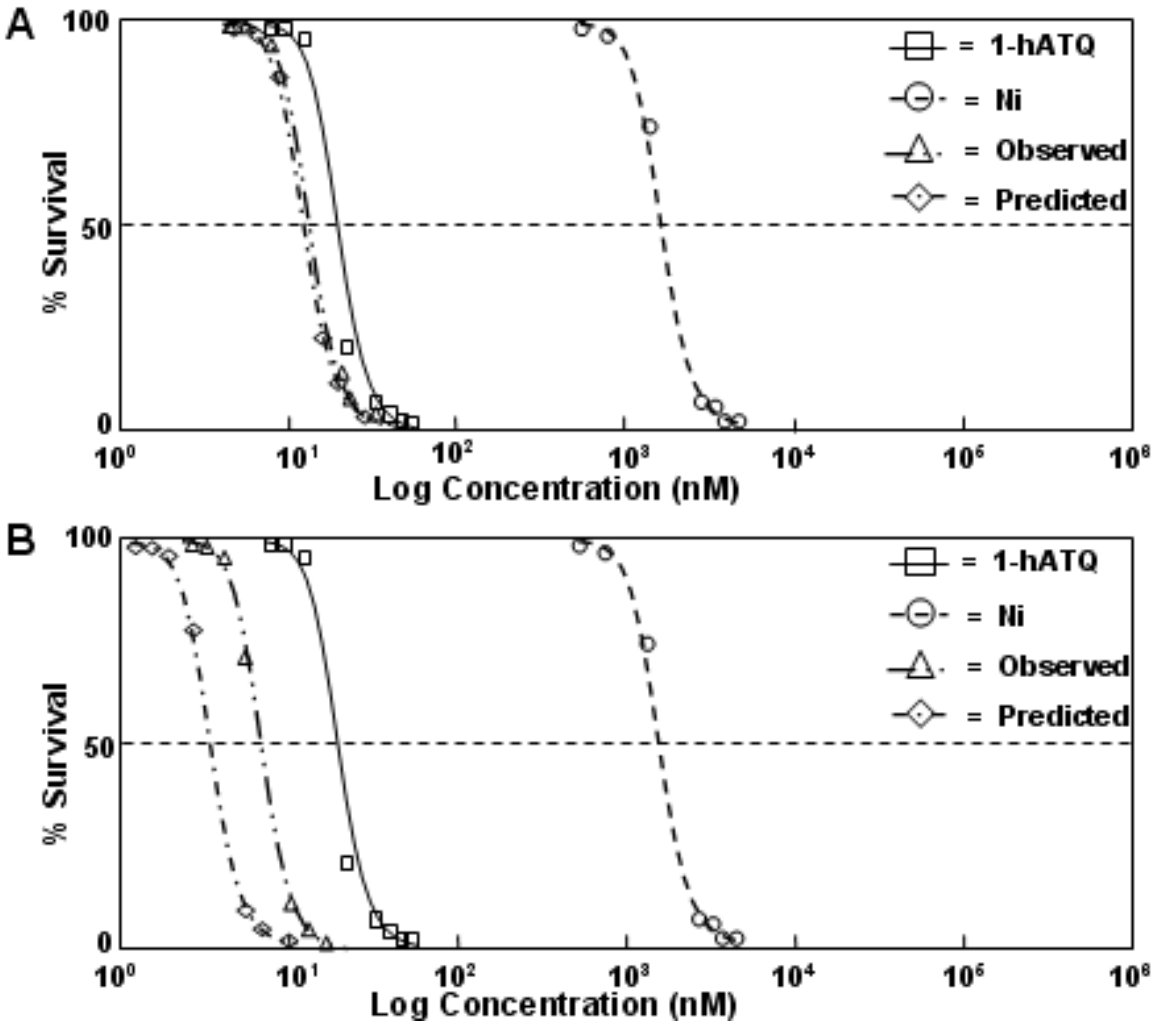

Figure 7.18 Concentration response curves of mixtures to *Hyalella azteca* under SSR conditions. 1-hATQ was varied while Ni was kept at a constant concentration. A. 1-hATQ + 100 nM Ni B. 1-hATQ + 1000 nM Ni.

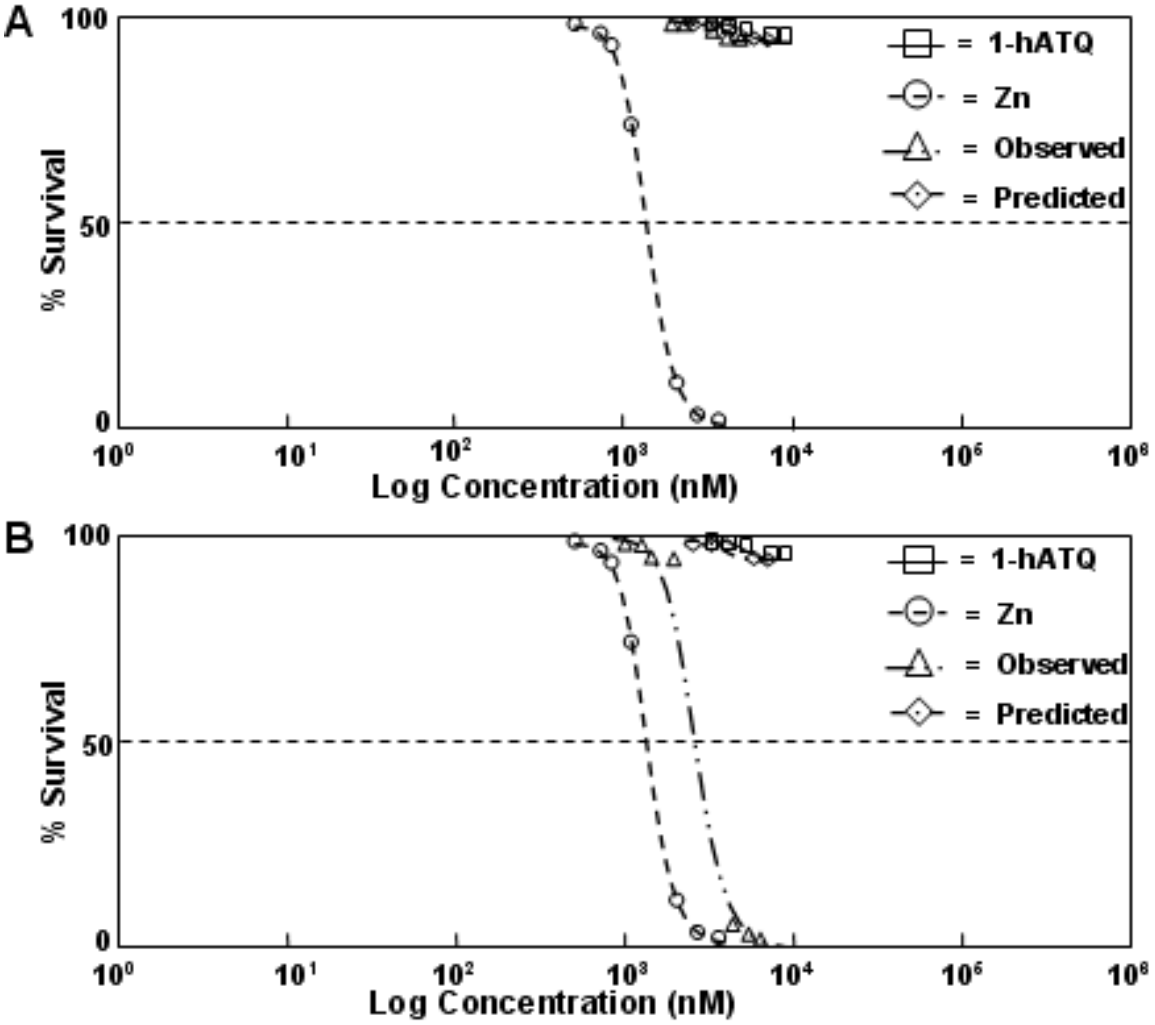

Figure 7.19 Concentration response curves of mixtures to *Hyalella azteca* under dark conditions. 1-hATQ was varied while Zn was kept at a constant concentration. A. 1-hATQ + 1 nM Zn B. 1-hATQ + 10 nM Zn.

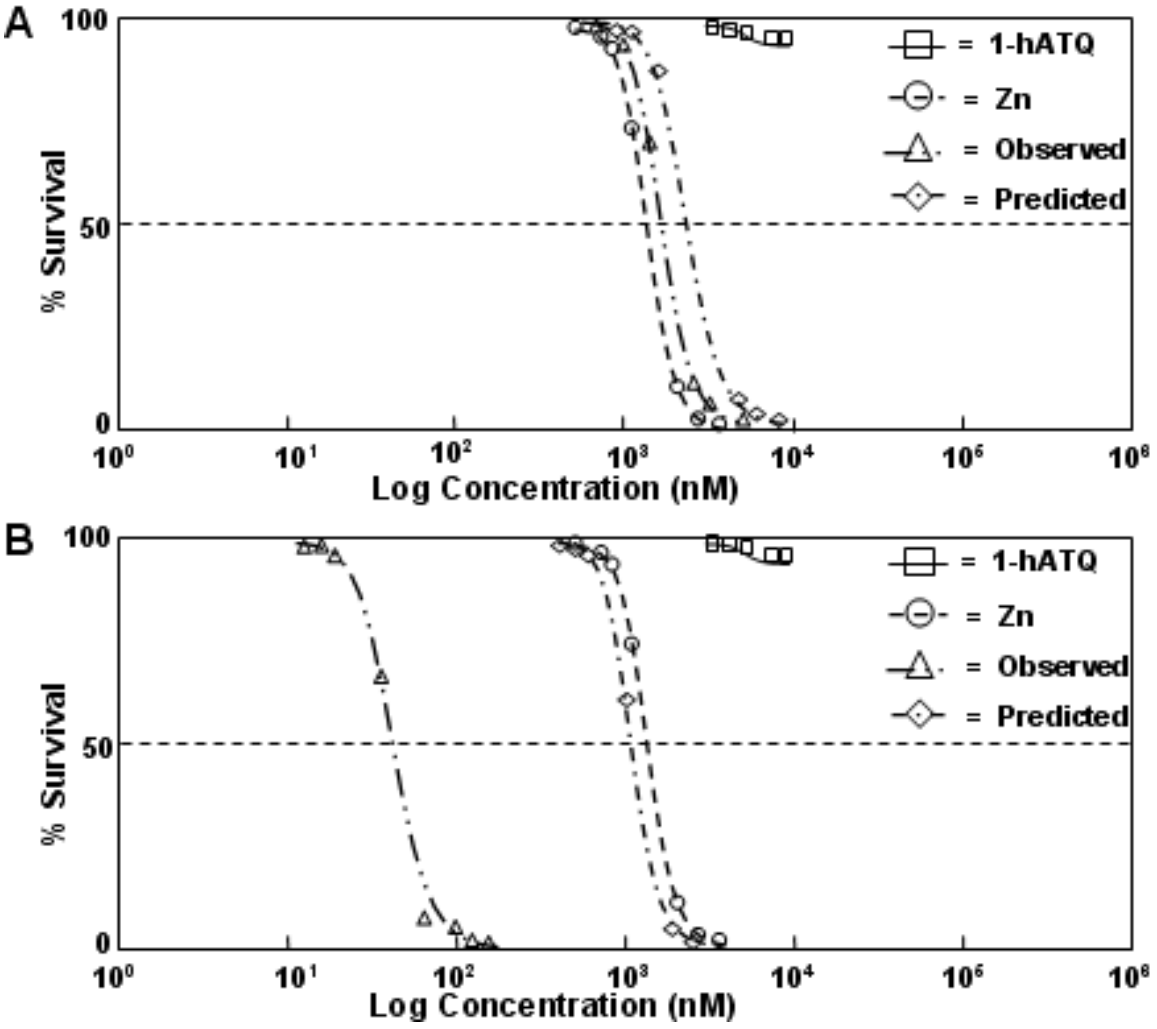

Figure 7.20 Concentration response curves of mixtures to *Hyalella azteca* under dark conditions. 1-hATQ was varied while Zn was kept at a constant concentration. A. 1-hATQ + 100 nM Zn B. 1-hATQ + 1000 nM Zn.

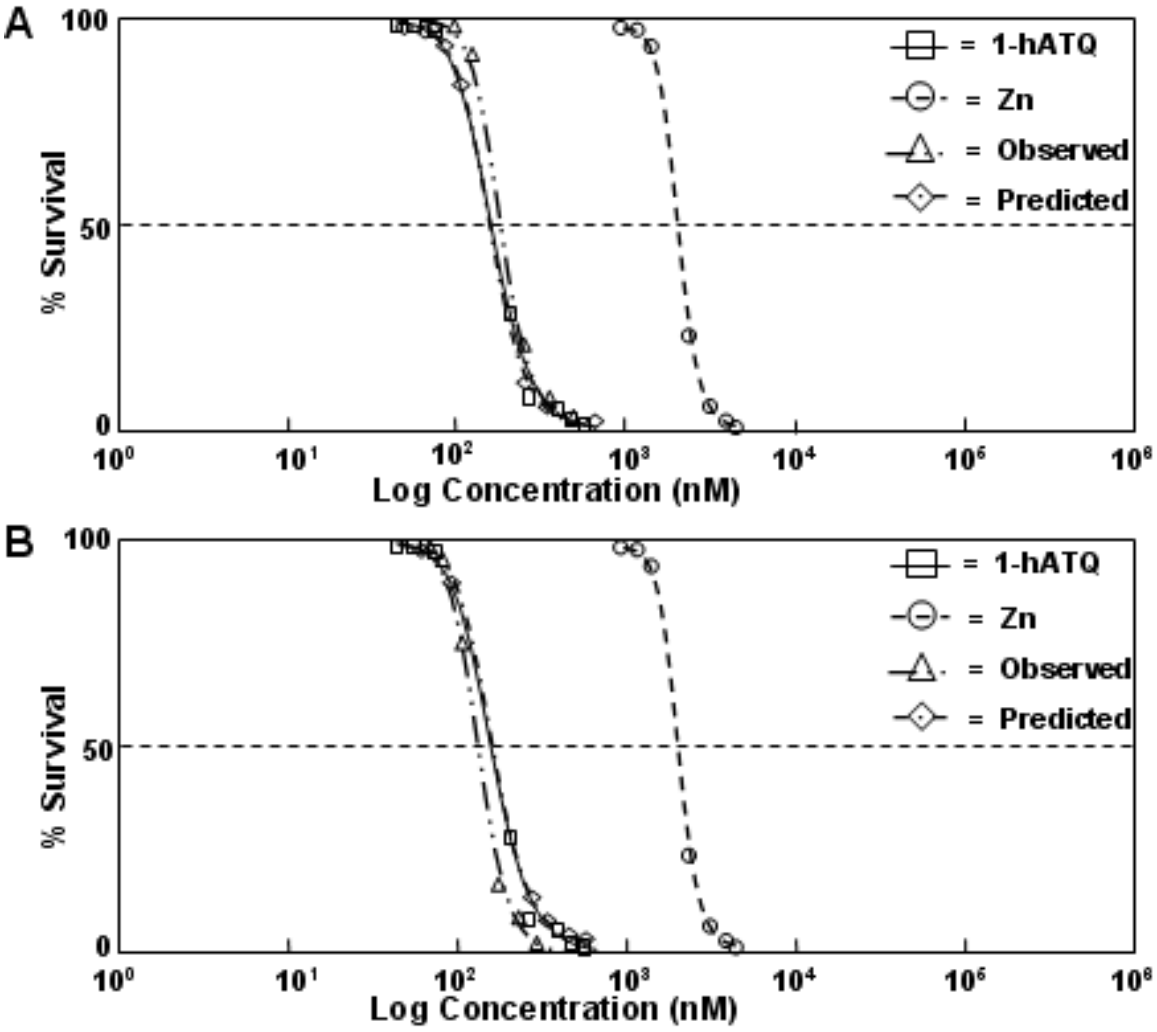

Figure 7.21 Concentration response curves of mixtures to *Hyalella azteca* under PAR conditions. 1-hATQ was varied while Zn was kept at a constant concentration. A. 1-hATQ + 1 nM Zn B. 1-hATQ + 10 nM Zn.

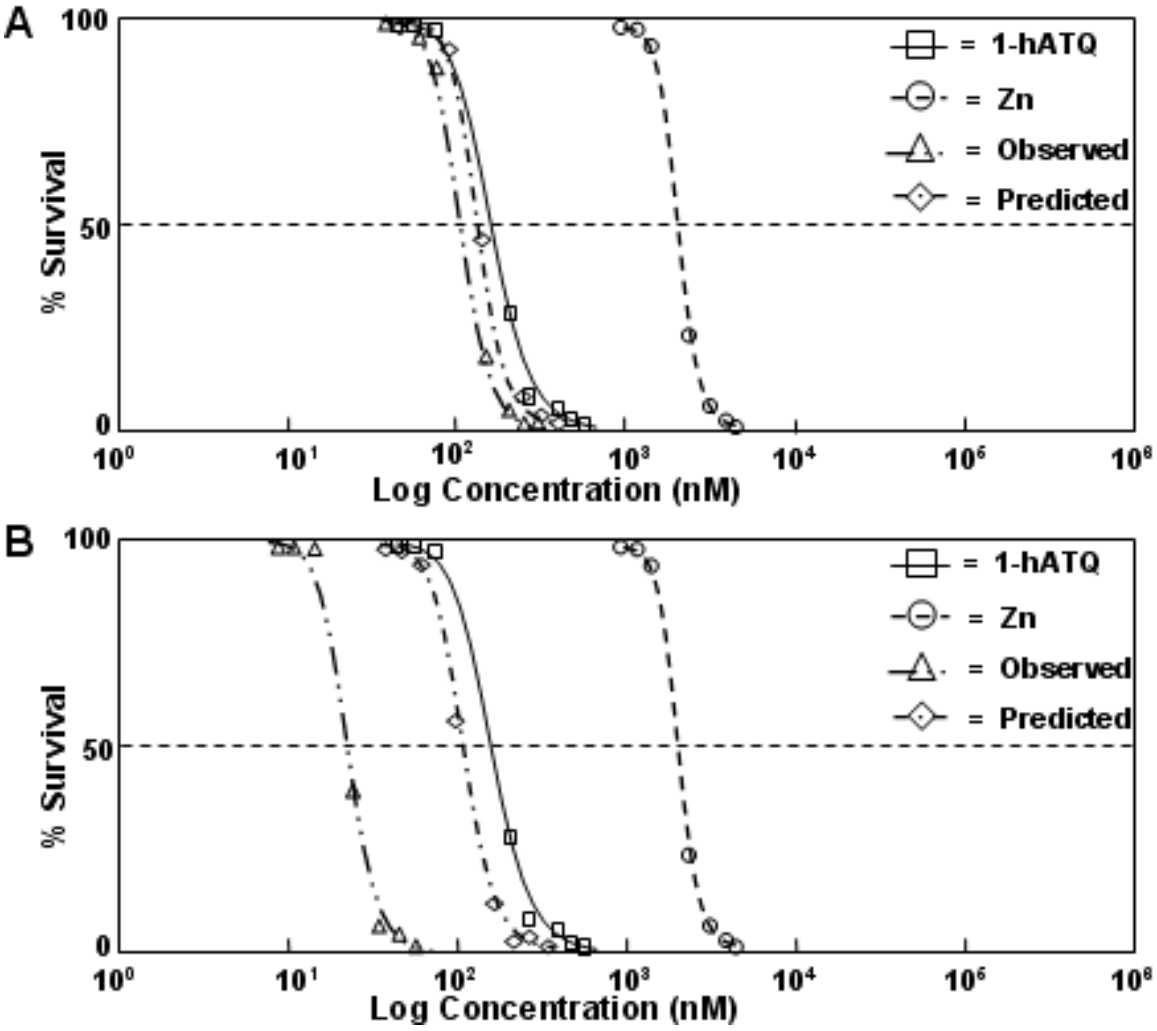

Figure 7.22 Concentration response curves of mixtures to *Hyalella azteca* under PAR conditions. 1-hATQ was varied while Zn was kept at a constant concentration. A. 1-hATQ + 100 nM Zn B. 1-hATQ + 1000 nM Zn.

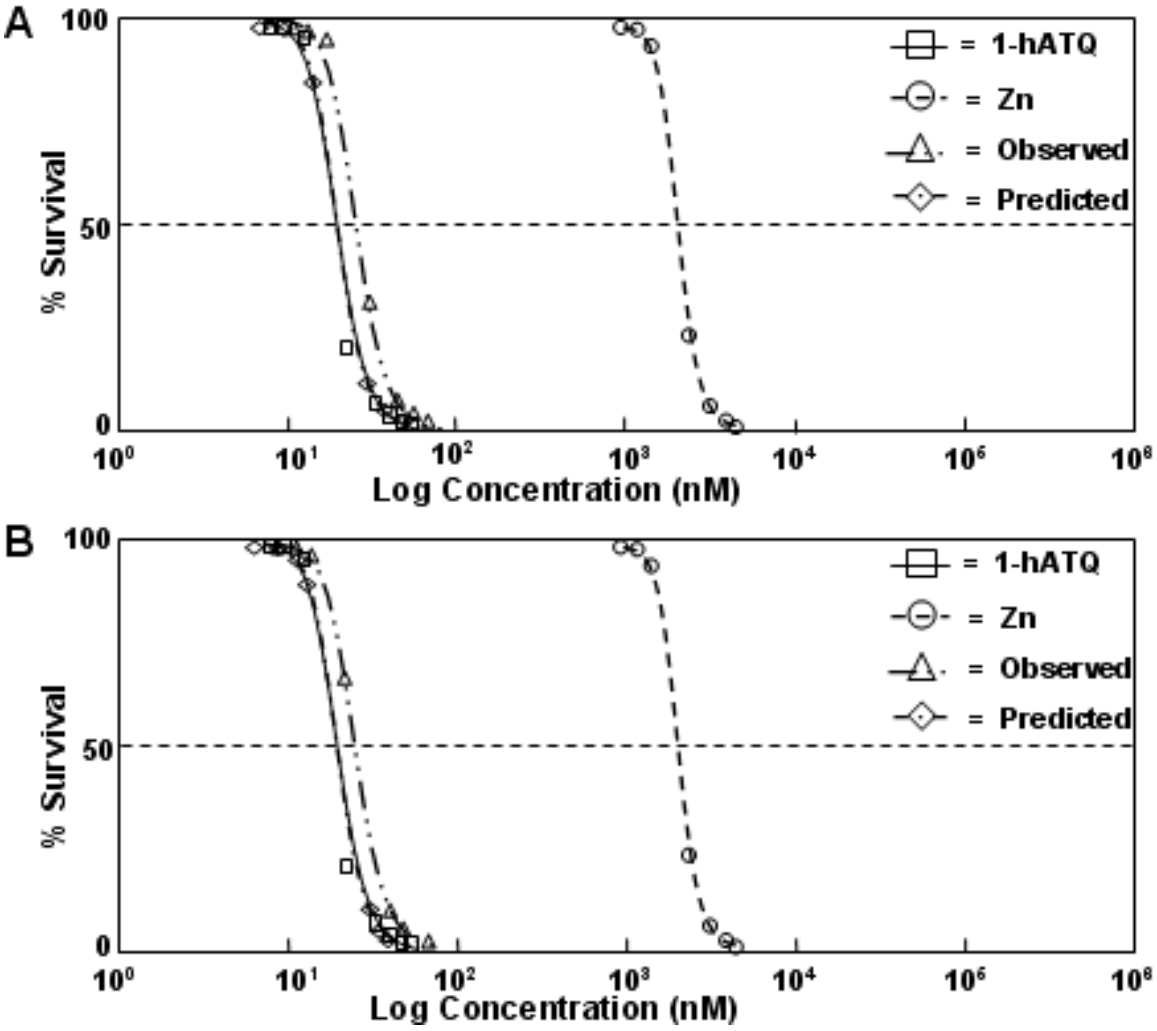

Figure 7.23 Concentration response curves of mixtures to *Hyalella azteca* under SSR conditions. 1-hATQ was varied while Zn was kept at a constant concentration. A. 1-hATQ + 1 nM Zn B. 1-hATQ + 10 nM Zn.

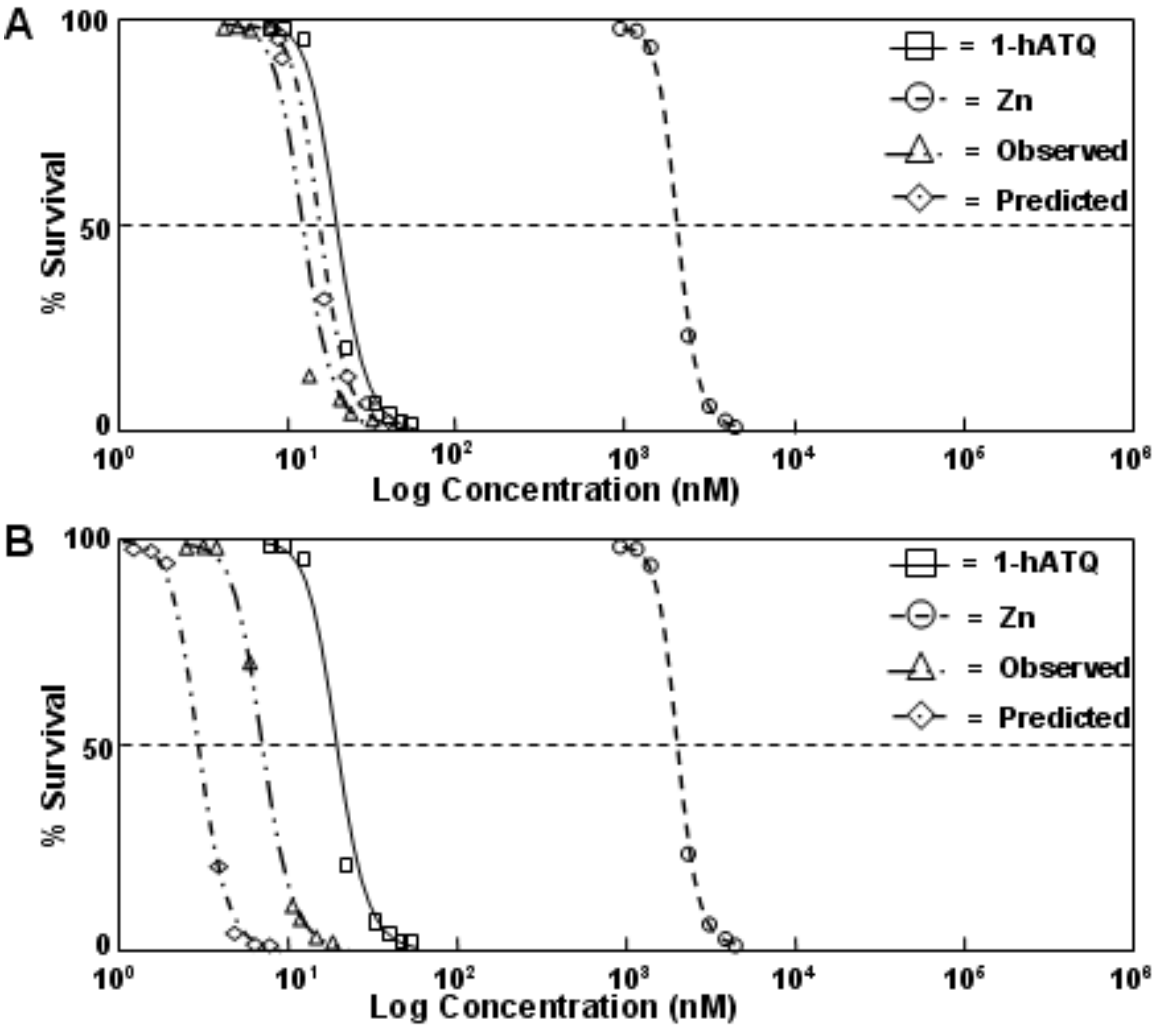

Figure 7.24 Concentration response curves of mixtures to *Hyalella azteca* under SSR conditions. 1-hATQ was varied while Zn was kept at a constant concentration. A. 1-hATQ + 100 nM Zn B. 1-hATQ + 1000 nM Zn.